Developing New Methods to Characterise Circulating Plasma Biomarkers in Abdominal Aortic Aneurysm

Pierfrancesco Lapolla Losasso

Nuffield Department of Surgical Sciences

St Catherine's College

University of Oxford

A thesis submitted for the degree of

Doctor of Philosophy

Michaelmas Term 2025

Developing New Methods to Characterise Circulating Plasma Biomarkers in Abdominal Aortic Aneurysm

Pierfrancesco Lapolla Losasso

St Catherine's College, University of Oxford

A thesis submitted for the degree of Doctor of Philosophy

Michaelmas Term 2025

Abdominal aortic aneurysms (AAAs) are progressive dilations of the abdominal aorta that carry a high risk of rupture and mortality if untreated. Current management relies on imaging-based surveillance and surgical repair at diameter thresholds; however, marked inter-individual variability in growth underscores the lack of personalised prediction tools. This thesis develops and refines a mass spectrometry-based pipeline for the absolute quantification of circulating proteins and metabolic profiling in AAA.

A bespoke isotopically labelled protein standard, the Oxford quantification conCATamer (OxConCAT), was designed to incorporate peptides from candidate AAA biomarkers. The construct was expressed in *E. coli* with complete ^15N incorporation, purified, and integrated into plasma proteomics workflows for absolute quantification via parallel reaction monitoring (PRM). Iterative optimisation addressed challenges in protein expression, digestion, and ion suppression, improving construct stability and proteotypic performance through computational redesign. In a dedicated pilot study of OxAAA plasma, OxConCAT peptides were successfully quantified, enabling evaluation of peptide chromatographic behaviour, heavy-to-light ratios, and protein-level fold changes. The combination of DIA-based discovery proteomics and PRM-based absolute quantification

facilitated the selection of robust quantotypic peptides. It demonstrated the feasibility of multiplexed protein measurement in plasma, with sufficient precision for downstream clinical studies.

In parallel, an optimised two-dimensional gas chromatography–mass spectrometry (GC×GC–MS) approach was developed for plasma metabolomics. Method development identified over 100 mass peaks (putatively assigned metabolites) across derivatised and non-derivatised fractions, and in a patient pilot study, 67 metabolites were confidently annotated. Comparative pre- and post-surgical analyses revealed significant systemic metabolic shifts involving lipid, amino acid, and oxidative metabolism, with cholesterol, octadecanoic acid, erythritol, glutamic acid, and citric acid emerging as key differentiators. These findings underscore the dynamic nature of the plasma metabolome during AAA surgery and suggest the potential of metabolomics for biomarker discovery and pathway-level insights.

Together, these proteomic and metabolomic pilot studies establish a dual workflow for biomarker discovery and validation in AAA. The OxConCAT pipeline provides a scalable, standardised, and precise method for absolute protein quantification, while metabolomics captures complementary biochemical changes with clinical relevance. The integrated platform is being applied to international cohorts (>400 patients) to develop and validate prediction models for AAA growth at 12 and 24 months, advancing biomarker-informed risk stratification and personalised surveillance strategies. Beyond AAA, the workflows described here may be adaptable to other vascular, metabolic, and inflammatory conditions, contributing to the advancement of precision medicine.

Acknowledgements

This thesis marks the culmination of a remarkable journey that began far from Oxford and has been shaped by the generosity, guidance, and friendship of many people to whom I owe my deepest gratitude.

I would first like to express my heartfelt thanks to my supervisors, Professors Regent Lee, Roman Fischer, and Ashok Handa, for their exceptional mentorship, patience, and unwavering support throughout this DPhil. Their insight, encouragement, and belief in this work have profoundly influenced both my research and my development as a clinician-scientist.

I am especially grateful to Professor Regent Lee, whose vision, rigour, and steady guidance have been the foundation of this entire journey. His encouragement and belief in my potential have carried me through challenges and shaped the way I think as both a researcher and a clinician-scientist. Working under his supervision has been one of the most formative and rewarding experiences of my academic life, and his example will continue to guide me well beyond this thesis.

I am deeply thankful to Professor Roman Fischer, whose scientific insight and proteomic expertise have been invaluable to this project. His generosity with time, knowledge, and advice has inspired me to approach complex problems with precision and curiosity. His passion for science and thoughtful guidance have greatly shaped my approach to research.

I wish to thank Professor Ashok Handa, whose clinical wisdom, perspective, and humanity have continually reminded me of the real-world purpose and responsibility behind this research. His mentorship has been both grounding and motivating, and his example of compassionate leadership has left a lasting impression.

I am grateful to Dr Sarah Flannery, Dr Lee Harris, and Dr Zhanru Yu for their invaluable expertise and assistance in laboratory proteomics and metabolomics work, and to Dr

Matteo Ferla for his generous guidance on the computational aspects of this project. I am also indebted to all members of Professor Benedikt Kessler Group at the TDI Mass Spectrometry Laboratory and the Professor Roman Fischer Clinical Proteomics Group for their collaboration, advice, and collegial spirit, which made the research environment both inspiring and formative.

My appreciation extends to Dr Sushma Shankar, Professor Ladislav Valkovič, and Mr Ed Sideso for their constructive evaluation and thoughtful feedback during my Transfer and Confirmation of Status, and to Professor Benedikt Kessler and Professor Matt Bown for their time and consideration in examining this thesis.

I am profoundly thankful to the Oxford University Clarendon Fund for its generous support, without which this research and my time at Oxford would not have been possible.

To my friends at St Catherine's College and across Oxford, thank you for your companionship throughout these years. A special mention goes to my best friends in Oxford, Maximilian Leopold Langefeld and Sunny Pydugadu, whose friendship, wisdom, and steadfast support have been a constant source of encouragement.

Finally, my deepest gratitude goes to my family, especially my mother and father, whose love, sacrifices, and faith have sustained me every step of the way. Their courage and perseverance have been my greatest inspiration, and every achievement in these pages belongs as much to them as to me.

Coming from where I began, reaching this point has been more than an academic achievement; it is a testament to perseverance, gratitude, and the belief that dedication and hope can bridge any distance. This journey, from its humble beginnings to Oxford, has shaped who I am, and I will carry its lessons with me always.

Table of Contents

Design, Synthesis, and Purification
2.7 Peptide Selection and Synthesis Criteria
2.8 Stable-Isotope Labelling via ^15N Incorporation
2.9 Challenges in Protein Expression and Folding
2.10 Purification Using Nickel Affinity Chromatography
2.11 Validation via Gel Filtration and Analytical QC

Analytical Workflow Optimisation
2.12 Integration of OxConCAT into Plasma Proteomics
2.13 Protease Digestion and Spike-In Strategies
2.14 LC–PRM/MS Method Development for Absolute Quantification

Results

Protein Behaviour and Stability Studies Results
2.15 Aggregation and Inclusion Body Formation
2.16 Iterative Troubleshooting for High-Yield Expression
2.16.1 Second to Fifth Purification Attempts
2.16.2 Freeze–Thaw Stability Testing
2.16.3 Final Gel Filtration and Buffer Optimisation
2.17 SDS-PAGE Confirmation of Purity

Discussion and Chapter Conclusion

Chapter 3 – Peptide Quantification and Selection Strategies

Introduction

Methods - Experimental Optimisation

Optimising Sample Preparation for Enhanced Peptide Quantification
3.1 Comparison of Loading Strategies (Co-Digestion, Sequential Digestion, Sandwich Loading)
3.2 Minimising Ion Suppression Effects

Refining Quantification through PRM Analysis
3.3 Peptide Competition and Signal Interference in PRM
3.4 Balancing Heavy and Light Peptide Ratios
3.5 Implementation of the Sandwich Loading Approach

Computational Methods - Optimisation of Peptide Fragment Arrangements
3.6 Introduction and Literature Review
3.6.1 Computational Background and Rationale
3.6.2 Application to OxConCAT Constructs

Chapter 4 – Pilot Proteomic Analysis of OxAAA Plasma
Introduction

Methods overview
DIA-Based Comparative Proteomic Profiling
4.1 Introduction and Experimental Design
4.2 Sample Collection, Preparation, and Digestion Strategies
4.3 DIA Data Acquisition and Analysis

Results

DIA-Based Comparative Profiling
4.4 Surgery-Associated Proteomic Changes in AAA Patients
4.4.1 Global proteomic reprogramming following surgical intervention

Absolute Quantification of OxConCAT Peptides Using Skyline
4.5 Introduction to the Quantification Workflow
4.6 Peak Identification and Extracted Ion Chromatogram (EIC) Integration
4.7 AL1L1 (Samples 01A, 01B)
4.7.1 APOA4_1 (Samples 01A, 01B)
4.8 Heavy-to-Light Peptide Ratio Calculation

Peptide-Level Quantification in the Patient Pilot Study
4.9 Experimental Design and Data Processing
4.10 Peptide-Level Analysis: NCHL1, ATRN, AL1L1, CRP, APOA4 Variants, CO8G
4.10.1 NCHL1 Peptide – GAGPESEPYIFQTPEGVPEQPTFLK
4.10.2 ATRN Peptide – YYTAINFVATPDEQNR
4.10.3 AL1L1 Peptide – GVVNVLPGSGSLVGQR
4.10.4 CRP Peptide – ESDTSYVSLK
4.10.5 APOA4_1 Peptide – LLPHANEVSQK
4.10.6 APOA4_2 Peptide – LGPHAGDVEGHLSFLEK
4.10.7 CO8G Peptide – RPASPSTIQPK
4.11 Grouped Protein-Level Analysis
4.11.1 Fold-Change Analysis and Log_2 FC Trends
4.11.2 Absolute Quantification (Log10 ng/µL Plasma)
4.11.3 Heatmaps: Median Quantities and Per-Patient Variability

Discussion
4.12 Interpretation of Technical and Biological Findings Determinants of Protein Quantification and Expression

Chapter 5 – OxConCAT Construct Redesign and Comparative Evaluation

Introduction

Rationale for Construct Redesign

5.1 Scientific motivations and analytical limitations of OxConCAT (AAAQconCAT-C002): Towards improving peptide quantification

Methods
Peptide Selection and Construct Refinement
5.2 Peptide Selection, Analytical Challenges, and Construct Refinement
5.3 Empirical validation using DIA overlap analysis with an automated script for peptide suitability
5.4 Peptide Junction Strategy and Linker Optimisation to enhance proteolytic efficiency

Results
Comparative Analysis of Constructs
5.5 Structural and Content Differences Between the Original OxConCAT (AAAQconCAT-C002) and Revised Versions
5.6 Theoretical Soundness: Proteotypic Value, Stability, and Predictability

Discussion
5.7 Discussion and Alignment with Research Goals

Chapter 6 – Metabolomics Analysis of Plasma Samples from the OxAAA Cohort

Introduction

Methods
Method Development and Workflow Optimisation
6.1 Identification of Plasma Metabolites via GC×GC–MS
6.2 Advantages Over Conventional 1D GC–MS

Metabolomic Profiling of OxAAA Plasma
6.3 Metabolite Extraction and Derivatisation Protocol
6.3.1 Sample Preparation
6.4 Data Acquisition and Comparative Chromatographic Performance

Results
6.5 Overview of Detected Metabolites and Annotation Confidence Levels
6.6 Comparative Coverage of Derivatised Fractions

Statistical Analyses
6.7 PLS–DA
6.8 Fold Change (FC) Analysis
6.9 Hierarchical Clustering Heatmap

List of Figures

List of Tables

List of Abbreviations

Abbreviation	Definition
AGI	Aneurysm Growth Index
AUC	Area Under the Curve
AUROC	Area Under the Receiver Operating Characteristic Curve
BH	Benjamini–Hochberg
BKY	Benjamini–Krieger–Yekutieli
CAD	Coronary Artery Disease
CMD	Cardiovascular Medicine Department
CRP	C-Reactive Protein
CV	Coefficient of Variation
DDA	Data-Dependent Acquisition
DIA	Data-Independent Acquisition
EDTA	Ethylenediaminetetraacetic Acid
EIC	Extracted Ion Chromatogram
ELISA	Enzyme-Linked Immunosorbent Assay
ESI	Electrospray Ionisation
EVAR	Endovascular Aneurysm Repair
FDR	False Discovery Rate
FMD	Flow-Mediated Dilation

Abbreviation	Definition
GC×GC–MS	Comprehensive Two-Dimensional Gas Chromatography–Mass Spectrometry
His-tag	Histidine Tag
HV	Healthy Volunteers
IL	Interleukin
ILT	Intraluminal Thrombus
IMAC	Immobilised Metal Affinity Chromatography
IPTG	Isopropyl β-D-1-thiogalactopyranoside
LC–MS/MS	Liquid Chromatography–Tandem Mass Spectrometry
LOD	Limit of Detection
LOQ	Limit of Quantification
MS	Mass Spectrometry
MTBE	Methyl tert-Butyl Ether
MSTFA	N-Methyl-N-(trimethylsilyl)trifluoroacetamide
MWCO	Molecular Weight Cut-Off
NAAASP	NHS Abdominal Aortic Aneurysm Screening Programme
OSR	Open Surgical Repair
OxConCAT	Oxford Quantification Concatemer
PAD	Peripheral Arterial Disease
PCA	Principal Component Analysis
PLS-DA	Partial Least Squares–Discriminant Analysis
ppm	Parts Per Million
PRM	Parallel Reaction Monitoring
PSM	Peptide Spectrum Match
QC	Quality Control
QconCAT	Quantitative Concatemer
RAAAS	Ruptured Abdominal Aortic Aneurysm
RNA	Ribonucleic Acid
SDS–PAGE	Sodium Dodecyl Sulphate Polyacrylamide Gel Electrophoresis
SEC	Size Exclusion Chromatography
SOP	Standard Operating Procedure
SRM	Selected Reaction Monitoring
TDI	Target Discovery Institute
TIC	Total Ion Chromatogram
TP	Timepoint
TVVN	Thames Valley Vascular Network

Statement of Contributions

Dr Sarah Flannery provided assistance with mass spectrometry data acquisition, instrument operation, and analysis. Dr Lee Harris contributed to protein expression and purification during the development of the OxConCAT workflow and the revised version of the protein construct. Dr Zhanru Yu assisted with laboratory-based metabolomics experiments. Dr Matteo Ferla provided guidance on the computational and bioinformatic aspects of the project. All experimental design, data interpretation, and thesis writing were carried out by the author.

Declaration on the Use of Artificial Intelligence Tools

Artificial intelligence–based tools were used in a limited and supportive capacity during the preparation of this thesis, primarily for language refinement, grammar checking, and improving clarity and readability of the text.

Chapter 1 – Scientific Background, Preliminary Work, and Research Framework

Introduction and Background

1.1 Background and Rationale

Abdominal aortic aneurysms (AAAs) are defined as permanent, localised dilatations of the abdominal aorta involving all three layers of the arterial wall. An AAA is usually diagnosed when the aortic diameter exceeds 30 mm or is more than 50% larger than the expected normal diameter (typically 14–30 mm) for a given individual.[1–3] Without prompt intervention, AAAs tend to enlarge gradually, eventually leading to rupture, a catastrophic event with high mortality. AAAs are roughly three times more common in men than in women and cause an estimated 6,000 deaths each year in the United Kingdom, contributing to about 200,000 cases worldwide.[4, 5] Risk factors for AAA development closely match those of other cardiovascular diseases and include advanced age, male sex, a positive family history, and cigarette smoking, with the latter being the most significant modifiable risk factor.[6, 7] Most AAAs are silent and remain symptom-free until rupture occurs. Ruptured AAAs (rAAAs) are associated with a high mortality rate of 85–90%. Even among patients who reach the hospital in time, survival rates are still limited, ranging from 50% to 70%. [8, 9] AAA pathogenesis often coexists with atherosclerotic conditions such as coronary artery disease (CAD),[10] cerebrovascular disease, and peripheral arterial disease (PAD), highlighting the systemic nature of the underlying vascular pathology. The standard of care for AAA management depends primarily on aneurysm size, anatomical location, rate of expansion, and the presence of comorbidities. Current intervention thresholds recommend repair when the aneurysm reaches 55 mm in diameter in men or 50 mm in women, or if rapid expansion is detected.

Surgical options include open surgical repair (OSR) and endovascular aneurysm repair (EVAR), with the choice influenced by anatomical suitability and patient risk profile (Figure 1).[11, 12]

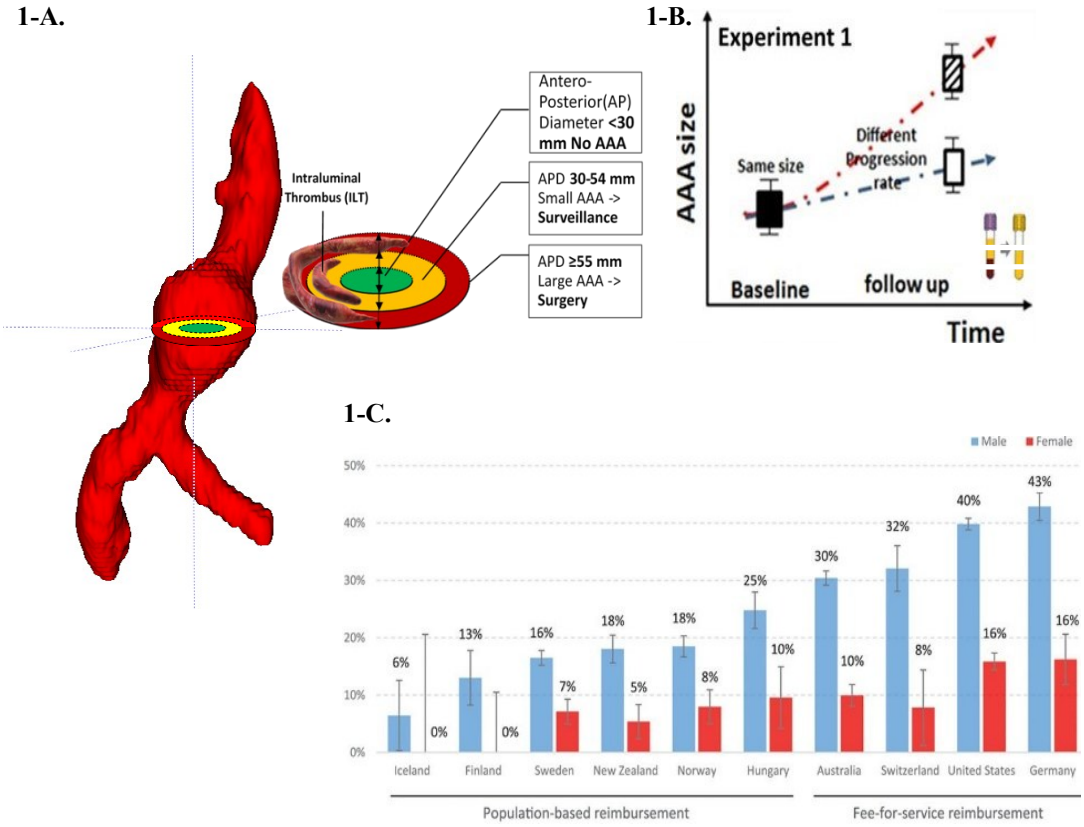

Figure 1. Clinical and Systemic Perspectives on Abdominal Aortic Aneurysm (AAA) Management. 1A: Three-dimensional reconstruction of an abdominal aortic aneurysm (AAA) from a computed tomography (CT) scan of a patient, processed using ITK-SNAP software for segmentation and visualisation. The rendering highlights the intraluminal thrombus (ILT) within the aneurysmal sac. It depicts the conventional size thresholds used to determine the need for surgical intervention (≥55 mm for men, ≥50 mm for women). 1B: Schematic representation of the heterogeneity in AAA progression observed during surveillance. Despite identical initial aneurysm sizes at baseline, different patients exhibit variable growth trajectories over time, highlighting the need for personalised surveillance strategies. Adapted from Lee et al., Annals of Surgery, 2020, with permission. 1C: Bar chart comparing the proportion of small AAA repairs and repairs in octogenarians across countries with different healthcare reimbursement models. In fee-for-service systems (e.g., the United States, Germany), a higher percentage of small aneurysms and elderly patients undergo surgical repair compared to countries with population-based reimbursement systems (e.g., Sweden, Norway). These differences suggest that financial incentives may influence treatment thresholds and clinical decision-making. The marked male predominance in AAA prevalence is well recognised and is thought to reflect sex-specific differences in vascular biology, hormonal protection (particularly oestrogen-mediated effects), inflammatory responses, and lifetime exposure to risk factors such as smoking. Data adapted from Beck et al., Circulation, 2016, with permission.

However, considerable international variation exists in the implementation and timing of AAA repair. These differences are, in part, driven by health system resources and financial incentives.[13] In cases where the aneurysm is below the surgical threshold (<55 mm), patients are enrolled in surveillance programmes involving regular abdominal ultrasound (US) to monitor aneurysm growth.[14] Importantly, not all aneurysms follow the same growth trajectory; some may remain stable for years, while others enlarge rapidly, necessitating a more individualised approach to monitoring. In the United Kingdom, the NHS Abdominal Aortic Aneurysm Screening Programme (NAAASP), introduced in 2009, invites all men during the year they turn 65 to undergo an initial abdominal ultrasound. The striking sex difference observed reflects the well-established male predominance in AAA prevalence and is likely attributable to sex-specific differences in vascular structure and remodelling, hormonal influences (notably oestrogen-mediated protective effects), inflammatory and immune responses, and differential lifetime exposure to major risk factors such as smoking. Once an AAA is diagnosed, NAAASP recommends periodic ultrasound surveillance. However, the frequency of these follow-up scans does not always align with international guidelines and often fails to consider individual growth patterns. As a result, many scans may be redundant, increasing patient burden and healthcare costs. It is estimated that approximately 2,500 new AAAs are diagnosed annually through the NHS, significantly contributing to surveillance workload and expenditure.[15, 16] These challenges highlight the need for more personalised, data-driven approaches to AAA monitoring and treatment decision-making. Emerging strategies, including biomarker profiling and systems biology approaches, hold promise for refining risk stratification and surveillance schedules, potentially reducing unnecessary imaging while improving patient outcomes.

1.2 The Plasma Proteome as a Source of Circulating Biomarkers

The human plasma proteome offers vast potential for improving disease diagnosis and monitoring, provided current analytical challenges are addressed. Plasma reflects the most comprehensive circulating proteome, containing classical liver-derived proteins (albumin, globulins, coagulation factors) as well as tissue-leakage proteins, immunoglobulins, and inflammatory mediators released through secretion, membrane shedding, or cellular turnover. [17] Most plasma proteins exist as diverse proteoform proteins with distinct structural or PTM-defined variants, shaped by glycosylation and proteolytic processing into bioactive fragments and other PTMs (e.g., phosphorylation, oxidation).[18] A defining feature of plasma proteomics is its extreme dynamic range; protein concentrations span over ten orders of magnitude, from abundant species such as albumin (35–50 g/L) to cytokines present in picogram quantities. This range creates major analytical challenges, demanding refined enrichment, fractionation, and detection strategies to access low-abundance biomarkers (Figure 2). Despite advances in high-resolution MS and antibody assays, only a few plasma proteins, such as troponin, CRP, and PSA, are used clinically. Most low-abundance plasma proteins remain unexplored. Two complementary discovery strategies have been proposed: (i) large-scale studies, which detect small effect sizes but require extensive resources, and (ii) phenotype-enriched ("lean") designs, which focus on extreme clinical presentations to maximise signal-to-noise with smaller cohorts. Continued innovation in sample processing, mass spectrometry, and data analysis will be essential to fully exploit the diagnostic potential of the plasma proteome.[19, 20]

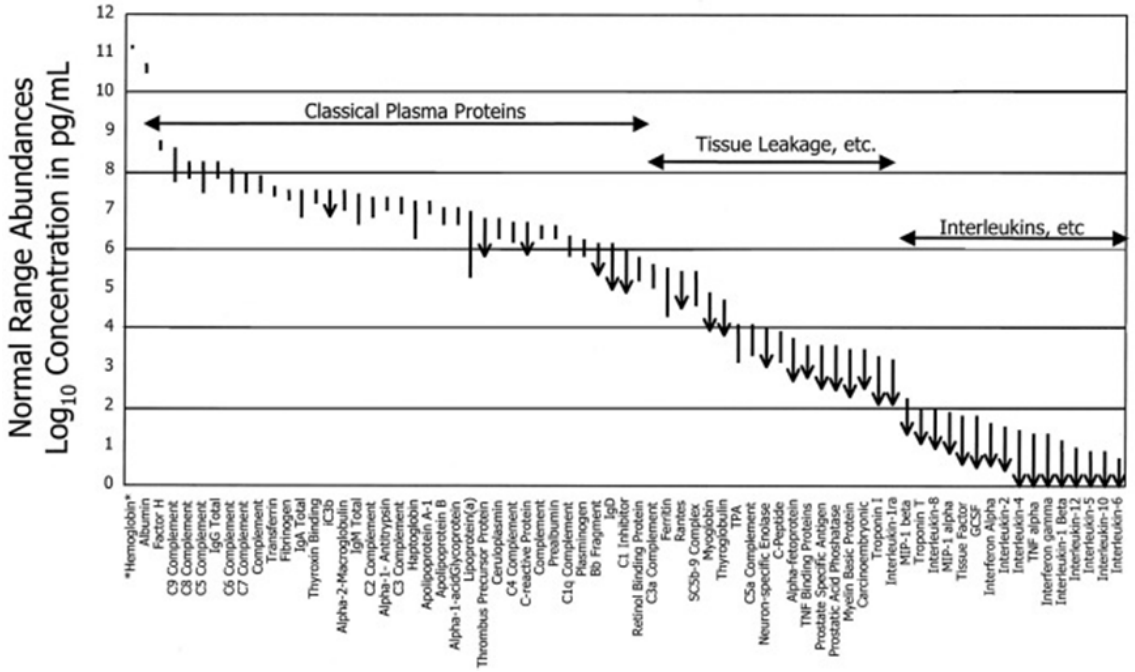

Figure 2. Dynamic range of human plasma protein concentrations. The chart illustrates the normal range abundances (on a $\log_{10}$ scale) of key plasma proteins, from classical plasma proteins such as albumin and immunoglobulins to lower abundance molecules like cytokines and interleukins. The vast dynamic range, spanning over 10 orders of magnitude, represents a significant analytical challenge in plasma proteomics. Adapted from The human plasma proteome. *Molecular & Cellular Proteomics* 2003 DOI: (10.1074/mcp.A300001-MCP200), with permission.

1.3 The Plasma Metabolome and Its Clinical Relevance

Metabolomics is a rapidly emerging field within the broader "*omics*" sciences that focuses on the comprehensive profiling of small-molecule metabolites in biological systems. These include amino acids, organic acids, sugars, lipids, and nucleotides, which are the downstream products of cellular biochemical processes and provide a dynamic snapshot of the physiological and pathological state of an organism. Unlike the genome, which remains relatively static, the metabolome is highly sensitive to internal and external perturbations, including genetic mutations, environmental exposures, drug treatments, and disease progression. As such, metabolomics offers unique insights into functional

biology and holds great promise for the identification of diagnostic, prognostic, and predictive biomarkers. Metabolomics approaches typically rely on high-throughput analytical platforms such as gas chromatography-mass spectrometry (GC-MS) and liquid chromatography-mass spectrometry (LC-MS).[21, 22]

These methods enable the detection, quantification, and structural annotation of metabolites in complex biological matrices, such as plasma, serum, urine, or tissue extracts. Importantly, metabolomics complements proteomics by capturing the functional consequences of protein activity and gene expression.[23, 24] It bridges the gap between molecular mechanisms and clinical phenotypes, thereby enhancing our understanding of disease pathways and physiological responses. In the context of abdominal aortic aneurysm (AAA), metabolomics offers an untapped opportunity to explore systemic metabolic changes associated with aneurysm formation, progression, and response to surgical intervention. Metabolic alterations may reflect oxidative stress, extracellular matrix turnover, immune activation, or vascular remodelling, all of which are hallmarks of AAA pathology. This thesis develops and optimises a robust plasma metabolomics workflow tailored for AAA samples. By integrating meticulous sample extraction, derivatisation, and GC×GC–MS analysis, the aim is to generate high-resolution metabolic profiles that can be interrogated for biomarker discovery and mechanistic insights. Ultimately, this strategy seeks to contribute to the development of more personalised, biology-driven approaches to AAA risk stratification and management. Before developing the analytical frameworks described above, initial studies within the OxAAA programme focused on functional vascular phenotyping.

Preliminary Work

To ground subsequent proteomic and metabolomic investigations in functional vascular measurements, the OxAAA programme initially focused on non-invasive vascular phenotyping. Endothelial dysfunction is a recognised feature of vascular disease. It can be assessed non-invasively using flow-mediated dilation (FMD), which measures brachial artery dilatation in response to increased shear stress.[25] In AAA patients, impaired FMD has been linked with faster aneurysm expansion, while surgical repair improves endothelial function, suggesting a systemic vascular contribution to aneurysm progression. Although promising, FMD is limited by operator dependence, equipment requirements, and variable reproducibility, restricting its wider clinical adoption. Building on these findings, the OxAAA programme evaluated models that combined physiological (FMD), anatomical (AAA diameter), and biochemical (circulating proteins) data. Multivariate approaches incorporating these parameters achieved strong predictive performance for aneurysm growth, with AUROC values of 0.92 at 12 months and 0.82 at 24 months for predicting 0% AAA growth.[26] I contributed to these studies, which demonstrated the potential of multimodal biomarker strategies. However, the complexity of requiring multiple assays and vascular measurements limits their clinical feasibility. To overcome these limitations, subsequent investigations sought to identify individual circulating proteins with sufficient predictive power to simplify biomarker models. By focusing on molecular markers that can be measured reproducibly and cost-effectively, the aim was to develop clinically feasible strategies for patient risk stratification. This shift in emphasis led to the exploration of the intra-luminal thrombus (ILT) as a potential source of disease-relevant proteins.

1.4 Proteomic Identification of Intraluminal Thrombus (ILT)-Derived Proteins: The Case of Attractin

Building on the success of the biomarker integration study,[26] subsequent efforts were directed toward identifying individual proteins with high predictive value for aneurysm growth. The focus turned to the intra-luminal thrombus (ILT), a hallmark of AAA pathology. ILT is metabolically active and releases proteins into circulation, making it a plausible source of circulating biomarkers. Histological and cytometric analyses have shown that ILT is rich in lymphocytic and inflammatory infiltrates, suggesting a role in modulating the vascular environment and potentially driving aneurysm progression. Using paired plasma and ILT tissue samples collected from OxAAA participants, a label-free proteomics workflow based on liquid chromatography–tandem mass spectrometry (LC–MS/MS) was employed. This high-resolution technique enabled comprehensive profiling of the ILT proteome and its correlation with plasma proteins in patients exhibiting divergent growth trajectories. From these data, a library of approximately 100 differentially expressed proteins, identified through differential abundance analysis comparing fast vs slow AAA growers, was compiled. Further targeted ELISA validation revealed Attractin as a promising biomarker. Attractin is a secreted glycoprotein implicated in immune regulation, T-cell activation, and inflammatory response. Crucially, its plasma levels were significantly elevated in patients with rapidly growing AAAs, and it was confirmed to be released directly from ILT. A simplified two-variable predictive model was then developed, incorporating plasma Attractin concentration and baseline AAA diameter. The model demonstrated high predictive power for aneurysm stability: AUROC = 0.85 for 0% growth prediction at 12 months. In clinical terms, this equated to: sensitivity = 54% (7/13 patients with no growth), specificity = 94% (46/49 patients with growth), overall accuracy = 85% (53/62 patients correctly classified).[27]

To facilitate interpretation, the Aneurysm Growth Index (AGI) was created, a probability score derived from the regression model. A cut-off score of 0.39 provided an optimal balance between sensitivity and specificity. Importantly, this two-variable model, based on plasma Attractin concentration and baseline AAA diameter, offers a potentially more clinically feasible solution than multi-marker or physiologically demanding algorithms. These findings not only underscore the utility of Attractin as a novel AAA biomarker but also illustrate how integrative proteomics can yield clinically actionable insights into complex vascular pathologies. The simplified model represents a significant step toward personalising AAA management by informing surveillance intervals and intervention timing based on individual growth risk (Figure 3). These findings motivated the development of a quantitative platform capable of precisely measuring candidate biomarkers such as Attractin in plasma.

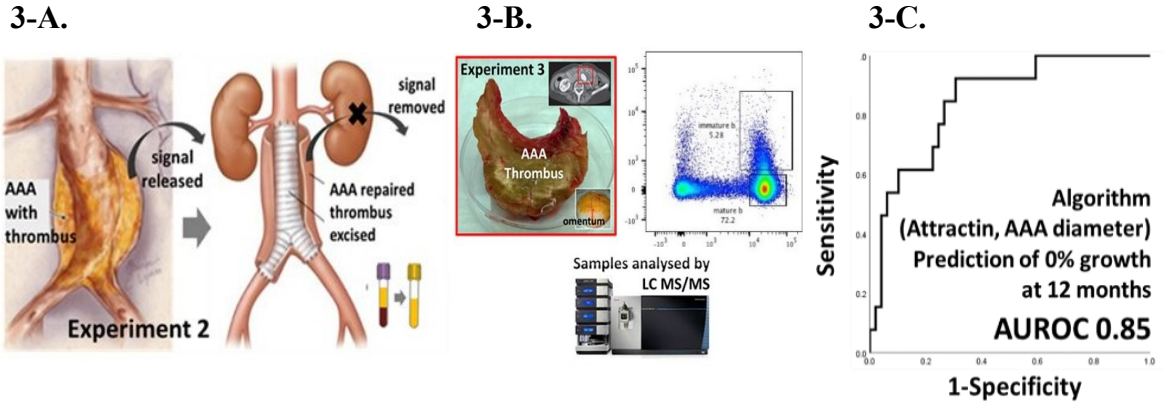

Figure 3. Validation of Attractin as a Predictive Biomarker for AAA Growth Based on ILT Proteomics. A Schematic illustrating the restoration of endothelial function following abdominal aortic aneurysm (AAA) surgical repair and removal of the intraluminal thrombus (ILT), supporting the hypothesis that ILT contributes to vascular dysfunction via immune signalling pathways. B: Fluorescence-activated cell sorting (FACS) flow cytometry of excised ILT demonstrates a dense lymphocytic infiltrate, implicating active immune processes in aneurysm progression. Liquid Chromatography-Tandem Mass Spectrometry (LC–MS/MS) analysis of ILT and matched plasma samples from the OxAAA cohort identified ~100 proteins associated with either fast or slow AAA growth phenotypes. Among these, Attractin emerged as a promising candidate biomarker. Orthogonal validation of Attractin was performed using enzyme-linked immunosorbent assay (ELISA) in plasma samples. C: In combination with AAA diameter, Attractin levels were integrated into a two-input prediction algorithm. Receiver operating characteristic (ROC) curve analysis shows that this algorithm predicts 0% AAA growth at 12 months with an AUROC of 0.85, demonstrating high diagnostic accuracy (sensitivity: 54%, specificity: 94%, accuracy: 85%) when applying a cut-off value of 0.39 to the Aneurysm Growth Index (AGI) (adapted from Lee et al., Ann Surg, 2020 with permission).

Quantification Methods in Proteomics

Proteomic quantification strategies span qualitative, semi-quantitative, and fully quantitative approaches, differing in precision and clinical relevance. Qualitative methods provide presence/absence data, useful for rapid screening but lacking abundance information. Semi-quantitative approaches, such as label-free MS and antibody arrays, estimate relative abundance across samples, balancing throughput and accuracy. Fully quantitative methods yield absolute concentrations, enabling clinical translation but requiring rigorous standardisation and specialised instrumentation. Selecting the right strategy is particularly critical in plasma proteomics, where the wide dynamic range demands both sensitivity and reproducibility (Figure 4).[28, 29]

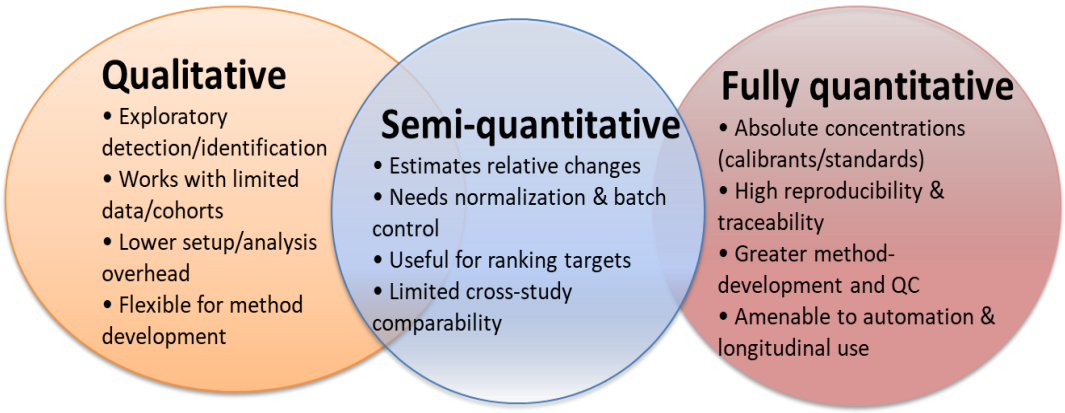

Figure 4. Comparison of qualitative, semi-quantitative, and fully quantitative proteomic readouts. Categories overlap; examples are illustrative rather than exhaustive. Qualitative methods detect presence/absence, quantitative approaches provide precise concentrations, and semi-quantitative methods offer relative abundance, balancing simplicity and accuracy. In practical terms, qualitative and semi-quantitative methods generally offer higher analytical throughput and are therefore well suited to discovery-driven and large-cohort studies, whereas fully quantitative approaches typically trade throughput for increased analytical robustness, reproducibility, and clinical traceability.

1.5 Qualitative and Semi-Quantitative Approaches

Qualitative proteomic analysis identifies proteins without measuring their abundance, yielding presence/absence information. A simple example is the lateral flow immunoassay (e.g., pregnancy test), which provides a binary visual output. In proteomics, untargeted LC–MS/MS ("shotgun") methods generate broad protein inventories by matching peptide fragmentation spectra to databases (e.g., Mascot, Sequest, Andromeda). These identifications are probabilistic, depending on peptide-spectrum matches, sequence coverage, and false discovery rate (FDR). While qualitative methods maximise coverage, they provide limited biological insight without follow-up quantification. Semi-quantitative approaches estimate relative abundance using MS signal intensity, fluorescence, or chemiluminescence, enabling group comparisons (e.g., disease vs. control) and offering a practical balance between throughput and depth.[30]

1.6 Analytical Platforms and Technologies

Proteomic measurements are commonly obtained using two broad classes of platforms: direct protein measurement by mass spectrometry (e.g., label-free bottom-up/shotgun and DIA approaches; targeted SRM/MRM (triple quadrupole) and PRM (high-resolution); and, for intact proteoforms, top-down MS) and affinity-based assays (e.g., antibody-based multiplexed platforms such as Olink™ proximity extension assays, protein/antibody microarrays, and aptamer-based assays such as SOMAscan™. [31] In label-free bottom-up MS, protein abundance is inferred from peptide ion intensities with appropriate normalisation across runs to enable comparisons between conditions; this approach is sensitive to ion suppression, sample complexity, chromatographic variability, and missing values. Affinity-based platforms typically provide relative (semi-quantitative) readouts proportional to binding signal, with absolute quantification achievable only with suitable

calibrators; they offer high multiplexing but can be affected by cross-reactivity, epitope availability, and matrix effects.

In antibody- or aptamer-based technologies, protein-specific binding reagents generate a signal proportional to target abundance, a proxy readout rather than direct protein measurement (in contrast to MS). These platforms are vulnerable to cross-reactivity or non-specific binding, batch effects and plate-to-plate variability, limited internal standards and calibration, signal saturation or compression near detection limits, and matrix effects in complex samples such as plasma.[32, 33] Resulting datasets typically report relative fold-changes or normalised expression units and often require validation by orthogonal methods (e.g., ELISA or targeted MS).

1.7 Pitfalls, Limitations, and Technical Considerations

While semi-quantitative data are invaluable for exploratory biomarker discovery, they must be interpreted cautiously: a change in signal intensity does not always correspond to a biologically meaningful change in protein abundance. Signal-to-noise ratios may differ across proteins, particularly low-abundance targets such as cytokines or growth factors. The lack of dynamic range coverage can lead to under-representation of rare but clinically significant proteins. Moreover, the measured signal may reflect total protein rather than the disease-relevant proteoform; modification-specific variants (e.g., phosphorylated Tau) can change independently of the total pool. Thus, these approaches are best viewed as hypothesis-generating tools that require downstream quantitative validation. [34, 35] These challenges have driven the evolution of targeted mass-spectrometry techniques capable of precise absolute quantification.

Targeted Mass Spectrometry

1.8 Absolute Quantification Using QconCAT

Quantitative proteomics aims to determine the absolute amount of a protein or peptide in a biological sample, typically reported in molar or mass concentration units (e.g., ng/mL, fmol/µL). These methods involve rigorous calibration using stable isotope-labelled standards (e.g., QconCATs, AQUA peptides), as well as calibration curves generated from serial dilutions of known standards and internal controls to account for variability in sample preparation and instrument performance. Quantitative Concatemer (QconCAT) technology provides a synthetic protein composed of concatenated isotope-labelled peptides, which serve as internal standards for multiple target proteins. During digestion, all labelled peptides are released with the same number of copies, allowing for direct comparison with the endogenous version of each peptide.[36] The concentration of the target analyte in label-free quantification (LFQ) is determined using equations such as:

$$LFQ\ intensity\ ratio = \frac{(Intensity\ of peptide\ A)}{(Intensity\ of\ standard\ A)} \times \frac{(Intensity\ of\ standard\ B)}{(Intensity\ of\ peptide\ B)}$$

Relative Quantification → Relative to a Reference e.g., 1 species compared to all species **Output = Ratios**

Absolute Quantification → Using a Calibration curve e.g., need a standard **Output = n of copies**

$$Absolute\ protein\ abundance = (Concentration\ of\ labeled\ peptide\ in\ sample) \times (Ratio\ of\ unlabeled\ to\ labeled\ peptide\ signal)$$

This technique allows for highly reproducible and accurate quantification, provided the following criteria are met: peptide uniqueness (sequence-specific to the target protein), complete digestion without missed cleavages, full label incorporation, and heavy/light peptide abundance measured within the linear dynamic range of the detector (mass spectrometer). Targeted proteomics methods, such as Parallel Reaction Monitoring (PRM) or Selected Reaction Monitoring (SRM), offer precise quantification with excellent sensitivity and specificity. When combined with labelled standards, PRM enables multiplexed quantification of dozens to hundreds of peptides in complex matrices such as plasma.[37] These approaches are especially valuable for validation studies, biomarker verification, and clinical translation, as they offer robustness and transferability between labs (Figure 5). [38, 39] Thus, QconCAT enables consistent absolute quantification across experiments and laboratories.

Figure 5. Applications of Absolute Protein Quantification. Absolute protein quantification by LC–MS provides precise concentration measurements that support diverse applications: biomarker development, cross-laboratory data validation, pharmaceutical and therapeutic monitoring, mathematical modelling, and analysis of protein complex stoichiometry. By offering absolute rather than relative abundance values, it underpins both rigorous research and clinical translation.

1.9 Analytical Challenges in Plasma and Quantitative Proteomics

Quantifying proteins in plasma remains technically challenging due to a dynamic range spanning over 10^9 between albumin and interleukins. This high range means high-abundance proteins masking low-abundance biomarkers, matrix effects reducing ionisation efficiency of target peptides, a vast PTM landscape, and variable digestion efficiency affecting peptide yield. [40] In data-dependent shotgun proteomics, a bottom-up mass spectrometry approach where proteins are digested into peptides and identified via database-matched spectra, ion suppression is particularly problematic. High-abundance peptides are preferentially selected for fragmentation, resulting in under-sampling of low-abundance features.[41] As a result, rare proteins may go undetected, or their measurements may exhibit high variance. Moreover, in the absence of internal standards, batch-to-batch variability in sample preparation, chromatography, and MS acquisition can distort inter-sample comparisons.[42] For this reason, rigorous experimental design, inclusion of controls, and downstream statistical normalisation are essential.[43] Protein quantification in complex samples poses challenges due to isoforms sharing similar sequences and carrying modifications, making discrimination difficult. Mass spectrometry lacks inherent quantitative ability without standards. Quantification typically involves using peptides, such as tryptic surrogates, recombinant, or synthetic peptides, as standards. However, stable-isotope-labelled synthetic peptides are costly, and recombinant protein expression may be unfeasible, especially for large or membrane proteins. Synthetic peptides encounter issues such as solubility, degradation, modification, and incomplete digestion, which can impact performance.

Incomplete or inconsistent proteolysis can bias abundance estimates. Measurement in current proteomic methods encounters numerous obstacles: affinity-based proteomics by proxy, such as the Olink™ and SOMAscan™ platforms, may experience issues with

specific proteins due to the lack of antibody or aptamer specificity, as well as the inability to differentiate proteoforms, leading to inconsistent results even between these modalities.[32, 44] Although real-time PCR pertains to nucleic-acid quantification, and the analogy here is conceptual, not mechanistic, its noise characteristics illustrate similar validation challenges: it exhibits different noise levels compared to other methods, requiring additional validation with targeted platforms such as mass spectrometry or ELISAs. Relative quantification on platforms such as SOMAscan™ and Olink™ introduces uncertainty for proteins below detection limits, as these platforms do not provide exact quantification and have unknown false-positive/negative identification rates and signal-to-noise ratios. Aptamer-based platforms like SOMAscan™ (SomaLogic, Inc.) may face challenges with target specificity in complex matrices, such as plasma, where a single aptamer may bind multiple targets. Inconsistencies in calibrator batches across large cohorts may cause intra-plate effects, and the absence of internal controls and standard curves makes it challenging to determine measurements within the linear dynamic range. [33] Additionally, amino acid substitutions can alter the binding properties of negatively charged aptamers, affecting quantification accuracy.

Untargeted proteomics, known as the shotgun approach, compares samples without prior assumptions.[45] However, protein identification relies on probability scores from fragment ions, leading to potentially erroneous but target/decoy-controlled identifications. Internal standards are not used, making absolute quantification impractical and limiting the analysis to qualitative protein profiling. Despite this, semi-quantitative comparisons of protein abundance between samples can be achieved through post-processing and normalisation procedures.[46]

The dynamic range of the plasma proteome and the prevalence of tryptic peptides pose unique challenges for shotgun proteomic analysis. Ion suppression, which occurs when

low-level peptides are less likely to become ionised during electrospray ionisation due to the proportional attraction of charges by the most abundant peptides, exacerbates these challenges, as low-level peptides may be under sampled.[47] To ensure precise protein quantification, it is imperative to appropriately handle discovery platforms, validate key findings with additional techniques, and compare results against reference standards (Table 1).

Table 1. Summary and Implications of Quantitative Methods.

Method	Description	Output	Strengths	Limitations
Qualitative	Protein identification only	Present/absent	Broad discovery	No concentration data
Semi-quantitative	Relative abundance	Fold-change	High throughput, broad coverage	Susceptible to noise, requires validation
Quantitative	Absolute protein levels	ng/μL, fmol/μL	High precision and reproducibility	Time- and resource-intensive

Protein quantification in complex biological matrices, such as plasma, remains constrained by both physicochemical and methodological limitations. While numerous analytical platforms have been developed to address these challenges, each carries inherent trade-offs that affect quantification accuracy and reproducibility. Aptamer-based methods may suffer from non-specific binding, charge-based interference, and batch-dependent variability. In contrast, antibody-based platforms can be affected by cross-reactivity, signal saturation, and calibration inconsistencies.

Similarly, real-time PCR assays, although highly sensitive, require orthogonal validation due to amplification variability and background noise.[48, 49] Shotgun proteomics, in contrast, provides broad discovery power but lacks inherent quantitative capacity in the absence of internal standards. It relies on probabilistic peptide-spectrum matching and

spectral counting, which can compromise confidence in estimates of low-abundance proteins and complicate isoform discrimination. As a result, absolute quantification remains challenging, and results must be interpreted within the limitations of each platform (Table 2).[50]

Table 2. Comparison of Protein Quantification Strategies in Complex Samples.

Method	Limitations	Notes
Synthetic Peptides	Expensive, prone to degradation, poor solubility, and incomplete digestion.	Used as standards but affected by proteolysis conditions.
Recombinant Proteins	Unfeasible for large/membrane proteins; expression difficulty.	May serve as standards for quantification.
Antibody-based (e.g., Olink™)	Antibody/aptamer specificity issues; signal-to-noise variability.	Lacks internal controls, sensitive to batch inconsistencies.
Aptamer-based (e.g., SOMAscan™)	Cross-reactivity, calibration inconsistencies, and amino acid substitutions affect binding.	Target specificity problems in plasma.
Shotgun Proteomics	Qualitative; lacks internal standards; ion suppression affects low-abundance peptides.	Identification via probability scores; semi-quantitative comparisons possible.
OxConCAT (QconCAT)	Requires initial construct design and expression optimisation.	Customisable, cost-effective, enables multiplexing and standardisation.

The OxConCAT (Oxford quantification Concatamer) strategy addresses key limitations in absolute quantification by enabling multiplexed, cost-effective, and standardised proteomic workflows. It offers significant benefits in large-cohort studies such as AAA, where accurate measurement of multiple low-abundance biomarkers is essential.[38, 51] Because each platform has inherent limitations, orthogonal validation using mass spectrometry, ELISA, or Western blot is necessary for confirming findings. Particularly in biomarker discovery, verification across multiple platforms increases confidence in clinical applicability.[52] Furthermore, a proper understanding of analytical range, linearity, and matrix effects is required to interpret results meaningfully and

reproducibly.[53] Robust quantification in plasma proteomics demands a balance between analytical depth, throughput, and cost. Qualitative and semi-quantitative methods enable discovery, while quantitative approaches are necessary for validation. Understanding the trade-offs and limitations of each technique is critical for designing reproducible and clinically translatable workflows in proteomics-based biomarker research. These constraints motivate the use of multiplexed, stable-isotope-labelled internal standards such as QconCAT/OxConCAT for absolute protein quantification in plasma. In the context of this thesis, a combination of semi-quantitative discovery platforms and targeted, absolute quantification workflows has been employed. This dual approach facilitates both the broad exploration of potential biomarkers and the rigorous validation of clinically actionable candidates, ultimately contributing to more precise and reproducible plasma biomarker profiling in AAA research.

Research Hypotheses

This thesis is founded on the central hypothesis that the development and implementation of novel MS-based quantitative workflows will enable high-throughput, scalable, and reproducible measurement of circulating biomarkers, ultimately improving the prediction of Abdominal Aortic Aneurysm (AAA) growth. The specific hypotheses are:

1. **OxConCAT as a methodological innovation**

   It is hypothesised that the OxConCAT recombinant protein standard, composed of concatenated isotopically labelled tryptic peptides, will provide a superior and more practical approach to protein quantification in plasma compared to semi-quantitative methods, as assessed by quantitative performance metrics including linearity, reproducibility, coefficients of variation, and robustness across batches and analytical

runs. By mimicking endogenous peptides, OxConCAT will enable precise, linear, absolute quantification of proteins and post-translational modifications, reduce variability introduced during sample preparation and MS acquisition, and improve reproducibility across sample batches and laboratories.

2. **AAA biomarker quantification and prediction**

   It is hypothesised that accurate, absolute quantification of a selected panel of AAA-related proteins, including Attractin, will enhance biomarker verification and support future development of AAA growth-prediction algorithms. This approach will allow detection of subtle but clinically meaningful changes in protein abundance and modifications, thereby improving patient stratification by aneurysm growth rate and risk category.

3. **Integrative omics approach**

   It is hypothesised that combining absolute proteomic data with metabolomic profiling (GC×GC–MS) will demonstrate improved analytical coverage and biological interpretability compared with single-omics approaches in capturing the complexity of AAA biology and enhance predictive modelling.

4. **Broader clinical application**

   It is hypothesised that incorporating OxConCAT-based absolute quantification into MS workflows can be applied in a generalisable manner beyond AAA to other vascular, metabolic, and inflammatory diseases at a methodological level. This approach has the potential to strengthen biomarker validation pipelines, improve inter-laboratory reproducibility, and support the development of standardised diagnostic assays. Ultimately, refining MS-based workflows through OxConCAT and integrative omics will advance precision medicine by enabling more accurate risk stratification, mechanistic understanding, and potentially therapeutic guidance.

Research Objectives

The overarching objective of this thesis is to develop and validate mass spectrometry-based workflows for the absolute quantification of circulating biomarkers, in order to improve the prediction of Abdominal Aortic Aneurysm (AAA) growth. The specific objectives are:

1. **Expand and characterise the OxAAA clinical cohort;**

   Collect longitudinal clinical and plasma data from AAA patients to provide a framework for biomarker validation and predictive modelling in a clinically relevant population.

2. **Design, synthesise, and validate the Oxford Concatemer (OxConCAT) standard;**

   Develop a stable-isotope-labelled artificial protein standard for absolute quantification of multiple target peptides, and evaluate its performance in terms of linearity, precision, reproducibility, and comparability with orthogonal methods.

3. **Implement and internally validate OxConCAT-based quantification in the OxAAA cohort;**

   Apply the OxConCAT standard to patient plasma samples, integrate the resulting proteomic data with clinical parameters, and assess its utility for biomarker verification.

4. **Externally validate AAA growth prediction models in an international cohort;**

   Test the refined prediction algorithm on ~400 plasma samples from AAA patients in the UK, Sweden, the Netherlands, and Japan, and evaluate performance using AUROC, sensitivity, specificity, and calibration metrics.

5. **Establish and optimise a GC×GC–MS metabolomics workflow;**

Develop a two-dimensional gas chromatography–mass spectrometry pipeline for the detection and quantification of plasma metabolites, including optimising derivatisation protocols to improve sensitivity and coverage.

6. **Combine absolute protein quantification with metabolomic signatures;** generate an integrated model of AAA progression and recovery, enabling more precise risk stratification and mechanistic insight.

Chapter 2 – Methodological Framework: Clinical Study Design and OxConCAT Development, Expression, and Protein Characterisation

Introduction

The methodological approach presented in this chapter builds directly on the rationale established in Chapter 1, in which the clinical and analytical challenges of circulating biomarker quantification in abdominal aortic aneurysm (AAA) were outlined. Despite advances in discovery proteomics, the clinical translation of candidate biomarkers remains constrained by the lack of reproducible methods for the absolute quantification of low-abundance plasma proteins across heterogeneous patient populations. This limitation necessitated the development of a rigorous, standardised platform that integrates clinical phenotyping with precise molecular quantification to enable evaluation of biomarker performance across disease stages and post-surgical outcomes.

This chapter establishes the dual methodological foundation of the thesis. The first component introduces the OxAAA clinical study framework, a prospective cohort designed to collect high-quality plasma samples under tightly controlled pre-analytical conditions and to provide comprehensive clinical metadata. This study structure ensures sample integrity suitable for both proteomic and metabolomic analyses, allowing biomarker dynamics to be interpreted within a well-defined clinical context. By linking molecular measurements with patient-level data, the OxAAA study provides a translational bridge between laboratory findings and clinical endpoints. The second component focuses on the development of the OxConCAT internal standard, a custom-engineered, isotopically labelled protein construct designed for absolute quantification of plasma biomarkers. Based on the Quantification Concatemer (QconCAT) principle, the

OxConCAT design integrates several refinements to improve analytical performance in complex biological matrices. These include rational peptide selection guided by proteotypic and physicochemical criteria, sequence optimisation to ensure efficient and reproducible proteolysis, and complete ^15N isotopic labelling to achieve uniform heavy-isotope incorporation. Collectively, these design features enable the OxConCAT construct to correct for digestion efficiency, ionisation variability, and matrix interference, ensuring precise and standardised quantification across analytical runs.

The following sections detail this comprehensive methodology. Sections 2.1–2.4 describe the OxAAA cohort design, patient recruitment, ethical approval, and sample collection procedures. Sections 2.5–2.11 outline the design, synthesis, and purification of the OxConCAT construct, including stable isotope labelling and protein expression strategies. Sections 2.12–2.14 address the integration of OxConCAT into LC–PRM/MS-based quantification pipelines and subsequent analytical optimisation, while Sections 2.15–2.17 discuss protein characterisation, behaviour, and stability, summarising the iterative troubleshooting and refinement steps undertaken to improve yield and reproducibility. Together, these elements define a unified methodological platform that connects clinical study design with quantitative proteomic precision and underpins all subsequent analyses in this thesis. It enables reliable, reproducible measurement of plasma biomarkers, providing the experimental foundation for the peptide-level quantification and optimisation strategies discussed in Chapter 3 (Peptide Quantification and Selection Strategies).

Methods

Methodological Framework of the OxAAA Study

This DPhil research was conducted within the Oxford Abdominal Aortic Aneurysm (OxAAA) Study, a prospective, longitudinal observational cohort approved by the Oxfordshire Research Ethics Committee (Ethics Reference No: 13/SC/0250). The study has been established to systematically investigate the molecular, structural, and functional characteristics of AAA, to improve risk prediction and guide personalised surveillance strategies. The OxAAA study is a comprehensive initiative to correlate biological markers with clinical trajectories in patients with AAA. It uniquely integrates serial measurements of circulating biomarkers (proteins, metabolites), radiological imaging, vascular function testing, and clinical follow-up data.[54] The study design permits a multi-dimensional analysis of AAA progression, with biomarker changes tracked over time and linked to clinical endpoints such as aneurysm expansion rate, surgical intervention, or rupture. A key strength of the study is access to well-characterised plasma and tissue samples collected from AAA patients at multiple clinically relevant time points, including pre-, peri-, and post-operative stages. This longitudinal design enables the evaluation of both biomarker dynamics and the biological effects of surgical repair on the vascular system. Notably, the study also includes healthy individuals without AAA, "Healthy Volunteers" (HV), serving as age-matched controls for biomarker comparisons and baseline reference values. This well-structured cohort thus provides an ideal platform for validating novel biomarker candidates, optimising quantification workflows, and evaluating predictive models in a clinically relevant setting. The work presented in this thesis is tightly integrated into this framework. It focuses on refining mass spectrometry-based workflows (proteomics and metabolomics) to support high-quality biomarker discovery and quantification in stored OxAAA samples.

2.1 Study Design and Patient Recruitment

Participants were recruited into three OxAAA study streams: S1 – Surveillance, comprising patients under imaging follow-up with AAA <5.5 cm; S2 – Surgical Referral, including new referrals with large AAAs (>5.5 cm) scheduled for elective repair; and S3 – Healthy Volunteers, age-matched controls without AAA (Table 3).

Table 3. Overview of the OxAAA Study Streams, Participant Groups, and Sampling Timepoints.

Stream	Description	Participants	Study Timepoints
S1: Surveillance	Existing AAA patients under surveillance at OUH and TVVN	Patients with AAA <5.5 cm	TP-1, TP-S, TP-F
S2: New Referrals	New patients referred for surgery with a large AAA (>5.5 cm)	Elective surgical candidates	TP-1, TP-2, TP-3, TP-4, TP-5, TP-F
S3: Healthy Volunteers	Control group with no AAA	Age-matched healthy individuals	TP-1, TP-F (optional repeat)

Timepoint definitions: TP-1: Baseline sampling at enrolment, TP-F: Follow-up sampling

Patient recruitment and sample collection were conducted over a multi-year period between 2021 and 2024 and were embedded within routine clinical care pathways at Oxford University Hospitals and affiliated vascular networks. The candidate independently coordinated and carried out all stages of participant recruitment and longitudinal sample collection for the OxAAA study. This included screening clinic lists and referral pathways for eligibility, liaising directly with vascular surgeons, specialist nurses, and imaging services, approaching potential participants during outpatient clinics or via postal invitation, and providing detailed verbal and written study information.

The candidate was responsible for obtaining written informed consent from all participants, ensuring confidentiality and compliance with ethical and governance requirements, and maintaining accurate recruitment and follow-up records. Research blood sampling was coordinated and performed in alignment with routine clinical visits, including surveillance imaging appointments and peri-operative timepoints, with the candidate organising sample collection schedules, tracking longitudinal timepoints, and ensuring protocol adherence across all study streams. Post-operative and follow-up sampling was actively coordinated by the candidate to maximise retention and completeness of paired samples.

Of 408 individuals invited to participate, 176 expressed interest and 127 were successfully enrolled, corresponding to an overall response rate of approximately 30%. Recruitment was staggered and cohort-specific, reflecting differences in surveillance frequency, surgical referral timing, and post-operative follow-up intensity across the three study streams. Throughout the study, research activities were integrated with standard clinical care to minimise participant burden while enabling high-quality longitudinal data and biospecimen collection.

This structured and candidate-led recruitment framework underpinned the generation of a well-characterised longitudinal plasma cohort, forming the foundation for the downstream proteomic and metabolomic analyses presented in this thesis. Table 3 summarises the resulting study streams, participant groups, and sampling timepoints derived from this integrated clinical–research approach.

2.2 Clinical and Biological Data Collection

At the time of recruitment and during follow-up visits, a comprehensive dataset was collected for each participant, including demographics (age, sex, ethnicity), lifestyle

factors (smoking status, BMI), medical and surgical history (comorbidities, medications), imaging data (AAA diameter via ultrasound and CT, aneurysm morphology), functional measurements, surgical intervention details (type of procedure, complications, outcomes), and longitudinal follow-up data (post-operative status, re-intervention, growth rate). In parallel, plasma samples were obtained using standardised venepuncture protocols and processed under stringent conditions to minimise pre-analytical variability.

2.3 Integration of Research and Clinical Timepoints

Research timepoints were aligned with routine clinical visits to maximise efficiency and patient convenience. In the surveillance group (S1), samples were collected during scheduled ultrasound assessments, while surgical patients (S2) provided pre- and post-operative samples to assess surgery-related biomarker changes. Healthy volunteers were sampled during dedicated appointments. This integration of clinical and research activities ensured efficient data capture, high compliance, and robust longitudinal datasets suitable for omics-based biomarker discovery (Figure 6).

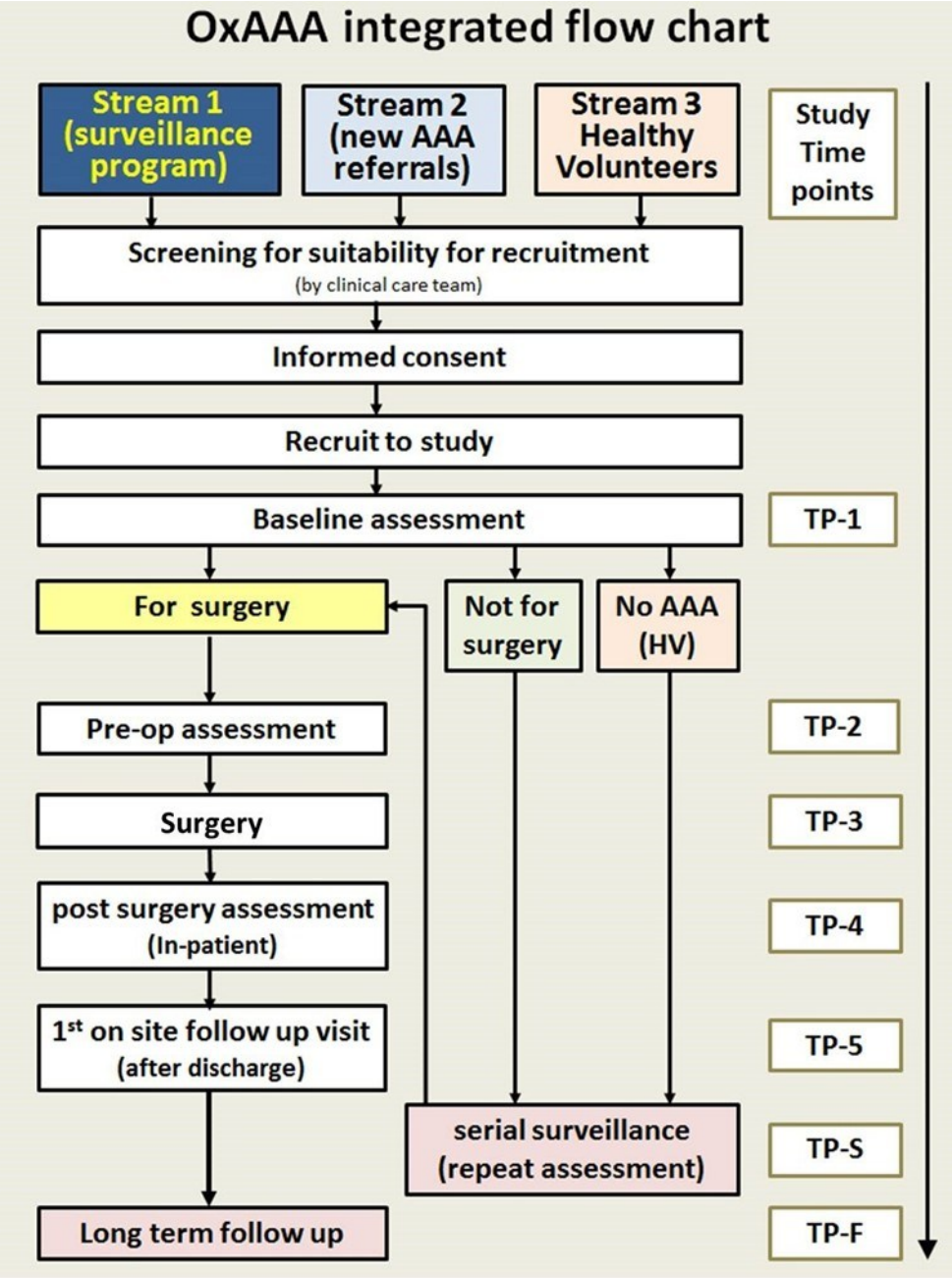

Figure 6. OxAAA Integrated Study Flowchart. Schematic of the OxAAA recruitment and workflow. Participants were enrolled into three streams: surveillance patients (S1), surgical referrals (S2), and Healthy Volunteers (HV). Following consent, baseline sampling (TP-1) was performed. Surgical patients contributed additional samples at the preoperative (TP-2), intraoperative (TP-3), inpatient (TP-4), and early follow-up (TP-5) stages. Non-surgical patients underwent serial surveillance (TP-S), and all participants were followed long term (TP-F). Study timepoints were aligned with clinical care to maximise sample quality and reduce participant burden. Although the study workflow comprises multiple clinical pathways and sampling timepoints, these were not treated as independent subgroups for analysis. Instead, the design enables longitudinal and paired comparisons within individuals, as well as aggregation of samples across clinically relevant categories where appropriate. This approach mitigates cohort fragmentation while preserving the ability to interrogate disease progression and surgery-related changes within a real-world clinical framework.

2.4 Sample Handling and Processing Strategies: Double-Step Centrifugation for Platelet-Free Plasma

At each time point, approximately 30 mL of venous blood was collected into EDTA tubes and processed within one hour at room temperature. Samples were fractionated into plasma, serum, red cells, and buffy coat, then stored at –80 °C. To ensure plasma integrity for proteomic and metabolomic analyses, a two-step centrifugation protocol was used to obtain platelet-free plasma: first spin, 12 min at 1300 × g; transfer of plasma to clean tubes; second spin, 15 min at 2500 × g; followed by aliquoting into pre-labelled cryovials and immediate freezing. This approach, standardised in 2010 and applied consistently thereafter, minimises pre-analytical variability and reduces artefactual release of proteins or metabolites.[55] All handling followed SOPs aligned with biobanking standards. Linked clinical and imaging data (CT, ultrasound, demographics, comorbidities, and surgical records) were extracted with consent to support longitudinal biomarker modelling and validation.

The OxConCAT Strategy

2.5 Conceptual Basis and Rationale

Accurate measurement of circulating proteins is a key challenge in clinical proteomics, especially for conditions like abdominal aortic aneurysm (AAA), where early detection and monitoring depend on subtle changes in protein levels. Traditional semi-quantitative proteomic methods, such as label-free quantification and antibody-based assays, are limited by their reliance on signal intensity, inter-assay variability, and issues such as cross-reactivity and limited dynamic range. To address these issues, the Oxford Concatemer (OxConCAT) strategy was developed to provide a precise, scalable approach

for absolute quantification using stable-isotope-labelled internal standards. OxConCAT builds on the QconCAT method, which involves creating synthetic proteins by concatenating peptide sequences from target proteins.[38] These constructs are produced in bacterial expression systems using isotope-labelled growth conditions, then enzymatically digested and used as internal standards in targeted mass spectrometry (MS) workflows. The OxConCAT approach aims to facilitate absolute protein quantification in plasma, supporting reliable biomarker validation, algorithm development, and clinical application in AAA prediction (Figure 7).

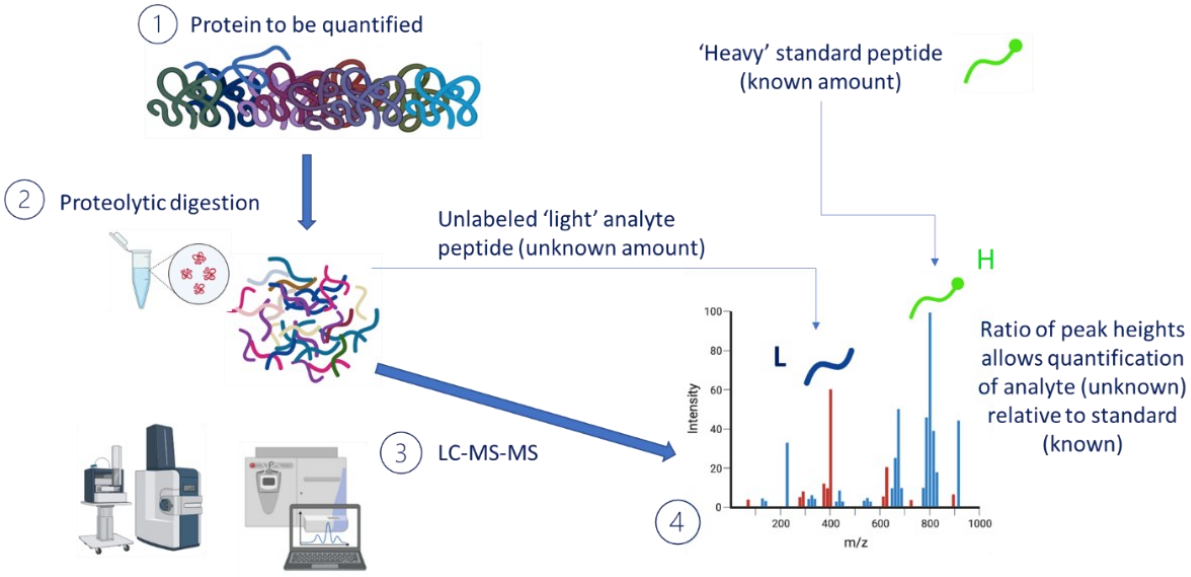

Figure 7. Overview of the OxConCAT protein quantification strategy. The construct comprises concatenated, ^15N-labelled peptides used as internal standards in LC–PRM/MS workflows.

The OxConCAT strategy aims to construct a single artificial protein comprising multiple proteotypic peptides from a selected panel of biomarker proteins. Each peptide in the OxConCAT construct is carefully selected based on previous empirical data and evaluated *in-silico* for optimal mass spectrometry (MS) performance, including high ionisation efficiency, reliable detectability, and minimal vulnerability to post-translational

modifications or enzymatic mis-cleavages. When expressed in a bacterial system supplemented with ^15N-labelled ammonium sulphate as the sole nitrogen source, all amino acids incorporated into the recombinant protein are stably isotope-labelled. After expression and purification, the OxConCAT protein undergoes tryptic digestion, producing a stoichiometrically defined isotope-labelled peptide pool. These heavy peptides are then spiked into digested plasma samples at known concentrations and analysed via liquid chromatography-parallel reaction monitoring-mass spectrometry (LC-PRM-MS). The absolute abundance of endogenous peptides is calculated from light/heavy peptide ratios and a known amount of spiked-in heavy peptide, enabling accurate quantification of the corresponding plasma proteins. This approach addresses key limitations of traditional peptide-based quantification methods. It removes the need to synthesise and handle multiple individual heavy-labelled peptides, instead enabling multiplexed quantification of numerous peptides from different proteins within a single assay. Each peptide within the recombinant standard acts as an internal reference for its corresponding endogenous analyte, thereby correcting for technical variability, digestion efficiency, and ion suppression. To ensure accurate quantification, the spiked-in protein must itself be precisely measured to determine the stoichiometric abundance of each constituent peptide. This represents an improvement over conventional heavy peptide standards, which are often prone to instability, adsorption losses, and concentration uncertainty during storage and sample preparation. [56]

2.6 Design Principles and Technical Advantages

The OxConCAT construct for this study was designed to target a panel of approximately 100 proteins previously identified through LC–MS/MS discovery work as being associated with AAA growth. For each target protein, two to three tryptic peptides were

selected based on the following criteria: length of 8–20 amino acids, uniqueness in mapping to the target protein, chemical stability, avoiding cysteine and methionine residues where possible, evidence of prior confident MS signal, and absence of known PTMs to ensure consistent fragmentation profiles.

Peptides were concatenated into a single synthetic open reading frame, encoded within the QCONCAT-c002 gene, and inserted into a pET28b vector; the final construct encoded 667 amino acids, including a His6 tag for affinity purification. The entire construct was synthesised and cloned by GenScript Biotech (UK) Limited and confirmed by Sanger sequencing. Complete construct protein sequence with His6-tag:

MAGKVIRGAGPESEPYIFQTPEGVPEQPTFLKLTWEAGADHNSNISEYIVEFEGN
KVTWKPQGAPVEWEEETVTNHTLRNHPNITFFVYVSNFTWPIKYYTAINFVATP
DEQNRVFHIHNESWVLLTPKGVVNVLPGSGSLVGQRINWDQPAEAIHNWIRIQG
STIPINQARPNRDNSQVNAVTVLTLLDKYQASTSNTVSKEGESHAENETKLFQFH
FHWGSTNEHGSEHTVDGVKEIINVGHSFHVNFEDNDNRYSAELHVAHWNSAK
VAEQTPLTALYVANLIKTIPIDGDFFSYTRVAFTGSTEIGRLGPHAGDVEGHLSFLE
KAVVLTLALVAVAGARLLPHANEVSQKSLADELALVDVLEDKDYSVTANSKGLT
SVINQKGAVHVVVAETDYQSFAVLYLERRPASPISTIQPKFLQEQGHREEDDVVS
EDLVQQDVQDLYEAGELKEDAQVAAEILEIADTPSGDKDLEADIIGDTSGHFQK
ESDTSYVSLKGYSIFSYATKAPLTKPLKGAGSSEPVTGLDAKLFLQFGAQGSPFL
KVEATFGVDESNAKDGLDAASYYAPVRADVTPADFSEWSKTPVISGGPYEYRTP
VITGAPYEYRGTFIIDPGGVIRGTFIIDPAAVIRYILAGVENSKLGGNEQVTRAGK
LAAALEHHHHHH

The construct included over 100 target peptides, organised in groups of three per protein for redundancy and cross-validation, with peptide order optimised to minimise unintended proteolysis or structural artefacts. To generate a fully ^15N-labelled OxConCAT protein, the QCONCAT-c002 construct was expressed in *E. coli* BL21 cells cultured in M9 minimal medium supplemented exclusively with ^15N-labelled ammonium sulphate. This ensures that all nitrogen atoms incorporated into the expressed protein are of the heavy isotope variant, enabling mass-shift discrimination from

endogenous peptides in MS analysis. The bacterial cultures were induced with IPTG and incubated under optimised conditions to maximise yield. Following cell lysis, the recombinant OxConCAT protein was purified using nickel-affinity chromatography via the His6 tag. The purified protein was validated using SDS-PAGE, UV absorbance, and preliminary MS to confirm complete isotope incorporation.

Yields typically reached 3–5 mg/L of culture, sufficient for thousands of spiking experiments given the low quantities (<100 fmol) needed for each analysis. Following purification, the OxConCAT protein was digested with trypsin under denaturing conditions to generate the heavy-labelled peptides. Enzymatic digestion was optimised to ensure complete cleavage at tryptic sites, minimising missed cleavages that could affect quantification accuracy. The resulting heavy peptide mixture was desalted and quantified using amino acid analysis or a bicinchoninic acid (BCA) assay. Known amounts of the heavy peptide mix were spiked into plasma digests from clinical samples (OxAAA cohort and international validation sets). The light-to-heavy ratios of the peptides were then quantified using PRM, with transitions selected based on prior optimisation.[19] As outlined in Section 1.9 Analytical Challenges in Plasma and Quantitative Proteomics, affinity-based assays provide proxy signals of abundance (binding readouts). In contrast, mass spectrometry provides direct detection of ions but requires appropriate standards for quantification.

Affinity- and mass spectrometry-based quantification methods each have inherent limitations. Affinity assays are prone to cross-reactivity, batch or plate effects, limited calibration, and matrix interference, with results often reported in relative rather than absolute units. Conversely, MS-based quantification relies on surrogate peptides and internal calibrants, and can be influenced by digestion efficiency, peptide solubility or stability, and proteolysis conditions. Moreover, the measured signal may correspond to

total protein rather than the biologically relevant proteoform, as post-translationally modified species (e.g., phosphorylated variants) can vary independently of total protein levels. In plasma, the extensive dynamic range and ion suppression further exacerbate missing values and hinder the detection of low-abundance peptides.

Within this context, the OxConCAT strategy offers a robust alternative for absolute quantification. Incorporating multiple labelled peptides within a single recombinant construct eliminates the need to synthesise and validate hundreds of individual standards, significantly improving cost-efficiency and scalability. Its design is fully customisable, allowing peptides to be updated or replaced in response to discovery findings or biomarker panel revisions. Multiplexing capability enables the simultaneous quantification of numerous biomarkers, a prerequisite for multivariate and algorithmic modelling. Furthermore, the use of a single, standardised construct enhances reproducibility across batches, platforms, and laboratories. In the setting of abdominal aortic aneurysm (AAA) research, where subtle proteomic shifts may correspond to critical clinical outcomes, the OxConCAT approach provides the precision, throughput, and flexibility required for reliable biomarker quantification across large patient cohorts.

Design, Synthesis, and Purification

2.7 Peptide Selection and Synthesis Criteria

When aiming to quantify a large panel of proteins, a key analytical challenge is creating a comprehensive set of peptide standards. This task becomes increasingly complex as the number of target proteins increases. To overcome this challenge, OxConCAT provides an innovative solution: the design and production of a single recombinant protein that contains concatenated, stable-isotope-labelled peptides representing the target proteins.

These synthetic constructs enable multiplexed quantification using just one standard. The OxConCAT process starts with *in silico* selection of peptides from a larger set of proteins of interest. Proteins are virtually digested into tryptic peptides, with only a few peptides, usually two or three per protein, chosen based on strict criteria. Peptides are evaluated for optimal detection by mass spectrometry, chemical stability, ionisation efficiency, and uniqueness within the proteome. Essential factors include avoiding internal cysteine residues, which can form disulfide bonds, and methionine residues, which are prone to oxidation (Table 4). Preference was given to peptides consistently identified and validated in proteomics studies, such as those listed in PeptideAtlas or previously used in PRM and MRM assays. Multiple Reaction Monitoring (MRM), also called Selected Reaction Monitoring (SRM), is a targeted LC–MS/MS mode on triple-quadrupole instruments in which a predefined precursor ion (Q1) is fragmented in Q2 and one or more predefined fragment ions are filtered in Q3.[57] Each precursor-fragment pair is a transition; quantification integrates the transition chromatograms and verifies expected ion ratios and retention time. Parallel Reaction Monitoring (PRM) is the analogous targeted mode on high-resolution, accurate-mass instruments (e.g., Orbitrap or Q-TOF): the precursor is isolated and fragmented once, and the full MS/MS spectrum is acquired at high resolution, allowing fragment-ion chromatograms to be selected post-acquisition with narrow mass tolerances. In practice, MRM often provides maximal sensitivity and high multiplexing, whereas PRM offers greater selectivity and interference checking; both typically use stable-isotope–labelled peptides for calibration and internal standardisation.[58]

The selected peptides are combined into a synthetic amino acid sequence encoded by a recombinant gene, which is ultimately expressed as a fusion protein in *E. coli*. The QconCAT gene construct used in this study, QCONCAT-c002, was synthesised and

cloned into a pET28b vector (GenScript AAAQconCAT-c002). The resulting artificial protein consists of 667 amino acids, including a His6-tag to aid purification. Each segment of the concatenated protein contains peptides from one of the ten core proteins in the discovery panel, with three peptides per protein, assembled in a specific sequence.

Table 4. Peptide Selection Criteria: summarising key considerations and rationale for choosing peptides to be included in the OxConCAT construct.

Criterion	Rationale
Absence of Cysteine	Avoid disulfide bond formation and cross-linking, which complicate analysis.
Absence of Methionine	Prevent oxidation artefacts that interfere with quantification.
Consistent Detection History	Preference was given to peptides that had been consistently identified in previous proteomics experiments.
High Ionisation Efficiency	Ensure stable and detectable signals during MS analysis.
Uniqueness	Peptides must be unique to target proteins to ensure specificity.
Avoid Post-translational Modification Sites	Prevent variability due to unpredictable modifications.
Presence in PeptideAtlas/Validated Databases	Use peptides with established use in PRM/MRM workflows.

2.8 Stable-Isotope Labelling via ^15N Incorporation

To enable absolute quantification, the OxConCAT protein was expressed in a heavy-isotope-labelled form. Specifically, ^15N incorporation was achieved by growing *E. coli* BL21 (DE3)-R3-pRARE2 in M9 minimal media containing ^15N-ammonium sulphate as the sole nitrogen source. This results in the entire expressed protein being labelled with ^15N, which can be distinguished by mass spectrometry due to the mass shift in the peptide fragments. Before synthesising with ^15N-labelled compounds, a test expression without labelling was conducted to optimise the expression and purification process. After

determining the best conditions, the expression was scaled up to 1 litre to generate sufficient material for downstream analysis.

2.9 Challenges in Protein Expression and Folding

Because OxConCAT is an artificial protein with no native structure, it is expressed in *E. coli* as inclusion bodies. The protein must be solubilised and properly refolded to allow purification. A critical thermodynamic factor in protein refolding is the Gibbs free energy of folding (ΔG_fold), defined by the equation:

$$\Delta G\_fold = \Delta H - T\Delta S$$

ΔG_fold = change in Gibbs Free Energy

ΔH = change in enthalpy

T = temperature in Kelvin

ΔS = change in entropy

Proteins fold into their native conformations, with the Gibbs free energy of folding (*ΔG_fold*) indicating thermodynamic stability. Negative *ΔG_fold* values denote a stable, energetically favourable state, while positive values suggest instability. Understanding ΔG_fold is key to protein stability, engineering, and assessing mutation or environmental effects, and is particularly relevant to misfolding disorders where altered energetics cause aggregation or loss of function. [106]

Where *ΔH* is enthalpy, *ΔS* is entropy, and *T* is the temperature in Kelvin. For successful folding, *ΔG_fold* must be negative. However, due to its synthetic nature, OxConCAT lacks well-defined folding domains and tends to aggregate. Solubilisation is therefore performed in 8 M urea, which disrupts hydrophobic interactions and stabilises the protein in an unfolded state.

2.10 Purification Using Nickel Affinity Chromatography

The His6-tagged OxConCAT protein was purified using nickel-affinity chromatography (Ni-IMAC), exploiting the strong coordination between histidine residues and nickel ions immobilised on the resin. In its denatured state (in urea), the OxConCAT binds tightly to the column, while other non-His-tagged proteins are washed away. A stepwise elution using imidazole, a histidine mimic, is then used to displace the bound OxConCAT protein from the resin. To enhance specificity, low imidazole concentrations (~10 mM) are used in the wash buffer to remove weakly bound contaminants, followed by high imidazole concentrations (250–500 mM) to elute the target protein. The selectivity of this process is driven by the strength of histidine-nickel interactions and the ability of imidazole to outcompete histidine for binding sites at high concentrations. Purity was further improved by subjecting the protein to a second round of purification using cobalt-based Talon resin, which provides superior selectivity through tighter binding to His-tags and lower non-specific binding. Finally, size-exclusion chromatography (SEC) using an S200 column was used to separate the OxConCAT from lower-molecular-weight contaminants based on size (Table 5).

Table 5. OxConCAT Protein Purification Workflow.

Step	Description	Purpose
Expression in *E. coli*	Expression of the synthetic OxConCAT gene in BL21 (DE3) Rosetta cells using ^15N-labelled M9 media.	Generate isotope-labelled recombinant protein.
Solubilisation in Urea	Lysis and solubilisation of inclusion bodies in 8M urea.	Keep the protein unfolded for purification.
Ni-NTA Affinity Purification	Histidine-tagged OxConCAT binds the nickel resin column.	Initial capture and isolation of the target protein.
Imidazole Wash & Elution	Low imidazole removes contaminants, and high concentration elutes OxConCAT.	Separate the target protein from non-specific binders.
IMAC (Talon Resin)	Use cobalt resin for higher purity capture.	Enhance specificity and yield.
Size Exclusion Chromatography	Separate protein by size using an S200 gel filtration column.	Final cleanup and removal of smaller contaminants.
Aliquoting & Storage	Aliquot and freeze OxConCAT into single-use tubes.	Prevent freeze-thaw degradation, preserve reproducibility.

2.11 Validation via Gel Filtration and Analytical QC

After the SEC, fractions were collected and analysed via SDS-PAGE to confirm molecular weight and assess purity. The first eluting fraction typically corresponds to the full-length OxConCAT protein, while later fractions contain smaller contaminants. Representative gels from each purification stage demonstrate the enrichment of the OxConCAT and confirm the success of the multi-step purification strategy (Figure 8).

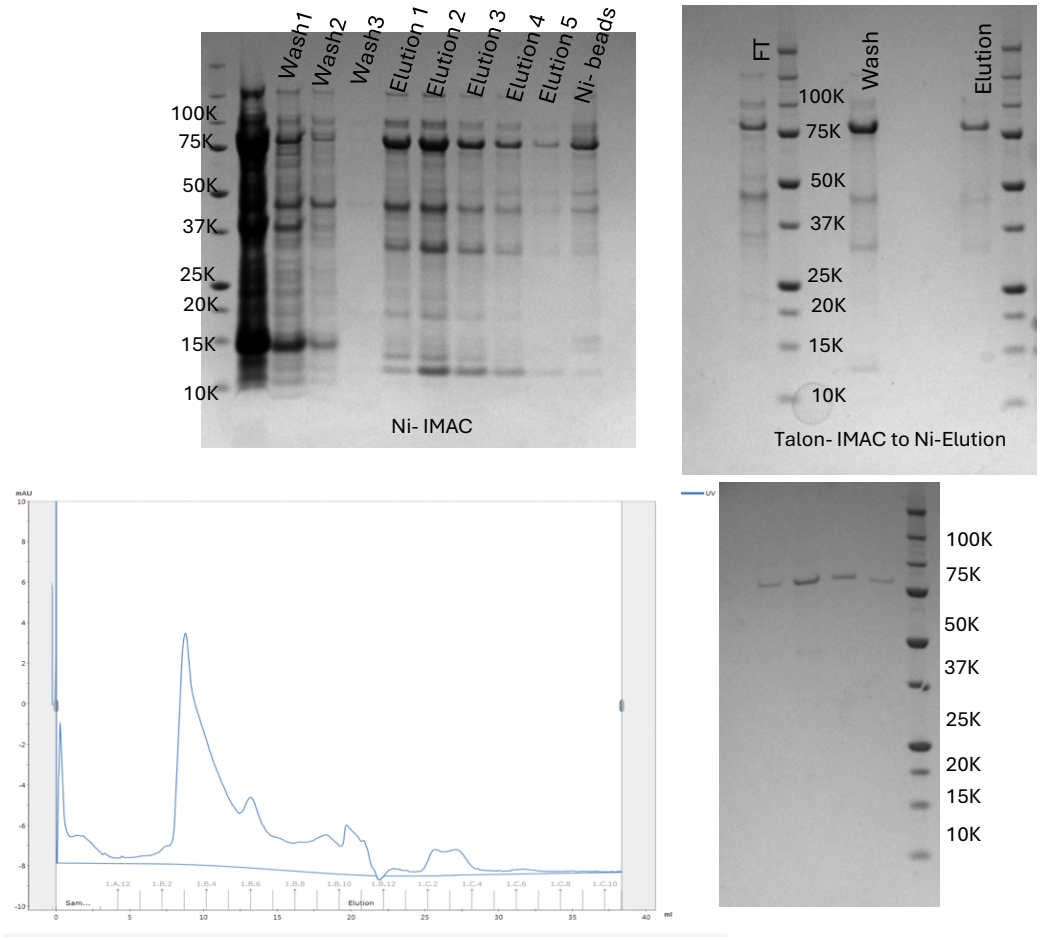

Figure 8. Validation of OxConCAT purification and Quality Control. SDS–PAGE analysis of Ni-IMAC, Talon, and SEC fractions demonstrating enrichment and purity. Top left: Ni-IMAC SDS-PAGE gel of all fractions. Top right: SDS-PAGE gel of Talon purification of pooled elution fractions. Bottom: Elution profile and SDS-PAGE from the S200 column loaded with the Talon Wash fraction showing the purified OxConCAT protein.

Analytical Workflow Optimisation

The OxConCAT strategy, as described earlier, forms the backbone of this absolute quantification pipeline. Once synthesised and purified, the OxConCAT protein, made of stable-isotope-labelled concatenated peptides, is added to plasma samples at a specific concentration. The OxConCAT construct remains consistent across all samples and serves as an internal standard, enabling absolute quantification of endogenous peptide targets

and assessing digestion efficiency and variability across sample batches. The proteomic analysis workflow begins with the enzymatic digestion of plasma samples, during which the OxConCAT construct is co-digested. The resulting peptide mixture, comprising both endogenous peptides and their labelled OxConCAT counterparts, is then subjected to LC–PRM/MS using a high-throughput system: the *Bruker TimsTOF Pro* coupled with *Evosep One LC*, which together allow rapid and highly sensitive peptide separation and quantification.[59]

2.12 Integration of OxConCAT into Plasma Proteomics

To accurately distinguish between the endogenous ("light") peptides and the synthetic ("heavy") standards derived from the OxConCAT construct, the protein was expressed in *E. coli* grown in M9 minimal media supplemented with ^15N-labelled ammonium sulphate. This labelling approach ensures that every nitrogen-containing position of the expressed OxConCAT protein is heavy-isotope labelled. Since nitrogen atoms are part of the peptide backbone and several side chains, the labelling causes a predictable mass shift, typically 20–40 Da per peptide, depending on its sequence. This mass difference is easily detected by MS, enabling precise quantification by comparing the intensities of heavy and light peptide pairs. The expression protocol required careful media preparation and optimisation of growth conditions. The minimal media contained essential vitamins and minerals, with ^15N as the sole nitrogen source. Regular optical density (OD600) monitoring was employed to ensure controlled bacterial growth and consistent expression rates.

2.13 Protease Digestion and Spike-In Strategies

Once purified, the OxConCAT protein was quantified, aliquoted, and stored under controlled conditions to prevent degradation from freeze-thaw cycles. For proteomic experiments, OxConCAT was added to plasma samples at known concentrations. Samples were then digested with trypsin, which cleaves both endogenous plasma proteins and the OxConCAT standard into peptides. Because the OxConCAT peptides are ^15N-labelled, they can be easily distinguished from the endogenous (light) peptides by their unique mass differences. The resulting peptide mixtures are analysed using LC-PRM/MS. The relative abundance of each target peptide is calculated by comparing the peak intensities of the endogenous (light) peptides to those of the labelled (heavy) standards. This allows for the absolute quantification of each protein in the panel. An additional synthetic protein not typically found in plasma is also added as an external control, with its heavy-labelled peptide standard, to ensure quantitative accuracy across all samples.

2.14 LC–PRM/MS Method Development for Absolute Quantification

Chromatographic and mass spectrometric parameters were optimised for selectivity and reproducibility. Narrow precursor ion windows improved specificity, while broad fragment-ion coverage enhanced confidence. Quantitative analysis was performed in Thermo PinPoint, extracting light/heavy ratios to derive absolute concentrations. The final workflow quantified proteins spanning four orders of magnitude, from high-abundance CRP to low-abundance Attractin, demonstrating broad dynamic range and analytical robustness (Figure 9).

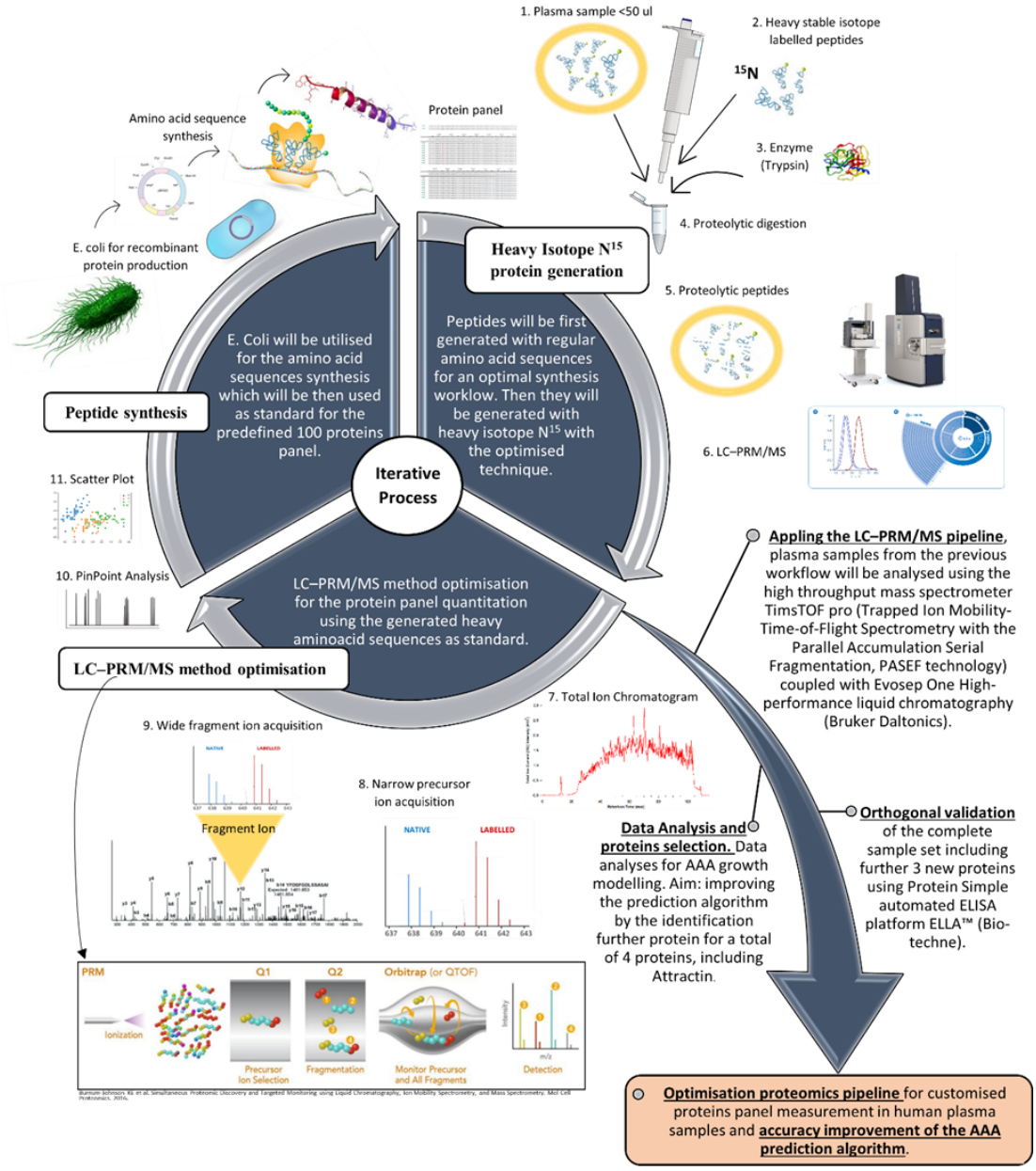

Figure 9. OxConCAT-based LC–PRM/MS pipeline. The process integrates peptide synthesis, ^15N-labelled protein expression in *E. coli*, and LC–PRM/MS optimisation for absolute quantification of predefined plasma protein panels. The iterative refinement of synthesis and analytical parameters enhances sensitivity and precision, supporting the improvement of the AAA biomarker prediction algorithm.

Results

Protein Behaviour and Stability Studies Results

The unique behaviour of the OxConCAT protein is fundamentally based on its primary amino acid sequence, which lacks the structural and physicochemical cues needed for native protein folding. In natural systems, proteins have evolved from simpler ancestral molecules, acquiring conserved domains and sequence motifs that enable them to fold efficiently and reliably into well-defined three-dimensional structures necessary for their biological roles. In contrast, the OxConCAT protein, an artificial chimaera composed of concatenated peptide sequences from unrelated proteins, lacks such evolutionarily conserved folding information. Therefore, it does not have the natural tendency to fold into a compact, stable tertiary structure.

2.15 Aggregation and Inclusion Body Formation

The OxConCAT construct exhibited atypical behaviour during recombinant expression in *E. coli*, aggregating into insoluble inclusion bodies rather than remaining in the soluble fraction. These dense deposits of misfolded protein required multiple washing steps before downstream use (Figure 10).

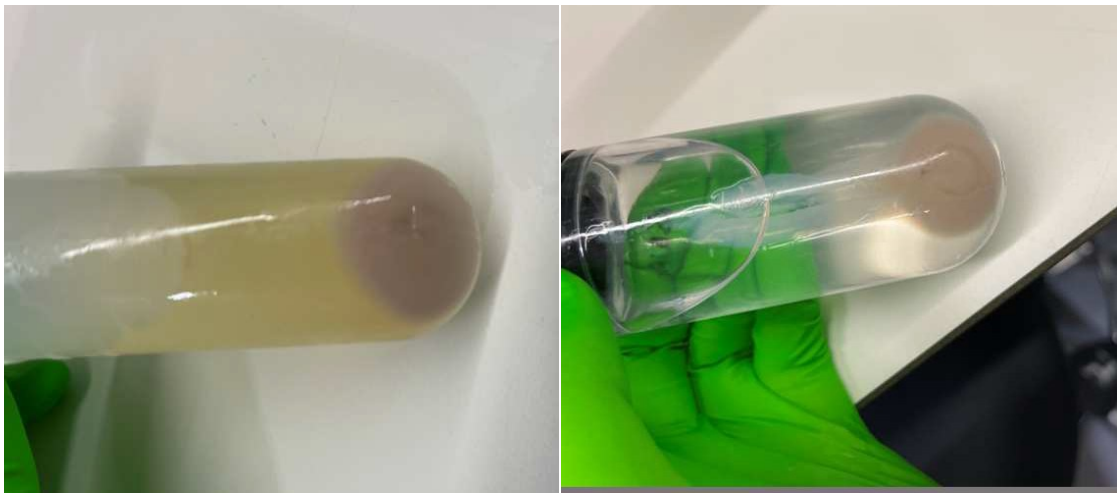

Figure 10. Inclusion Body Pellet Preparation. Photographs showing the OxConCAT protein pellet before (left) and after (right) the washing procedure. The images highlight the pronounced tendency of the recombinant OxConCAT protein to form insoluble inclusion body aggregates during expression.

In native systems, molecular chaperones guide proper protein folding, stabilise hydrophilic surfaces, and prevent aggregation. However, artificial constructs like OxConCAT, comprising concatenated peptides from unrelated proteins, lack evolutionary folding pathways and structural motifs, making them inherently prone to misfolding and precipitation. Their lack of defined domains or hydrophobic cores reduces solubility and increases the risk of aggregation. Aggregation arises when unfolded proteins expose hydrophobic residues, promoting intermolecular interactions that become thermodynamically more favourable than maintaining correctly folded conformations. This imbalance is intensified during overexpression, where translational rates exceed folding capacity, leading to inclusion body formation.[60]

OxConCAT artificial design also results in high thermolability: repeated freeze–thaw cycles or prolonged exposure at room temperature cause irreversible denaturation and fragmentation. Unlike native proteins, it lacks internal stabilising features such as disulfide bonds or compact tertiary structures, rendering it fragile during handling. To

mitigate degradation, purified OxConCAT is now aliquoted into single-use PCR-grade vials at final-use concentrations. This prevents freeze–thaw cycling and improves downstream MS consistency. Additional refinements included stringent temperature control, minimal agitation, and optimised purification buffers to preserve integrity. Despite ongoing improvements, OxConCAT purity and long-term stability remain active areas of development essential for maximising the potential of this absolute quantification platform.

2.16 Iterative Troubleshooting for High-Yield Expression

The development and implementation of the OxConCAT construct for absolute protein quantification required extensive optimisation and troubleshooting across multiple experimental iterations. Following Talon™ immobilised metal affinity chromatography, the His-tagged OxConCAT construct was recovered in a concentrated eluate with a final volume of 450 µL at a measured concentration of 0.22 mg/mL (Figure 11).

11-A

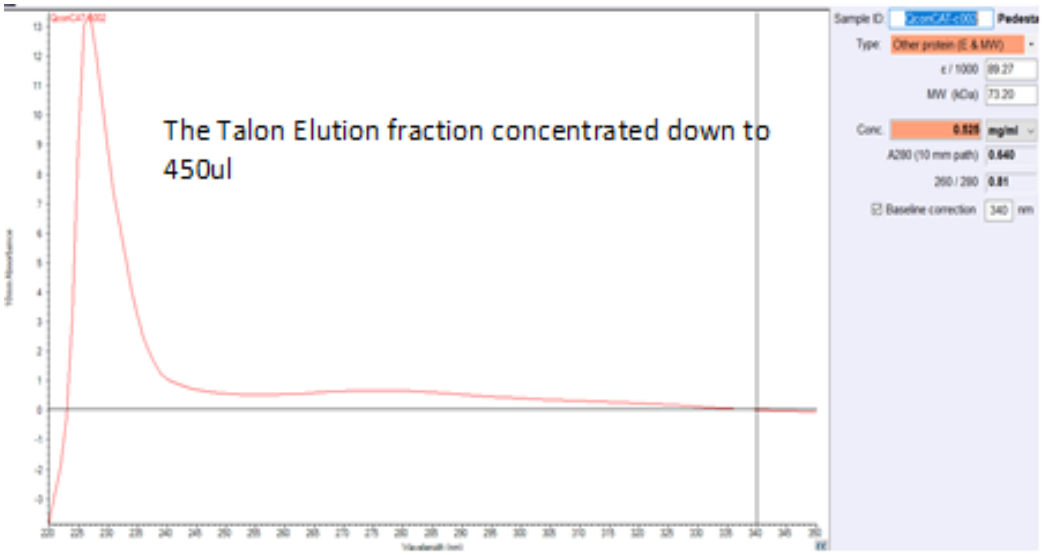

11-B

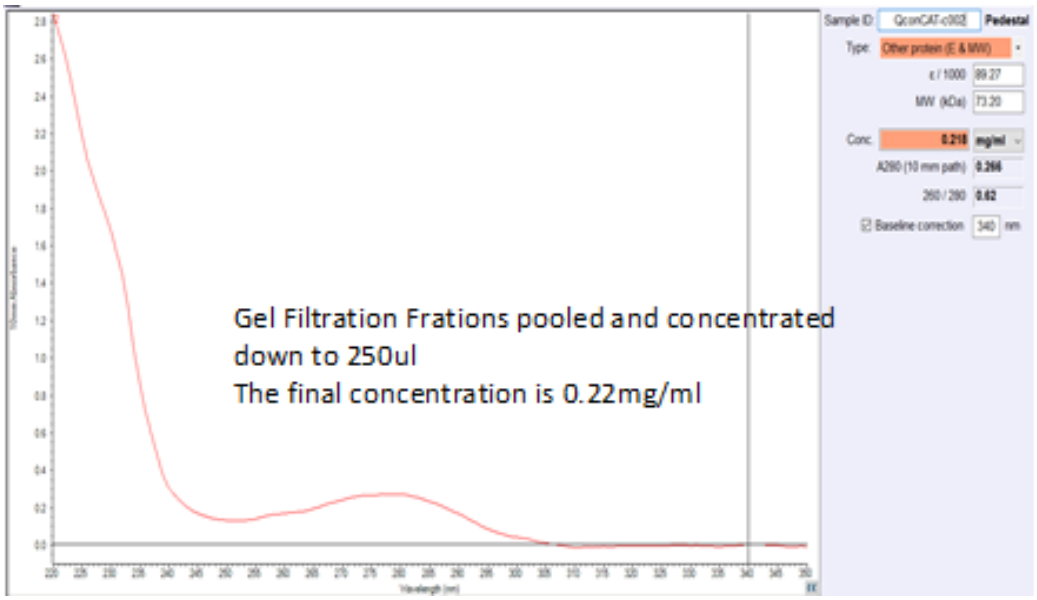

Figure 11. NanoDrop™ Spectra of Purified OxConCAT Protein. Representative Nanodrop traces showing the absorbance profiles of OxConCAT samples after the Talon™ elution (11-A) and following gel filtration (11-B). The Talon elution fraction was concentrated to 450 µL, while the pooled gel filtration fractions were concentrated to 250 µL, yielding a final protein concentration of 0.22 mg/mL. The distinct 280 nm absorbance peak confirms the high purity and recovery of the OxConCAT protein after sequential purification.

Subsequent production runs showed reduced reproducibility, with lower yield and decreased purity. The principal issues were partial degradation of the OxConCAT construct and co-purification of contaminants. A structured troubleshooting and optimisation workflow was implemented to identify process variables contributing to these outcomes and to mitigate them (Figures 12-14). Collectively, these observations indicate that the construct is susceptible to degradation and purity loss under certain processing conditions.

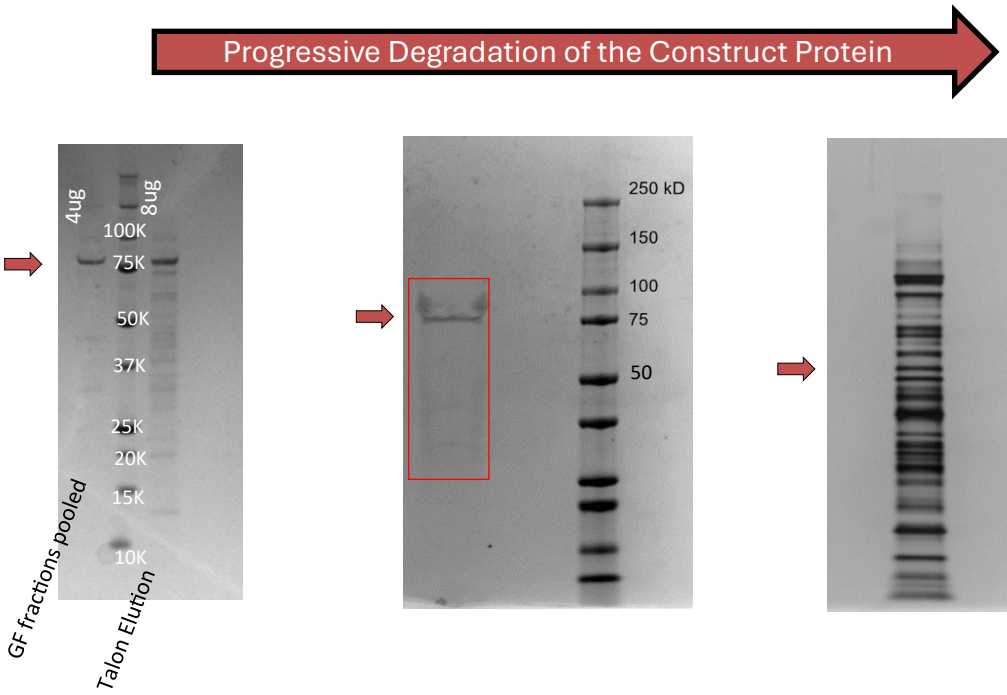

Figure 12. SDS–PAGE Analysis of Purified OxConCAT Protein. SDS–PAGE gel showing a prominent band at approximately 75 kDa, corresponding to the full-length OxConCAT protein.

Figure 13. Early Degradation of the OxConCAT Construct. Coomassie-stained SDS–PAGE gel demonstrating the gradual fading of the ~75 kDa band corresponding to the OxConCAT construct, indicative of initial degradation. The molecular weight ladder is shown on the right.

Figure 14. Advanced Degradation of OxConCAT After Handling. Ultra-sensitive silver-stained SDS–PAGE gel comparing the same OxConCAT fraction after repeated freeze–thaw cycles and short-term handling at room temperature. Extensive peptide degradation is observed, with a reference molecular weight ladder on the right.

2.16.1 Second to Fifth Purification Attempts

Second Purification Attempt: Inclusion Body Processing and Refolding

The second experimental iteration aimed to refine the isolation of inclusion bodies, increase overall yield, and enhance the purity of the OxConCAT protein. The approach used a gradient refolding protocol with the AKTA system and a Talon™ column, enabling controlled buffer exchange and improved handling of unfolded protein species. Additionally, the workflow was modified to pre-aliquot protein fractions into single-use tubes, thereby reducing degradation caused by repeated freeze–thaw cycles in downstream MS applications. However, despite careful optimisation of each step, the overall outcome remained suboptimal. SDS-PAGE analysis of gel filtration fractions (Lanes 14–25) revealed no clear band for the OxConCAT protein. Additionally, Talon elution fractions (Lanes 5–12) showed only faint traces of the target protein. These findings indicate that the overall protein expression yield was much lower than expected, suggesting inefficiencies in transcription/translation or inclusion body formation during expression (Figure 15).

15-A

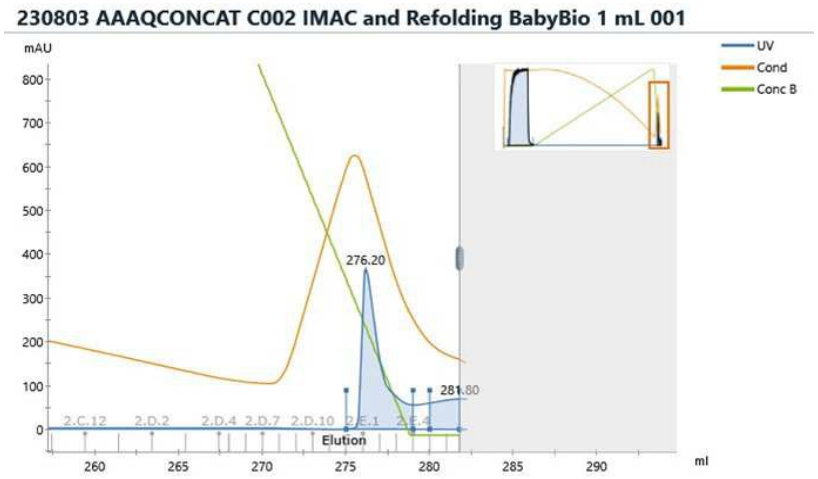

15-B

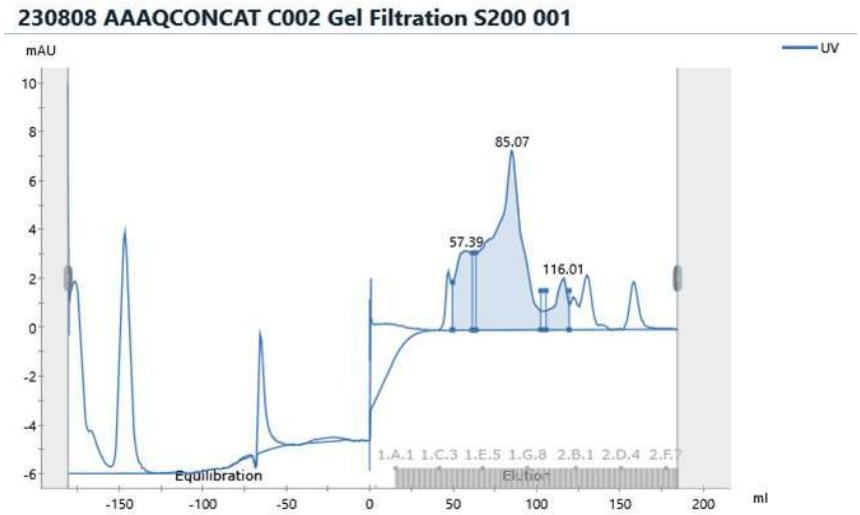

Figure 15. Second purification attempt of the OxConCAT C002 construct using IMAC and gel filtration chromatography. 15-A. IMAC (1 mL BabyBio Ni^{2+} column) with gradient refolding was followed by size-exclusion chromatography (Superdex S200 10/300 GL). **15-B.** Chromatograms show low-yield elution peaks and the absence of a significant peak at the expected ~75 kDa retention volume.

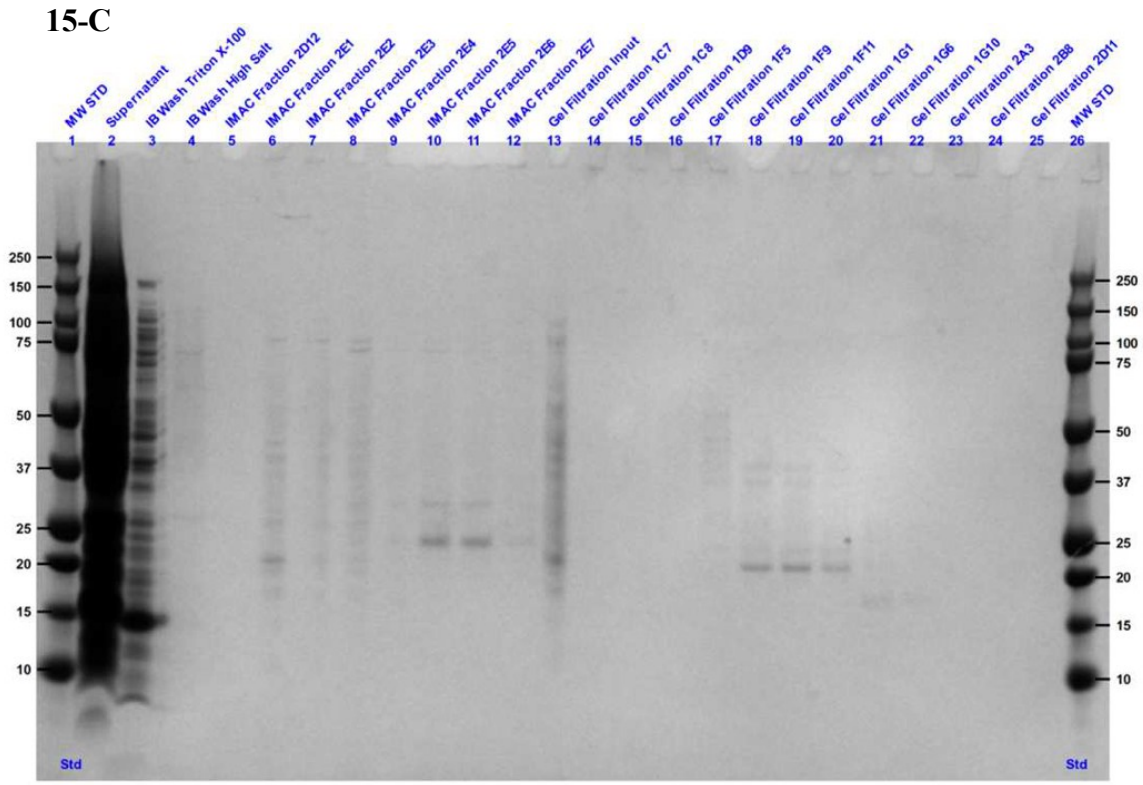

Figure 15-C. SDS–PAGE gel (12% Bis-Tris) showing all purification fractions. Lane labels identify wash buffers, IMAC eluates (F6–F12), and gel filtration fractions (1–25). No prominent band was visible at ~75 kDa, with only faint signals in IMAC eluates (lanes 7–12) and early SEC fractions (lanes 14–19). Lanes 1 and 26 represent molecular weight standards. These findings indicated that further purification or refolding steps would be unproductive until the low expression yield was resolved. Consequently, subsequent efforts focused on smaller-scale expression (50 mL cultures) and optimisation of bacterial growth and induction conditions. Figure reproduced in collaboration with Dr Lee Harris (University of Oxford).

Third Attempt: Temperature and Expression Rate Variability

To investigate the effect of expression kinetics on OxConCAT solubility and stability, two induction protocols were tested: slow expression at 18 °C for four h and rapid expression at 37 °C for the same duration. Given the unstructured nature of OxConCAT, it was hypothesised that faster expression might promote inclusion body formation and aid recovery after refolding.

SDS–PAGE of the 18 °C culture revealed faint but distinct OxConCAT bands (lanes 9–11), confirmed by a minor peak on the Superdex 200 Increase 10/300 GL chromatogram. In contrast, no detectable expression or elution peaks were observed from the 37 °C induction. The findings suggest that moderate, low-temperature expression supports limited but consistent protein production, whereas rapid expression favours aggregation or degradation. Overall, slower induction at 18 °C improved solubility and folding efficiency, albeit with reduced yield, indicating that controlled, low-rate expression conditions were preferable for generating retrievable OxConCAT protein (Figure 16).

16-A

18 °C (overnight – slow expression rate)
OxConCAT Synthesis and Purification (50 mL)

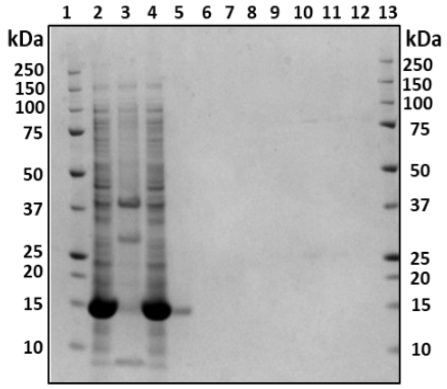

Position	Sample ID
1	MW STD Precision Plus Protein (Bio-Rad)
2	Supernatant
3	Pellet
4	Flowthrough
5	Wash 1
6	Wash 2
7	Wash 3
8	Wash 4
9	Elution 1
10	Elution 2
11	Elution 3
12	1 mL Nickel Resin after Elutions
13	MW STD (Bio-Rad)

Figure 16. SDS-PAGE analysis of OxConCAT expression at two different temperatures (50 mL scale). **16-A**: Expression at 37 °C for 4 hours (rapid induction).

16-B

37 °C (4 hrs – rapid expression rate)
OxConCAT Synthesis and Purification (50 mL)

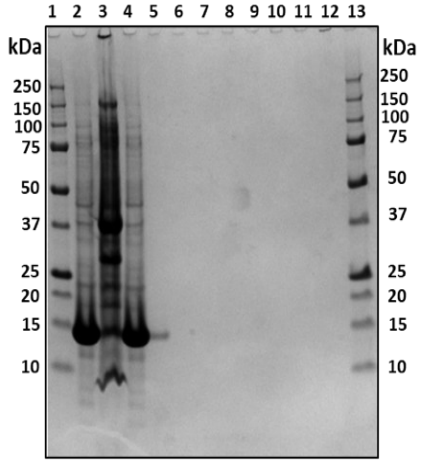

Position	Sample ID
1	MW STD Precision Plus Protein (Bio-Rad)
2	Supernatant
3	Pellet
4	Flowthrough
5	Wash 1
6	Wash 2
7	Wash 3
8	Wash 4
9	Elution 1
10	Elution 2
11	Elution 3
12	1 mL Nickel Resin after Elutions
13	MW STD (Bio-Rad)

Figure 16-B: Expression at 18 °C overnight (slow induction). The 18 °C overnight expression yielded better band resolution and reduced contaminant background, indicating improved OxConCAT solubility, although the overall expression level remained low. The 37 °C condition failed to show a discernible band at the expected OxConCAT size, suggesting possible degradation or aggregation - figure reproduced in collaboration with Dr Lee Harris (University of Oxford).

Fourth Attempt: Returning to Overnight Low-Temperature Expression

Building on prior results, a 1 L culture was expressed overnight at 18 °C to improve OxConCAT recovery. The experiment focused on maintaining solubility and yield by using a rapid, gravity-flow refolding protocol and denaturing purification under 8 M urea to prevent aggregation and proteolysis. Induction was increased to 500 µM IPTG to enhance expression levels. IMAC purification revealed a distinct UV peak at 19–21 mL corresponding to histidine-tagged OxConCAT, followed by a smaller secondary peak suggesting minor misfolded species (Figure 17). Pooled fractions (D5–D9) underwent gel filtration using a Superdex 200 Increase 10/300 GL column, yielding a broad but clearly defined peak near the expected 75 kDa elution volume. SDS–PAGE confirmed the presence of OxConCAT with partial degradation, indicating modest success in recovery under denaturing conditions but persistent instability during processing.

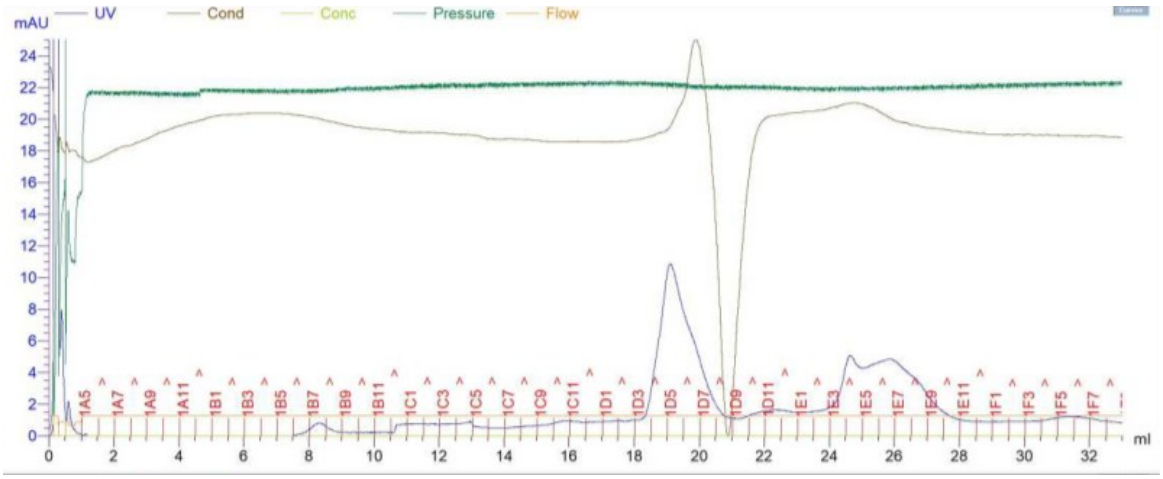

Figure 17. IMAC purification chromatogram from the fifth OxConCAT synthesis and purification attempt. Chromatogram showing imidazole-gradient elution of His-tagged OxConCAT protein under denaturing conditions. A defined UV peak at 19–21 mL indicates the primary elution of the target protein (fractions D5–D9), with a secondary broader peak between 25–28 mL corresponding to minor contaminants or partially folded species. Conductivity and pressure traces remained stable throughout, confirming consistent column performance during purification.

Fifth Experiment: Successful High-Yield Expression and Denaturing Purification

In the fifth experiment, OxConCAT was expressed at 1 L scale in E. coli Rosetta cells under optimised conditions (18 °C overnight induction with 500 µM IPTG) to maximise yield and maintain construct integrity. Following lysis and centrifugation, IMAC purification produced strong bands at ~75 kDa in elution fractions 2–3, corresponding to the OxConCAT protein, alongside minor ~25 kDa contaminants likely representing host proteins or degradation products. Most of the expressed protein was retained in the insoluble fraction, consistent with inclusion body formation.

To reduce co-eluting contaminants, pooled eluates were concentrated using 50 kDa MWCO filters, effectively retaining the target protein while removing smaller species. The inclusion of molecular weight standards (lanes 1 and 12) confirmed the expected size of OxConCAT. The final yield was 1.04 mg/mL, aliquoted into 48 × 50 µL PCR tubes, flash-frozen, and stored at –80 °C. This optimised protocol improved purity, stability, and reproducibility for downstream MS quantification (Figure 18).

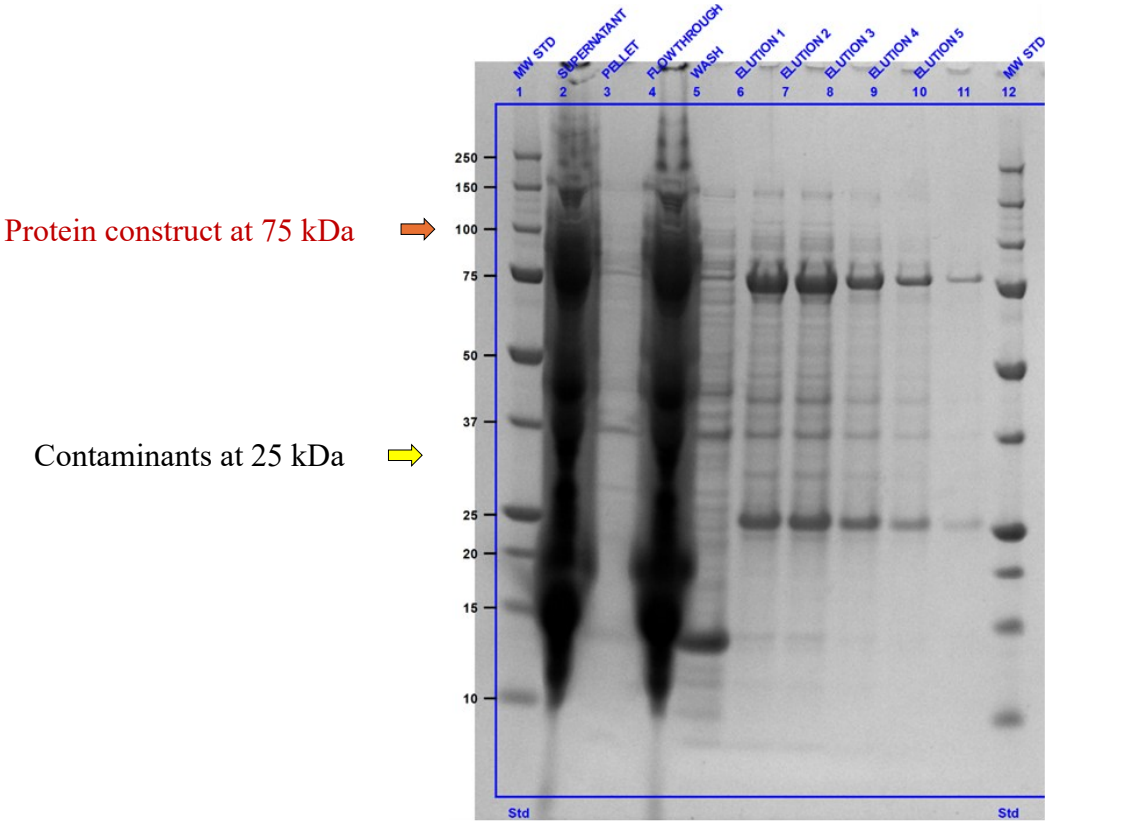

Position	Sample ID
1	MW STD Precision Plus Protein (Bio-Rad)
2	Supernatant
3	Pellet
4	Flowthrough
5	Wash
6	Elution 1
7	Elution 2
8	Elution 3
9	Elution 4
10	Elution 5
11	N/A
12	MW STD Precision Plus Protein (Bio-Rad)

Figure 18. SDS–PAGE analysis of OxConCAT purification following 1 L expression at 18 °C with 500 µM IPTG induction. Lane 1 & 12: molecular weight standards (Bio-Rad Precision Plus). Lane 2: supernatant showing soluble protein fraction after lysis. Lane 3: pellet containing predominantly insoluble OxConCAT inclusion bodies. Lane 4: flow-through with unbound proteins. Lane 5: wash fraction removing weakly bound species. Lanes 6–10: IMAC elutions 1–5 showing enriched OxConCAT bands at ~75 kDa (strongest in elutions 2–3) and minor contaminants at ~25 kDa, consistent with host-derived or degraded fragments. The gel confirms successful expression and recovery of OxConCAT, supporting downstream refinement by size-exclusion and controlled aliquoting for LC–MS quantification. Figure reproduced in collaboration with Dr Lee Harris (University of Oxford).

2.16.2 Freeze–Thaw Stability Testing

To evaluate the OxConCAT protein stability during storage, a freeze–thaw experiment was conducted. Artificial constructs like OxConCAT, lacking native folding domains, are often prone to conformational instability and precipitation upon temperature variation. Aliquots were collected before and after concentration with a 50 kDa MWCO centrifugal concentrator (Amicon, Millipore), then split into fresh and freeze–thawed (–80 °C overnight, rapid thaw at room temperature) samples. All were analysed by SDS–PAGE (12% Bis-Tris) to assess degradation or banding changes.

Results showed no discernible differences between fresh and freeze–thawed samples, either before or after concentration. The OxConCAT protein remained intact with a consistent ~75 kDa band, indicating structural stability after a single freeze–thaw cycle in denaturing buffer (8 M urea). However, contaminant bands near 25 kDa persisted, suggesting incomplete removal of smaller bacterial byproducts or truncated fragments, likely due to partial aggregation or membrane retention during filtration. Further purification via SEC or buffer exchange into 6 M guanidine hydrochloride was therefore recommended. The final OxConCAT stock (1.04 mg/mL) was aliquoted into 48 × 50 µL PCR tubes, snap-frozen, and stored at –80 °C for subsequent LC–MS applications (Figure 19).

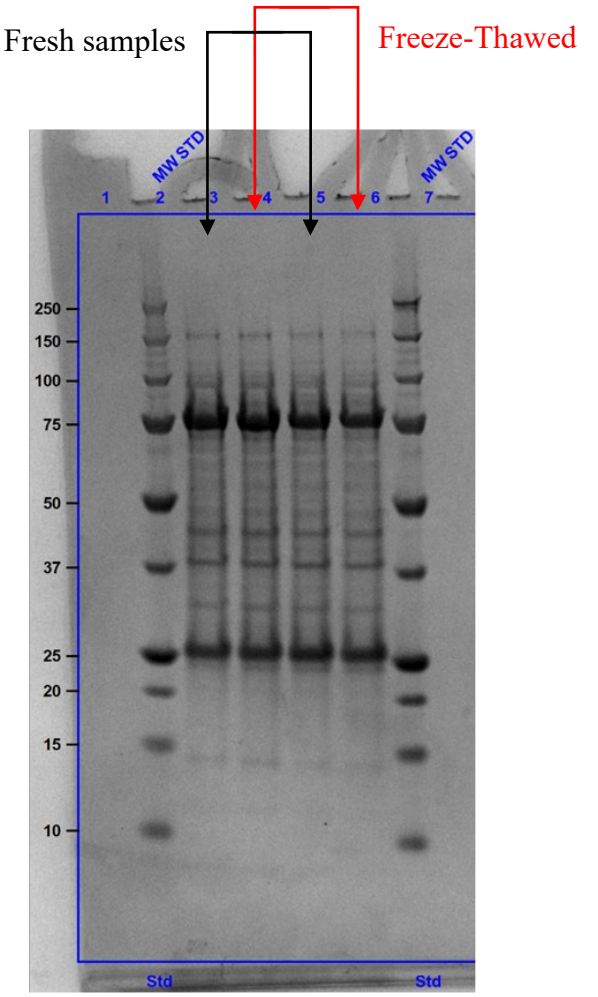

Position	Sample ID
1	N/A
2	MW STD Precision Plus Protein (Bio-Rad)
3	Pre-Concentration (50 kDa MWCO)
4	Pre-Concentration (50 kDa MWCO) Freeze-Thawed (-80 C)
5	Post-Concentration (50 kDa MWCO)
6	Post-Concentration (50 kDa MWCO) Freeze-Thawed (-80 C)
7	MW STD Precision Plus Protein (Bio-Rad)

Figure 19. SDS–PAGE analysis of OxConCAT samples before and after a freeze–thaw cycle. Lane 2 & 7: MW standards (Bio-Rad Precision Plus). Lanes 3–4: pre-concentration (fresh and freeze–thawed). Lanes 5–6: post-concentration (fresh and freeze–thawed). The 75 kDa band indicates intact OxConCAT across all conditions, confirming stability after a single freeze–thaw cycle. Persistent ~25 kDa bands represent low-molecular-weight contaminants. Figure reproduced in collaboration with Dr Lee Harris (University of Oxford).

Table 6. Summary of Experimental Findings.

Experiment	Scale	Expression Condition	Refolding Method	Outcome
1	1 L	18 °C overnight	Gravity flow + quick on-column	Successful expression and high yield (0.22 mg/mL)
2	1 L	18 °C overnight	AKTA-Talon gradient refolding	No detectable protein post-gel filtration
3	50 mL	18 °C / 37 °C	Talon + Superdex	Faint bands; low recovery
4	1 L	18 °C + 500 µM IPTG	Denaturing purification	Improved expression; persistent contaminants
5	1 L	18 °C overnight	8 M Urea purification	Purified 0.15 mg OxConCAT; freeze-thaw sensitive

2.16.3 Final Gel Filtration and Buffer Optimisation

Following several optimisation cycles, the most effective purification strategy for OxConCAT involved direct application onto a Superose 6 Increase 10/300 GL column under denaturing conditions. The protein was first buffer exchanged into 8 M urea, 50 mM HEPES (pH 7.5), 500 mM NaCl, and 5% glycerol to maintain solubility and prevent aggregation. This denaturing environment was critical for stabilising the unstructured construct, which otherwise precipitated during native purification.

The final chromatogram (Figure 20) showed three distinct peaks at 8.84, 12.00, and 13.55 mL. The central peak at 13.55 mL (Peak C) corresponded to OxConCAT, confirmed by SDS–PAGE analysis. Peak quantification identified Peak C as the dominant fraction (area = 63.04 mAU×mL; concentration = 0.296 mg/mL), representing the purest and most abundant form used for downstream experiments.

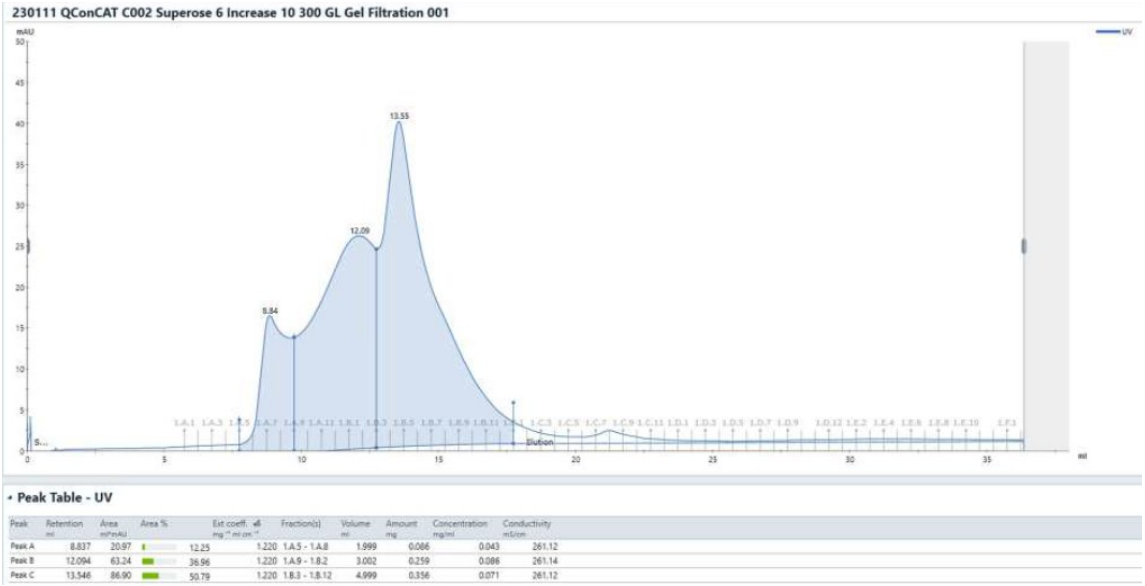

Figure 20. Final size-exclusion chromatogram of OxConCAT under denaturing conditions. Size-exclusion chromatogram (Superose 6 Increase 10/300 GL) of the final OxConCAT purification following buffer exchange into 8 M urea buffer: three prominent peaks (A–C) were observed, with Peak C (13.55 mL) corresponding to the OxConCAT construct, confirmed by SDS–PAGE as the most abundant and pure fraction.

Fractions A9–B8 were pooled, concentrated, and analysed by SDS–PAGE, which showed a clear 75 kDa band with minimal contaminants. The Superose 6 column provided improved resolution over Superdex 200, making it more suitable for large, aggregation-prone constructs. The final yield was 0.15 mg (150 µL at 1 mg/mL), aliquoted into 15 × 10 µL PCR tubes, snap-frozen, and stored at –80 °C.

This final purification established that maintaining 8 M urea throughout, combined with high-salt and glycerol buffering, prevents precipitation and enhances reproducibility. Direct denaturing injection onto Superose 6 yielded a stable, high-purity OxConCAT preparation suitable for scalable PRM-based proteomic applications.

2.17 SDS-PAGE Confirmation of Purity

As part of the final validation of the purification process, a 12% Bis-Tris SDS-PAGE gel was run on the final pooled fractions after Superose 6 gel filtration and buffer exchange. The gel (Figure 21) shows a clear, prominent band at approximately 75 kDa, corresponding to the expected molecular weight of the OxConCAT construct. The presence of this distinct band, with minimal background signals and no secondary bands, further confirmed the high purity and specificity of the final product. This analysis represents a crucial quality control step before aliquoting and long-term storage. Importantly, no degradation or fragmentation products were observed in this lane, indicating that the denaturing buffer conditions and rapid sample handling effectively preserved the structural integrity of the construct during the purification workflow.

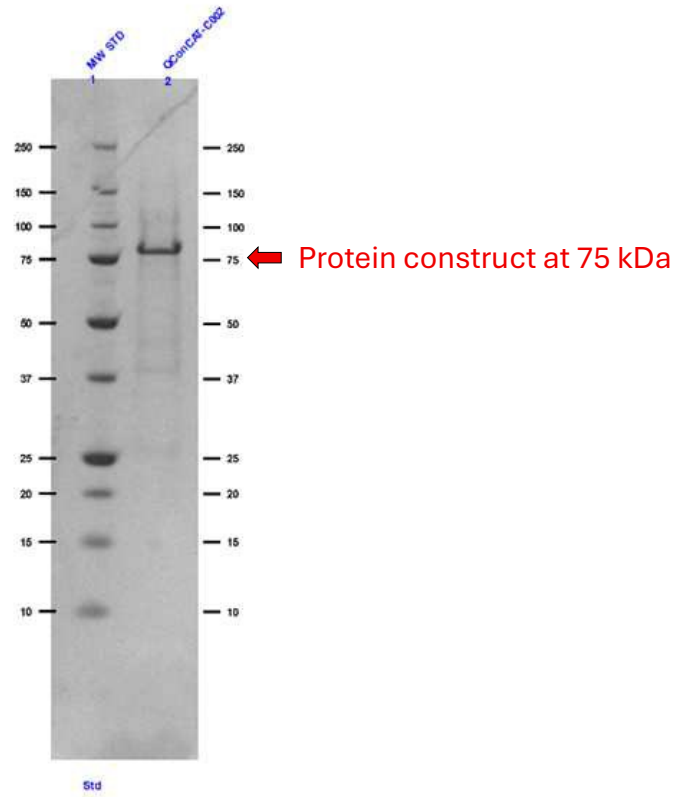

Figure 21. SDS-PAGE (12% Bis-Tris) analysis of final Superose 6 gel filtration fractions. A distinct band at ~75 kDa confirmed the successful recovery and purity of the OxConCAT construct.

The refinement of the OxConCAT synthesis and purification process culminated in the successful production of a reliable, high-purity, stable protein standard. This standard is now ready for downstream LC–PRM/MS-based quantification across hundreds of AAA plasma samples, providing the analytical foundation for internal and external validation of the AAA growth prediction algorithm.

Discussion and Chapter Conclusion

The methodological strategy developed in this chapter laid the foundation for the analytical framework underpinning this thesis. By integrating a well-defined clinical cohort with a proteomic quantification platform, it bridged the translational gap between biological sample collection and absolute molecular measurement. The combination of the OxAAA clinical study design with the OxConCAT quantification approach created a coherent, scalable system that supports biomarker validation and future clinical translation.

The OxAAA study design ensured systematic recruitment, uniform plasma preparation, and consistent data acquisition across patients, thereby minimising pre-analytical variation, a principal source of bias in clinical proteomics. The inclusion of matched pre- and post-surgical plasma samples allowed dynamic evaluation of biomarker fluctuations associated with AAA intervention. This rigorous clinical approach provided the biological and logistical foundation for the subsequent analytical developments described in this thesis.

In parallel, the OxConCAT construct was conceptualised, designed, and experimentally validated as a next-generation internal standard for absolute quantification of plasma proteins. The design phase focused on selecting representative, quantotypic peptides that exhibit stable ionisation, limited post-translational modification, and reproducible

chromatographic behaviour. Rational sequence optimisation enabled efficient proteolysis, while complete ^15N incorporation ensured isotopic uniformity and accurate co-elution with endogenous peptides. Through these refinements, the OxConCAT approach addressed key analytical limitations inherent to traditional QconCAT and label-free quantification methods.

The experimental implementation of OxConCAT was iterative and data-driven. Early expression trials revealed inclusion body formation and aggregation, necessitating optimisation of induction temperature, IPTG concentration, and buffer composition. These adjustments resulted in marked improvements in solubility and yield. Successive purification cycles using nickel-affinity chromatography and gel filtration achieved high purity and structural homogeneity, as verified by SDS-PAGE and UV absorbance profiles. Furthermore, freeze–thaw testing confirmed that the construct maintained structural stability and quantitative performance under typical storage conditions, an essential criterion for reproducibility in longitudinal studies.

Collectively, these outcomes demonstrate that the optimised OxConCAT construct provided a reproducible, stable, and scalable solution for multiplexed quantification of candidate plasma biomarkers. Its development represents a critical methodological advance, enabling the transition from discovery-based proteomics to precise, standardised, and clinically relevant quantification. The successful synthesis, purification, and validation of OxConCAT now allow its deployment in targeted mass spectrometry assays, where digestion efficiency and peptide robustness can be systematically evaluated.

The next chapter, Chapter 3 - Peptide Quantification and Selection Strategies, builds directly upon this methodological foundation. It examines the analytical performance of the OxConCAT construct under varying digestion and loading conditions, assesses the

optimisation of the heavy-to-light peptide ratio, and refines the criteria for selecting quantotypic peptides for clinical application. In doing so, it translates the methodological advances achieved here into quantitative precision and biological interpretability, thereby advancing the overall objective of developing a reliable, translatable biomarker quantification platform for AAA. These validated protocols form the analytical basis for the quantitative evaluations described in Chapter 3.

Chapter 3 – Peptide Quantification and Selection Strategies

Introduction

Accurate and reproducible peptide quantification underpins the translation of targeted proteomics into a reliable platform for biomarker validation. Building on the OxConCAT construct developed in Chapter 2, this chapter optimises peptide-level quantification workflows to obtain consistent and interpretable absolute measurements in plasma. Although the OxConCAT approach provides a stoichiometric internal standard, its accuracy depends on the behaviour of individual peptides during digestion, ionisation, and detection. Variability in solubility, digestion efficiency, or chromatographic recovery can bias quantification, particularly in complex biological matrices. Here, these sources of variability were systematically examined and minimised through iterative empirical refinement, controlled loading experiments and computational modelling. The first part of the chapter details optimisation of digestion and loading strategies, including co-digestion, sequential digestion, and a novel "sandwich" loading approach to maximise peptide recovery and minimise ion suppression. These experiments established standardised protocols for OxConCAT-based absolute quantification in PRM workflows. In parallel, a computational framework combining random permutation, Markov-chain modelling, and thermodynamic scoring was implemented to predict sequence arrangements with improved solubility, stability, and proteolytic accessibility, accelerating construct refinement. Finally, a targeted case study of APOA4 peptides illustrates how structural and biochemical properties can differentially affect detectability and quantification.

Together, these empirical, computational, and peptide-specific analyses establish a standardised framework for absolute quantification in plasma proteomics. This chapter thus forms the methodological bridge between construct development (Chapter 2) and clinical application (Chapter 4) in the OxAAA study.

Methods - Experimental Optimisation

Optimising Sample Preparation for Enhanced Peptide Quantification

Accurate peptide quantification is essential in proteomic studies, particularly in absolute quantification approaches based on OxConCAT methodologies. This chapter explores the impact of different sample loading strategies on signal intensity and quantification reliability in mass spectrometry-based proteomics. This section evaluates experimental comparisons between co-digestion, sequential digestion, and sandwich loading methods. The goal is to establish an optimised workflow that ensures consistent peptide detection and minimises signal suppression effects.

3.1 Comparison of Loading Strategies (Co-Digestion, Sequential Digestion, Sandwich Loading)

Co-Digestion Approach

To assess the effect of matrix complexity on signal uniformity, co-digestion was first tested. Co-digestion involves mixing the OxConCAT and plasma digest before mass spectrometric analysis. This method is widely believed to improve sample homogeneity,

facilitating quantification. However, the co-digestion strategy may result in attenuation of signal intensity for specific peptides, likely due to matrix-related effects and competition between peptides for ionisation, and consistent with a non-uniform distribution of peptide signals across different replicates. The variability introduced by this approach poses challenges for achieving reproducible and accurate quantification, ultimately limiting its applicability in clinical and biomarker discovery settings. Furthermore, it was observed that peptides exhibit varying degrees of signal loss, suggesting that some may be more prone to competition effects than others. Because co-digestion may still lead to peptide-specific ion suppression (as evidenced in Table 7), we evaluated a sequential digestion and spiking workflow.

Sequential Digestion and Spiking

An alternative method involves digesting OxConCAT separately before adding it to the plasma digest. This method is expected to maintain a constant peptide standard concentration across samples, mitigating competition effects observed in co-digestion. By spiking equal amounts of OxConCAT digest into each plasma digest, the variability in peptide ionisation may be reduced, leading to improved consistency in quantification. Additionally, this method may align with absolute quantification principles by maintaining a known and reproducible concentration of OxConCAT peptides per sample. The reproducibility of this approach could allow for standardisation across multiple experimental batches, making it a preferred method in high-throughput proteomics studies and ensuring that the heavy peptide standard consistently reaches the mass spectrometer in the same quantity across all samples, thereby improving accuracy.

Sandwich Loading Strategy

A further refinement involves sandwich loading, in which peptides are preloaded into the tip, followed by buffer, plasma digest, and additional buffer. This approach is designed to reduce variability introduced by sequential loading and to achieve a more uniform peptide distribution, thereby representing a potential improvement over conventional loading methods. The advantage of sandwich loading may lie in its ability to reduce handling variability and ensure that peptides are uniformly introduced into the mass spectrometer. Furthermore, sandwich loading may help preserve peptide integrity, reducing the risk of degradation or incomplete digestion that can lead to erroneous quantification results. This method is expected to provide more consistent peptide detection, particularly for peptides susceptible to suppression effects (Table 7).

Table 7. Comparison of Sample Preparation Strategies for OxConCAT-Based Peptide Quantification.

Sample Preparation Method	Description	Advantages	Limitations	Suitability for Quantification
Co-digestion	OxConCAT and plasma are digested together in a single step	- Simple and time-efficient - No separate handling required	- High signal suppression - Potential peptide loss - Inconsistent across replicates	✗ Limited reproducibility and accuracy
Sequential Digestion + Spiking	OxConCAT is digested separately and spiked into already digested plasma	- Reduces matrix effects - Improved peptide consistency - Aligned with absolute quantification principles	- Requires precise pipetting - Slightly more labour-intensive	✓ High reproducibility and reliability
Sandwich Loading	Sequentially loads peptide standard, buffer, plasma digest, and buffer into the tip	- Uniform peptide distribution - Minimises handling variation - Preserves peptide integrity	- Requires careful technique - May not eliminate suppression for highly competitive peptides	✓ Optimised signal stability and retention
Ion Suppression Awareness	Identification and mitigation of peptide suppression during ionisation	- Helps refine peptide panel - Enables targeted optimisation	- Requires peptide-specific assessment and possibly redesign of OxConCAT constructs	⚠ Complementary strategy for refinement

3.2 Minimising Ion Suppression Effects

Ion suppression, where peptides with higher ionisation efficiency dominate the MS signal, remains a major source of bias in peptide quantification, particularly in complex plasma matrices; co-eluting peptides can reduce signal intensity for weaker species, leading to underestimation of their abundance. Characterising peptide-specific susceptibility to suppression is therefore essential for refining peptide selection and digestion protocols to improve analytical precision. To address these challenges, a range of digestion and loading strategies was designed to control competitive ionisation in OxConCAT plasma mixtures. Instead of relying solely on co-digestion, the refined workflow incorporates separate digestion of OxConCAT standards followed by defined post-digest spiking, ensuring uniform delivery of heavy peptides to the mass spectrometer. Maintaining a consistent peptide-to-protein ratio across analytical runs was prioritised to support reproducibility. Four loading strategies, including sequential digestion and "sandwich" loading, were implemented to explore ways to minimise matrix effects and improve retention-time consistency. These workflows are intended to enhance reproducibility and signal linearity, thereby supporting robust absolute quantification in biomarker studies. Subsequent sections describe their comparative evaluation and validation for clinical proteomic applications.

Refining Quantification through PRM Analysis

Parallel Reaction Monitoring (PRM) is a valued tool in targeted proteomics, providing high selectivity and sensitivity for peptide quantification. This chapter explores the optimisation of PRM-based workflows, with a focus on sample loading strategies and their effects on signal intensity and measurement accuracy. A critical aspect of this optimisation involves titration experiments to determine the impact of heavy and light

peptide competition and the effectiveness of sandwich loading methods in mitigating variability. Additionally, the chapter examines the feasibility of implementing these strategies at a larger scale and addresses practical considerations for improving quantification accuracy and reproducibility.

3.3 Peptide Competition and Signal Interference in PRM

One of the primary challenges in PRM-based quantification is the competition between heavy and light peptides. Excessively high concentrations of heavy peptides can suppress the detection of light ones, leading to signal distortion. This effect has been observed in previous peptide quantification studies and remains an important consideration when designing experimental workflows.[58] To evaluate this phenomenon, titration-based optimisation of heavy-to-light peptide ratios is typically performed, including conditions where plasma background is present at varying concentrations.[61–63] At elevated heavy peptide concentrations, light peptide detection becomes increasingly complex, necessitating careful calibration of peptide inputs. The optimal ratio for minimising competition effects while maintaining accurate quantification can be established through systematic PRM analysis. The competition effect is often peptide-specific, with certain peptides exhibiting greater susceptibility to suppression than others. Understanding these behaviours enables strategic optimisation of relative peptide concentrations and chromatographic conditions to minimise co-elution and ensure quantification.

3.4 Balancing Heavy and Light Peptide Ratios

Beyond direct signal suppression, peptide competition introduces additional challenges in absolute quantification. Given the necessity of knowing the exact number of heavy

peptides introduced into each sample, precise calibration steps are critical. To achieve quantitative precision, it is essential to ensure that heavy peptides reach the mass spectrometer in equal amounts across all samples, independent of total protein concentration in the plasma digest. This requires meticulous sample preparation, with controlled digestion and spiking steps to maintain consistency.[64] Furthermore, variations in sample matrix composition may influence peptide ionisation efficiency (e.g., elevated lipid content can suppress hydrophobic peptides), even when heavy peptide concentrations are constant.[65, 66] The influence of plasma conditions on peptide signal intensities should be examined, and alternative normalisation strategies may be required to correct for these effects.

3.5 Implementation of the Sandwich Loading Approach

To mitigate peptide competition and enhance quantitative consistency, various sample loading strategies were evaluated, with emphasis on the sandwich loading approach. The sandwich loading method, in which peptides are layered between buffer and plasma digest, in this method, peptides are pre-loaded into the tip, followed by buffer, plasma digest, and an additional buffer layer, was evaluated to promote uniform peptide distribution and to reduce variability from sequential loading. Although this configuration added an extra preparation step, it was predicted to improve signal stability relative to conventional loading and mitigate ionisation competition. Its benefits in reducing ionisation competition outweigh the minor increase in workload. Implementation across larger experimental cohorts proved feasible, though reproducibility depended on precise buffer layering and pipetting technique, which was not formally evaluated. Automated sample preparation platforms may further reduce operator-induced variability and enhance consistency. Standardisation of buffer composition also emerged as a critical

factor. Minor adjustments to ionic strength or pH improved peptide retention and reduced carryover effects. Future studies should evaluate alternative buffer formulations to stabilise peptide interactions and ensure uniform elution across diverse peptide chemistries. Given the inherent complexity of plasma, matrix components can still influence peptide ionisation efficiency, even under optimised loading conditions. Combining sandwich loading with depletion or fractionation strategies may further reduce matrix interference and enhance detection sensitivity. The sandwich loading approach is introduced as a practical and scalable strategy aimed at mitigating ion suppression and supporting PRM-based peptide quantification. This configuration can be integrated into OxConCAT-based workflows for absolute quantification. Ongoing refinements, including automated handling and optimised buffer systems, are expected to enhance reproducibility and analytical precision further, supporting more accurate biomarker discovery and clinical proteomic applications (Table 8).

Table 8. Comparison of PRM-based peptide quantification strategies.

Aspect	Description	Considerations
Peptide Competition	High heavy peptide concentrations suppress light peptide signals; peptide-specific suppression observed.	Optimise peptide selection to reduce suppression.
Titration Strategy	Used to determine optimal heavy/light ratios for minimal competition and accurate quantification.	Identify the ratio with the best signal-to-noise for target peptides.
Heavy/Light Ratio Calibration	Ensures consistent heavy peptide input across samples; critical for absolute quantification accuracy.	Track input peptide amounts precisely across runs.
Sandwich Loading	Peptides and buffer layers are used to minimise variability; this improves signal consistency and reduces suppression.	Minimise pipetting errors; consider automated loading.
Large-Scale Implementation	Feasible with a slight increase in complexity; automation can enhance reproducibility.	Balance throughput with reproducibility and accuracy.
Mitigating Matrix Effects	Complex plasma matrix impacts ionisation: buffer adjustments and depletion strategies suggested.	Explore buffer composition and cleanup techniques.

Computational Methods - Optimisation of Peptide Fragment Arrangements

3.6 Introduction and Literature Review

The development of OxConCAT constructs for absolute protein quantification requires precise optimisation of peptide fragment arrangement. These concatenated proteins, composed of multiple quantotypic peptides, act as stoichiometric internal standards for mass spectrometry-based quantification. However, their performance depends not only on peptide selection but also on the thermodynamic and structural stability of the concatenated construct. Inappropriate peptide ordering may expose hydrophobic residues, promote aggregation, and reduce digestion efficiency, ultimately compromising quantification accuracy. This study aimed to enhance OxConCAT stability through computational optimisation of peptide arrangement. By permuting peptide order and evaluating free energy, folding efficiency, and aggregation propensity, the objective was to identify arrangements that minimise instability while preserving proteolytic accessibility. Computational modelling thus complements empirical optimisation by addressing a key design challenge, achieving structural robustness in an inherently artificial protein.

3.6.1 Computational Background and Rationale

The folding behaviour and stability of proteins, including OxConCAT constructs, depend on a delicate balance of hydrophobic and hydrophilic interactions, secondary structure formation, and backbone flexibility. Misfolding or exposure of hydrophobic cores promotes aggregation and inclusion body formation, phenomena frequently observed during recombinant expression.[36] Sequence optimisation guided by thermodynamic modelling can help mitigate these issues by minimising total free energy and

conformational disorder. Modern computational protein design frameworks integrate several strategies, Monte Carlo simulations, genetic algorithms, and deep learning–driven prediction models, to evaluate thousands of potential sequence permutations. AlphaFold, for instance, provides accurate structural predictions that can be used to assess folding potential before synthesis. Incorporating such tools allows prediction of structurally stable peptide arrangements, minimisation of aggregation-prone motifs, and assessment of secondary structure compatibility between adjacent peptides.[67]

3.6.2 Application to OxConCAT Constructs

The principles outlined above were applied to optimise OxConCAT design using a stepwise computational workflow. Evolutionary and energy-based optimisation algorithms were applied to explore multiple permutations of the OxConCAT sequence. Each configuration was scored using thermodynamic and solvation energy metrics to estimate structural feasibility.[68] The objective was to lower free energy and reduce hydrophobic exposure while preserving protease accessibility and isotopic labelling compatibility. Iterative modelling cycles refined these parameters, identifying near-optimal arrangements predicted to form more stable and soluble constructs than the original sequence. This computational refinement extends beyond simple sequence shuffling. Secondary structure predictions and disorder propensity analyses were incorporated to evaluate how neighbouring peptides influence folding kinetics and solubility. The inclusion of flexible linker sequences and strategic peptide ordering was explored to minimise steric clashes and enhance accessibility for tryptic digestion, critical for achieving consistent peptide release in quantitative workflows.

3.6.3 Relevance to Proteomic Applications

OxConCAT technology has transformed targeted proteomics by enabling absolute quantification of proteins via isotope-labelled synthetic standards. Yet, despite extensive

optimisation of peptide selection and digestion protocols, the arrangement of peptide fragments within constructs remains underexplored. Structural instability and aggregation continue to limit yield and reproducibility.[56] By integrating computational modelling into the OxConCAT design pipeline, this study provides a framework for rational construct optimisation that precedes laboratory synthesis, improving expression efficiency, digestion uniformity, and long-term stability. Ultimately, this combined computational–experimental strategy supports the creation of thermodynamically optimised OxConCAT standards with enhanced solubility and structural resilience. These improvements strengthen the reliability of absolute quantification in plasma proteomics and contribute to advancing OxConCAT technology for biomarker discovery and clinical translation.

3.7 Peptide Fragment Selection and Initial Model Design

A predefined set of peptide fragments representing control proteins was used as the initial dataset. Three representative peptides were selected from each protein to serve as building blocks for concatenation. The initial construct, hereafter termed the "original model," was generated using AlphaFold3 (AF3), a state-of-the-art deep-learning algorithm for protein structure prediction.[69] Peptides were arranged according to their natural sequence order within the source proteins, establishing a baseline model for subsequent computational optimisation. The original sequence was considered the baseline for optimisation and served as a reference point from which subsequent modifications and refinements were made. This unoptimised configuration served to evaluate the inherent instability associated with natural peptide ordering.

3.8 Sequence Optimisation Strategies (Random Permutation, Markov Chain, Metal-Binding Motifs)

A multi-stage optimisation pipeline was implemented to refine the concatenated peptide sequence and enhance its structural and thermodynamic properties. Each generation employed distinct computational strategies to explore sequence permutations and identify energetically favourable configurations. The optimisation process was divided into multiple generations, each incorporating different methods to refine the sequence progressively.

1. Random Permutation (Generation I): In the first generation, the peptide fragments were randomly shuffled, generating a set of candidate sequences for analysis. This permutation step provided a broad range of sequence variations, establishing a diverse pool of candidates from which to select for further optimisation.

2. Markov Chain-Based Selection (Generations II-V): This stage introduced probabilistic weighting to preserve favourable motifs. In the following generations, the top 10% of models from each iteration were analysed to identify recurring pairwise and triplet fragment occurrences. A Markov chain algorithm was applied to bias sequence generation toward recurring, high-scoring motifs while preventing redundancy. This method allowed for more targeted exploration of sequence permutations, enhancing the likelihood of finding sequences with improved stability.

3. Zinc Incorporation: Some of the peptide fragments in the study contained a zinc-finger domain, which is known to play a key role in protein stability. After Generation I, Zinc coordination sites were modelled in silico to assess their effect on predicted folding stability. This step provided valuable insights into how the inclusion of metal ions could affect the overall stability of the concatenated sequence.

4. Selective Concatenation (Generation VI): By Generation 6, high-scoring subsequences from previous generations were concatenated to form longer peptide sequences. At this stage, subsequent optimisation proceeded autonomously, requiring minimal manual adjustment, as the computational methods had already refined the sequence arrangement to a high degree of stability. This final selective concatenation step aimed to consolidate high-stability subsequences into an optimised construct.

Computational scoring was carried out using AlphaFold3-based predictions, with energy minimisation techniques applied to further refine the models. Thermodynamic stability was quantified as absolute ΔG, where more negative values indicate enhanced stability. This scoring method provided a direct way to compare the stability of different sequence permutations and track improvements over successive generations.

3.9 Computational Modelling, Thermodynamic Scoring, and Sequence Refinement

Structure Generation: For each sequence permutation, AlphaFold3 was used to generate predicted 3D structures. This allowed for a visual and structural comparison of the various sequence permutations to evaluate their potential stability.

The process began with energy minimisation, where models underwent FastRelax minimisation: this technique optimises protein structures by adjusting atomic positions to achieve lower energy configurations, thereby improving the accuracy of the stability predictions. To assess thermodynamic stability, absolute ΔG values were calculated for each model. These values serve as a quantitative measure of protein stability, with more negative results indicating better stability. To visualise the overall similarity between different sequence permutations, a *t-SNE* (t-distributed Stochastic Neighbour

Embedding) analysis was performed using *Jaccard* distance-based metrics: this clustering approach helped identify groups of similar sequences, offering valuable insights into the relationship between sequence permutations and their structural characteristics.

A comprehensive sequence scoring and refinement strategy guided the optimisation process. The composite stability metric was used to evaluate the sequences, incorporating a variety of factors that contribute to protein stability:

- Hydrophobic Exposure Penalties: Sequences were penalised for exposing hydrophobic residues to the surface, as this can lead to aggregation and reduced solubility.
- Secondary Structure Compatibility: Sequences that aligned poorly with secondary structure predictions, such as alpha-helices and beta-sheets, received lower scores. Maintaining proper secondary structure is crucial for protein folding and stability.
- Backbone Flexibility Constraints: Flexibility in the protein backbone was also considered, with penalties assigned to sequences that exhibited excessive rigidity, as this could hinder proper folding and function.[70, 71]

Experimental Optimisation Results

Data-Driven Refinement of OxConCAT Peptide Selection

The development of OxConCAT constructs for absolute quantification in proteomics involves careful peptide selection to ensure precise and consistent measurements. Initially, peptides are selected based on theoretical digestion patterns, but their suitability must be verified through experimental analysis. This section addresses the challenges faced in peptide candidate selection, the refinement process guided by empirical data, and

the implications for targeted quantification using Parallel Reaction Monitoring (PRM). It also explores the role of titration experiments, sample loading techniques, and iterative improvements to target peptide identification, emphasising the importance of experimental validation in enhancing quantification workflows.

3.10 Theoretical vs Empirical Selection Strategies

OxConCAT constructs were designed by selecting peptides from theoretical *in silico* digestions of target proteins. This involves predicting tryptic cleavage sites and selecting peptides of optimal length and physicochemical properties. The expectation is that these peptides will ionise efficiently, fragment well in mass spectrometry, and provide reliable quantification of their respective proteins. However, early-stage OxConCAT development does not guarantee that all theoretically selected peptides will perform well in real-world analyses. Experimental validation is essential to confirm peptide detectability and signal consistency. Observations from previous PRM data indicated that some peptides fail to ionise efficiently or co-elute with interfering species, leading to poor reproducibility. However, peptides that were initially assumed to be optimal displayed unexpected fragmentation behaviour, affecting their suitability for absolute quantification (Table 9). This empirical feedback loop informed the next generation of OxConCAT design and guided peptide inclusion for downstream quantification.

Table 9. OxConCAT Peptide Selection Summary.

Aspect	Description	Implication
Titration Findings	Assessed minimum detectable concentrations; revealed suppression patterns.	Improves understanding of peptide behaviour across concentration ranges.
Signal Suppression	Light peptide signal reduction at high heavy concentrations; peptide-specific suppression noted.	Necessitates ratio optimisation and loading control in quantification workflows.
Refinement Strategy	Iterative refinement based on PRM performance; only reliable peptides are retained in the construct.	Establishes a data-driven pipeline for future OxConCAT design.
Peptide-Specific Adjustments	Excluded poorly ionising or high-variability peptides; added validated alternatives.	Enhances robustness and precision of quantification workflows.

3.11 Validation through Experimental Data

To address these limitations, a systematic evaluation of peptide performance was undertaken. This involved analysing PRM data to identify peptides that generate strong, reproducible signals across biological replicates. Candidate peptides were evaluated against four criteria: (i) signal intensity; high, stable response across injections; (ii) endogenous detectability; co-detection of the light peptide with the heavy-labelled OxConCAT analogue; (iii) fragmentation quality; clear, reproducible fragment-ion spectra; and (iv) low interference; minimal matrix effects and limited co-elution. Building on these analyses, the OxConCAT construct was refined by choosing the best-performing peptide for each target protein. This refinement step ensures that the final construct retains only peptides empirically demonstrated to support absolute quantification. The revised selection strategy contrasts with the initial theoretical approach, highlighting the importance of ongoing experimental feedback in OxConCAT design. Figure 22 summarises the filtering pipeline from initial nomination to final inclusion.

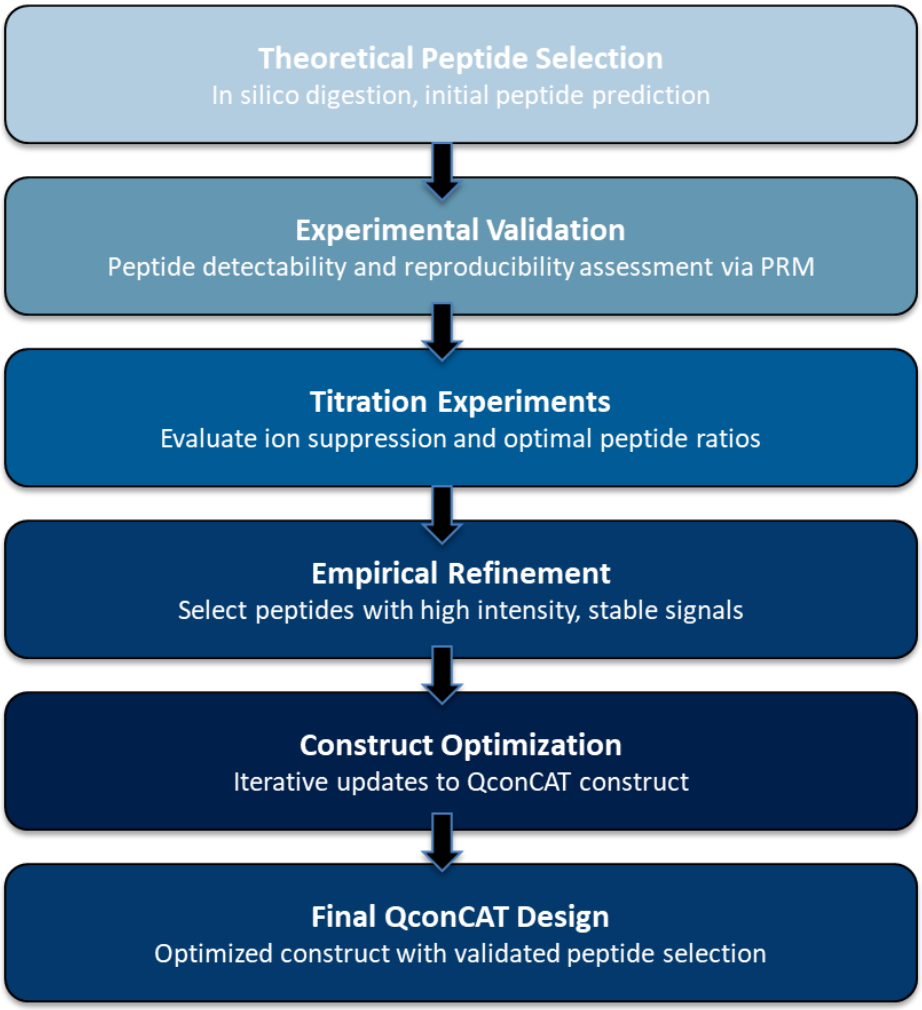

Figure 22. Step-by-Step Refinement of Peptide Selection for OxConCAT-based Quantification.

3.12 Managing Signal Suppression and Variability

Ion suppression arising from competition between heavy-labelled OxConCAT peptides and endogenous counterparts may be a principal source of bias. Titrations demonstrated that elevated heavy inputs attenuate light-peptide signals, with peptide-specific susceptibility. This peptide-specific behaviour underscores the influence of physicochemical properties on ionisation efficiency and detectability in plasma.

To define optimal quantification conditions, PRM analyses were performed at varying concentrations to determine each peptide detection threshold (see Sections 3.14 and related Figure 23). Peptides exhibiting strong ionisation efficiency remained quantifiable at lower concentrations, while those prone to suppression required adjusted loading ratios. Consequently, peptide-specific calibration is required; assuming uniform ionisation across peptides is untenable. Future OxConCAT designs should de-prioritise poorly ionising peptides and optimise heavy:light ratios to limit distortion. A data-driven redesign strategy was implemented, integrating empirical evidence from previous proteomics datasets to select peptides with proven detectability and stable ionisation. Iterative evaluation through PRM allowed the identification of a subset of high-performing peptides that now form the foundation for next-generation OxConCAT constructs. To further stabilise delivery, we explored loading configurations (including "sandwich" layering); their performance is evaluated in sections 3.18–3.20. While its performance is assessed later, the approach illustrates the rationale for integrating computational peptide prediction with empirical evaluation. Systematic assessment of peptide behaviour through titration experiments, PRM analysis, and historical performance review provides a structured framework for refining OxConCAT design. The experimental evidence supporting these observations, including peptide titration data, signal suppression effects, and loading configuration comparisons, is presented in detail in Sections 3.14–3.20 and the corresponding figures. Establishing standardised criteria for peptide selection, loading configuration, and analytical workflow development will be essential to ensure reproducibility and quantitative precision in OxConCAT-based absolute quantification of plasma proteins.

Titration strategy

The accurate quantification of peptides in proteomics relies on well-optimised methodologies that ensure reproducibility and precision. OxConCAT-based absolute quantification plays a crucial role in targeted proteomics, but its effectiveness depends on carefully selected peptides, optimised titration strategies, and controlled sample loading approaches. This section explores the refinement of OxConCAT constructs through titration experiments, ranking of peptide intensities, and systematic loading strategies to minimise variability and enhance signal consistency in PRM workflows.

We implemented titrations to (i) define peptide-specific heavy:light windows that avoid suppression while maintaining sensitivity, and (ii) rank peptides by robustness under matrix load. Criteria and results are detailed in sections 3.13–3.14.

The key challenges discussed in this chapter involve determining and improving peptide selection criteria for OxConCAT constructs and evaluating titration experiments to identify the optimal heavy-to-light peptide ratio, analysing how different sample loading methods impact quantification reproducibility, addressing ion suppression and peptide competition issues, and exploring strategies to incorporate OxConCAT-based quantification with clinical biomarker validation. By systematically optimising these variables, we aimed to establish a workflow that improves OxConCAT quantification, ensuring consistency and reliability across multiple experiments and biological sample types. OxConCAT constructs are designed using *in silico* digestion models that select peptides based on predicted tryptic cleavage efficiency, physicochemical properties, and expected ionisation behaviour. However, these theoretical selections often fail to account for real-world mass spectrometry performance. Empirical validation is essential to determine which peptides are truly detectable under experimental conditions and which

may suffer from low ionisation efficiency, poor fragmentation, or high interference from matrix effects. The challenges identified in the initial OxConCAT design include peptides exhibiting poor ionisation efficiency, leading to weak or undetectable signals; overlapping fragmentation patterns that complicate PRM-based quantification; peptides showing retention shifts or co-elution with interfering species, which reduces accuracy; and the presence of modifications or sequence characteristics that influence detectability, such as methionine oxidation or cysteine alkylation. To refine OxConCAT design, PRM data were analysed to identify peptides that consistently produce strong, reproducible signals. A ranking system was established based on the following criteria:

1. Signal Intensity: Peptides exhibiting the highest and most stable signal intensities were prioritised.
2. Presence of Endogenous Counterparts: Peptides, where both the heavy (OxConCAT) and light (endogenous) versions were consistently detected, were preferred.
3. Fragmentation Efficiency: Peptides generating precise and reproducible fragment ion spectra were considered ideal.
4. Minimal Interference: Peptides with minimal ion suppression and low background noise were prioritised.

A key insight from this ranking approach was the identification of highly variable peptides that deviated significantly from the expected dynamic range.

3.13 Determining Optimal Heavy-to-Light Ratio

To determine the optimal ratio between OxConCAT-derived heavy peptides and their endogenous light counterparts, titration experiments were performed across a range of

heavy peptide concentrations. The purpose of these experiments was to identify the highest heavy input that does not suppress the corresponding light peptide signal, to assess the linearity of quantification across different ratios, and to ensure that endogenous peptides remain consistently detectable alongside their labelled analogues. Excessive heavy peptide concentrations may reduce the apparent intensity of light peptides, leading to ion suppression and inaccurate quantification. Conversely, insufficient heavy input may compromise measurement precision. Overall, an intermediate heavy-to-light ratio was found to provide the most balanced performance, maintaining both accuracy and reproducibility across peptides.

3.14 Evaluating Peptide Robustness Across Concentrations

Beyond establishing the optimal heavy-to-light ratio, titration experiments were employed to assess peptide behaviour across a range of concentrations, providing critical insights into ion suppression dynamics, retention stability, and overall detectability. By plotting signal intensities at multiple titration points, characteristic patterns of suppression, peak broadening, and retention shifts were identified. Several peptides exhibited stable signal intensities throughout all titration levels, confirming their suitability for absolute quantification. In contrast, others demonstrated substantial variability, reflecting susceptibility to ion suppression or chromatographic instability. Peptides observed in the wash fraction towards the end of the gradient likely exhibited excessive interaction with the chromatographic stationary phase, suggesting the need for refined loading or gradient conditions. Figure 23 summarises the detectability of individual peptides under different titration conditions. Each column represents a specific heavy-to-light ratio, and each row corresponds to an OxConCAT peptide sequence. Green-highlighted entries indicate peptides that were consistently detected with stable

intensities, whereas grey fields denote non-detectable or inconsistently detected peptides. The consistent presence of green-highlighted peptides across multiple titration levels indicates strong ionisation efficiency and minimal influence from competitive suppression or matrix effects. These peptides, therefore, represent reliable candidates for inclusion in refined OxConCAT constructs. Conversely, non-highlighted peptides displayed variable or absent detection, likely due to suboptimal ionisation, interference from co-eluting species, or retention time drift, all of which can undermine reproducibility in quantitative proteomics.

Across titration points, peptides clustered into two behaviours: (i) robust-stable intensity, consistent RT, and minimal suppression; and (ii) labile-variable intensity, peak broadening, or RT drift. Signals detected predominantly in the post-gradient wash indicate excessive stationary-phase interaction and warrant gradient or loading adjustments. Figure 23 presents a detection matrix (rows: peptides; columns: heavy:light conditions): green denotes consistent detection; grey denotes absent/inconsistent detection. Green-dominant peptides were retained for subsequent constructs; variable peptides were excluded or flagged for further optimisation. Physicochemical correlates of robustness included moderate hydrophobicity, optimal length (8–16 aa), and predictable charge state, reinforcing the need for empirical screening beyond in-silico predictions.

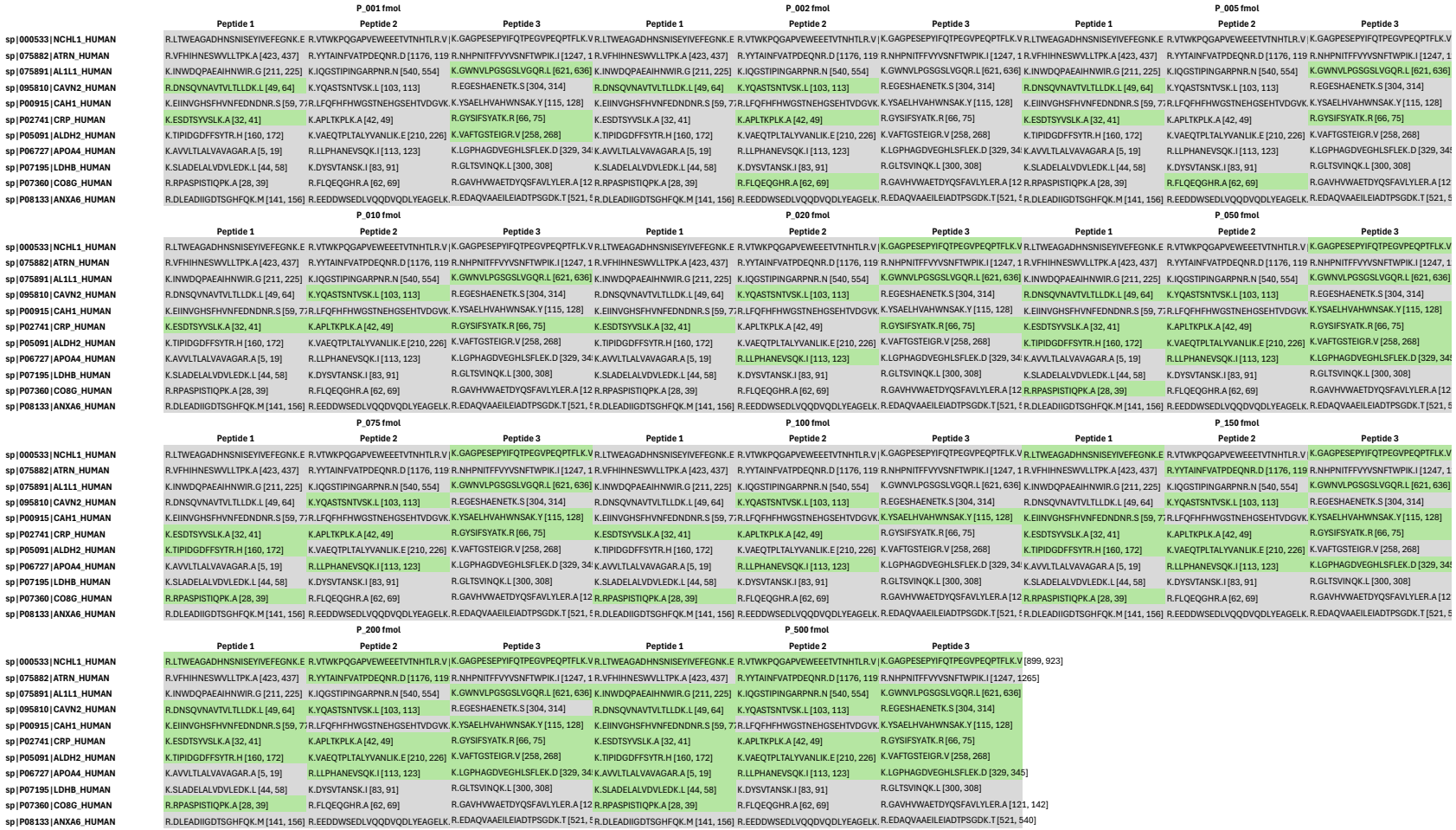

Figure 23. Detection matrix across heavy:light titrations. Figure showing peptide detectability across varying heavy-to-light (H/L) ratios in PRM titration experiments. Each column represents a specific H/L titration condition, and each row corresponds to a OxConCAT peptide. Green-highlighted peptides were consistently detected with stable signal intensity across titrations, indicating strong ionisation efficiency and robustness for quantitative analysis. Grey entries denote peptides that were undetected or inconsistently detected, likely due to ion suppression, low ionisation efficiency, or co-elution effects. These results identify a subset of peptides that maintain reliable performance under variable loading conditions, supporting their selection for absolute quantification workflows.

The distribution of green-highlighted peptides across titration levels delineates the optimal concentration window where detection remains both sensitive and stable. Adjusting the heavy-to-light ratio within this range improved the detectability of low-abundance peptides and minimised signal suppression. The findings also highlighted that certain peptides, while theoretically suitable, underperformed under experimental conditions, underscoring the necessity of empirical validation rather than relying solely on in silico peptide predictions. This empirical insight was particularly valuable for refining digestion protocols and optimising peptide loading, ensuring that target peptides were quantifiable even in the presence of complex plasma matrices.

Physicochemical factors such as hydrophobicity, peptide length, sequence composition, and charge state play central roles in determining ionisation efficiency and fragmentation quality. Peptides with highly hydrophobic sequences or poor fragmentation behaviour often showed inconsistent signals, even when present in sufficient concentrations. This observation reinforces the importance of experimental screening to verify theoretical predictions and exclude peptides with unstable or inconsistent performance. By integrating these empirical data, the QconCAT design process evolved into an iterative workflow, combining computational peptide selection with validation-based exclusion of underperforming candidates.

The refined dataset enabled targeted construct design improvements. Peptides demonstrating stable and reproducible detection across all titration points (green) were retained for subsequent OxConCAT iterations, ensuring that only the most analytically reliable candidates were included. This rational selection process enhances construct precision, expands the quantifiable dynamic range, and improves reproducibility in PRM-based absolute quantification workflows. It also allows more accurate stoichiometric

balancing of heavy and light peptide components, reducing competitive ionisation effects and signal distortion.

Beyond construct optimisation, these findings have broader methodological implications. The titration results informed the selection of spiking concentrations to prevent overloading of the OxConCAT internal standard, which can suppress endogenous peptide signals. They also provided guidance for chromatographic optimisation by identifying peptides prone to co-elution or retention anomalies, enabling gradient fine-tuning and improved separation. In clinical plasma applications, where matrix effects can significantly distort ionisation, this knowledge supports the implementation of customised sample preparation strategies that enhance reproducibility and quantitative confidence. Ultimately, this titration matrix functions as a diagnostic map to understand peptide behaviour under competitive ionisation conditions. It bridges the gap between theoretical design and functional quantification performance, offering a framework for systematically evaluating peptide robustness before integration into large-scale OxConCAT workflows. Through this approach, empirical titration analysis directly informed construct refinement, sample loading optimisation, and chromatographic stability improvements, strengthening the analytical reliability of the OxConCAT quantification pipeline.

Figure 24 provides a complementary overview of chromatographic performance for a representative titration experiment. The total ion chromatogram (TIC) and base peak chromatogram (BPC) illustrate peptide elution over time, revealing distinct peaks corresponding to different peptides within the OxConCAT construct. The high-intensity peak near 20 minutes indicates the elution of late-binding or hydrophobic peptides, highlighting the necessity for optimised gradient conditions and balanced sample loading strategies to ensure consistent detection across all peptides.

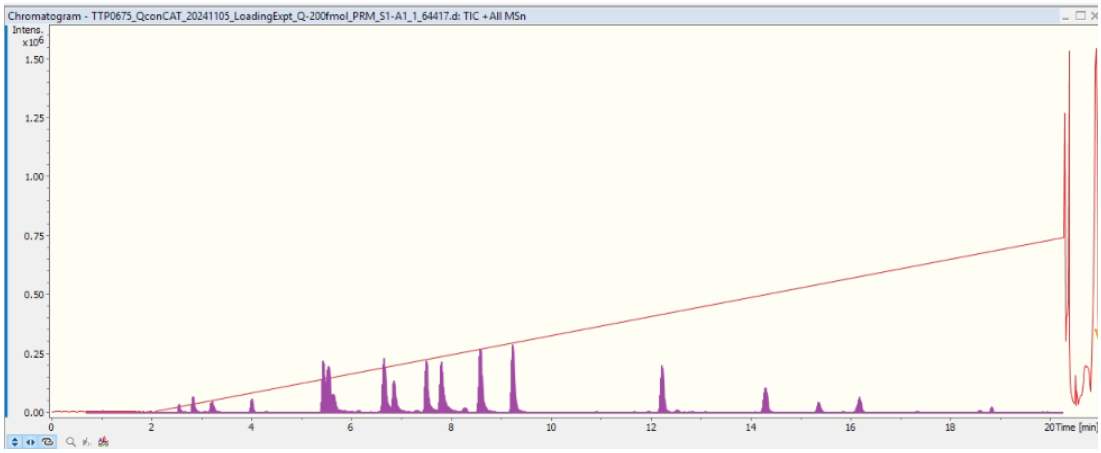

Figure 24. Chromatographic Overview of PRM Acquisition for 200 fmol OxConCAT. Total ion chromatogram (TIC, purple) and base peak chromatogram (BPC, red) from a PRM run of a 200 fmol OxConCAT sample in which n=21 target peptides were detected. The BPC shows the most intense ions at each time point, while the TIC reflects cumulative fragment ion signals across the gradient. The gradual intensity rise indicates peptide elution, with a distinct late peak (~20 min) corresponding to hydrophobic peptides, highlighting the importance of optimised gradient and loading conditions for consistent ionisation and resolution.

3.15 Addressing Competition Effects During Loading

A major challenge in OxConCAT-based quantification is the competition between co-eluting peptides for ionisation. This issue was particularly pronounced in cases where high concentrations of heavy peptides suppressed the signals of their light counterparts. To mitigate this effect, several strategies were evaluated, including adjusting the peptide loading order: experiments compared different sequences of heavy and light peptide introduction to determine the optimal approach. Additionally, buffer composition was optimised, with buffer conditions refined to minimise retention variability and enhance peptide solubility. Furthermore, widening PRM acquisition windows involved adjusting PRM parameters to accommodate peptides with minor retention time shifts, thereby improving overall detection rates.

Careful control of sample loading conditions may enhance detection rates and quantification accuracy, highlighting the importance of standardised preparation

protocols. Refining OxConCAT-based peptide quantification requires a comprehensive approach that incorporates peptide selection, titration optimisation, and sample loading strategies. These key improvements may boost reproducibility, signal consistency, and accuracy in PRM workflows.

Iterative Refinement of OxConCAT Design

Quantitative Concatemer (QconCAT) technology provides a platform for absolute protein quantification, offering high precision and reproducibility in targeted proteomics. Its success, however, relies heavily on optimal peptide selection and fine-tuning of experimental parameters. While theoretical predictions guide the initial construct design, empirical validation is essential to ensure consistent performance in complex biological matrices. This section outlines the iterative refinements undertaken to optimise peptide selection and heavy-to-light ratio calibration, forming the foundation for accurate and reproducible quantification.

Refining Peptide Selection for OxConCAT Constructs

Peptide selection followed established theoretical criteria, including optimal length for tryptic digestion, favourable amino acid composition, and high predicted ionisation efficiency, while excluding sequences susceptible to post-translational modifications or miscleavages. Unique, protein-specific peptides were prioritised to prevent cross-detection of homologous sequences. However, experimental analyses revealed that some theoretically suitable peptides produced weak signals, poor fragmentation, or high interference in plasma matrices. To address this, an iterative empirical validation process

was implemented. Peptides were systematically ranked using PRM data based on signal intensity, fragmentation quality, and reproducibility across replicates (sections 3.18-4.20). Only peptides meeting these performance thresholds were retained in the final construct (Section 4.9, Figure 41). This data-driven refinement ensured that selected peptides displayed detectability and consistent quantification, improving the overall reliability of the QconCAT workflow.

Optimising Heavy-to-Light Peptide Ratios

A key challenge in OxConCAT-based quantification is achieving an appropriate balance between heavy-labelled (QconCAT-derived) and endogenous light peptides. Excessively heavy peptides can cause ionisation competition, leading to signal suppression, whereas insufficient levels reduce quantitative precision. Titration experiments were conducted to evaluate peptide response curves and determine the dynamic range for accurate measurement. Results revealed that an intermediate heavy-to-light ratio provided optimal quantification, maintaining sensitivity without inducing suppression. This iterative optimisation established the concentration window that supports both reproducibility and accuracy, reducing artefacts linked to ionisation competition. The resulting refinement can enhance the robustness of OxConCAT-based absolute quantification and ensure reliable application to complex biological samples.

3.16 Enhancing Reproducibility and Biomarker Applicability

The refined OxConCAT workflow was systematically evaluated for its ability to deliver robust and reproducible protein quantification. Methodological improvements, including optimised peptide selection, titration-based calibration of heavy-to-light ratios, and

refined sample preparation, significantly enhanced detection sensitivity and measurement consistency. Compared with earlier iterations, the optimised workflow demonstrated improved peptide detectability and more substantial quantitative precision, underscoring the value of iterative optimisation in achieving reliable performance across complex plasma samples. The development of OxConCAT-based quantification relied on an ongoing feedback cycle that integrated theoretical peptide design with empirical validation. By refining peptide selection based on experimental data and optimising isotope ratios, this study established a reproducible framework for absolute quantification in targeted proteomics. These cumulative refinements strengthened the analytical robustness of the OxConCAT platform and its potential application in biomarker discovery. Subsequent work is directed towards expanding validated peptide libraries, exploring alternative digestion protocols, and incorporating advanced analytical methods to enhance sensitivity and reproducibility. This iterative process ensured continual improvement of OxConCAT-based workflows. (Figure 25).

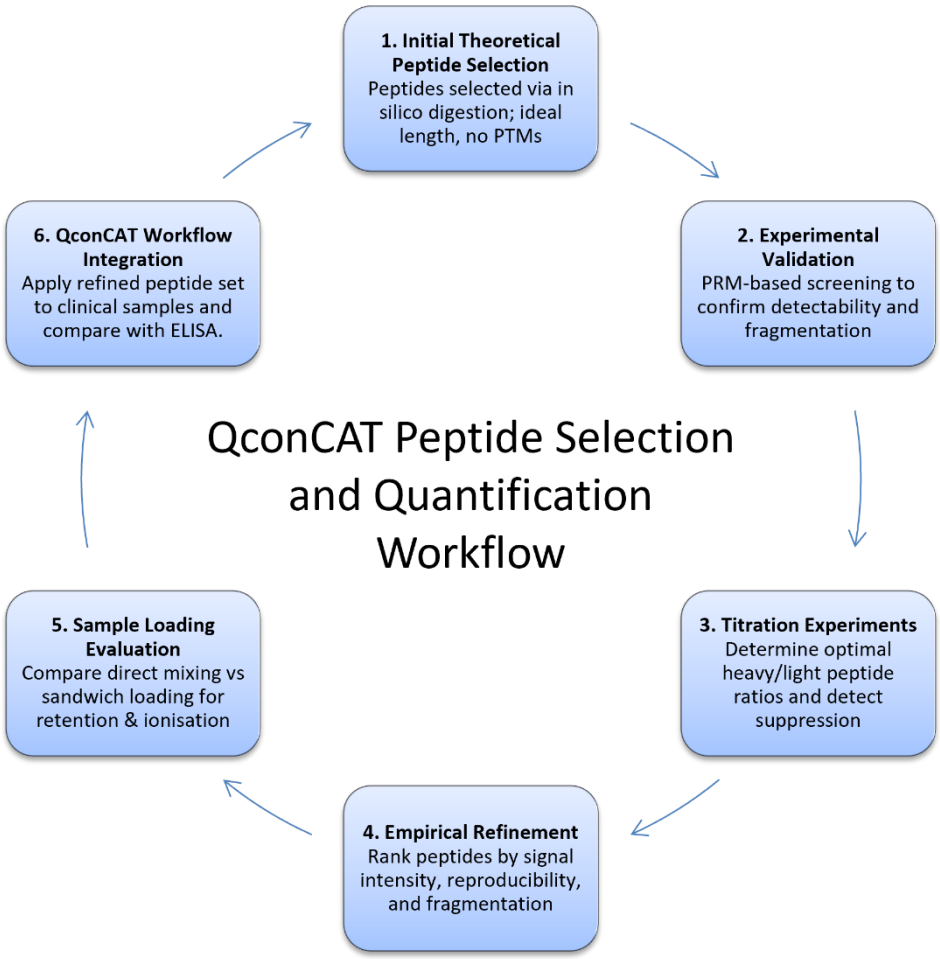

Figure 25. Iterative Workflow for Refining OxConCAT-Based Peptide Quantification. This diagram illustrates the stepwise strategy for optimising OxConCAT peptide selection and quantification. Starting with theoretical peptide predictions, each stage, experimental validation, titration, empirical refinement, loading evaluation, and clinical integration, builds toward a robust and reproducible workflow. The circular layout reflects the iterative nature of refinement, ensuring continual improvement based on experimental feedback.

Computational Optimisation Results

3.17 Results and Analysis: Score Progression, Generational Ranking, and Stability Predictions

This section presents the computational optimisation results for the OxConCAT construct, focusing on thermodynamic stability (ΔG), generational score progression, and the influence of metal coordination on structural robustness.

Successive generations were evaluated to assess improvements in folding energy and to identify convergence trends within the optimisation pipeline. As summarised in Table 10, the distribution of thermodynamic scores across generations demonstrated progressive refinement, with evident variability in stability metrics.

The best-performing model (Gen 2, ΔG = −1814) represented a 12% improvement in thermodynamic potential compared with the original sequence (Table 10). Later generations did not surpass this performance, indicating a plateau in optimisation efficiency. The incorporation of zinc resulted in better structural scoring, suggesting the importance of metal coordination in stabilising the construct.

Table 10. Thermodynamic Score Progression.

Generation	Mean Score (ΔG)	Standard Deviation	Best Score	25th Percentile	50th Percentile	75th Percentile	Worst Score
Original	-1547	66	-1595	-1571	-1547	-1524	-1500
Gen1	-1335	187	-1728	-1497	-1329	-1192	-935
Gen2	-1611	90	-1814	-1667	-1619	-1573	-1064
Gen3	-1569	310	-1764	-1662	-1618	-1556	1644
Gen4	-1631	80	-1790	-1678	-1639	-1593	-1245
Gen5	-1611	95	-1807	-1663	-1617	-1579	-982
Gen6	-1591	97	-1811	-1647	-1600	-1555	-1071

Computational Approach

The optimisation of peptide fragment arrangements was carried out using a brute-force permutation method combined with iterative refinement. From the initial OxConCAT sequence, 1,000 permutations were generated and evaluated for thermodynamic potential. The top-performing sequences were subsequently refined using evolutionary algorithms to enhance stability and folding efficiency.

Generations and Ranking of Optimised Sequences

In the first generation, peptide fragments were randomly shuffled to create a diverse set of sequence configurations. The second through fifth generations employed a Markov chain-based approach, incorporating frequency weighting for high-performing fragment pairs and triplets derived from earlier iterations. As shown in Table 10, the second generation achieved the most substantial improvement, while later generations yielded limited additional gains, suggesting convergence toward a local optimum.

By the sixth generation, a hybrid strategy was adopted in which the best-performing subsequences were concatenated and randomly interchanged to increase sampling diversity. Although this approach generated alternative high-scoring variants, the median thermodynamic potential remained lower than that of the second generation, confirming that the best configuration likely resided within the Gen 2 solution space.

Sequence clustering using t-distributed Stochastic Neighbour Embedding (t-SNE) and k-nearest-neighbour analyses revealed that approximately 82% of all sequences were more closely related to gen2_250 than to gen6_238, indicating strong local convergence within the optimisation landscape (Table 11).

Table 11. Ranking of Optimised Sequences.

Index	Sequence ID	Whole Score	Quantile to Lead
1	gen2_250	-1850.6	3
2	gen6_238	-1841.1	0
3	gen2_206	-1829.8	82.8
4	gen5_016	-1827.5	0.8
5	gen4_095	-1824.4	51.4
6	gen2_079	-1821.9	57.3
7	gen2_082	-1816.2	74.4
8	gen4_066	-1808.2	47.8
9	gen5_077	-1804.7	24.3
10	gen3_118	-1802.6	17.5

These findings suggested two main possibilities: either the search space had been insufficiently sampled, warranting further exploration using more advanced algorithms, or the optimisation had reached its theoretical limit under current modelling constraints.

Sequence Scoring and Refinement

The scoring framework incorporated hydrophobic exposure penalties, secondary structure compatibility, and backbone flexibility. As illustrated in Figure 26**,** the distribution of scores demonstrated that most sequences clustered between −1800 and −1600 ΔG, indicating moderate yet consistent improvements. The best-performing sequence achieved a 12% increase in thermodynamic potential relative to the original model and a 20% improvement over random permutations.

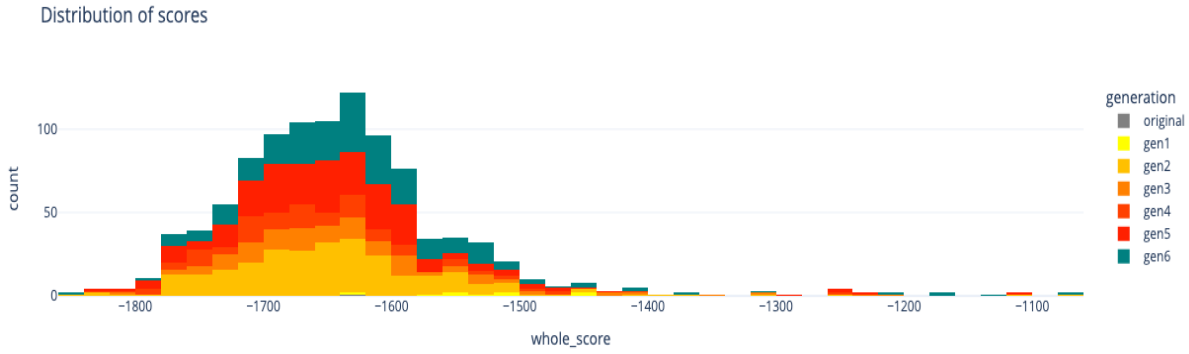

Figure 26. Distribution of stability scores (ΔG) across generations. This figure shows the spread of thermodynamic scores across all optimisation generations, with the original sequence in grey and subsequent generations colour-coded. The concentration of high-performing models around −1600 ΔG indicated diminishing returns in later generations. Figure reproduced in collaboration with Dr Matteo Ferla (University of Oxford).

Visual inspection of the predicted secondary structures confirmed these trends. The original peptide structure (Figure 27) was predominantly disordered, containing sparse α-

helices and β-sheets. The peptide fragment arrangement (Figure 28) illustrated extensive coil regions with limited secondary organisation, explaining the relatively low thermodynamic stability of the unoptimised native construct.

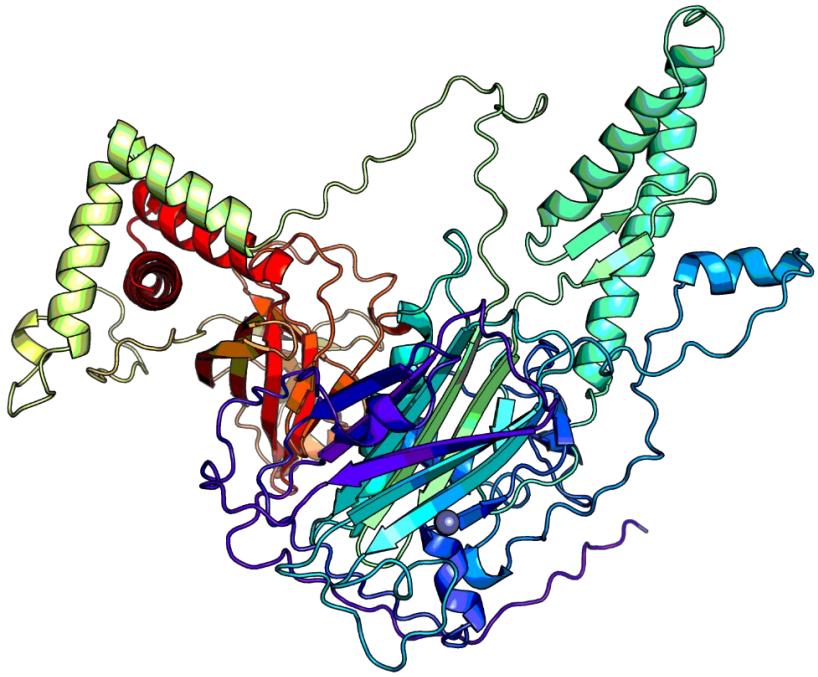

Figure 27. Original Peptide Structure. The non-optimised native OxConCAT construct exhibited extensive random coil regions with few ordered elements. Figure reproduced in collaboration with Dr Matteo Ferla (University of Oxford).

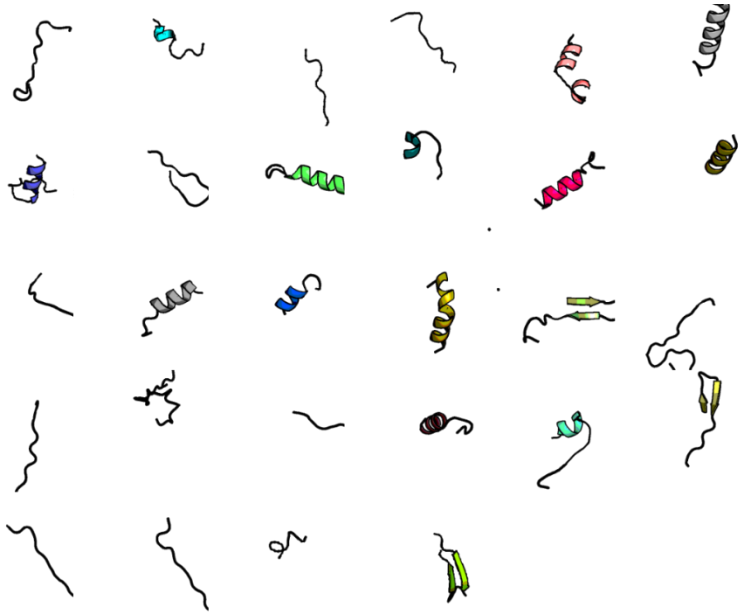

Figure 28. Peptide Fragment Arrangements in the Original Sequence. This image illustrates the secondary structure distribution in the original sequence, highlighting the native arrangement of peptide fragments. The black lines represent random coil regions, while coloured elements indicate secondary structures (alpha-helices and beta-sheets). Figure reproduced in collaboration with Dr Matteo Ferla (University of Oxford).

The original sequence (grey) maintains its distinctiveness from subsequent generations. The optimised sequences tend to cluster centrally, indicating convergence in thermodynamic characteristics. Higher-generation variants (red and blue) exhibit increased diversity, suggesting ongoing sequence evolution (Figure 29).

Figure 29. t-SNE Clustering of Sequence Variants. This figure visualises the relationships between different sequence variants using t-distributed Stochastic Neighbour Embedding (t-SNE). Each dot represents a sequence variant, with colours corresponding to other generations. Optimised generations clustered centrally in thermodynamic space, demonstrating convergence in folding characteristics and minor diversification in higher iterations. Figure reproduced in collaboration with Dr Matteo Ferla (University of Oxford).

Compared to the original sequence, the structural compactness has improved, indicating an overall enhancement in thermodynamic stability. Some regions of random coil persist, suggesting scope for further optimisation. This represents the final, best-optimised structure attained after six generations of refinement. The structure, obtained in Generation 2, exhibits increased compactness, characterised by a higher prevalence of helices and beta-sheets. A substantial reduction in random coil regions signifies enhanced structural stability. The remaining weak points highlight potential areas for additional refinement, possibly through further modifications in residue packing (Figure 30).

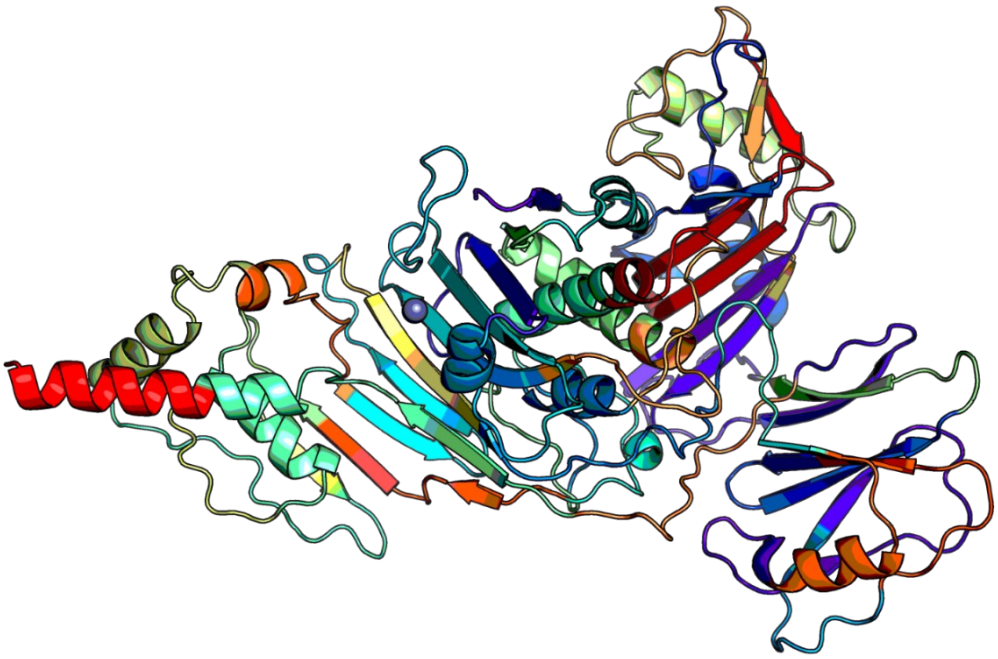

Figure 30. Optimised Structure in Generation 2. The best-performing OxConCAT sequence after computational refinement showed enhanced structural integrity and reduced disorder. Figure reproduced in collaboration with Dr Matteo Ferla (University of Oxford).

Experimental Comparison of Loading Strategies

Loading strategies and "Sandwich" loading experiment

3.18 Introduction and Experimental Overview

The accuracy and reproducibility of OxConCAT-based absolute quantification depended on multiple parameters, including peptide selection, sample preparation, and data acquisition. Among these, the method of sample loading was identified as a critical determinant of quantitative consistency. Variations in peptide recovery, ionisation efficiency, and chromatographic behaviour often originated from differences in how samples were introduced into the instrument.

To address this, a series of controlled experiments was conducted to compare multiple loading strategies and identify the most effective method for achieving reproducible peptide quantification. The comparison focused on co-digestion, pre-mixed digestion, sequential loading (P-then-Q), and a modified "sandwich" loading approach. Control analyses were also performed using plasma-only and OxConCAT-only digests (hereafter referred to as QConCAT with "Q" for simplicity) to establish baseline peptide profiles and verify normalisation accuracy.

Experimental Overview and Sample Loading Strategies

A comparative study was conducted to evaluate six distinct sample loading methods, each designed to assess the reproducibility and efficiency of peptide quantification in QconCAT-based workflows. These methods included:

- Co-Digestion (CD): Plasma and QconCAT peptides were digested together with a calculated injection of 200 ng plasma and 200 fmol QconCAT.
- Mix (M): 200 ng plasma digest and 200 fmol QconCAT digest were prepared separately and mixed before loading onto Evotips.
- P-then-Q (P–Q): 200 ng plasma digest was first loaded onto an Evotip, followed by 200 fmol QconCAT (OxConCAT) on the same tip.
- Sandwich Loading (S): 200 ng plasma (5 µL) was pipetted into the bottom of an Evotip, followed by 10 µL 0.1% formic acid (with air gaps above and below), and finally 200 fmol QconCAT in 5 µL.
- Plasma-only (P): 200 ng plasma digest only.
- QconCAT-only (Q): 200 fmol OxConCAT digest only.

Control experiments using plasma-only and QconCAT-only digests were analysed separately to assess background interference and confirm normalisation accuracy. Each loading method was tested in triplicate using both Parallel Reaction Monitoring (PRM) and Data-Independent Acquisition (DIA) workflows. The primary goal was to determine which approach minimised peptide loss, improved reproducibility, and yielded consistent quantitative performance.

3.19 Comparative Evaluation of Sample Loading Strategies (Co-Digestion, Sequential Digestion, Sandwich Loading)

The comparative evaluation of loading strategies revealed distinct differences in peptide recovery, signal intensity, and reproducibility across methods. Among all approaches, the Mix (M) method demonstrated the most consistent performance, exhibiting minimal variability in heavy peptide signal intensities and reduced OxConCAT (QconCAT) peptide loss.

The Co-Digestion (CD) method, while conceptually advantageous for ensuring uniform peptide representation, introduced moderate variability. Several peptides showed lower-than-expected intensities, likely due to digestion competition or matrix effects affecting peptide detectability.

The P-then-Q (P–Q) method produced greater variability than anticipated. Although sequential loading was expected to enhance peptide distribution, the non-uniform dispersion of peptides within the Evotip resulted in retention-time shifts and irregular intensities, limiting reproducibility.

Contrary to initial expectations, the Sandwich Loading (S) technique, developed to reduce ion suppression by layering plasma, buffer, and QconCAT digest, did not provide measurable improvements. Although initially hypothesised to reduce ion suppression, experimental evaluation did not support this. Instead, it introduced additional complexity without enhancing peptide recovery or ionisation stability. Air gaps and multi-layer buffer steps appeared to increase signal variability, particularly for heavy peptides. Overall, these findings collectively indicated that direct mixing of QconCAT and plasma digests before loading was identified as the most reproducible and effective strategy for consistent peptide recovery and stable signal intensity in absolute quantification workflows, providing the optimal balance between simplicity, reproducibility, and signal consistency for PRM-based OxConCAT analyses (Figure 31).

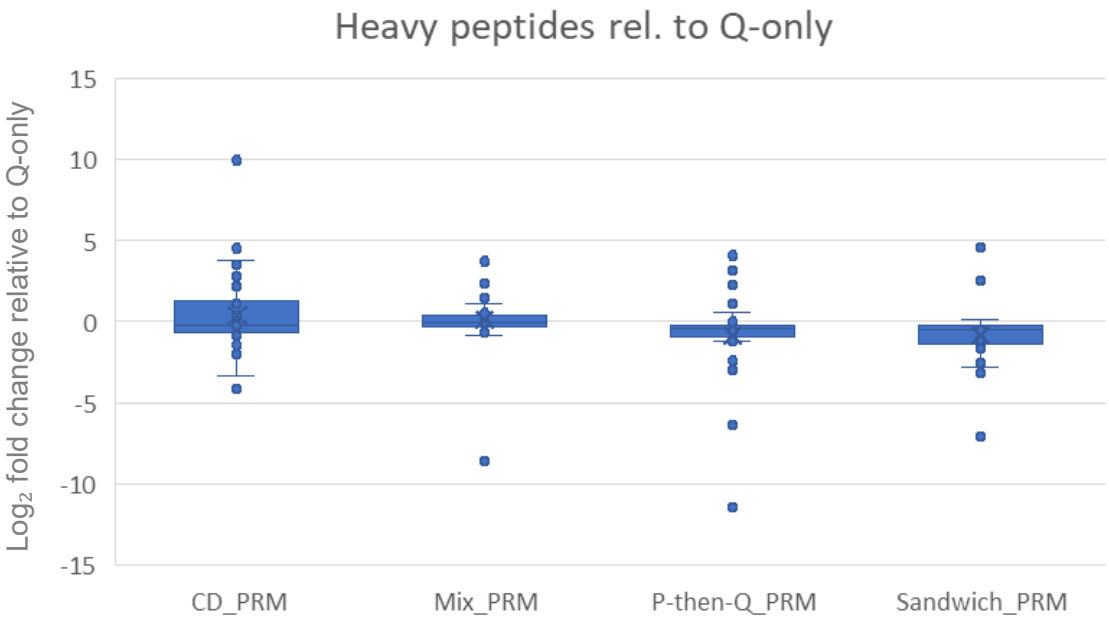

Figure 31. Effect of loading strategy on heavy-peptide signal. Box plot showing log_2-transformed total fragment peak areas of heavy peptides across four PRM loading strategies: Co-digestion (CD_PRM), Mixed digest (Mix_PRM), Plasma-then-QconCAT (P–then–Q_PRM), and Sandwich loading (Sandwich_PRM), all normalised to the QconCAT-only (Q-only) control. Greater dispersion in CD_PRM indicated inconsistent peptide recovery, whereas Mix_PRM and Sandwich_PRM showed tighter distributions and improved signal stability. The y-axis represents the log_2 fold change in heavy-peptide peak area relative to Q-only. A value of 0 indicates equal intensity, positive values correspond to enhanced recovery, and negative values reflect suppression or loss. The log_2 transformation normalised the scale, facilitating comparison across methods. Figure reproduced in collaboration with Dr Sarah Flannery (University of Oxford).

To quantitatively assess analytical precision in the sample mixing experiment, peptide-level coefficients of variation (%CV) were calculated from heavy fragment ion peak areas across technical replicates within each loading condition. For each workflow, the median %CV across peptides was determined.

The median %CV values were as follows:

- CD_DIA: 13.40%
- CD_PRM: 12.83%
- Mix_DIA: 12.06%

- Mix_PRM: 6.48%
- P-then-Q_DIA: 10.60%
- Q_DIA: 14.81%
- Q_PRM: 11.31%
- Sandwich_DIA: 9.43%
- Sandwich_PRM: 10.20%

Across acquisition strategies and loading conditions, median %CV values ranged from 6.48% to 14.81%. PRM-based measurements demonstrated lower median variability in certain conditions (e.g., Mix_PRM 6.48%) compared with corresponding DIA analyses. All workflows exhibited median %CV values within ranges generally considered acceptable for targeted proteomic quantification experiments. These results provide a numerical assessment of intra-condition reproducibility and directly address the precision of the heavy peptide quantification workflow.

3.20 Key Findings: Heavy Peptide Recovery and Variability

To evaluate the impact of each loading strategy, total fragment peak areas were $\log_2$-transformed and normalised against QconCAT-only values, allowing direct comparison of peptide intensities across conditions. The Mix (M) method demonstrated the least variability in heavy peptide signal intensities, with minimal loss of QconCAT peptides compared to other methods. Co-digestion (CD) introduced moderate variability, with several peptides showing lower-than-expected signals consistent with matrix-dependent differences in proteolysis. In contrast, the P-then-Q strategy produced inconsistent heavy/light ratios, likely due to variable capture of QconCAT peptides when applied after plasma onto a partially saturated C18 bed. The sandwich loading approach, designed to

stabilise QconCAT recovery by pre-binding it to the C18 resin, did not significantly alter chromatographic elution or reduce ion suppression. Empirically, sandwich loading provided no clear advantage over alternative methods, and variability remained highest for several heavy peptides, indicating that tip capacity and loading reproducibility were the dominant influencing factors (Figure 32). These findings suggested that direct mixing of plasma and QconCAT digests before loading offered the most reliable approach for QconCAT-based quantification, ensuring minimal peptide loss and consistent recovery across replicates.

- K.**GVVNVLPGSGSLVGQR**.L [621, 636] (AL1L1)
- R.**DNSQVNAVTVLTLLDK**.L [49, 64] (CAVN2)
- K.**EIINVGHSFHVNFEDNDNR**.S [59, 77] (CAH1)
- K.**YSAELHVAHWNSAK**.Y [115, 128] (CAH1)
- K.**ESDTSYVSLK**.A [32, 41] (CRP)
- K.**APLTKPLK**.A [42, 49] (CRP)
- K.**VAEQTPLTALYVANLIK**.E [210, 226] (ALDH2)
- K.**VAFTGSTEIGR**.V [258, 268]
- K.**AVVLTLALVAVAGAR**.A [5, 19] (APOA4)
- R.**LLPHANEVSQK**.I [113, 123] (APOA4
- K.**LGPHAGDVEGHLSFLEK**.D [329, 345] (APOA4)
- R.**RPASPISTIQPK**.A [28, 39] (CO8G)

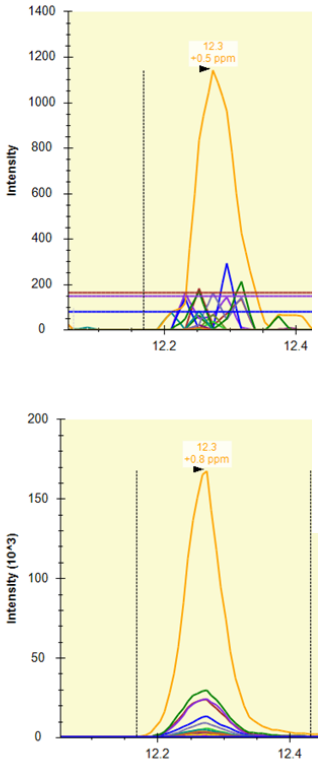

Figure 32. PRM chromatograms illustrating endogenous (light) and stable isotope-labelled (heavy) peptides across loading strategies. Representative PRM chromatograms are shown, with the upper panel displaying the endogenous (light) peptide and the lower panel showing the corresponding stable isotope-labelled (heavy) peptide. Across loading strategies, endogenous peptide signals varied in magnitude, and several targets fell below the integration threshold. A representative light peptide eluted at ~12.3 min with sub-ppm mass error and consistent fragment co-elution; however, peak areas differed by loading method, leading to intermittent non-detection for some strategies. In contrast, the heavy peptide showed consistent detection across conditions, implicating loading capacity at the C18 stage rather than LC elution differences.

Endogenous peptides detected included AL1L1, CAVN2, CA1, CRP, ALDH2, APOA4, and C8G, indicating biological relevance of the panel. Only a subset of light peptides was consistently detected across all loading conditions, with others falling below the detection threshold. This indicated that sample loading techniques influenced endogenous peptide quantification, likely through matrix effects, ion suppression, or retention shifts. Fragmentation patterns of light peptides closely resembled those of their heavy counterparts, confirming that OxConCAT provided a reliable internal reference. However, light peptides generally exhibited lower intensities, underscoring the difficulty of quantifying low-abundance peptides within complex biological matrices.

From the light peptide quantification analysis, the LGPHAGDVEGHLSFLEK (Figure 33, left peptide) suggests an abundance higher than 200 fmol, which is the expected OxConCAT concentration. This implies that this peptide might be overestimated due to stronger ionisation efficiency or lower interference from the sample matrix. Conversely, LLPHANEVSQK (Figure 33, right peptide) appears less abundant than OxConCAT, indicating potential underestimation caused by ion suppression or inefficient fragmentation. These conflicting results within the same protein highlight a fundamental challenge in absolute quantification: not all peptides behave the same, even when derived from the same protein and identical stoichiometry.

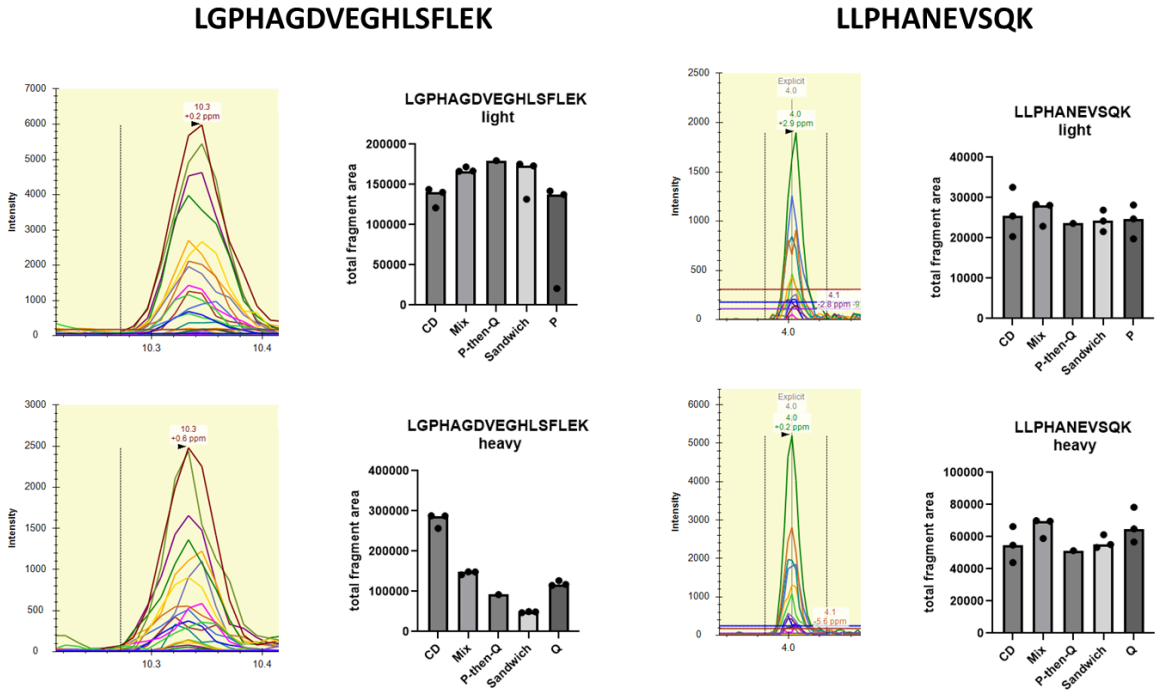

Figure 33. Inconsistencies in Light Peptide Quantification. Two APOA4-derived light peptides displayed conflicting quantification results, highlighting peptide-specific behaviour in OxConCAT-based absolute quantification. The peptide LGPHAGDVEGHLSFLEK appeared to exceed the expected 200 fmol OxConCAT concentration, whereas LLPHANEVSQK yielded a lower apparent abundance. Figure reproduced in collaboration with Dr Sarah Flannery (University of Oxford).

Peptide-Level Divergence Within a Single Protein and Selection of Quantotypic Peptides – the APOA4 Case Study

This observed divergence in quantitative behaviour between two peptides originating from the same protein prompted a deeper investigation into the underlying causes. To better understand these discrepancies, APOA4 was selected as a case study to examine how the sequence location, structural context, digestion efficiency, and analytical performance contribute to peptide-specific differences, and how these factors inform the selection of robust quantotypic peptides for absolute quantification. In targeted proteomics, individual tryptic peptides act as analytical surrogates for their parent

proteins. However, peptides from the same protein can display divergent quantitative behaviour due to sequence-specific biochemical properties, structural context, or analytical artefacts. Careful peptide selection is therefore essential for robust inference at the protein level.

3.21 Peptide Location within the APOA4 Sequence

Two tryptic peptides from APOA4 were evaluated in this study:

1. LLPHANEVSQK (APOA4_1) – located near the C-terminus, immediately upstream of the recombinant His-tag in the OxConCAT construct.
2. LGPHAGDVEGHLSFLEK (APOA4_2) – located within the central region of the protein.

Mapped positions (approximate):

...LGPHAGDVEGHLSFLEK.....LLPHANEVSQK.....HHHHHH

↑ (mid-region) ↑ (C-terminal)

3.22 Structural and Proteolytic Considerations

The peptide LLPHANEVSQK demonstrated a considerable increase in fold abundance in the subsequent pilot study quantification, situated at the C-terminal region near the terminus of the native protein, consistent with solvent exposure and efficient tryptic release at the C-terminus. This region exhibits fewer structural constraints. Trypsin efficiency is generally high in this area, as cleavage occurs after K. The peptide LGPHAGDVEGHLSFLEK, which consists of 17 amino acids, does not show a significant increase in fold abundance in the quantification study. It may be affected by incomplete digestion due to the presence of bulky, acidic, or glutamate residues. Missed cleavages are probable, given that the G–D–V–E–G–H sequence presents challenges for

trypsin. Furthermore, secondary structural constraints may be present if the peptide is buried within a domain or associated with lipids.

3.23 Technical Sources of PRM/MS Quantification Bias

LLPHANEVSQK utilised as a standard SRM/PRM peptide: short, no known modification, with a basic K at the end, resulting in a high response. In contrast, LGPHAGDVEGHLSFLEK is less optimal: it is longer, produces more complex fragmentation, and shows greater variability (Table 12).

Table 12. Comparison of physicochemical and mass spectrometric properties between two representative peptides used in SRM/PRM analysis.

Feature	**LLPHANEVSQK**	**LGPHAGDVEGHLSFLEK**
Length	11 aa	17 aa
Charge state	Likely +2	Likely +3
m/z	~600–700	~900–1000
MS detectability	High (ideal length, clean fragmentation)	Intermediate (longer, possible interference)
Retention time	Late (hydrophobic)	Mid-range

Suppose the same protein exhibits varying peptide responses. In that case, plausible explanations include proteolytic processing (e.g., increased prevalence of C-terminal fragments that elevate LLPHANEVSQK), degradation or conformational changes that expose some regions while masking others, and lipophilic interactions (e.g., lipid-associated conformations of APOA4 that obscure mid-region peptides). Another likely explanation is endogenous post-translational modification of the target protein: site-specific modifications (e.g., glycosylation, oxidation, deamidation) at or near a surrogate

peptide can shift mass, alter charge state, impede tryptic cleavage, or change chromatographic behaviour, thereby depressing the measured signal for the unmodified peptide while leaving other peptides relatively unaffected.

3.23.1 Observed Divergence in Quantitative Behaviour

Inconsistencies in light peptide quantification: the figure presented above (Figure 33) illustrates two APOA4 peptides in both endogenous ("light") and OxConCAT ("heavy") forms across various loading strategies. It is observed that the peptide LGPHAGDVEGHLSFLEK frequently exhibited higher abundance than the OxConCAT (~200 fmol), which may suggest over-integration, enhanced ionisation, or diminished suppression effects. Conversely, the peptide LLPHANEVSQK often demonstrated lower abundance relative to the OxConCAT, indicating potential underestimation due to ion suppression, inefficient fragmentation, or retention time shifts. Heavy peptides displayed stable signals, implying that the variability primarily resulted from endogenous light peptide detection. The challenges encountered in Light Peptide detection and quantification are significant, as many light peptides approached or reached the detection limit, thereby elevating variability. Retention time drift posed complications for PRM integration, with certain peptides necessitating manual adjustments to peak boundaries. The utilisation of a Q-only DIA file enhanced retention time alignment and peak selection for PRM analysis.

Regarding implications for absolute quantification, it is essential to consider peptide-specific effects prior to selecting a single peptide as a quantifier. Averaging multiple validated peptides per protein may mitigate the impact of outliers. Moreover, the criteria for choosing quantotypic peptides should encompass digestion stability, high response, low coefficient of variation (CV), and clean co-elution with heavy standards. Quality

control evidence for APOA4 LLPHANEVSQK indicates that cleaner chromatographic profiles, consistent RT, and low variability in the heavy form are retained as the primary quantotypic peptide. LGPHAGDVEGHLSFLEK: Retained for monitoring but excluded from primary quantification due to overestimation and higher variability in the light form (Table 13)**.** The recommendation from this case peptide analysis is the use of LLPHANEVSQK for APOA4 quantification, and to avoid relying solely on LGPHAGDVEGHLSFLEK unless digestion and interference issues are resolved. When multiple peptides are available, compare EICs, assess dot product (idotp), and filter by CV before averaging.

Table 13. Summary: The Differential Effects of Peptides on Variability.

Factor	**LLPHANEVSQK**	**LGPHAGDVEGHLSFLEK**
C-terminal, more accessible	✓	✗
Short, ideal for PRM	✓	✗
Digestion efficiency	High	Variable
Possible post-op cleavage effect	✓	✗
PTMs/missed cleavages are likely.	No	Yes
Signal variability	Low	High
Biologically meaningful region	Possibly yes	Less clear

3.24 Challenges in Light Peptide Detection and Quantification

While heavy-labelled peptides produced stable and reproducible signals, the detection of endogenous (light) peptides proved substantially more challenging due to their low abundance and proximity to the limit of detection. In several cases, peptides originating

from the same protein yielded inconsistent quantification results, such as the APOA4 pair, where one peptide indicated higher abundance than expected, while another suggested depletion. These discrepancies highlight the influence of peptide-specific behaviour and raise the question of whether averaging multiple peptides per protein might provide more reliable quantification. Retention time variability also complicates data interpretation. Several light peptides eluted later than their heavy counterparts, likely due to post-translational modifications such as glycosylation or sialylation that alter hydrophobicity, charge, and cleavage efficiency.

To address these shifts, a Q-only DIA run was used as a reference for peak alignment, and data were normalised using $\log_2$-transformed fragment ion areas relative to Q-only controls, improving consistency across loading conditions. Among all tested approaches, direct co-loading of OxConCAT and plasma digests prior to injection yielded the most reproducible results, showing minimal retention variability and optimal peptide recovery. In contrast, sandwich and sequential P-then-Q loading introduced unnecessary complexity and higher variability, while co-digestion suffered from digestion competition effects. Overall, reliable quantification of light peptides remains limited by sensitivity, peptide-specific variability, and matrix effects. Future optimisation will focus on improved peptide selection, enhanced detection sensitivity for low-abundance species, and refined retention alignment to strengthen the reproducibility of OxConCAT-based absolute quantification workflows.

Discussion

3.25 Interpretation of Experimental Optimisation

The experimental optimisation described in this chapter represents a critical advancement in transforming the OxConCAT construct from a conceptual tool into a quantitatively reliable analytical standard. Through the systematic comparison of digestion and loading strategies, including co-digestion, sequential digestion, and the innovative sandwich-loading approach, clear improvements were achieved in peptide recovery, reproducibility, and sensitivity. These optimisations directly addressed one of the principal challenges in targeted proteomics: the variable digestion efficiency and matrix-driven ion suppression that compromise quantitative accuracy in plasma samples. By modulating the concentration of heavy-labelled OxConCAT to endogenous peptides, the workflow established optimal heavy: light ratios that maintained linearity across concentration ranges, reduced competitive suppression, and enhanced signal-to-noise consistency. The titration experiments revealed that peptide-specific behaviour, rather than total protein concentration, largely governs reproducibility, emphasising the need for empirical validation of each quantotypic peptide. Collectively, these results demonstrate that analytical precision in PRM-based quantification can be substantially improved through fine-tuned control of digestion conditions and spike-in design.

3.26 Insights from Computational Modelling

Complementary to the empirical optimisation, the computational modelling framework developed in Sections 3.6–3.9 identified configurations with reduced aggregation propensity; results are summarised in Section 3.17. By applying random permutation,

Markov-chain modelling, and thermodynamic scoring, multiple generations of in silico constructs were evaluated to predict sequence stability, solubility, and proteolytic accessibility. The iterative modelling approach successfully identified configurations that minimised aggregation-prone motifs and improved predicted cleavage uniformity, features that correlated well with the empirical performance of peptides later validated experimentally. The optimisation of peptide fragment arrangement through computational methods yielded moderate but measurable thermodynamic gains, demonstrating the potential of sequence permutation as a viable strategy for enhancing peptide stability. The best sequence identified after 1,000 permutations exhibited a 12 % improvement in predicted thermodynamic stability relative to the initial construct. However, subsequent generations did not achieve further enhancement, indicating a point of diminishing returns. This plateau suggested that a brute-force optimisation strategy relying solely on random permutation and iterative refinement was limited in its ability to explore the broader sequence space and was unlikely to produce substantial additional gains in protein stability.

This pattern underscored a key limitation of the applied approach, the rapid convergence of the optimisation landscape. While early iterations produced tangible benefits, later rounds failed to generate new high-scoring configurations, indicating that the search space became locally saturated. To overcome this constraint, future optimisation frameworks should integrate evolutionary algorithms, tournament-based selection, or deep learning–driven models capable of navigating more complex, multidimensional sequence spaces. Such advanced frameworks could identify non-obvious but high-potential configurations that simple permutation methods might overlook.

A notable finding from the modelling was the stabilising effect of metal coordination. Incorporating zinc atoms into specific motifs after Generation I consistently improved

model stability scores. This observation reinforced the structural role of zinc-finger–like domains in promoting proper folding and increasing rigidity. Metal coordination appeared to stabilise local secondary structures and reduce disorder, suggesting that the deliberate inclusion of metal-binding residues could serve as an effective design principle for enhancing construct stability. The principal outcomes of this analysis were threefold. First, early random permutation cycles produced a measurable 12 % improvement in predicted stability, but subsequent gains plateaued, confirming the limitations of exhaustive heuristic optimisation. Second, zinc incorporation markedly improved structural stability, underscoring the potential of metal-assisted folding mechanisms. Third, t-SNE analysis of the optimisation trajectory revealed early convergence within the explored sequence space. While secondary-structure stability improved, residual local disorder persisted, highlighting opportunities for refinement through targeted sequence modification or spacer insertion.

Future optimisation strategies should therefore aim to expand sampling diversity and integrate machine-learning approaches capable of recognising complex sequence–stability relationships. Deep learning and hybrid modelling frameworks could enable the exploration of previously inaccessible configurations. At the same time, refined energy functions and residue-level scoring models would more accurately capture the physicochemical determinants of stability. In parallel, experimental validation of the highest-scoring constructs remained essential to verify computational predictions. In-vitro assays assessing expression yield and thermal stability would provide empirical confirmation of the model-derived insights. Overall, this work demonstrated the utility of computational modelling as a proof of concept for systematic sequence optimisation within OxConCAT design. The observed 12 % stability improvement confirmed that rational sequence permutation could enhance thermodynamic resilience, while also

revealing the limitations of purely stochastic approaches. The integration of script-guided modelling, metal-coordination strategies, and empirical validation represented the most promising direction for future OxConCAT construct design, as further explored in Chapter 5.

3.27 Analytical and Methodological Implications

Together, the experimental and computational findings establish a unified methodological platform that enhances both the precision and scalability of OxConCAT-based quantification. The dual optimisation strategy, combining empirical iteration with predictive modelling, yielded a workflow capable of addressing multiple analytical bottlenecks simultaneously: incomplete digestion, ion suppression, and peptide variability. This integrated approach transforms OxConCAT from a static internal standard into a dynamic system adaptable to different analytical contexts, including high-complexity plasma and potentially other biofluids. From a methodological perspective, this chapter reinforces the importance of peptide-level validation within quantitative proteomics. Rather than assuming uniform behaviour across peptides, each candidate was evaluated for chromatographic consistency. Such rigorous screening ensures that only the most stable, quantotypic peptides contribute to downstream quantification, thereby increasing the robustness of biomarker assessment in translational studies.

3.28 Case Study Integration: APOA4 Peptide Divergence

The APOA4 case study exemplifies the biological and analytical complexity inherent in peptide quantification. Despite originating from a single protein, APOA4 peptides displayed markedly different quantitative behaviours, reflecting both technical and biological influences. From a technical standpoint, co-eluting background ions and local hydrophobic interactions affected PRM peak quality, leading to differential detectability between light and heavy peptide forms. Biologically, structural flexibility and post-translational modification potential likely contributed to incomplete proteolysis and variable recovery. By dissecting these factors, the APOA4 analysis provided insight into how peptide selection can bias quantification if empirical behaviour is not carefully evaluated. The findings support the notion that even within well-characterised proteins, peptide-specific stability and accessibility must be verified experimentally before inclusion in absolute quantification panels. As a rule for panel curation: retain peptides that (i) co-elute with their heavy standards, (ii) exhibit CV ≤20% across replicates, (iii) maintain linearity over the titration window, and (iv) show no evidence of systematic interference or missed cleavages; retain a secondary peptide for monitoring where feasible. These lessons directly inform future OxConCAT design iterations, where structural and physicochemical diversity should be deliberately incorporated to ensure broad peptide robustness.

3.29 Summary and Future Directions

In summary, this chapter has demonstrated that comprehensive optimisation, spanning sample preparation, peptide competition control, and computational sequence design, can significantly enhance the reliability and reproducibility of quantitative proteomics

workflows. The integration of modelling and experimental evidence yielded a refined analytical strategy that is both data-driven and empirically validated. The improvements achieved here form the foundation for applying the optimised OxConCAT standard to real-world clinical samples. The following chapter, Chapter 4 - Pilot Proteomic Analysis of OxAAA Plasma, extends these findings to patient-derived specimens, evaluating the translational performance of the developed workflow in quantifying circulating biomarkers of abdominal aortic aneurysm progression.

Chapter 4 – Pilot Proteomic Analysis of OxAAA Plasma

Introduction

This chapter presents the pilot application of the optimised OxConCAT-based quantitative proteomics workflow to plasma samples collected within the OxAAA study. Building upon the methodological development and validation described in preceding chapters, this section demonstrates the translation of the refined analytical pipeline, comprising stable-isotope-labelled internal standards, optimised digestion protocols, and targeted PRM quantification, into a clinical context. The overall aim was to evaluate the practical feasibility, precision, and interpretative value of the OxConCAT strategy when applied to complex biological matrices such as human plasma obtained from patients with AAA before and after surgical intervention. To place the targeted quantification results within a broader biological and analytical framework, a complementary data-independent acquisition (DIA) analysis was first performed. The DIA component provided a discovery-level overview of global proteomic variation and confirmed expected post-surgical trends related to inflammation, immune activation, and metabolic remodelling. DIA was solely included as a contextual exploratory tool, not as a primary quantitative approach. Because of the complex and highly dynamic nature of plasma, DIA methods may exhibit limited sensitivity for certain proteins that ionise poorly or co-elute with abundant species; DIA sensitivity also depends heavily on instrument, library, and matrix. Consequently, some OxConCAT targets, such as APOA4 and Attractin, were not detected in the DIA dataset, most likely due to spectral library coverage and matrix interference rather than biological absence or low abundance. These targets were, however, quantified with high confidence by PRM, which offers greater selectivity and sensitivity through the use of isotope-labelled internal standards. Following the exploratory DIA analysis, the

OxConCAT internal standard was applied to the same plasma samples to enable absolute quantification using parallel reaction monitoring (PRM). This targeted approach focused on a predefined set of robust, quantotypic peptides validated in earlier optimisation experiments. The use of ^15N-labelled OxConCAT peptides ensured precise internal calibration, correcting for ion suppression, digestion variability, and chromatographic fluctuations. The inclusion of DIA alongside PRM represents a parallel analytical design: DIA establishes the global proteomic context and verifies overall data quality, while PRM delivers accurate, absolute quantification of clinically relevant targets central to the OxAAA study. Together, these approaches support both the analytical robustness and translational potential of the OxConCAT-based workflow, providing the foundation for large-scale absolute quantification across the whole OxAAA cohort and future international validation studies.

The chapter is structured first to outline the study design, experimental setup, and data acquisition parameters (Sections 4.1–4.3), followed by DIA-based comparative profiling (Sections 4.4–4.4.1), which provides the broader proteomic context for targeted quantification. Sections 4.5–4.12 present the absolute quantification workflow, peptide-level analyses, and cohort-level results, including fold-change and variability assessments. Finally, Section 4.12 integrates technical and biological interpretation, linking peptide detectability and matrix effects to protein expression patterns relevant to AAA pathophysiology. Collectively, this pilot study illustrates the translation of the OxConCAT strategy from methodological development to clinical application, establishing a foundation for large-scale absolute quantification within the OxAAA cohort and future validation studies.

Methods Overview

The pilot proteomic study of OxAAA plasma samples was designed to evaluate the performance of the optimised analytical workflow under real clinical conditions. Plasma aliquots collected at defined peri-operative timepoints were processed using the platelet-poor plasma (PPP) double-centrifugation protocol described in Chapter 2 to ensure platelet-free matrices and minimise pre-analytical variability. Following protein denaturation, reduction, alkylation, and enzymatic digestion, each sample was divided into two analytical streams.

To situate the targeted results within a broader biological context, a contextual data-independent acquisition analysis was performed on aliquots from the same plasma samples. The DIA component provided an unbiased, global overview of proteomic variation, helping to visualise overall trends and confirm the expected post-surgical shifts in inflammatory and metabolic proteins. However, given the complexity of plasma matrices and the need for consistent peptide detection, DIA was primarily used to provide context on peptide coverage and signal behaviour, rather than serving as the primary quantification method for OxConCAT targets. Some proteins of clinical relevance, such as APOA4 and Attractin, were not detected in the DIA dataset, likely due to spectral library limitations, peptide ionisation behaviour, or interference from highly abundant plasma proteins, rather than inherently low abundance. The combination of DIA and PRM therefore served complementary purposes: DIA offering exploratory insight into global proteomic alterations associated with surgery, and PRM delivering accurate, absolute quantification of predefined targets. This dual strategy ensured that the OxConCAT-based workflow was evaluated not only for analytical precision but also for biological relevance within the broader proteomic landscape of AAA. Therefore, the first stream employed the

DIA method to achieve comprehensive, unbiased protein coverage. DIA spectra were processed using spectral library-based identification and quantitative alignment across runs to assess proteome-wide expression patterns between pre- and post-surgical samples. The second stream implemented parallel reaction monitoring (PRM) for targeted absolute quantification of predefined OxConCAT peptides. Stable-isotope-labelled OxConCAT (^15N) standards were spiked into digested plasma at known concentrations prior to LC–MS analysis. The PRM method was optimised for dwell time, collision energy, scheduled windows, targeted transitions count, and iRT/RT calibration to maximise sensitivity and linearity across transitions (see Sections 3.18–3.23 and Figures 30–33). Together, these complementary approaches allowed simultaneous global profiling and quantitative validation within the same pilot cohort. The integrated design enabled assessment of both global proteomic changes and the quantitative reliability of OxConCAT peptides as internal standards, thereby establishing proof-of-principle for large-scale implementation in the complete OxAAA study.

DIA-Based Comparative Proteomic Profiling

4.1 Introduction and Experimental Design

The current pilot analysis represents a significant step in applying OxConCAT-based absolute quantification to investigate proteomic changes in platelet-poor plasma (PPP) in patients undergoing surgery. Its primary aim is to evaluate the feasibility, reproducibility, and robustness of the OxConCAT method for detecting and quantifying specific proteins before and after surgery. The study seeks to determine whether OxConCAT-based workflows can provide meaningful insights into protein expression changes related to physiological stress, recovery, and surgical impact. To address this, 20 paired plasma

samples were analysed, each collected at two time points: TP3 (before surgery) and TP5 (after surgery). The patient pilot cohort analysed in this section comprised ten individuals undergoing elective open surgical repair (OSR) for abdominal aortic aneurysm. Key cohort characteristics and sampling details are summarised below:

- Cohort size: 10 patients
- Sex: 9 male, 1 female
- Age at surgery: median 70 years (range 64–83)
- Baseline AAA diameter: median 5.75 cm (range 3.9–8.5 cm)
- Surgical approach: 100% open surgical repair (OSR), elective
- Major comorbidities: hypertension (80%), type 2 diabetes (30%), coronary heart disease (20%), cerebrovascular disease (10%)
- Baseline sampling (TP3): collected pre-operatively during routine surgical assessment
- Follow-up sampling (TP5/TPF): collected post-operatively at clinical follow-up visits, ranging from early recovery (~1–4 months) to long-term follow-up (up to ~4 years)

Full patient-level demographic, clinical, laboratory, and medication data, including exact sampling dates, are provided in Supplementary Table S1.

These time points were selected based on the hypothesis that significant proteomic changes occur in response to surgical trauma, immune activation, coagulation, and metabolic shifts. Using PRM and DIA mass spectrometry techniques aimed to identify proteins with differential expression and assess the effectiveness of various sample

processing strategies, digestion methods, and normalisation techniques. Additionally, due to challenges in detecting low-abundance peptides, this study also compares the efficiency of different digestion approaches to evaluate how consistently they recover peptides across different experimental setups. The results from this pilot will help improve OxConCAT workflows for larger clinical studies, advancing biomarker discovery and absolute quantification in human plasma proteomics.

4.2 Sample Collection, Preparation, and Digestion Strategies

Each patient sample was meticulously collected and processed to minimise variability. A total volume of 200 µL of plasma was obtained per patient, with 190 µL allocated for lipidomics study and 10 µL reserved for proteomic analysis. To ensure the integrity and stability of plasma proteins, the samples were immediately diluted 10-fold with RIPA buffer and stored at -80°C until analysis. The 10 µL proteomics fraction was diluted to 100 µL with RIPA buffer and aliquoted into 10 tubes for subsequent experiments.

Sample Preparation Protocol

To ensure consistent sample preparation, the following protocol was implemented: 1/10 Plasma Dilution, where 10 µL of plasma was combined with 90 µL of RIPA buffer, vortexed, placed on ice, and aliquoted into ten 10-µL fractions for storage at -80°C. For 1/100 Plasma Dilution, 2 µL of 1/10 plasma was mixed with 18 µL of RIPA buffer and vortexed. Regarding OxConCAT Stock and Dilutions: 1/10 OxConCAT (100 ng/µL), 10 µL of OxConCAT stock (1 mg/mL), was diluted with 90 µL of RIPA buffer. For 1/100 OxConCAT (10 ng/µL), 20 µL of 1/10 OxConCAT was diluted with 180 µL of RIPA buffer.

Experimental Design and Digestion Strategies

The study used a comparative approach to evaluate different digestion strategies for protein extraction and quantification. The following experimental conditions were assessed:

- 10 µg Plasma Digest: Plasma proteins were digested separately without adding QconCAT peptides to serve as a control.
- 10 µg Co-Digest: Plasma proteins and QconCAT peptides were digested together to ensure uniform peptide representation before analysis. For 10 µg plasma, 750 ng QconCAT was spiked in.
- 1 µg Co-Digest: Using 1/100 diluted plasma, 1 µg of plasma protein was combined with 75 ng QconCAT per digest to assess lower input feasibility.

Digestion Protocol

Protein digests were performed using the SP3 method.[72] QconCAT stock at 1 µg/µL was diluted either 1-fold or 100-fold with RIPA buffer. Plasma samples were diluted 10-fold or 100-fold, and 2 µL of plasma was combined with 7.5 µL of QconCAT or RIPA buffer. RIPA was used explicitly due to compatibility with SP3 cleanup. Magnetic beads were prepared by combining hydrophilic and hydrophobic beads in equal volume on the day of the experiment. The sample preparation steps were as follows: Bead Binding: 2 µL of the bead mix was added to 10 µL of the sample, followed by 27 µL of acetonitrile, and mixed at room temperature for 18 minutes at 1000 rpm. Cleanup Steps: Samples were placed on a magnet, and the supernatant was removed after 2 minutes. Beads were washed sequentially with 70% ethanol and acetonitrile before being resuspended in 45 µL of ammonium bicarbonate buffer (pH 8). Digestion: Proteins were digested overnight at

37°C with trypsin at a ratio of 1:25 enzyme to substrate. Peptide Elution: Digested peptides were removed from beads and acidified with 1% trifluoroacetic acid (TFA).

Mass Spectrometry Analysis

For label-free quantification, either 2% or 20% of the sample was loaded onto Evotips for LC-MS analysis. Peptides were separated using an Evosep One LC system and analysed on a Bruker timsTOF Pro mass spectrometer operating in diaPASEF mode. The acquisition settings included 8 diaPASEF scans per TIMS-MS scan, 100 ms accumulation and ramp time, 25 m/z isolation windows spanning 475-1000 m/z, and Ion mobility-dependent collision energy increasing from 20 eV to 59 eV. For PRM analysis, 2% of plasma-only digests were analysed alongside a 200 fmol OxConCAT tryptic digest using PRM-PASEF mode.

4.3 DIA Data Acquisition and Analysis

Data were examined using DIA-NN v1.9.2 against a predicted spectral library derived from the UniProt human proteome database (UP000005640, downloaded in January 2025).[73] The analysis considered peptides 7–30 amino acids in length, allowing one missed cleavage. Subsequently, data were processed in Perseus [74] with normalisation and imputation performed alongside Log2 transformation of protein intensity values. Filtering was applied to retain proteins present in at least 70% of samples within a single group. Proteins detected in at least 70% of samples within at least one group were retained, balancing data completeness and cohort coverage while avoiding biases introduced by overly stringent (≥80%) or permissive (≤50%) thresholds. Missing values were imputed using a downshifted normal distribution (Perseus default). Statistical analysis involved a paired Student's t-test with Benjamini-Hochberg FDR correction at a

5% threshold ($q<0.05$). All differential abundance analyses comparing pre- and post-operative samples were performed using paired statistical tests, explicitly accounting for within-patient matching.

Results

DIA-Based Comparative Profiling

The analytical workflows described above were applied to OxAAA plasma samples to assess proteomic variation before and after surgery and to validate the technical robustness of the optimised methods. DIA provided a global overview of protein abundance patterns, enabling both qualitative and quantitative comparison across patient timepoints. The resulting datasets were processed through predicted spectral libraries and subjected to multivariate statistical analysis to identify proteins contributing most strongly to intergroup variation. To visualise these global proteomic differences, two complementary approaches were employed. Volcano plot analysis (Section 4.4) was used to highlight proteins showing statistically significant fold changes between pre- and post-operative samples, providing a direct view of differential expression trends. Principal Component Analysis (PCA) and loadings plot interpretation (Section 4.4.1) were then used to explore overall data structure, clustering behaviour, and the principal contributors to observed variance. Together, these analyses delineate the proteomic landscape of the OxAAA pilot cohort and establish the biological and analytical context for subsequent absolute quantification using the OxConCAT internal standard.

4.4 Surgery-Associated Proteomic Changes in AAA Patients

The volcano plot offers a global overview of changes in protein levels between two conditions. Proteins with high statistical significance (log p-value) and large fold changes (log2 difference) are highlighted, helping to identify key regulated proteins. The analysis was based on paired comparisons between pre-operative (TP3) and post-operative (TP5/TPF) samples from the same individuals, thereby controlling for inter-individual variability. This provides a clear visual summary of proteomic changes between the two clinical states, with several notable patterns emerging. Upregulated proteins (right quadrant), such as IGKV3-7, IGKV1-39, IGLV2-11, CFH, and A1BG, show significant increases after surgery. Many of these are immunoglobulin components or inflammation-related molecules, indicating activation of immune response pathways post-surgery. The increased levels of FCGR3A and HP (haptoglobin) further support an inflammatory or acute-phase response. Downregulated proteins (left quadrant), including APOD, KNG1, BCHE, and C5, are significantly decreased after surgery. These likely reflect metabolic remodelling, lipid transport, or complement activity, suggesting suppressed metabolic or immune-modulatory functions during recovery or systemic stress. Highly significant proteins (top of the plot), such as GPLD1, C8B, C8G, PLTP, and F9, display both high–$\log_{10}$ (p-values) and moderate fold changes, indicating consistent differential abundance across samples with strong statistical support. These proteins may represent potential candidates for future targeted validation. Proteins annotated with cRAP (Common Repository of Adventitious Proteins, CRAPome),[75] like cRAP-C5 and cRAP-ALB, may signal background contamination or common plasma proteins observed in proteomic workflows. Their constant detection highlights the importance of careful data curation and peptide validation (Figure 34). This analysis identifies a set of statistically significant and biologically relevant proteins whose abundance changes after surgery. These results

match expected physiological responses, such as inflammation, immune modulation, and metabolic shifts. Proteins that pass the 5% FDR threshold should be studied further as potential peptide markers for surgical response and may be prioritised for targeted quantification using PRM or OxConCAT-based methods in future validation studies.

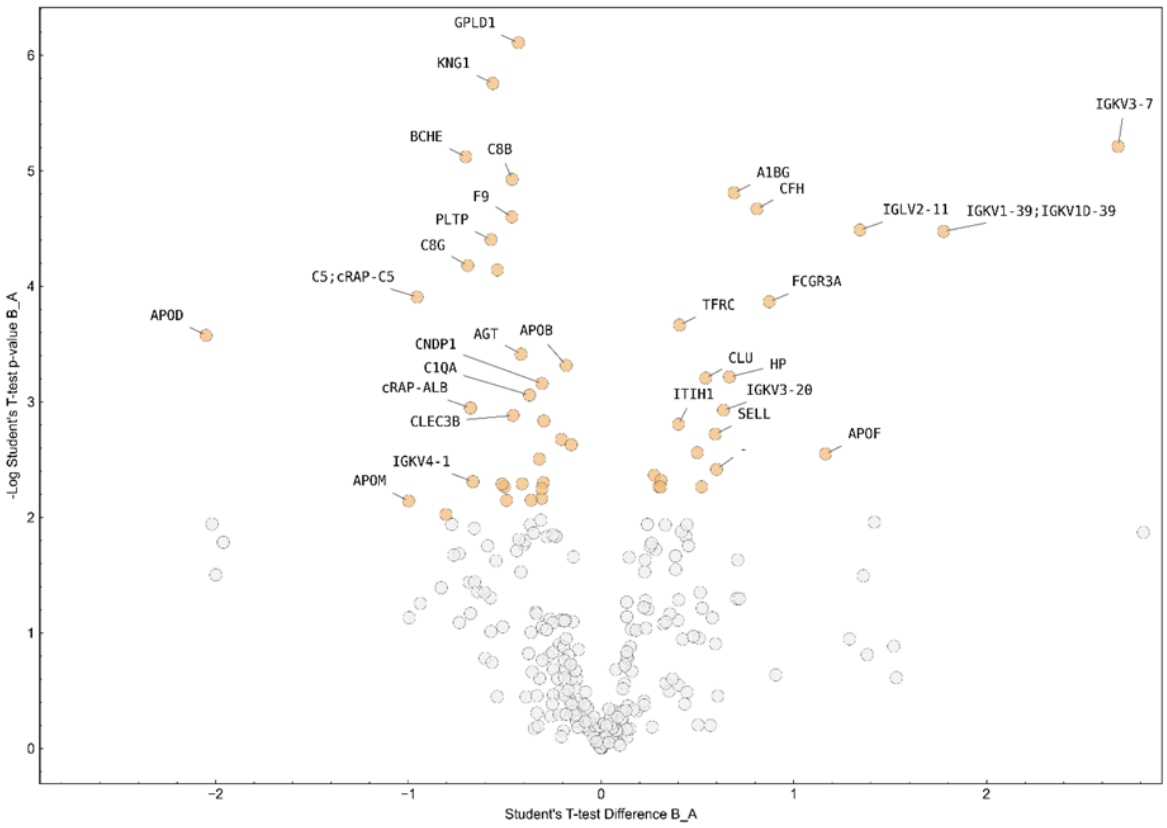

Log_2 fold change (post-surgery − pre-surgery)

Figure 34. Surgery-associated changes in plasma protein abundance following AAA repair. The volcano plot shows the relationship between statistical significance and the magnitude of change in protein levels comparing post-surgical (Condition B) versus pre-surgical (Condition A) plasma samples. The x-axis displays the log_2 fold change (Student's t-test difference, B − A), with positive values indicating proteins upregulated after surgery and negative values indicating downregulation relative to the pre-surgical state. The y-axis presents the $-log_{10}$ transformed p-values from the Student's t-test. Proteins exceeding the 5% false discovery rate (FDR, $q < 0.05$) threshold are highlighted in orange. Annotated proteins represent those with both large fold changes and high statistical significance. Figure reproduced in collaboration with Dr Sarah Flannery (University of Oxford).

4.4.1 Global proteomic reprogramming following surgical intervention

Principal Component Analysis (PCA)

The PCA plot shows how samples are spread out based on their proteomic profiles. Group A (pre-surgery, blue) and Group B (post-surgery, red) are separated along Component 1 (18%) and Component 2 (15.7%), indicating a major shift in longitudinal protein expression. Cluster tightness indicates data consistency and experimental reproducibility. The variance explained by PC1 and PC2 indicates systematic proteomic differences between pre- and post-operative samples. This analysis provides a comprehensive overview of the dataset's variance and highlights patterns that distinguish the two clinical states. Although PCA was performed as an unsupervised exploratory analysis, sample labels reflect paired pre- and post-operative measurements from the same patients. A spatial separation between pre-surgical (blue) and post-surgical (red) samples is observed, especially along Component 1, which accounts for the largest source of variation. This separation indicates significant proteomic reprogramming following surgical intervention in AAA patients, reflecting biological changes such as inflammation, wound healing, immune activation, or metabolic remodelling. Pre-Surgical Samples (Group A, blue) tend to cluster on the right side of the PCA space (positive Component 1 values), indicating shared proteomic features before intervention. This clustering reflects baseline consistency among patients before surgery, suggesting a stable pre-operative proteomic state. Post-Surgical Samples (Group B, red) are spread toward the left and upper areas of the PCA plot, showing a wider dispersion, which may reflect individual differences in physiological responses to surgery. Some patients (e.g., 06B, 02B) display substantial divergence, possibly due to patient-specific factors like recovery status, inflammatory responses, or comorbidities. Component contribution and explained variance: The combined contribution of Component 1 (18%) and Component 2 (15.7%) accounts for a

significant portion of the dataset variability, together capturing 33.7% of variance and separating TP3 and TP5 samples along PC1, indicating reproducible surgery-associated proteomic shifts. Although this does not explain all variance, it supports the detected changes and justifies further statistical analysis of differentially expressed proteins. Data quality and reproducibility, demonstrated by relatively tight clustering within each group, especially among pre-surgical samples, indicate high technical reproducibility and consistency in sample processing and mass spectrometry analysis. The more dispersed distribution in Group B is biologically plausible, reflecting the heterogeneity of post-surgical responses. This confirms that surgery causes a measurable and consistent shift in the plasma proteome of AAA patients. The separation of sample groups along principal components supports the biological importance of the observed changes and highlights the usefulness of unsupervised multivariate analysis in identifying overall proteomic patterns (Figure 35).

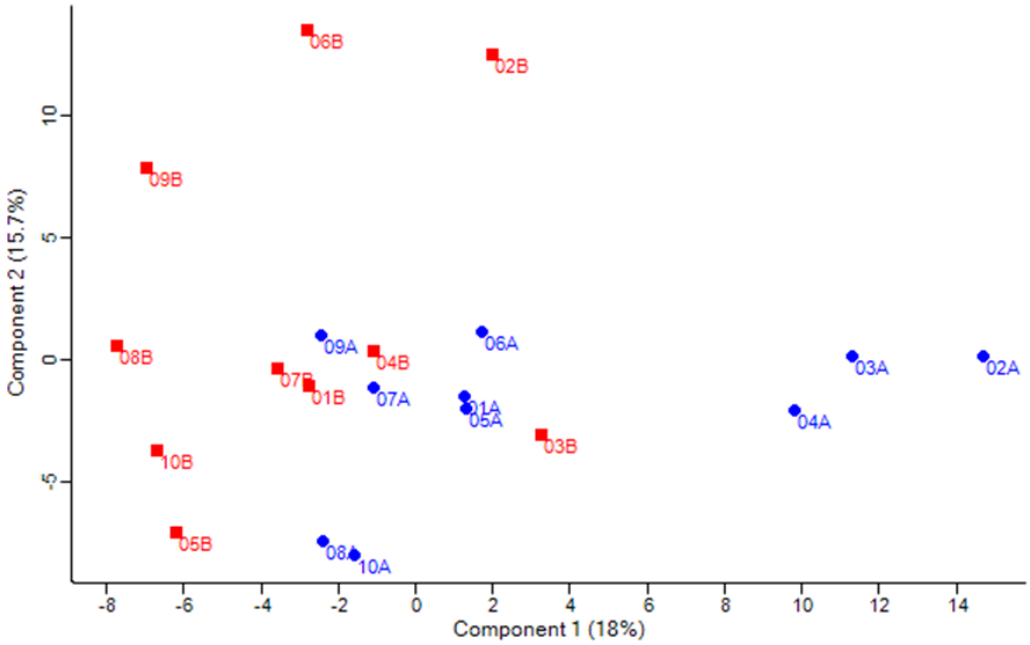

Figure 35. Global separation of pre- and post-surgical plasma proteomes following AAA repair. PCA plot, created in Perseus, shows the reduction in dimensionality of proteomic data from samples collected before surgery (Group A, blue circles) and after surgery (Group B, red squares). The x-axis (Component 1) captures 18% of the total variance, while the y-axis (Component 2) accounts for an additional 15.7%. Each point represents a single patient sample, and clustering reflects similarities in overall protein expression profiles. Figure reproduced in collaboration with Dr Sarah Flannery (University of Oxford).

PCA Loadings Analysis

This loading plot offers a mechanistic view of the biological factors underlying the separation between pre- and post-surgical samples. Proteins influencing Component 1 (horizontal axis), such as KRT1, KRT2, KRT6B, KRT10, and KRT14, appear on the far right of this axis, indicating a substantial contribution to the variance it explains. These keratin proteins are typically linked to epithelial cell structure, stress response, and wound healing, highlighting their relevance in the post-operative physiological state. Their prominent placement likely reflects increased tissue remodelling and repair processes following surgery. In contrast, proteins with strong negative loadings on Component 1, including PF4, ARFGAP3, and IGKV3-7, are positioned on the left-hand side of the plot

and are inversely associated with the post-surgical state, likely reflecting features of the pre-operative plasma proteome or proteins downregulated following surgery. Proteins influencing Component 2 (vertical axis), including ORM1, IGLV2/C7, SAA2, CRP, and PZP, are enriched along this axis, implying their involvement in a distinct yet related biological pathway. These proteins are well-known acute-phase reactants and inflammatory mediators, with upregulation commonly seen in response to trauma or inflammation. Their high loadings suggest they play a significant role in shaping post-surgical inflammatory and immune responses. Proteins in the central cluster form a dense group that remains near the origin, indicating minimal contribution to group separation. These proteins display consistent expression across conditions, serving as a stable proteomic background that improves the interpretability of more variable markers. Outlier proteins with negative loadings, such as PF4, ARFGAP3, and IGKV3-7, positioned on the far left of Component 1, may be downregulated after surgery or act as markers of pre-surgical physiology. Their displacement from the origin indicates inverse correlations with post-operative proteomic trends (Figure 36). This loading analysis complements the PCA scores plot by identifying the specific proteins responsible for sample variation. Keratin family proteins (KRTs) are clear markers of surgical stress and tissue repair, while ORM1, CRP, and SAA2 highlight the systemic inflammatory response following surgery. When combined with differential abundance data (e.g., volcano plots) and unsupervised clustering (e.g., heatmaps), these multivariate methods improve the

resolution and understanding of proteomic changes, supporting future translational efforts

i0 n clinical proteomics.

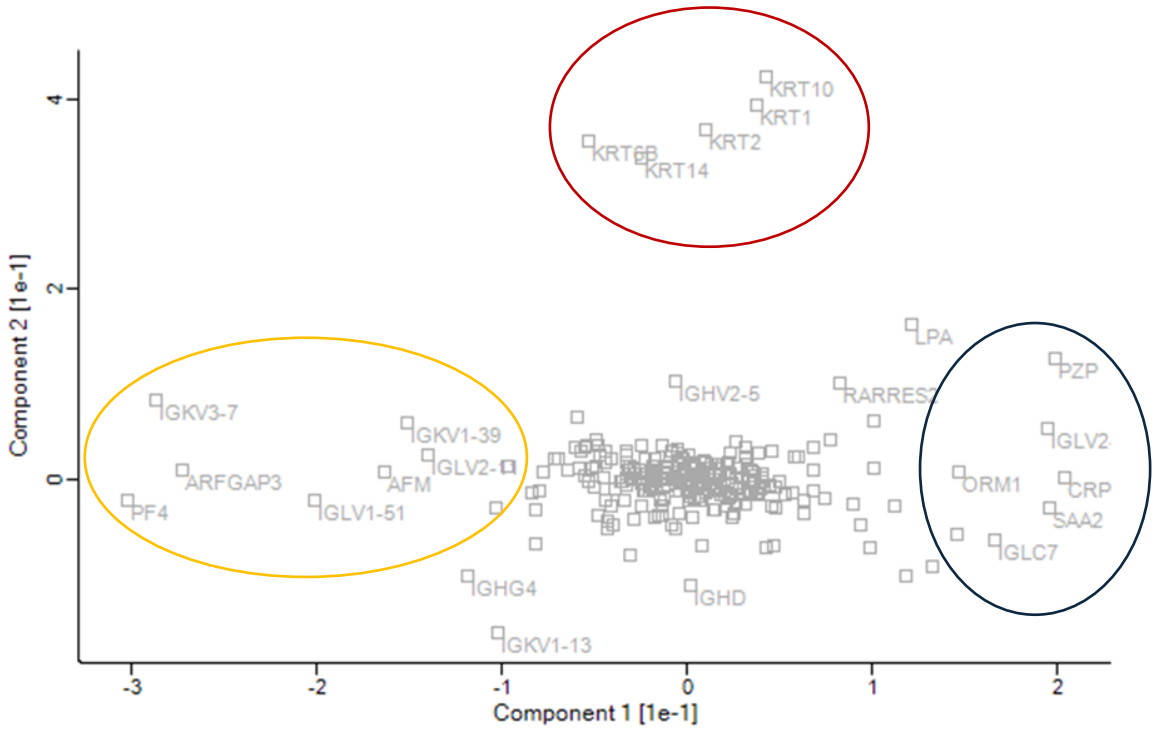

Figure 36. Proteins driving surgery-associated variance in the plasma proteome. Principal Component Analysis (PCA) loadings plot illustrates how individual proteins contribute to the separation of samples seen in the PCA scores plot. The axes represent Component 1 and Component 2, which together account for the amount of the variance in the dataset. Each square stands for a protein, and its distance from the origin reflects the strength of its contribution to sample separation along the respective principal component. Proteins located furthest from the centre are considered the most influential in driving group differences. Proteins with strong positive loadings along Component 1 (right-hand side) are associated with the post-operative state and include acute-phase and inflammatory markers such as CRP, SAA2, ORM1, and PZP. In contrast, proteins with strong negative loadings along Component 1 (left-hand side), including PF4, ARFGAP3, and immunoglobulin-related proteins (e.g. IGKV3-7), are associated with the pre-surgical state or show inverse correlation with post-operative proteomic changes. Figure reproduced in collaboration with Dr Sarah Flannery (University of Oxford). Figure reproduced in collaboration with Dr Sarah Flannery (University of Oxford).

Absolute Quantification workflow of OxConCAT Peptides Using Skyline

4.5 Introduction to the Quantification Workflow

In this pilot, stable-isotope–labelled OxConCAT peptides were used to obtain absolute quantification of target peptides in plasma using Skyline. In the case of the OxConCAT construct, peak intensity measurements provide key data for absolute quantification. "Skyline was used to analyse extracted-ion chromatogram (EIC) peaks/transitions, determine peptide concentrations, and verify quantification using internal heavy-labelled standards. This section outlines the methods for identifying peaks, measuring their areas, and calculating absolute peptide concentrations in plasma samples. It also details how to normalise quantifications to the total protein content to enable reliable comparisons across samples. These procedures underpin the absolute quantification results reported in this chapter.

4.6 Peak Identification and Extracted Ion Chromatogram (EIC) Integration

Accurate peak identification is essential for reliable quantification. Peak selection in Skyline was based on retention time matching to OxConCAT standards and on signal quality. Signal-to-noise ratio was also considered, with only peaks that had intensity significantly above background being selected. For heavy versus light peptides, heavy-labelled internal standards were used to normalise light peptide intensities. Figures 37 and 38 display representative extracted ion chromatograms, highlighting retention time consistency and peak intensity differences.

4.7 AL1L1 Peptide (Samples 01A and 01B)

One of the peptides analysed is K.GVVNVLPGSGSLVGQR.G, derived from the AL1L1 protein. Its chromatographic data show peptide detection from sample 01A, with the x-axis representing retention time (in minutes) and the y-axis indicating intensity (in ion counts). The top panel shows the light peptide EIC, with a low but distinct peak at ~12.1 minutes, consistent with the expected retention time. The bottom panel presents the heavy peptide trace at the same retention time, serving as the internal standard reference. Each coloured trace represents different fragment ions (transitions), collectively forming a composite peak for quantification. The modest light peptide signal indicates a lower endogenous abundance of the AL1L1 peptide in this specific sample. Although the signal is relatively faint, the peak has a Gaussian shape and matches the heavy standard in retention time, confirming confident peak integration. This chromatogram forms the basis for calculating the light-to-heavy ratio and determining the absolute concentration of AL1L1 in plasma sample 01A (Figure 37).

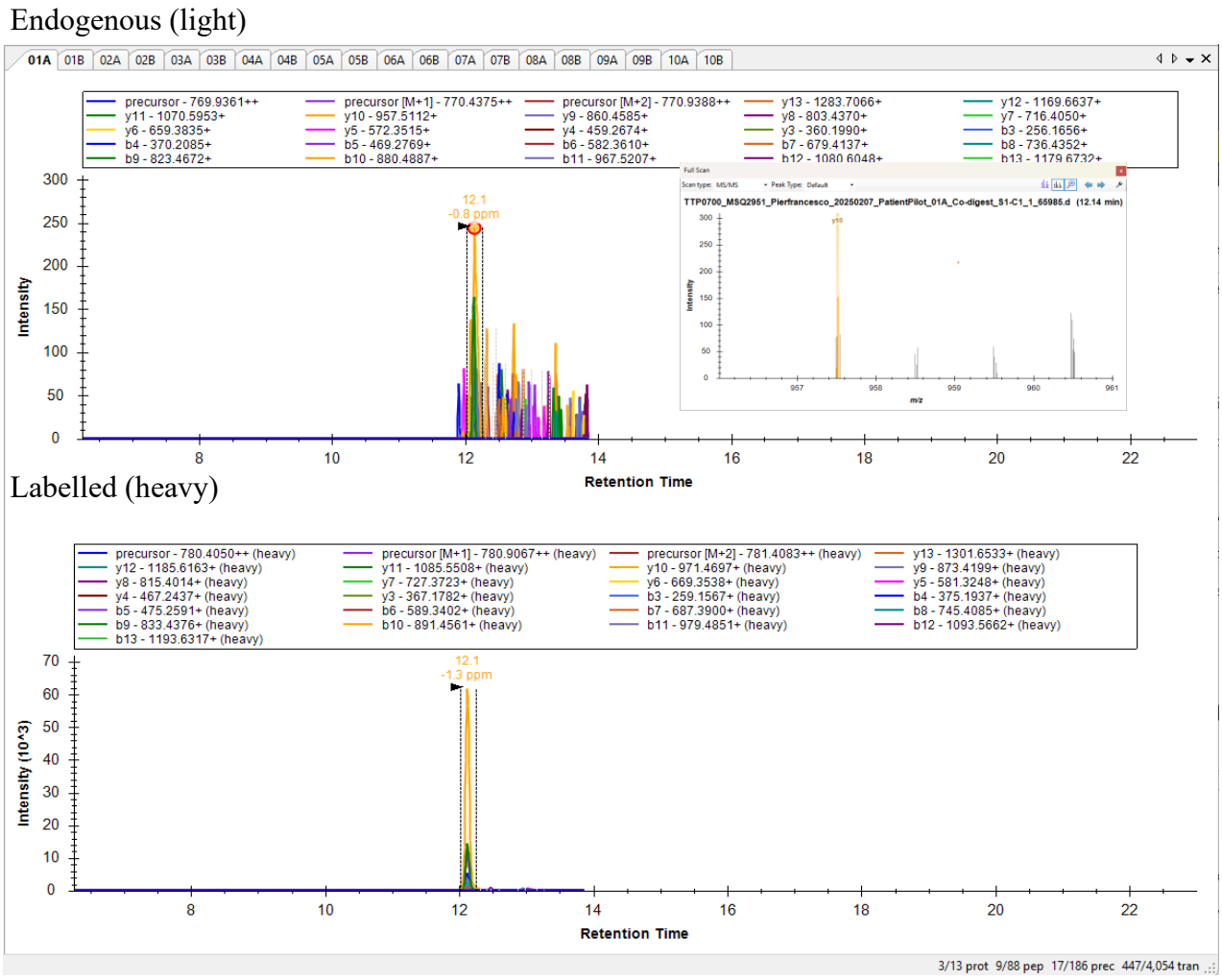

Figure 37. The chromatogram of AL1L1 peptide sample 01A (pre-operative). Retention time and intensity profiles for the AL1L1 peptide in sample 01A are shown. The upper panel displays extracted ion chromatograms for the endogenous (light) peptide, while the lower panel shows the corresponding stable isotope-labelled (heavy) peptide. Multiple monitored fragment ions (b and y ions) are displayed for each peptide, with light and heavy transitions clearly distinguished. The representative quantotypic fragment ion (y10) is highlighted for the peak and used for peptide quantification, while additional fragment ions serve as confirmatory transitions. The observed mass accuracy (ppm error) for the monitored transitions is indicated to provide additional confirmation of fragment ion identity and measurement quality. Co-elution of light and heavy fragment ions at ~12.1 minutes confirms transition specificity and analytical robustness.

The same peptide was analysed post-surgery, AL1L1 peptide 01B, with overlaid extracted ion chromatograms for the light and heavy forms. The layout matches that of Figure 37 to allow direct comparison. A well-defined peak appears at approximately 12.0 minutes, confirming the expected retention time of the peptide. The top panel shows the light

(endogenous) peptide trace, indicating a significant increase in intensity compared to the same peptide in sample 01A. The bottom panel presents the heavy-labelled standard peptide with a steady peak, serving as an internal reference. Here, the sharp increase in light peptide intensity indicates a significantly higher concentration of the AL1L1 peptide in this sample. The overlapping retention times for light and heavy peptides confirm co-elution, ensuring accurate quantification. The stability of the heavy peptide signal allows for confident calculation of the absolute peptide amount using intensity ratios. This figure highlights the importance of internal standards in correcting potential variability in sample processing or instrument performance (Figure 38).

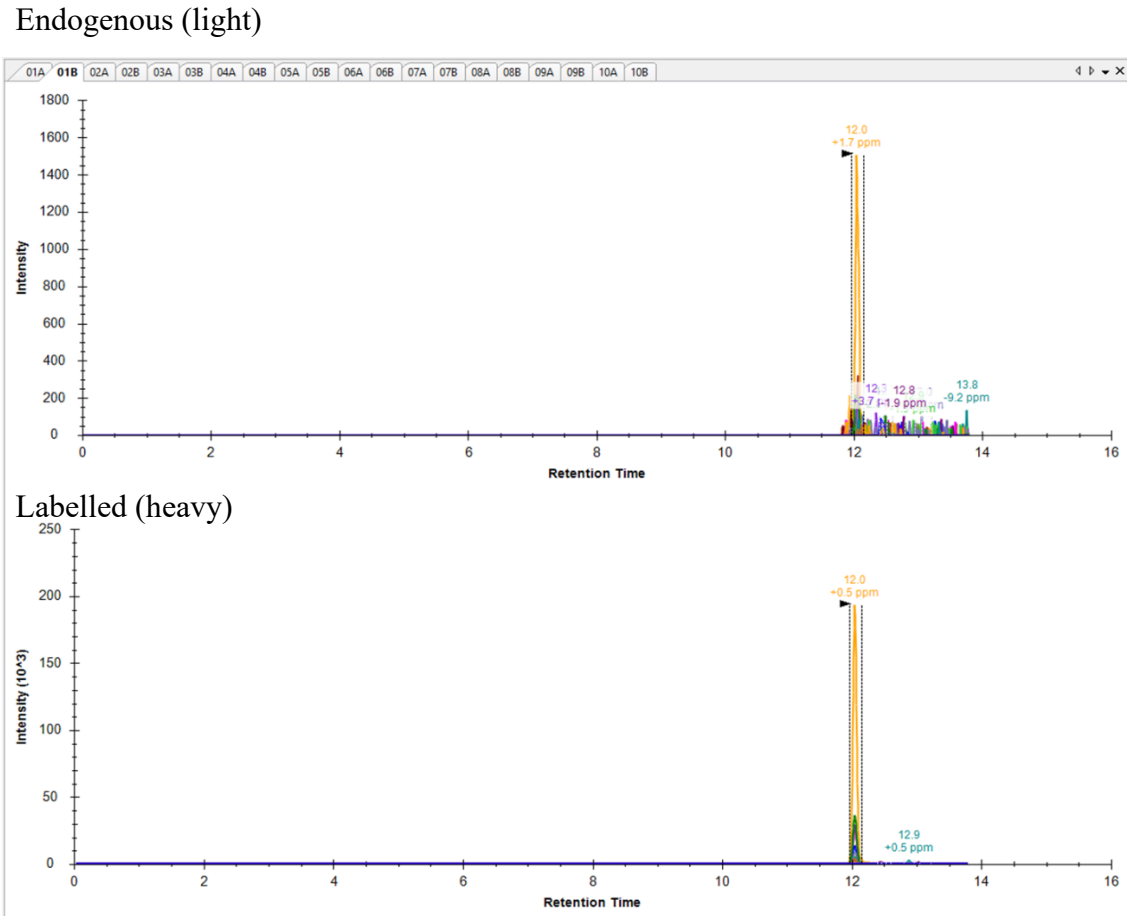

Figure 38. The chromatogram of AL1L1 peptide sample 01B (post-operative). Representative PRM chromatograms are shown, with the upper panel displaying the endogenous (light) peptide and the lower panel showing the corresponding stable isotope-labelled (heavy) peptide. A noticeably higher intensity of the light peptide at the same retention time (~12.0 minutes) compared with sample 01A indicates increased endogenous AL1L1 peptide abundance in the post-operative sample.

Peak Area Integration

The peak area represents the total ion intensity detected for a specific peptide. Manual integration was performed in Skyline to ensure accurate baseline correction, where I_t The intensity at time *t*, and Δ*t* represents time intervals between scans.

$$Peak\ Area\ = \sum_{t=t_{start}}^{t_{end}} I_t \cdot \Delta t$$

The process involved defining the retention time window: peak areas were obtained by (i) defining a retention time window centred on the expected peptide apex, (ii) adjusting baselines to remove background, and (iii) summing intensities across the window.

4.7.1 APOA4_1 Peptide (Samples 01A and 01B)

Another example of peak integration is provided by the APOA4_1 peptide (R.LLPHANEVSGK.I). Figures 39 and 40 show the light and heavy EICs for samples 01A (pre-surgery) and 01B (post-surgery), respectively. A clear and distinct peak appears around 3.9 minutes, aligning with the expected retention time. The top panel presents the intensity profile of the light (endogenous) peptide. The bottom panel displays the corresponding heavy-labelled standard (QconCAT-derived peptide). The light peptide exhibits a well-defined, Gaussian-shaped peak with minimal background noise, confirming successful detection. The heavy peptide also elutes at the same retention time, indicating co-elution and precise quantification. The consistent fragment ion traces increase confidence in both identification and quantification. The light-to-heavy intensity ratio derived from these peaks is used to determine the absolute concentration of APOA4 in the digested plasma sample (Figure 39).

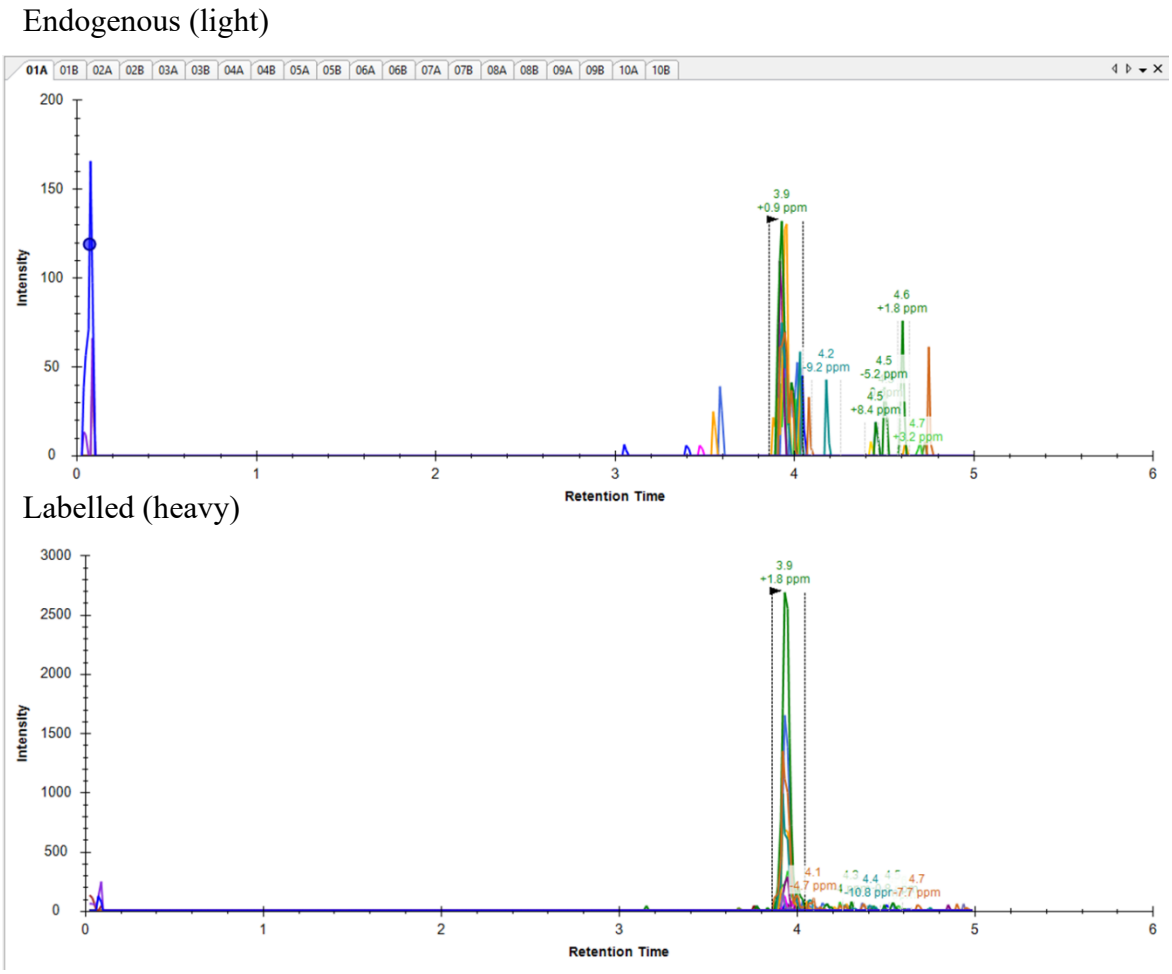

Figure 39. Extracted peak areas for the APOA4_1 sample peptide 01A (pre-surgery). Representative PRM chromatograms are shown, with the upper panel displaying the endogenous (light) peptide and the lower panel showing the corresponding stable isotope-labelled (heavy) peptide. A clear peak is observed at approximately 3.9 minutes, matching the expected retention time. The strong endogenous signal indicates detection of the APOA4_1 peptide in the pre-surgical sample.

The same peptide (R.LLPHANEVSGK.I) is analysed post-surgery (01B) and displayed in this figure, showing the extracted ion chromatograms for both light (endogenous) and heavy (OxConCAT standard) peptide transitions. The peak elutes at approximately 3.9 minutes of retention time, closely matching the expected retention time values for this peptide based on the OxConCAT standard. The upper panel shows the extracted ion chromatogram for the light (endogenous) peptide, with a well-resolved peak centred at

about 3.9 minutes, indicating reliable detection within the expected retention window. The lower panel corresponds to the heavy (OxConCAT standard) peptide, also showing a strong and symmetrical peak at the same retention time (~3.9 min), confirming co-elution. Although APOA4 showed a marked increase in abundance by PRM, it did not appear as differentially abundant in the latest DIA dataset. This discrepancy most likely reflects matrix-related limitations of DIA in plasma (dynamic range constraints, co-elution with abundant proteins, and spectral library dependency), rather than a true absence of change. In contrast, PRM with isotope-labelled OxConCAT standards provides higher sensitivity and selectivity, enabling robust quantification of APOA4 even when DIA signals are weak or non-significant. Spectral library dependency and variable ionisation efficiency may reduce DIA detection confidence. In contrast, the PRM workflow, supported by isotope-labelled OxConCAT standards, offers higher sensitivity, selectivity, and quantitative precision, enabling measurement of APOA4 even when undetected or statistically insignificant in DIA analysis.

The peak is well-resolved and symmetrical, indicating high-quality chromatography and reliable peak integration. The intensity of the light peptide is significantly higher, especially compared to earlier samples (e.g., sample 01A), suggesting a greater endogenous concentration of APOA4 in this plasma sample. The co-elution of multiple transitions with low mass error (shown by ppm values) and the consistent apex at approximately 3.9 minutes increases confidence in peptide identity. Quantification is based on the integration of this light peak area relative to the heavy standard, allowing for absolute concentration estimates in fmol per μL of plasma (Figure 40).

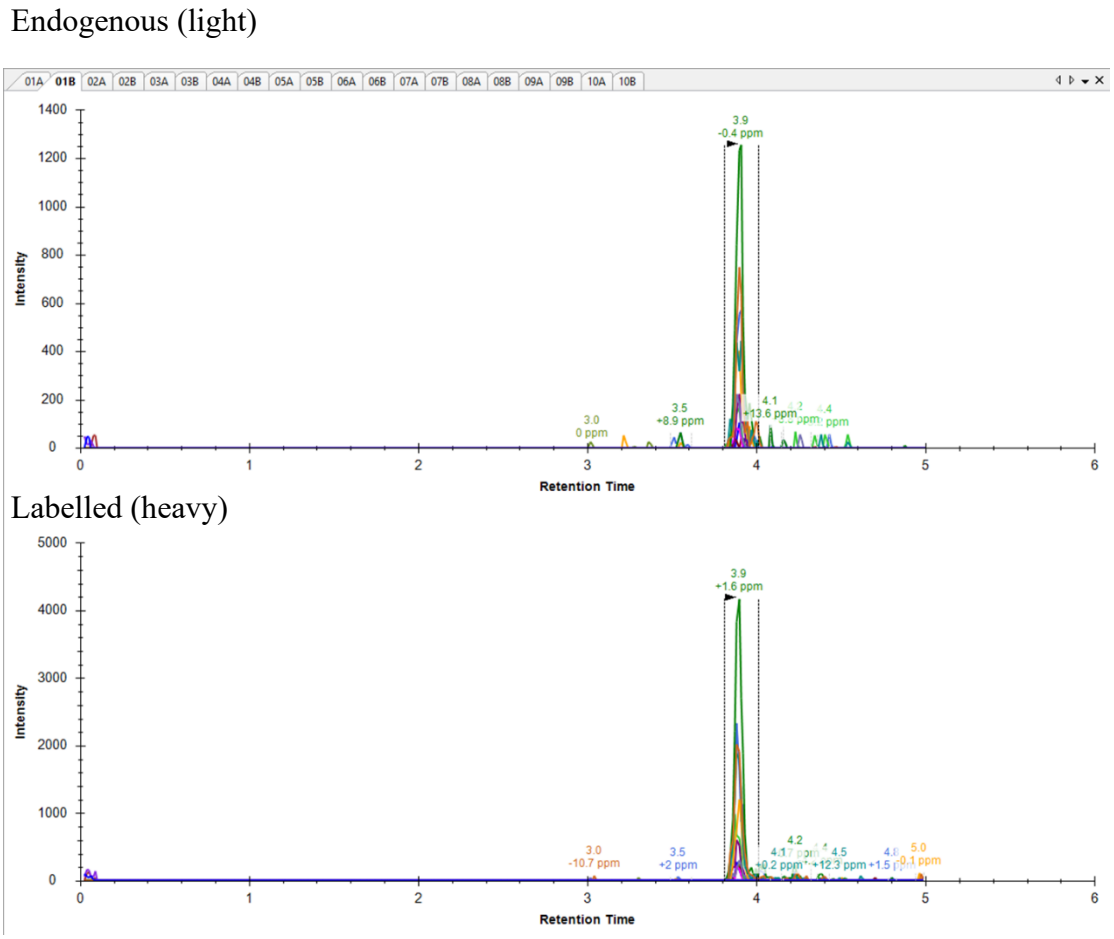

Figure 40. Chromatogram displaying the peak area integration for the APOA4_1 peptide (R.LLPHANEVSGK.I) in sample 01B (after surgery). The upper panel shows the endogenous (light) peptide, while the lower panel shows the corresponding stable isotope-labelled (heavy) peptide. Both panels display consistent transitions and symmetrical peak shapes with co-elution at ~3.9 minutes, confirming peptide identity and reliable quantification. The clear elution profile with minimal background noise supports accurate absolute quantification of APOA4 in plasma.

4.8 Heavy-to-Light Peptide Ratio Calculation

To normalise peptide quantification (Table 14), peak intensity ratios between heavy and light peptides were calculated using the formula:

$$Ratio = \frac{Peak_{light}}{Peak_{heavy}} \times fmol_{heavy}\ injected$$

Where:

$Peak_{heavy}$: Integrated peak area for the heavy isotope-labelled peptide.

$Peak_{light}$: Integrated peak area for the light endogenous peptide.

$fmol_{heavy}$: Known amount of heavy peptide injected.

Table 14. Absolute quantification of APOA4_1 based on OxConCAT signal for peptide LLPHANEVSGK in a patient pre- (01A) and post- (01B) surgery.

Sample	Heavy Intensity	Light Intensity	fmol Light	fmol Light in Digest	fmol Light per µL Plasma
01A	2750	125	9.09	454.54	2272.73
01B	4200	1200	57.14	2857.14	14285.71

Each column represents a different stage of normalisation and absolute quantification for the peptides.

1 *Heavy Intensity & Light Intensity*: raw Skyline peaks for the heavy-labelled OxConCAT peptide and the endogenous (light) peptide.

2 *fmol Light*: amount of light peptide injected, calculated from the light:heavy ratio assuming 200 fmol heavy standard.

$$fmol\ Light\ = \frac{Light\ Intensity}{Heavy\ Intensity} \times fmol\ Heavy\ Injected$$

For Sample 01A:

$$\frac{125}{2750} \times 200 = 9.09\ fmol$$

For Sample 01B:

$$\frac{1200}{4200} \times 200 = 57.14\ fmol$$

3 *fmol Light in Digest*: total amount of light peptide in the full digest (here, 50× the injected volume). This step accounts for the fact that only a fraction of the total digest was injected into the LC-MS.In this case, 1/50th of the digest was loaded, meaning the total peptide amount in the digest is:

$$fmol\ Light\ in\ Digest = fmol\ Light \times 50$$

For Sample 01A:

$$9.09 \times 50 = 454.54\ fmol$$

For Sample 01B:

$$57.14 \times 50 = 2857.14\ fmol$$

4 *fmol Light per µL Plasma*: back-calculated concentration in the originating plasma, taking into account that only 20% (10 µg of 50 µg) of the protein from 1 µL plasma was digested (×5 scaling). The total digest originated from 1 µL of plasma, containing 50 µg of protein (assuming an approximate plasma protein concentration of 50 mg/mL, i.e. 50 µg per µL). Since only 20% (10 µg) was digested, the total plasma concentration is scaled accordingly:

$$fmol\ Light\ per\ \mu L\ Plasma\ =\ fmol\ Light\ in\ Digest\ \times 5$$

For Sample 01A:

$$454.54 \times 5 = 2272.73\ fmol/\mu L$$

For Sample 01B:

$$2857.14 \times 5 = 14285.71\ fmol/\mu L$$

To further illustrate the calculations, an additional example for the AL1L1 peptide (K.INWDQPAEAIHNWIR.G) is shown here (Table 15), applying the same calculations.

Table 15. Additional example of quantitation for the AL1L1 peptide.

Sample	Heavy Intensity	Light Intensity	fmol Light	fmol Light in Digest	fmol Light per µL Plasma
01A	60000	250	0.83	41.67	208.33
01B	200000	1500	1.50	75.00	375.00

The integration of peak intensities and heavy-to-light peptide ratios enables precise absolute quantification in OxConCAT-based workflows. By scaling peptide amounts to total plasma protein content, robust and reproducible results are achieved. In future work, these manual calculations could be supplemented with fully automated quantification workflows in Skyline, improving consistency and scalability for larger cohort analyses.

Peptide-level Absolute Quantification Analysis of Patient Pilot Study using OxConCAT

4.9 Experimental Design and Data Processing

To assess the performance of our bespoke peptide construct (C-002) in a clinically relevant matrix, we conducted a pilot study on platelet-poor plasma (PPP) from ten patients undergoing surgical intervention. For each patient, blood draws were collected at two defined time-points: pre-operative (TP3) and post-operative (TP5), ≥ 1 month after surgery. Samples were processed using a standardised SP3 digestion protocol with co-digestion of 200 fmol OxConCAT standard and endogenous plasma proteins (see Section 2.2).

Peptide candidates for inclusion in the C-002 OxConCAT standard were selected through a comprehensive screening process involving eleven target proteins of interest, including NCHL1, ATRN, AL1L1, CRP, APOA4, and CO8G. Selection was based on stringent analytical and technical criteria designed to ensure robust absolute quantification in plasma using LC–MS/MS. Selection criteria focused on robust dual detectability, meaning peptides had to show consistent and high-confidence detection in both light (endogenous) and heavy (OxConCAT-derived) forms across co-digest experiments. Only peptides with minimal ion suppression and reproducible signals across spike-in conditions were retained.

Peptides were tested under both post-digest spike-in (heavy peptides added after digestion) and co-digest (OxConCAT digested alongside plasma proteins) conditions. Only peptides with minimal signal suppression or interference in both setups were kept for further analysis. Candidates were also evaluated for favourable physicochemical

properties, including stable retention time, effective fragmentation, and absence of interfering peaks. These qualities were essential for ensuring clear peaks, consistent quantification, and successful integration into targeted PRM workflows.

Preliminary screening revealed heterogeneous peptide performance across the panel. The peptides from CAH1, LDHB, and ANXA6 consistently failed to meet these criteria, displaying low signal intensity, inconsistent detection, or significant suppression, likely due to poor ionisation efficiency or unfavourable hydrophobicity. As a result, these peptides were excluded from analysis. Conversely, peptides from CRP, APOA4 (LLPHANEVSQK and LGPHAGDVEGHLSFLEK), CO8G, ATRN, AL1L1, and NCHL1 demonstrated consistent detection in both endogenous ("light") and OxConCAT ("heavy") forms across co-digest conditions, meeting the criteria for quantitative reliability. In contrast, peptides from CAVN2 and ALDH2 were detected in the heavy form but failed to yield quantifiable endogenous signals due to low abundance, interference, or suppression, and were therefore excluded from primary quantification. Following this refinement, the final OxConCAT standard comprised seven peptides representing six target proteins, each selected for its quantitative reliability and compatibility with clinical plasma analysis (Figure 41). The limited detectability of several candidate peptides reflects the challenges of absolute quantification in complex plasma matrices, where low endogenous abundance, co-eluting interferences, ion suppression, and peptide-specific physicochemical properties (e.g. poor ionisation or suboptimal tryptic behaviour) can prevent robust signal extraction. In addition, co-digestion introduces variable competition for trypsin and may increase miscleavage or reduce recovery for certain sequences. For this reason, Figure 41 was used as an explicit QC filter to retain only peptides showing consistent dual detectability (light and heavy) for downstream quantification.

Legend

- GREEN **Light & Heavy**: Detected in both endogenous (light) and OxConCAT (heavy) peptides across co-digest.
- YELLOW **Suppressed / Limited**: Detection inconsistent or only observed in different spike-in condition.
- GREY **Not Detected**: Peptide not observed reliably across any condition.

	TTP0700_MSQ2951_20250207_PatientPilot_10ugCoDigest_Skyline.sky		
	Peptide 1	**Peptide 2**	**Peptide 3**
sp|O00533|NCHL1_HUMAN	R.LTWEAGADHNSNISEYIVEFEGNK.E [630, 653]	R.VTWKPQGAPVEWEEETVTNHTLR.V [749, 771]	K.GAGPESEPYIFQTPEGVPEQPTFLK.V [899, 923]
sp|O75882|ATRN_HUMAN	R.VFHIHNESWVLLTPK.A [423, 437]	R.YYTAINFVATPDEQNR.D [1176, 1191]	R.NHPNITFFVYVSNFTWPIK.I [1247, 1265]
sp|O75891|AL1L1_HUMAN	K.INWDQPAEAIHNWIR.G [211, 225]	K.IQGSTIPINGARPNR.N [540, 554]	K.GVVNVLPGSGSLVGQR.L [621, 636]
sp|O95810|CAVN2_HUMAN	R.DNSQVNAVTVLTLLDK.L [49, 64]	K.YQASTSNTVSK.L [103, 113]	R.EGESHAENETK.S [304, 314]
sp|P00915|CAH1_HUMAN	K.EIINVGHSFHVNFEDNDNR.S [59, 77]	R.LFQFHFHWGSTNEHGSEHTVDGVK.Y [91, 114]	K.YSAELHVAHWNSAK.Y [115, 128]
sp|P02741|CRP_HUMAN	K.ESDTSYVSLK.A [32, 41]	K.APLTKPLK.A [42, 49]	R.GYSIFSYATK.R [66, 75]
sp|P05091|ALDH2_HUMAN	K.TIPIDGDFFSYTR.H [160, 172]	K.VAEQTPLTALYVANLIK.E [210, 226]	K.VAFTGSTEIGR.V [258, 268]
sp|P06727|APOA4_HUMAN	K.AVVLTLALVAVAGAR.A [5, 19]	R.LLPHANEVSQK.I [113, 123]	K.LGPHAGDVEGHLSFLEK.D [329, 345]
sp|P07195|LDHB_HUMAN	K.SLADELALVDVLEDK.L [44, 58]	K.DYSVTANSK.I [83, 91]	R.GLTSVINQK.L [300, 308]
sp|P07360|CO8G_HUMAN	R.RPASPISTIQPK.A [28, 39]	R.FLQEQGHR.A [62, 69]	R.GAVHVWAETDYQSFAVLYLER.A [121, 142]
sp|P08133|ANXA6_HUMAN	R.DLEADIIGDTSGHFQK.M [141, 156]	R.EEDDWSEDLVQQDVQDLYEAGELK.W [167, 191]	R.EDAQVAAEILEIADTPSGDK.T [521, 540]

Figure 41. Peptide-level detection performance in the OxConCAT patient pilot study. Summary of peptide detectability across eleven target proteins in platelet-poor plasma (PPP) samples from the OxAAA patient pilot study. Detection consistency was evaluated for both endogenous ("light") and OxConCAT-derived ("heavy") peptides under co-digest conditions. Green indicates peptides reliably detected in both light and heavy forms across all samples; yellow denotes suppressed or limited detection, observed inconsistently or only under specific spike-in conditions; and grey marks peptides not reliably detected under any condition. This classification guided peptide inclusion in the final OxConCAT standard panel used for absolute quantification. Limited detectability for a subset of peptides is expected in plasma co-digest experiments due to low endogenous abundance and matrix-dependent ion suppression/interference; therefore, this figure was used as a QC gate to prioritise peptides with robust dual detectability for absolute quantification.

An additional optimisation step confirmed 200 fmol per digest as the optimal spike-in concentration. This level provided consistent detection across peptides of varying abundance, strong signal intensity without saturating the detector, and improved detection of low-abundance targets compared to lower spike-in concentrations (e.g., 50 or 100 fmol). Therefore, this 200 fmol spike-in was adopted for all downstream analyses, offering the best balance between signal clarity, dynamic range, and quantification robustness across the entire peptide panel. Digested peptides were injected (2% of each digest) onto an Evosep One LC system coupled to a timsTOF Pro operating in diaPASEF mode. Each run comprised 8 diaPASEF windows per TIMS scan (100 ms accumulation/ramp time) spanning 475–1000 m/z with ion mobility-dependent collision

energies (20–59 eV). For targeted verification, PRM-PASEF was performed on a subset of transitions.

Absolute peptide quantification was performed using Skyline-daily (version 25.1) to process LC–PRM/MS data derived from patient plasma samples. Peptide peak areas and fragment ion intensities were integrated and normalised against heavy-labelled OxConCAT standards, yielding fmol/µL plasma and ng/µL plasma concentrations per peptide. Absolute values represent peptide quantities per µL of plasma; protein concentrations in ng/mL can be easily derived by applying molecular-weight scaling under the assumption of a 1:1 peptide–protein stoichiometry. Data for each peptide were analysed in GraphPad Prism v10.4.2, where fold-change analyses (post- vs pre-surgery) were performed using paired t-tests, and 95% confidence intervals were calculated. Peptides were assessed for significant post-surgical changes and quantification consistency, guiding peptide inclusion for downstream absolute quantification and analyses.

Building on this initial evaluation, before performing cohort-level fold-change analysis, a comprehensive pilot test was conducted on Patient 01, who was chosen for detailed quantification of all detectable proteins and peptides from the OxConCAT panel. This initial analysis helped evaluate the detectability, chromatographic performance, and quantitative responsiveness of each peptide, validating the absolute quantification pipeline before scaling up to the group Pilot patient analysis (n=10 pairs, before and after surgery).

Quantitative analysis of peptide-level fold changes was conducted using Skyline (for peak integration) and GraphPad Prism (for statistical evaluation).

Peptide selection and signal extraction protocols were optimised for accuracy and reproducibility. For Patient 01, to test absolute quantification, a manual, labour-intensive, meticulous approach was employed to ensure precision. Specifically, for each peptide (light and heavy form), the top three most intense fragment ions were individually identified and manually selected after thorough inspection of peak shape, retention time consistency, and reproducibility across replicates. Fragment peak heights were summed to obtain the most accurate light/heavy ratio, which was then used to calculate the absolute concentration (fmol/µL) based on the known OxConCAT spike-in amount. This method ensured high-precision quantification and enabled estimation of pre- versus post-surgical protein levels.

For the patient pilot cohort (n=10), a streamlined and scalable method was applied. For each peptide, the single most intense fragment peak was selected automatically for both peak height and peak area quantification. Consistent peak boundaries were used across all samples, enabling direct pre- and post-comparisons. For each patient, fold change was expressed relative to the pre-surgery baseline (baseline = 1). Group differences were assessed with paired t-tests, and Benjamini–Hochberg FDR control was applied to adjust for multiple testing (reported as q-values). Analysis proceeded at two levels: patient-level QC (manual verification of peak identity and integration) to ensure valid measurements, and cohort-level statistics to quantify overall trends. All quantification outputs were validated through fragment ion inspection, ensuring robustness of the resulting fold-change analyses presented in Section 4.10.

4.10 Peptide-Level Evaluation: Quantification and Signal Characteristics of NCHL1, ATRN, AL1L1, CRP, APOA4 Variants, CO8G

To support the interpretation of group-level results presented in later sections, the performance of individual peptides across all patient samples was examined, focusing on absolute quantification, chromatographic behaviour, and consistency in light/heavy signal ratios. Data from a representative Patient 01 were analysed in detail to illustrate typical chromatographic profiles, fragment ion behaviour, and quantification consistency observed across the cohort. These figures exemplify characteristic signal patterns rather than outlier behaviour, providing a reference for subsequent comparative analyses. All statistical evaluations across the cohort were performed using summed top-3 transitions per peptide to ensure harmonised quantification criteria. The six proteins evaluated, NCHL1, ATRN, AL1L1, CRP, APOA4, and CO8G, were selected based on stringent analytical and biological criteria described in Section 4.9. These targets consistently met performance thresholds for dual detectability, co-elution accuracy, and minimal ion suppression across co-digest experiments, confirming their suitability for absolute quantification. For statistical comparisons, the top transition was computed and the corresponding peak height and areas used to derive quantitative metrics. Importantly, these proteins also represent biologically relevant pathways implicated in AAA pathophysiology, including inflammation (CRP), complement activation (CO8G), lipid metabolism (APOA4), and thrombus-associated signalling (ATRN, NCHL1, AL1L1). Collectively, this subset provides a balanced evaluation of both technical performance and clinical relevance within the OxConCAT quantitative framework.

4.10.1 NCHL1 Peptide – GAGPESEPYIFQTPEGVPEQPTFLK

The peptide GAGPESEPYIFQTPEGVPEQPTFLK, derived from NCHL1 protein, exhibited robust chromatographic behaviour and high signal clarity across all patient samples (n=20; 10 pre- and 10 post-surgery). Both endogenous (light) and OxConCAT (heavy) peptides showed excellent co-elution at ~16.2 min retention time with well-defined, symmetrical peaks and minimal matrix interference (Figure 42). The heavy standard provided consistent peak shapes across conditions, validating its use for absolute quantification. In Patient 01, the absolute plasma concentration of NCHL1 peptide measured with the top-peak fragment was:

Pre-Surgery: 9581.6 fmol/µL, equivalent to 26.05 ± 3.09 ng/µL plasma

Post-Surgery: 4556.8 fmol/µL, equivalent to 12.39 ± 1.65 ng/µL plasma

This represents a ~2.1-fold decrease post-operatively. Fragment ion intensities and light/heavy ratios corroborated the reduced post-surgical decrease (Figure 42A, right panels).

42-A

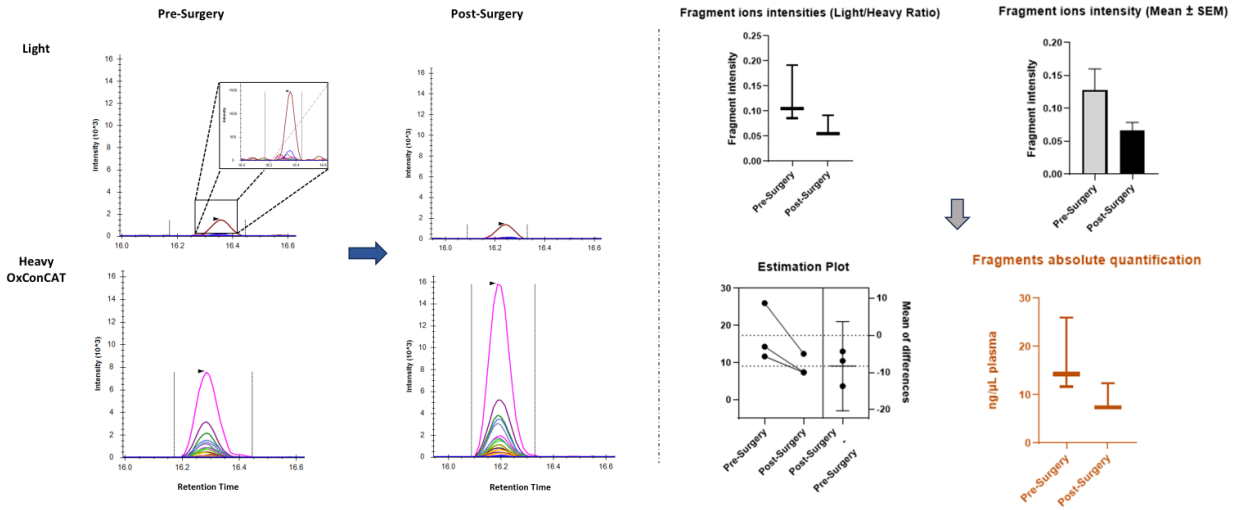

Absolute Quantification output

Time Point	fmol/µL	ng/µL (±SEM)
Patient 01 (Pre - Surgery, time 0h)	9581.6	26.05 ± 3.088
Patient 01 (Post - Surgery, time ≥ 1 month)	4556.8	12.39 ± 1.65

Figure 42A. Absolute Quantification of NCHL1 in an Individual AAA Patient. Skyline chromatograms and quantitative output for the OxConCAT-derived peptide NCHL1 (GAGPESEPYIFQTPEGVPEQPTFLK) from Patient 01, showing light (endogenous) and heavy (OxConCAT) traces before and after surgery. Fragment ion intensities and estimation plots indicate a marked reduction in NCHL1 levels post-surgery. The absolute quantification table summarises the fmol/µL and ng/µL values, confirming a postoperative decrease in protein abundance.

In the pilot level analysis across the whole patient cohort (n=10), normalised peak height and area under the curve (AUC) measurements were extracted and analysed in Skyline and Prism.

Peak Height (fmol/µL plasma): Significant reduction post-surgery ($p < 0.001$)

Peak Area (fmol/µL plasma): Significant reduction post-surgery ($p < 0.001$)

Normalized fold-change (pre-surgery = 1) decreases to ~0.35 post-surgery ($p < 0.0001$)

Absolute concentrations (ng/µL plasma) in the pilot cohort confirmed the same trend, supporting strong biological relevance (Figure 42B).

42-B

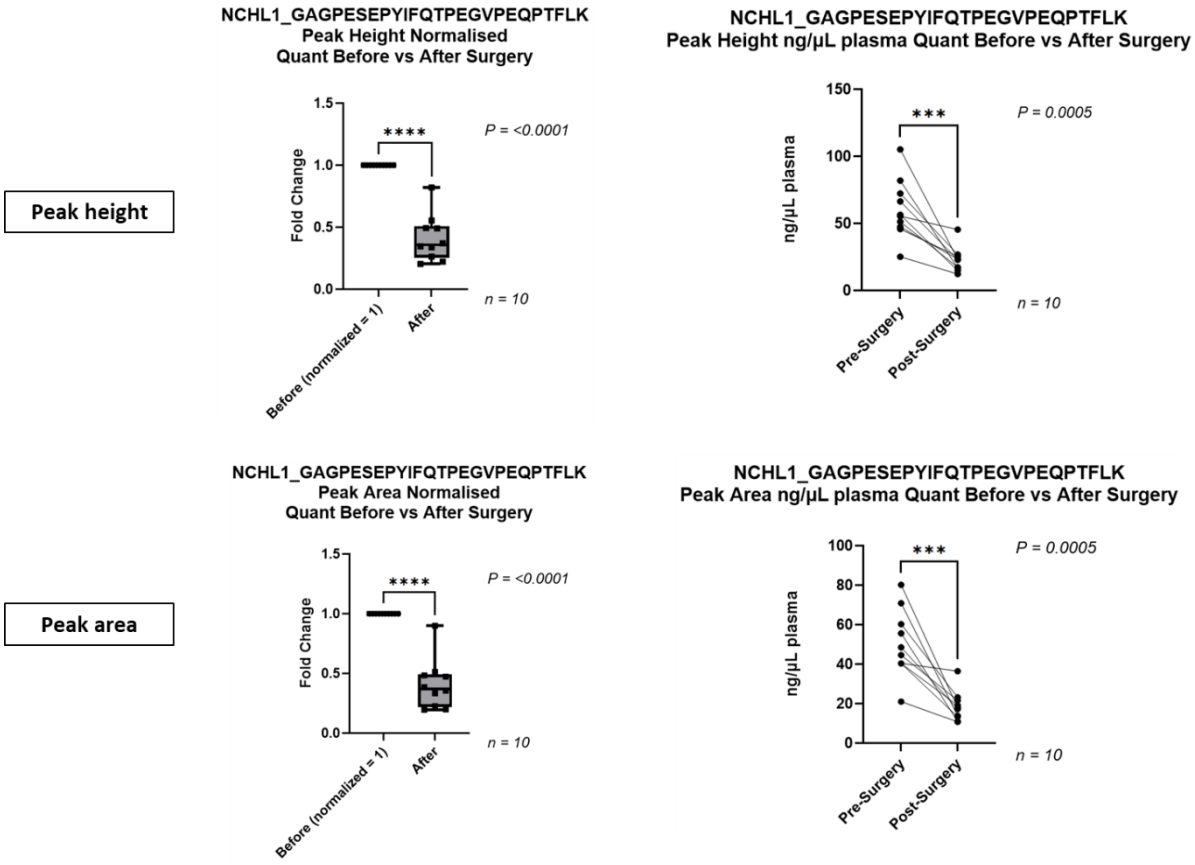

Figure 42B. NCHL1 Absolute Quantification Across the Pilot AAA Cohort. Quantitative evaluation of the NCHL1 peptide (GAGPESEPYIFQTPEGVPEQPTFLK) across the OxAAA pilot cohort (n = 10), comparing plasma samples collected before surgery (TP3) and after surgery (TP5/TPF). Left panels show box-and-whisker plots (minimum to maximum) of log_2-normalised fold change based on peak height and peak area measurements. Boxes represent the interquartile range (IQR), the central line denotes the median, whiskers extend to the minimum and maximum values, and all individual data points are displayed. Right panels show paired individual plasma concentrations (ng/µL) with connecting lines illustrating within-patient longitudinal changes. A consistent postoperative decrease in NCHL1 levels is observed across both quantification approaches (paired statistical testing: ****P < 0.0001; ***P = 0.0005).

This peptide displayed excellent detectability, stable ionisation efficiency, and clear quantification dynamics across both individual and cohort analyses. The observed statistically significant decline in NCHL1 levels post-surgery supports its inclusion in ongoing absolute quantification workflows.

4.10.2 ATRN Peptide (YYTAINFVATPDEQNR)

The next peptide evaluated was ATRN. This exhibited reliable detection across both pre- and post-surgical samples in the entire patient cohort. In Patient 01, precise and reproducible co-elution of light and heavy OxConCAT-derived peaks was observed at ~12.6 min retention time (RT), indicating good chromatographic behaviour despite minor tailing (likely due to matrix complexity or high peptide abundance) (Figure 43A). Notably, the signal intensity for both peptide forms was well above background, supporting confident quantification across timepoints.

Absolute Quantification (Patient 01):

Pre-surgery: 862.9 ± 138.5 ng/µL.

Post-surgery: 357.8 ± 64.4 ng/µL.

This corresponds to a ~2.5-fold reduction in plasma ATRN levels post-operatively, with statistical significance ($p = 0.032$). These values represent peptide mass concentrations (ng/µL plasma) derived directly from LC–MS peak areas using labelled internal standards. Conversion to protein-level concentration (ng/mL) can be readily obtained through molecular-weight scaling under a 1:1 peptide–protein assumption. The fragment ion intensities showed a consistent and marked decrease in light-to-heavy ratios post-surgery, confirming an actual reduction in circulating peptide levels rather than variability in detection or technical artefacts. Estimation plots demonstrated a uniform downward trend for ATRN across both absolute values and log-transformed intensities, suggesting robust peptide behaviour even in the context of plasma matrix interference.

43-A

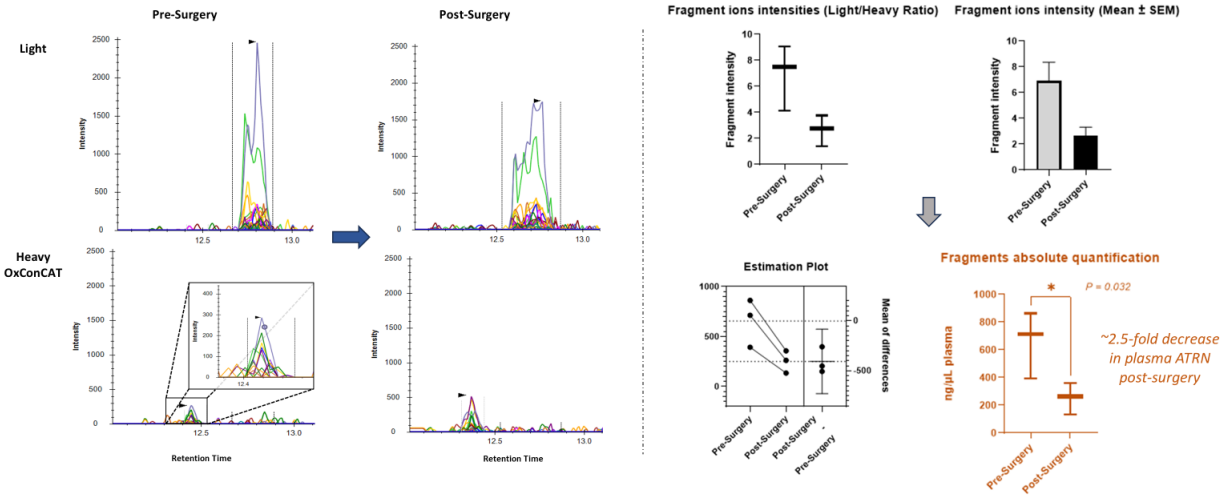

Absolute Quantification output	Time Point	fmol/µL	ng/µL (±SEM)
	Patient 01 (Pre - Surgery, time 0h)	453690	862.9 ± 138.5
	Patient 01 (Post - Surgery, time ≥ 1 month)	188146	357.8 ± 64.4

Figure 43A. Absolute Quantification of ATRN in an Individual AAA Patient. Skyline chromatograms and quantitative output for the OxConCAT-derived peptide ATRN (YYTAINFVATPDEQNR) from Patient 01, showing co-eluting light (endogenous) and heavy (OxConCAT) traces at ~12.6 min. Absolute quantification yielded 862.9 ± 138.5 ng/µL pre-surgery and 357.8 ± 64.4 ng/µL post-surgery, indicating an approximately 2.5-fold decrease in plasma ATRN levels ($p = 0.032$). Fragment ion intensities showed a consistent reduction in light-to-heavy ratios, confirming an actual postoperative decrease in circulating peptide abundance.

Quantification in the patient pilot cohort (*n=6*) confirmed a statistically significant reduction in both peak height (fmol light/uL plasma): $p < 0.05$ and Peak Area: $p < 0.05$. Normalised fold-change analyses (Skyline/Prism) confirmed this pattern, with ~60–70% reduction in ATRN peptide levels post-surgery and consistent downregulation in all 6 patients analysed (remaining four excluded due to outliers or poor signal quality) (Figure 43B).

43-B

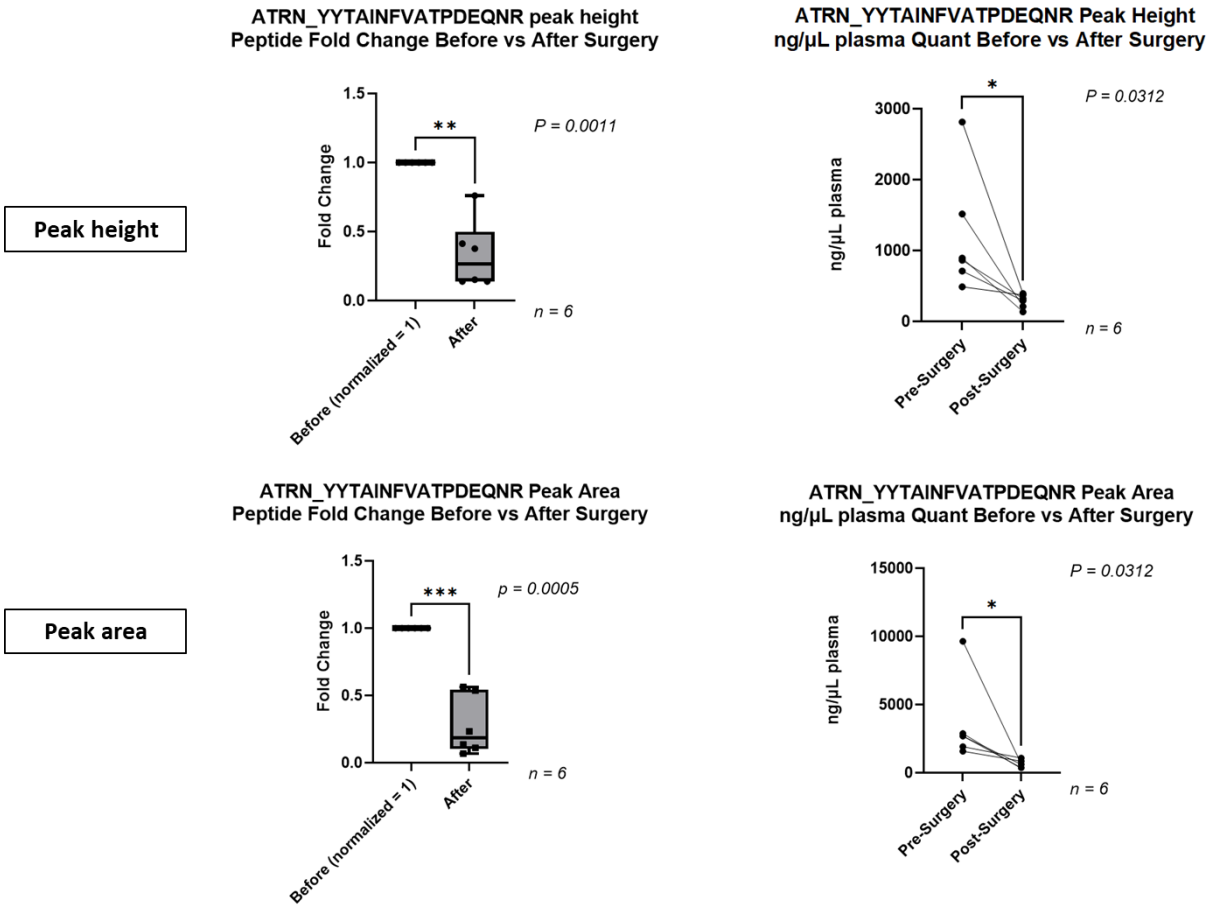

Figure 43B. ATRN Absolute Quantification Across the Pilot AAA Cohort. Quantitative assessment of the ATRN peptide (YYTAINFVATPDEQNR) in paired plasma samples from the OxAAA pilot cohort (n = 6), comparing pre-surgical (TP3) and post-surgical (TP5/TPF) time points. Left panels show box-and-whisker plots (min–max) of log_2-normalised fold change for peak height and peak area measurements. Boxes represent the interquartile range (IQR), the central line denotes the median, whiskers indicate the full data range (minimum to maximum), and all individual data points are displayed. Right panels show paired individual plasma concentrations (ng/µL) with connecting lines illustrating within-patient longitudinal changes. Both peak height and peak area analyses demonstrate a statistically significant postoperative reduction in ATRN levels (paired testing, p = 0.0312; fold-change analyses: **p = 0.0011; ***p = 0.0005), indicating a consistent decrease in peptide abundance following surgery.

The ATRN peptide demonstrated excellent detectability and dynamic response to surgical intervention, confirming its suitability for absolute quantification workflows. Despite minor intensity variability, the magnitude and consistency of ATRN depletion suggest this

peptide sensitively reflects post-surgical proteomic change with translational potential. It remains a reliable quantitative marker, and its performance supports continued inclusion in both cohort-level and individual-level analyses of AAA surgical impact.

4.10.3 AL1L1 Peptide (GVVNVLPGSGSLVGQR)

This peptide exhibited suboptimal chromatographic behaviour compared to other panel members. While detectable in Patient 01 and across the cohort, signal intensities were consistently low, and co-elution of light and heavy peaks was less distinct, occurring at ~12.1 min RT (Figure 44A). Low ionisation efficiency and potential matrix suppression effects likely contributed to poor signal-to-noise ratios, particularly evident in the pre-surgery light peptide traces (Figure 44A inset). Despite these limitations, quantification was possible with careful manual inspection and integration of the top three fragment peaks. Quantitative Summary for patient 01 results in pre-surgery: 0.3 ± 0.17 ng/µL and post-surgery values: 0.5 ± 0.03 ng/µL. The absolute quantification indicated a modest increase post-surgery (~1.6-fold rise); however, this change was not statistically significant, given the large variability in the pre-surgery measurement.

44-A

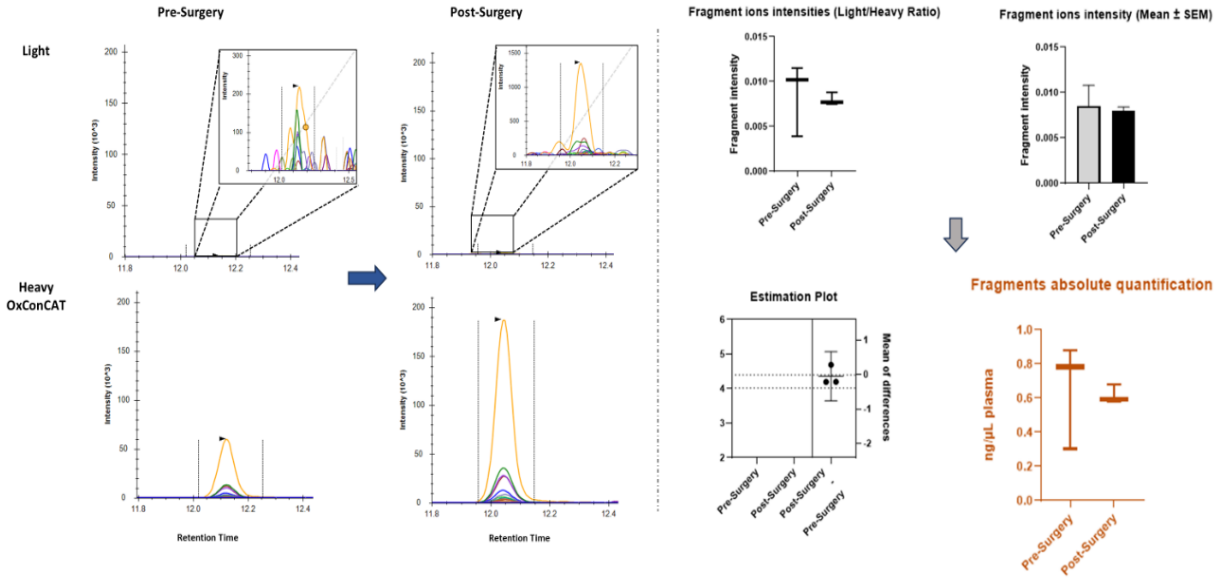

Absolute Quantification output

Time Point	fmol/µL	ng/µL (±SEM)
Patient 01 (Pre - Surgery, time 0h)	197.49	0.3 ± 0.17
Patient 01 (Post - Surgery, time ≥ 1 month)	385.75	0.5 ± 0.03

Figure 44A. Absolute Quantification of AL1L1 in an Individual AAA Patient. Skyline chromatograms for the OxConCAT-derived peptide AL1L1 (GVVNVLPGSGSLVGQR) from Patient 01, showing detectable but low-intensity light (endogenous) and heavy (OxConCAT) traces eluting at ~12.1 min. Signal-to-noise ratios were reduced, likely due to low ionisation efficiency and matrix suppression effects. Quantification yielded 0.3 ± 0.17 ng/µL pre-surgery and 0.5 ± 0.03 ng/µL post-surgery, representing a modest (~1.6-fold) but statistically non-significant increase in plasma concentration.

Statistical evaluation of the patient cohort (n = 10) showed no significant changes in either peak height (fmol light/uL plasma) or Peak Area. Fold-change analyses demonstrated a neutral response with average ratios close to 1.0 (pre vs post), as shown in the cohort box plots (Figure 44B). These findings suggest intra-patient consistency but poor inter-patient robustness, making this peptide less reliable for population-level analysis.

44-B

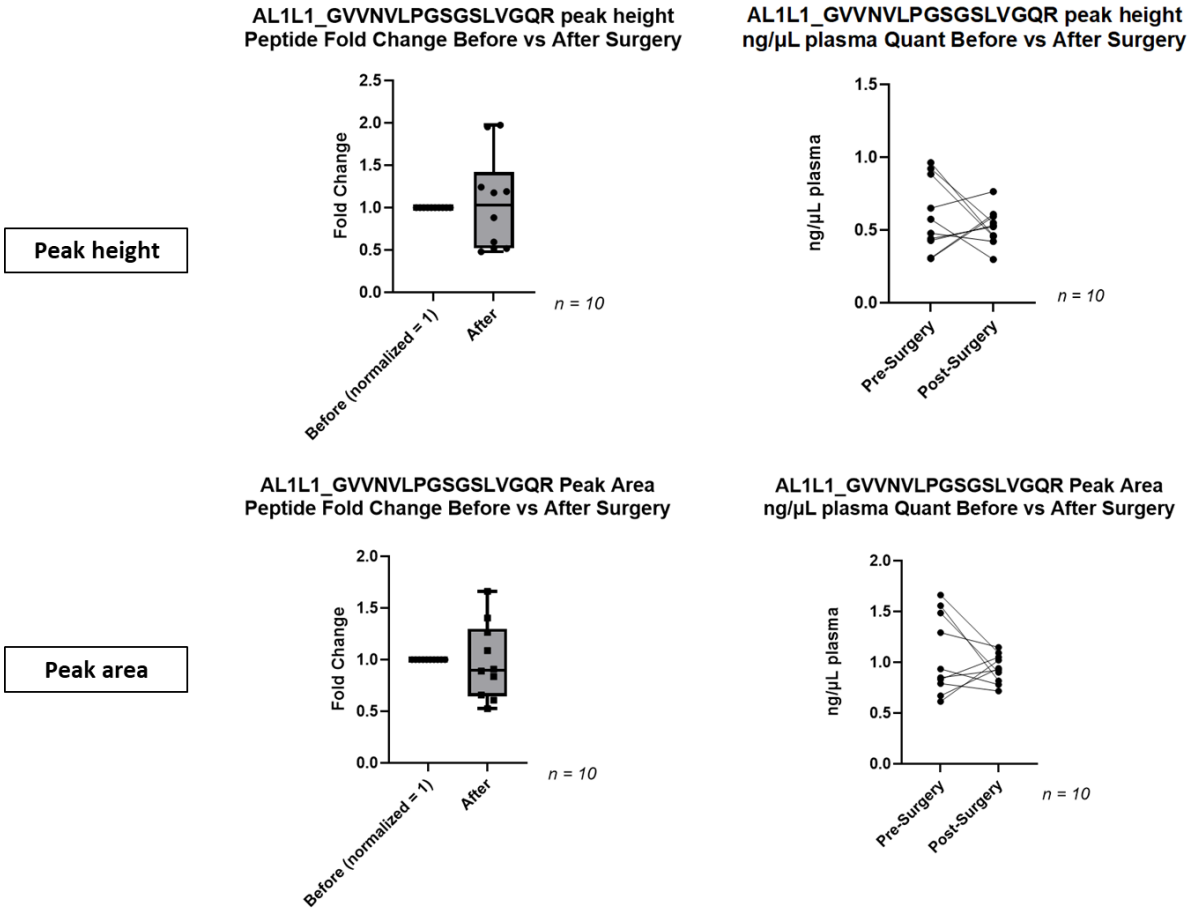

Figure 44B. AL1L1 Absolute Quantification Across the Pilot AAA Cohort. Quantitative analysis of the AL1L1 peptide (GVVNVLPGSGSLVGQR) across the OxAAA pilot cohort (n = 10), comparing plasma samples collected before surgery (TP3) and after surgery (TP5/TPF). Left panels display box-and-whisker plots (minimum to maximum) of $\log_2$-normalised fold change derived from peak height and peak area measurements. Boxes represent the interquartile range (IQR), the central line indicates the median, whiskers extend to the minimum and maximum values, and all individual data points are shown. Right panels depict paired individual plasma concentrations (ng/µL) with connecting lines illustrating within-patient longitudinal changes. No statistically significant postoperative differences were observed in either peak height or peak area. Fold-change values remained close to 1.0, indicating relative stability of AL1L1 levels following surgery. Although detectable, the limited dynamic range and greater variability suggest reduced suitability of this peptide for robust biomarker quantification.

Although technically measurable, the AL1L1 peptide showed limited dynamic range and poor response to surgical intervention. The small fold-change across patients, along with low absolute concentrations, indicates this peptide was susceptible to ion suppression and may not be suitable for reliable biomarker development. Overall, its inclusion in the panel

remains exploratory, and further optimisation or peptide substitution may be necessary for future studies focused on high-confidence quantification of AL1L1.

4.10.4 CRP Peptide (ESDTSYVSLK)

The CRP-derived peptide ESDTSYVSLK showed strong and consistent chromatographic performance across all patient samples. Both light and heavy OxConCAT forms co-eluted effectively at approximately 6.6 min RT, with minimal matrix interference and well-defined peak shapes in both pre- and post-surgical samples (Figure 45A). Notably, fragment ion intensities were consistently high, providing excellent signal-to-noise ratios for both light and heavy peptides. These features allowed for confident manual selection and integration of the top three fragment peaks for precise quantification. Pre-surgery absolute quantification of the top-peak fragment was 2.79 ± 0.15 ng/µL and 2.33 ± 0.34 ng/µL post-surgery. The data suggested a modest ~1.2-fold decrease post-operatively; however, this difference did not reach statistical significance for patient 01 individually (Figure 45A).

45-A

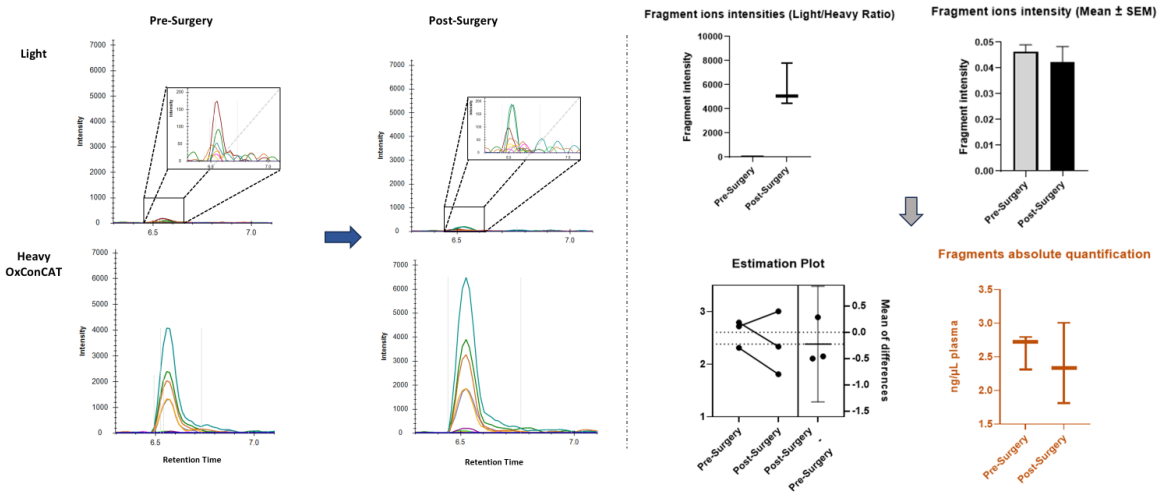

Absolute Quantification output

Time Point	fmol/µL	ng/µL (±SEM)
Patient 01 (Pre - Surgery, time 0h)	2477.6	2.79 ± 0.15
Patient 01 (Post - Surgery, time ≥ 1 month)	2070.2	2.33 ± 0.34

Figure 45A. Absolute Quantification of CRP in an Individual AAA Patient. Skyline chromatograms and quantitative output for the OxConCAT-derived CRP peptide (ESDTSYVSLK) from Patient 01, showing strong co-elution of light (endogenous) and heavy (OxConCAT) traces at ~6.6 min. The peptide exhibited excellent chromatographic performance and high fragment ion intensities, enabling precise quantification. Absolute concentrations were 2.79 ± 0.15 ng/µL pre-surgery and 2.33 ± 0.34 ng/µL post-surgery, indicating a modest (~1.2-fold) but non-significant postoperative decrease.

Across the patient pilot cohort (n = 10), this peptide consistently showed significant downregulation post-surgery, with the following observations (Figure 45B): peak height significant decreases ($p < 0.001$) in light peptide intensity, and a considerable reduction ($p < 0.01$) in the peak area for all patients. Fold-change analysis confirms a consistent suppression of CRP peptide signal with normalised post-operative values averaging ~0.5-fold relative to pre-operative levels.

45-B

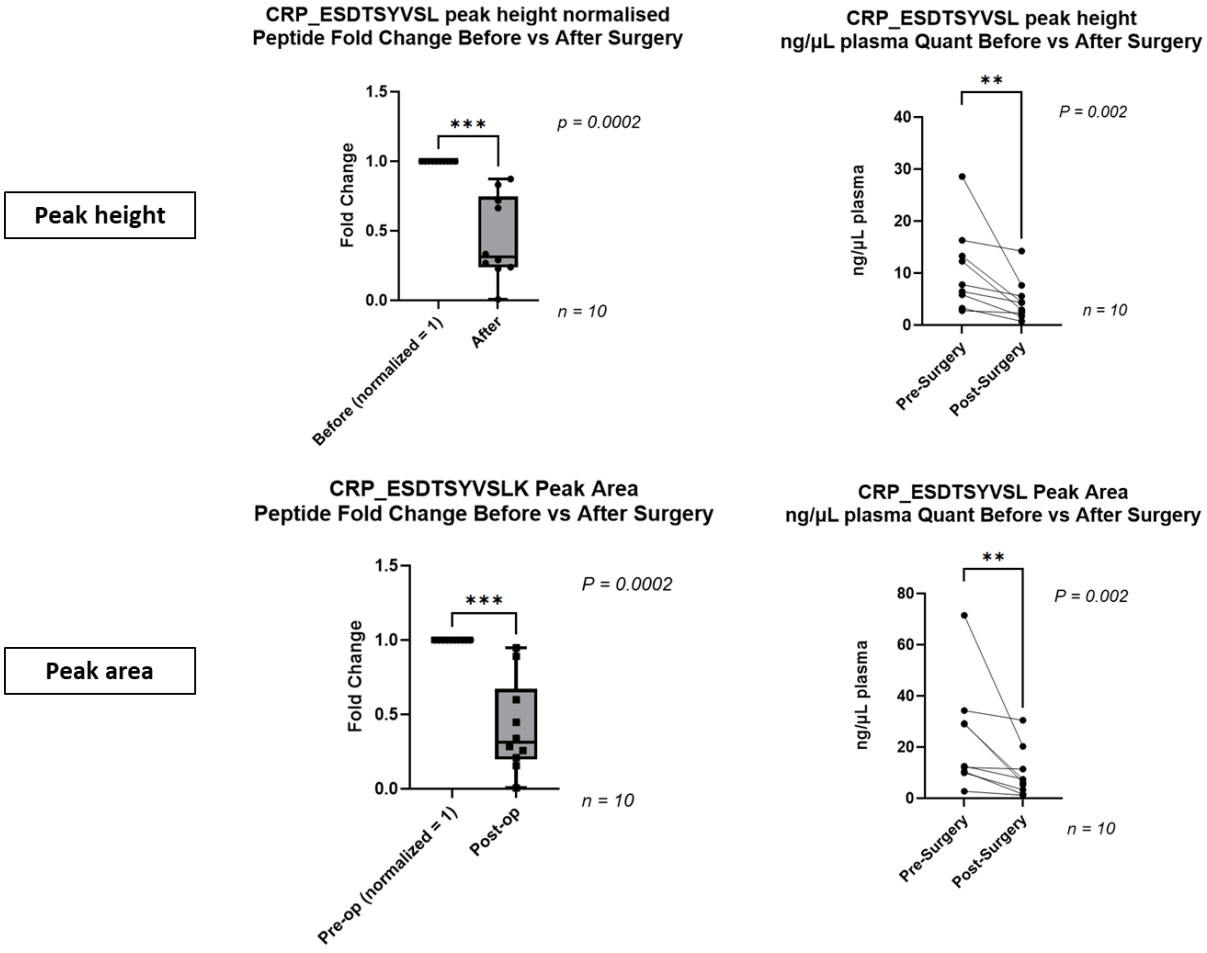

Figure 45B. CRP Absolute Quantification Across the Pilot AAA Cohort. Quantitative assessment of the CRP peptide (ESDTSYVSLK) across the OxAAA pilot cohort (n = 10), comparing plasma samples collected before surgery (TP3) and after surgery (TP5/TPF). Left panels display box-and-whisker plots (minimum to maximum) of log_2-normalised fold change derived from peak height and peak area measurements. Boxes represent the interquartile range (IQR), the central line denotes the median, whiskers extend to the minimum and maximum values, and all individual data points are shown. Right panels present paired individual plasma concentrations (ng/µL) with connecting lines illustrating within-patient longitudinal changes. A statistically significant postoperative reduction in CRP abundance is observed across both peak height and peak area quantification approaches (paired statistical testing: ***P = 0.0002; **P = 0.002). The approximately 0.5-fold decrease in fold-change analysis reflects a consistent suppression of circulating CRP levels in the post-operative samples.

This peptide demonstrated excellent detectability, a robust dynamic range, and clear post-surgical responsiveness, making it a highly reliable biomarker for monitoring inflammatory status in AAA patients. The sharp decline in peptide levels after surgery

likely reflects the acute-phase nature of CRP and supports its utility in perioperative monitoring. Due to its strong performance metrics, CRP (ESDTSYVSLK) remains a key candidate in the biomarker panel and a positive control for absolute quantification in plasma.

4.10.5 APOA4_1 Peptide (LLPHANEVSQK)

This peptide displayed strong and distinct chromatographic peaks in both pre- and post-surgery plasma samples, with clear co-elution of light and heavy transitions at ~3.9 min RT. The peak shape was sharp and symmetrical, especially for the heavy OxConCAT peptide (Figure 46A). Notably, post-surgery light signals were markedly elevated, showing a substantial increase in intensity relative to pre-surgery. The light-to-heavy fragment ion ratio increased significantly, confirming enhanced detection sensitivity and quantifiability post-surgery (pre-operatively, the highest peak fragment was 3.24 ± 0.34 ng/µL and post-operatively, 19.85 ± 0.75 ng/µL). The retention time reproducibility and low background noise further supported its stable chromatographic behaviour in complex plasma.

46-A

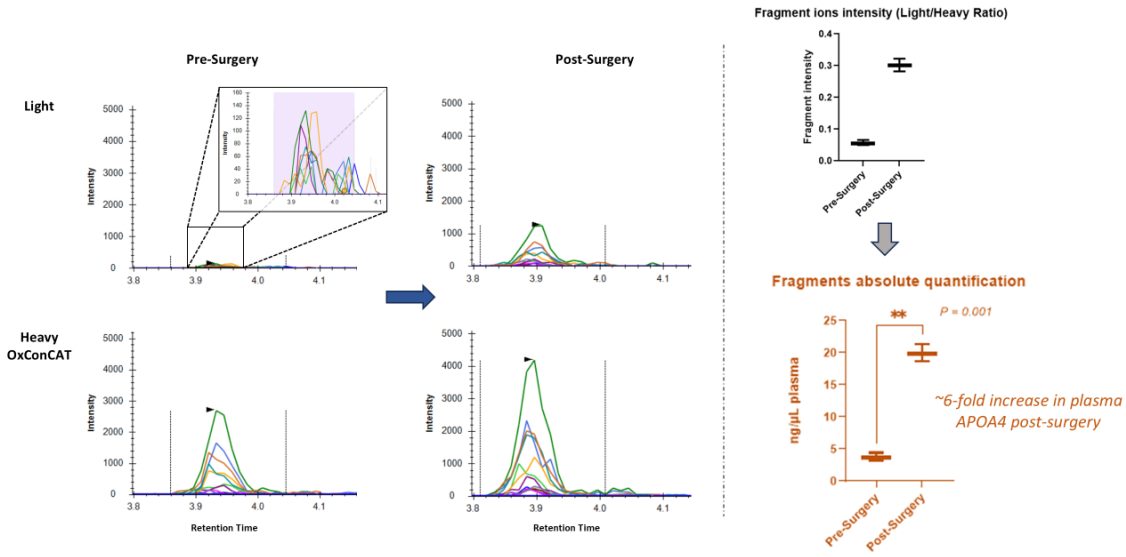

Absolute Quantification output

Time Point	fmol/µL	ng/µL (±SEM)
Patient 01 (Pre - Surgery, time 0h)	2453.53	3.24 ± 0.34
Patient 01 (Post - Surgery, time ≥ 1 month)	15021.56	19.85 ± 0.75

Figure 46A. Absolute Quantification of APOA4 in an Individual AAA Patient. Skyline chromatograms and quantitative output for the OxConCAT-derived APOA4 peptide (LLPHANEVSQK) from Patient 01, showing distinct and well-resolved light (endogenous) and heavy (OxConCAT) peaks co-eluting at ~3.9 min. The post-surgery light signal showed a substantial intensity increase, reflected by a significant rise in the light-to-heavy fragment ion ratio. Absolute quantification yielded 3.24 ± 0.34 ng/µL pre-surgery and 19.85 ± 0.75 ng/µL post-surgery, corresponding to an approximately 6-fold increase in plasma APOA4 concentration ($p = 0.001$). The peptide displayed excellent chromatographic fidelity and reproducibility.

This represented an approximately 6-fold increase in APOA4, with low intra-patient variability ($p = 0.001$; Figure 46A). The high absolute concentrations and low SEM reflect excellent quantification fidelity.

Pilot cohort-wide analyses showed consistent and significant increases in both peak height and area across patients. Peak height measurements increased ($p < 0.01$), with box plots showing an upward shift in the post-surgery group (Figure 46B).

Peak Area likewise increased ($p < 0.01$), mirroring the peak height trend and confirming the dynamic range of the peptide response. Fold-change analyses revealed a ~4.5-fold median increase in plasma APOA4 peptide post-surgery, indicating this peptide is highly responsive to surgical intervention and physiologic stress.

46-B

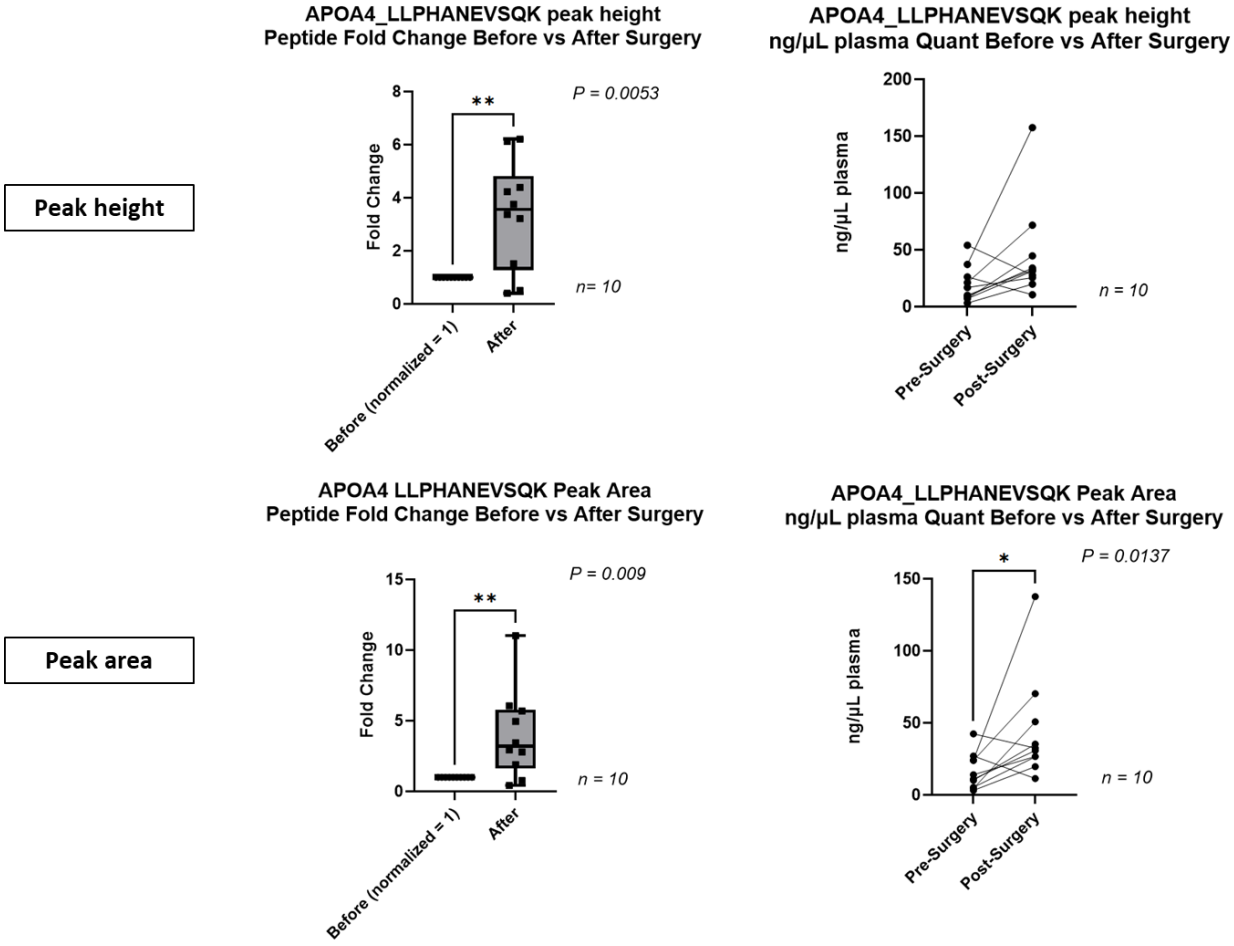

Figure 46B. APOA4_1 Absolute Quantification Across the Pilot AAA Cohort. Quantitative assessment of the APOA4 peptide (LLPHANEVSQK) across the OxAAA pilot cohort (n = 10), comparing plasma samples collected before surgery (TP3) and after surgery (TP5/TPF). Left panels display box-and-whisker plots (minimum to maximum) of log_2-normalised fold change derived from peak height and peak area measurements. Boxes represent the interquartile range (IQR), the central line denotes the median, whiskers extend to the minimum and maximum values, and all individual data points are shown. Right panels present paired individual plasma concentrations (ng/µL) with connecting lines illustrating within-patient longitudinal changes. A statistically significant postoperative increase in APOA4 abundance is observed across both peak height and peak area quantification approaches (paired statistical testing: P = 0.0053 for peak height; P = 0.009 and P = 0.0137 for peak area measures). Fold-change analysis indicates a marked elevation in APOA4 levels following surgery.

The APOA4 peptide demonstrated excellent chromatographic and quantitative performance, with high signal intensity, broad dynamic range, and statistically significant fold-changes across patients. It is consistently upregulated post-surgery, reflected in both absolute and relative quantification metrics. Due to high abundance, low variability, and considerable fold-change, LLPHANEVSQK is one of the strongest-performing peptides in the AAA panel, providing high-confidence quantitative data suitable for both individual and cohort-level analysis. Its inclusion in future predictive models is warranted and supported by both biological and technical performance.

4.10.6 APOA4_2 Peptide (LGPHAGDVEGHLSFLEK)

The peptide LGPHAGDVEGHLSFLEK showed moderate to strong chromatographic performance, with well-defined peak shapes and consistent retention times (~4.1 min RT). Fragment ion co-elution was satisfactory, although some variability in intensity across transitions was observed. The signal was sufficiently above baseline noise, with consistent light/heavy fragment ion ratios that enabled reliable peak identification and quantification. Despite a slight variation in signal intensity, the peptide was confidently detected in all samples from Patient 01 and throughout the cohort. In the 10-patient pilot, this peptide showed an upward trend in abundance after surgery, although it did not reach statistical significance. Peak height quantification (ng/µL) yielded a median of about 25 ng/µL before surgery and about 35 ng/µL after. Peak Area quantification (ng/µL) had a median of around 30 ng/µL pre-surgery and approximately 50 ng/µL post-surgery. Fold-change analysis suggested a trend toward increased abundance after surgery (mean fold-change around 1.5–1.7), but high variability within patients limited statistical power (Figure 47). Although LGPHAGDVEGHLSFLEK showed suitable chromatographic and

ionisation behaviour, it did not display a consistent or statistically significant change after surgery across the pilot study. This may reflect biological variability in APOA4 regulation or peptide-specific sensitivity to sample matrix effects. Despite suitable chromatographic performance, the peptide did not show a statistically significant change and warrants validation in a larger cohort. Its current performance suggests limited usefulness, but it could complement other APOA4 peptides in multi-peptide quantification strategies.

47

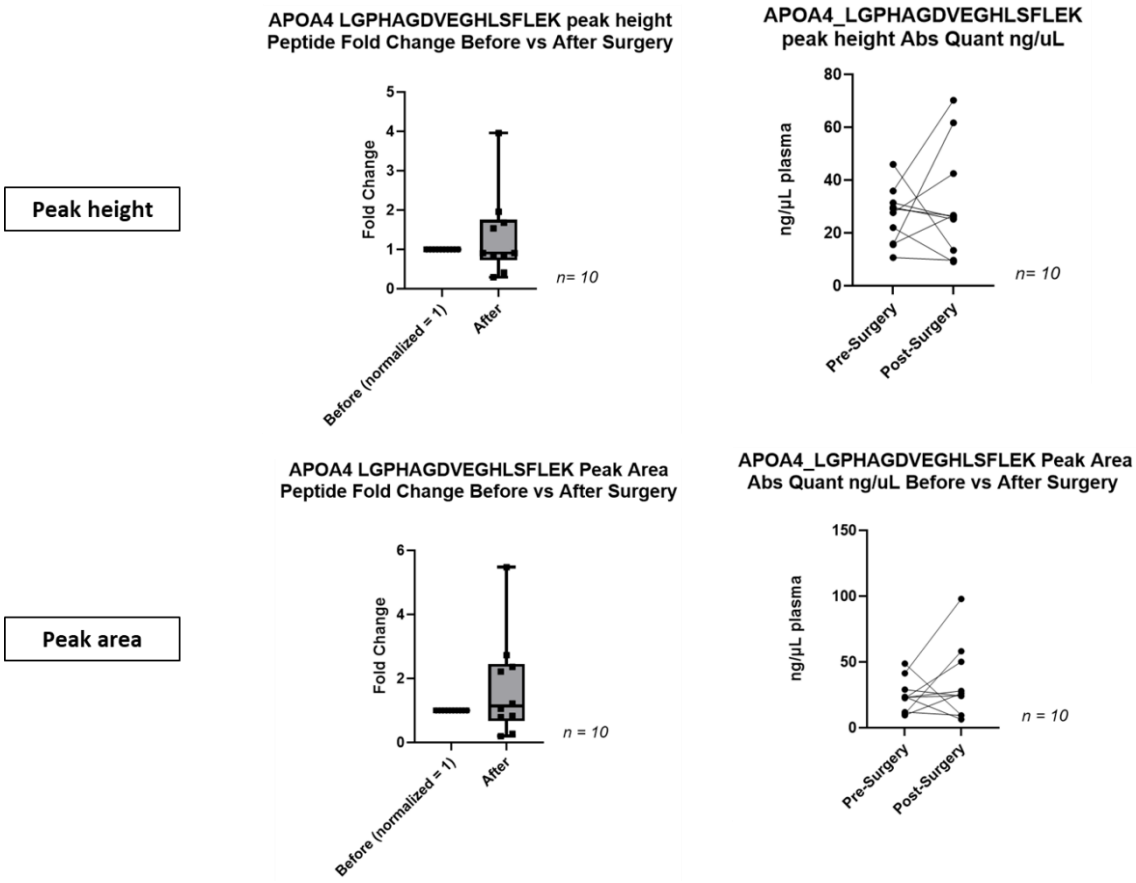

Figure 47. APOA4_2 Absolute Quantification Across the Pilot AAA Cohort. Quantitative evaluation of the APOA4 peptide (LGPHAGDVEGHLSFLEK) across the OxAAA pilot cohort (n = 10), comparing plasma samples collected before surgery (TP3) and after surgery (TP5/TPF). Left panels display box-and-whisker plots (minimum to maximum) of log_2-normalised fold change derived from peak height and peak area measurements. Boxes represent the interquartile range (IQR), the central line denotes the median, whiskers extend to the minimum and maximum values, and all individual data points are shown. Right panels present paired absolute plasma concentrations (ng/µL) with connecting lines illustrating within-patient longitudinal changes. A trend toward increased APOA4_2 abundance following surgery is observed in both peak height and peak area measurements; however, inter-individual variability limits statistical significance in this pilot cohort.

4.10.7 CO8G Peptide (RPASPSTIQPK)

The peptide RPASPSTIQPK exhibited strong chromatographic behaviour, with clear and consistent co-elution of light and heavy forms in both pre- and post-surgery samples. Retention times were steady (~5.4 min RT), with sharp, well-resolved peaks (Figure 48A). Signal-to-noise ratios were high, and minimal matrix interference was detected. Fragment ion traces were reliable and reproducible, enabling confident quantification. Manual peak integration verified excellent ionisation efficiency. The three most intense fragment ions were used for quantification in patient 01. For the entire cohort, the highest peak was consistently chosen for both peak height and peak area measurements (Pre-surgery: 13.14 ± 1.30 ng/µL and post-surgery: 9.17 ± 0.25 ng/µL). This translated to an approximate 1.5-fold decrease in plasma CO8G levels post-surgery, which reached statistical significance (p = 0.034) in patient 0.

48-A

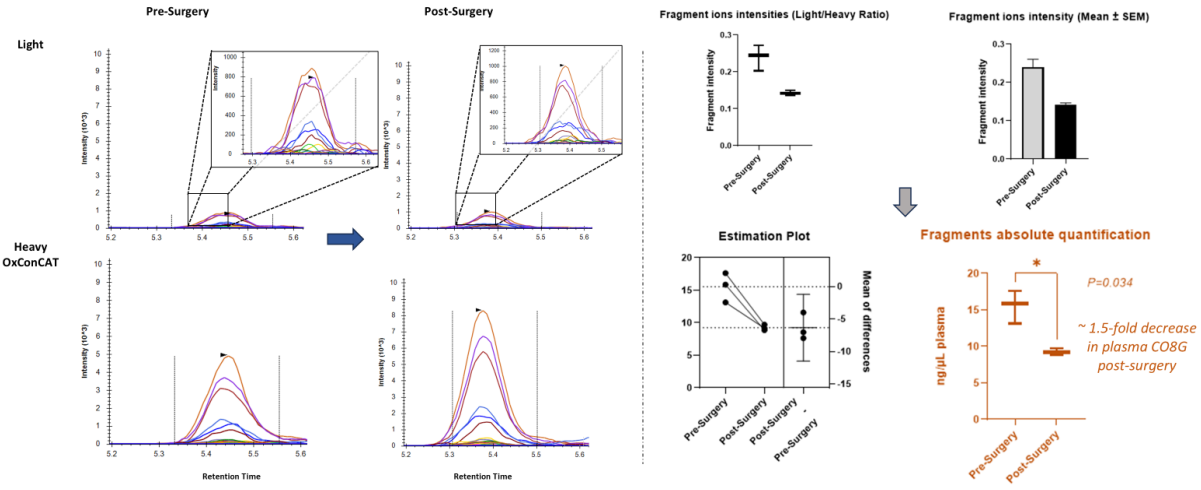

Absolute Quantification output	Time Point	fmol/µL	ng/µL (±SEM)
	Patient 01 (Pre - Surgery, time 0h)	10157.67	13.14 ± 1.30
	Patient 01 (Post - Surgery, time ≥ 1 month)	7088.38	9.17 ± 0.25

Figure 48A. Absolute Quantification of CO8G in an Individual AAA Patient. Skyline chromatograms and quantitative output for the OxConCAT-derived CO8G peptide (RPASPSTIQPK) from Patient 01, showing sharp co-elution of light (endogenous) and heavy (OxConCAT) traces at ~5.4 min with excellent signal-to-noise ratios. Quantitative analysis yielded 13.14 ± 1.30 ng/µL pre-surgery and 9.17 ± 0.25 ng/µL post-surgery, indicating an approximately 1.5-fold decrease in plasma CO8G levels (p = 0.034). The fragment ion intensities and estimation plots confirmed a consistent postoperative reduction in circulating peptide abundance.

In the patient cohort (*n = 10*), both peak height and peak area analyses demonstrated a significant reduction in peptide abundance post-surgery. Key results include peak height quantification $p < 0.0001$, Peak Area quantification $p = 0.0001$, and Fold-change (peak height) mean ~0.6-fold post-surgery, $p < 0.0001$. Fold-change (Peak Area) mean ~0.6-fold post-surgery, $p < 0.0001$. Box plots indicated a consistent and significant reduction in CO8G levels post-surgery across the cohort, with low intra-patient variability (Figure 48B).

48-B

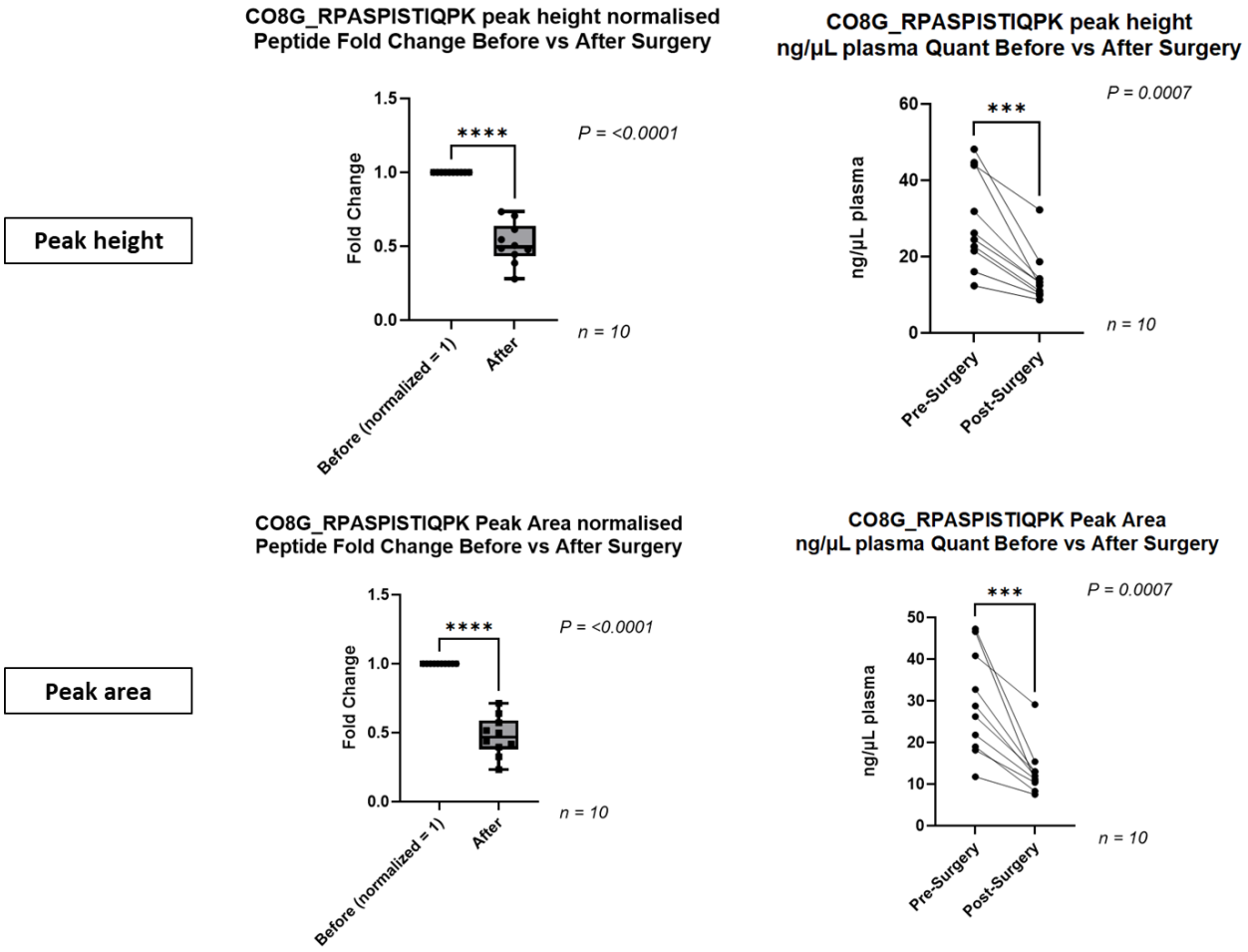

Figure 48B. CO8G Absolute Quantification Across the Pilot AAA Cohort. Quantitative evaluation of the CO8G peptide (RPASPSTIQPK) across the OxAAA pilot cohort (n = 10), comparing plasma samples collected before surgery (TP3) and after surgery (TP5/TPF). Left panels show box-and-whisker plots (minimum to maximum) of log_2-normalised fold change derived from peak height and peak area measurements. Boxes represent the interquartile range (IQR), the central line denotes the median, whiskers extend to the minimum and maximum values, and all individual data points are displayed. Right panels present paired absolute plasma concentrations (ng/µL) with connecting lines illustrating within-patient longitudinal changes. A significant and consistent postoperative reduction in CO8G abundance is observed across both quantification approaches (paired statistical testing: peak height P = 0.0007; peak area P = 0.0007; fold-change analyses P < 0.0001). The concordant decrease across analytical formats supports the robustness and reproducibility of CO8G quantification within the OxConCAT workflow.

RPASPSTIQPK proved to have reliable peak integration and a responsive peptide for absolute quantification of CO8G. Its significant decrease post-surgery, reproducibility across patients, and high-quality chromatographic characteristics support its utility as a potential biomarker candidate.

The peptide reliably detected post-surgical reductions, supporting its inclusion in future targeted panels aimed at clinical monitoring and outcome prediction. CO8G is together with Attractin part of the 3 key peptides that emerged from the previous OxAAA study published in Annals of Surgery, which I have co-authored (Integrated Plasma and Tissue Proteomics Reveals Attractin Release by Intraluminal Thrombus of Abdominal Aortic Aneurysms and Improves Aneurysm Growth Prediction in Humans, Lee et al), where thrombus-derived protein release and postoperative systemic decreases were described. Specifically, analyses of the tissue culture supernatant revealed 3 proteins that were: (i) uniquely present in intra-luminal thrombus; (ii) released by intra-luminal thrombus; (iii) systemic levels reduced after AAA surgery;(iv) different between fast and slow growth AAAs, and this is highly important as it validates previous important discovery data.

These peptide-level assessments reveal differing performance among the OxConCAT components, offering important technical and biological insights (Table 16). While peptides such as APOA4_1, NCHL1, ATRN, CRP, and CO8G showed excellent detectability, strong ionisation, and clear responses to surgical intervention, others, most notably AL1L1, faced technical limitations like low ionisation efficiency, signal suppression, and inconsistent quantification. Specifically, AL1L1 did not meet reliability criteria in several samples and was excluded from fold-change analyses, while APOA4_2, though consistently detectable, exhibited a modest and variable response after surgery. Overall, five out of six peptides demonstrated reliable performance, supporting their use in both absolute quantification workflows and biomarker development.

The changes observed in NCHL1, CRP, APOA4_1, ATRN, and CO8G across the patient cohort may highlight their potential clinical utility in monitoring systemic responses to surgery. These findings provide important context for interpreting the group-level fold-change analyses in the next section and underscore the importance of thorough peptide evaluation before their application in clinical proteomics.

Table 16. Summary of peptide-level performance and post-surgical trends in the OxConCAT patient pilot study. Evaluation of chromatographic quality, detection rate, and quantitative reliability for target peptides included in the OxConCAT C-002 construct. Peptides showing consistent detection and post-surgical changes (e.g., CRP, APOA4_1, ATRN, CO8G) were considered highly reliable for absolute quantification and biomarker analysis.

Peptide	Chromatographic Quality	Quant Detection Rate	Post-Surgical Trend	Quant Reliability
NCHL1	Excellent	100%	↓ Significant	High
ATRN	Good	100%	↓ Significant	High
AL1L1	Poor	~60%	– Not significant	Low
CRP	Excellent	100%	↑ Significant (group)	High
APOA4_1	Excellent	100%	↑↑ Highly significant	Very High
APOA4_2	Good	100%	↑ Modest, variable	Moderate
CO8G	Excellent	100%	↓ Significant ($p<0.001$)	High

4.11 Grouped Protein-Level Analysis

4.11.1 Fold-Change Analysis and Log_2 FC Trends

To assess the overall impact of surgical intervention on absolute protein concentrations, fold-change analysis was conducted for each quantified AAA panel protein before and after surgery across 10 paired patient samples. Normalised fold-change values (post-operative/pre-operative) were calculated for each peptide, and significance was determined using paired t-tests corrected for multiple comparisons with the False Discovery Rate (FDR) method (Benjamini, Krieger, Yekutieli) at a Q threshold of 1% (Figure 49).[76] This allowed identification of peptides showing significant expression changes post-surgery.

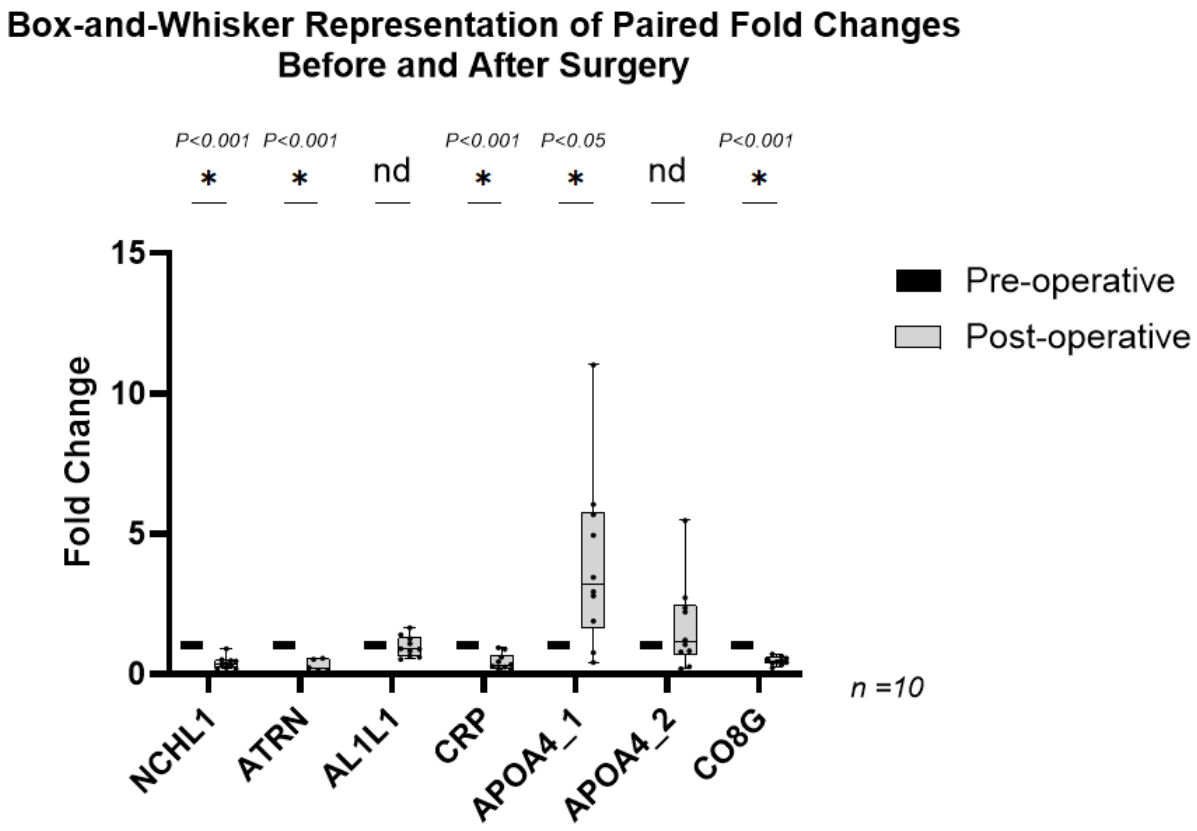

Figure 49. Distribution of Paired Fold Changes in Targeted Peptides Before and After Surgery. Box-and-whisker plots (min–max with all individual data points shown) illustrate post-operative fold changes relative to pre-operative baseline (normalised to 1.0) for each targeted peptide (n = 10). Fold change was derived from absolute quantification data. Each data point represents an individual patient, preserving the paired longitudinal structure of the cohort and explicitly accounting for within-subject variability. Statistical significance was evaluated using paired Student's t-tests with Benjamini–Hochberg FDR correction (Q = 0.01, 1%). Asterisks denote significant differences (*P < 0.05; **P < 0.001), and 'nd' indicates no significant difference. Consistent with the individual peptide analyses presented in Figures 42–48, NCHL1, ATRN, CRP, and CO8G showed significant postoperative decreases, whereas APOA4_1 demonstrated a significant increase following surgery. This representation avoids distributional assumptions inherent to bar plots with error bars and provides a transparent visualisation of inter-individual variability and paired changes.

Summary of Test Parameters:

Parameter	***Description***
Test	*Paired t-test with FDR correction*
FDR Method	*Benjamini, Krieger, Yekutieli (Two-stage step-up)*
Desired FDR (Q)	*1.0%*
Total Comparisons	*7 peptides across 6 proteins*
Figure Reference	*Grouped fold-change bar plot with P-values (Figure 49)*

Key Findings from Fold-Change Group Analysis

The grouped fold-change plot (Figure 49) highlights several statistically significant changes in plasma protein concentrations post-surgery, summarised in Table 17.

Table 17. Key findings from fold-change group analysis of plasma proteins pre- and post-surgery. Summary of mean fold changes, statistical significance, and direction of change for target peptides in the OxConCAT pilot study. Significant decreases were observed for NCHL1, ATRN, CRP, and CO8G, while APOA4_1 showed a marked post-operative increase.

Protein	**Peptide ID**	**Mean Fold Change**	**P-value**	**Q-value**	**Significance**	**Direction of Change**
NCHL1	GAGPESEPYIFQTPEGVPEQPTFLK	0.41	<0.001	0.00001	**Yes**	↓ Post-op
ATRN	YYTAINFVATPDEQNR	0.27	<0.001	0.00036	**Yes**	↓ Post-op
AL1L1	GVVNVLPGSGSLVGQR	~1.0	ns	ns	No	Neutral
CRP	ESDTSYVSLK	0.41	<0.001	0.00021	**Yes**	↓ Post-op
APOA4_1	LLPHANEVSQK	4.0	<0.05	0.0086	**Yes**	↑ Post-op
APOA4_2	LGPHAGDVEGHLSFLEK	1.72	ns	ns	No	↑ Post-op (NS)
CO8G	RPASPISTIQPK	0.47	<0.001	0.000003	**Yes**	↓ Post-op

Note: "ns" = not significant; ↓ and ↑ denote decrease and increase post-operatively.

Protein-Level Trends

Significant Responders: APOA4_1 (LLPHANEVSQK) showed approximately a 4-fold increase after surgery, indicating consistent upregulation across the patient group. This was the only peptide notably increased post-operatively ($p = 0.0141$, $q = 0.0086$). NCHL1, ATRN, CRP, and CO8G all displayed statistically significant decreases, suggesting these proteins are suppressed after surgery, potentially reflecting reduced systemic inflammation or changes in vascular-related protein turnover. Non-Responders / Inconclusive: AL1L1 showed no significant change ($p = 0.890$), with a fold change near 1, indicating poor detectability or stability. APOA4_2 (LGPHAGDVEGHLSFLEK) increased following surgery (1.72-fold), but this was not statistically significant ($p = 0.186$, $q = 0.094$). The higher variance of this peptide likely masked significance despite showing a consistent trend.

The grouped analysis confirms post-surgical modulation of several key AAA panel proteins, particularly APOA4 and CO8G. The divergent behaviour of APOA4 peptides highlights the importance of multi-peptide validation for reliable quantification, as only one of the two peptides reached statistical significance. In contrast, CO8G and CRP showed measurable decreases after surgery, which may reflect aspects of the vascular or systemic response to AAA repair. This dataset demonstrates the feasibility of using the OxConCAT-based absolute quantification strategy to track plasma protein concentrations over time in a clinical study.

4.11.2 Absolute Quantification Analysis (Log10 ng/µL Plasma)

85To translate fold-changes into absolute concentrations, peptide abundances (fmol per µL plasma) were calculated using heavy-to-light ratios and known spike-in amounts and then converted to ng/µL (Figure 50). These values correspond to peptide-level mass

concentrations obtained from LC–MS analysis and were used as direct indicators of plasma abundance. Concentrations are plotted on a $\log_{10}$ scale for each peptide, with boxplots illustrating inter-patient variability pre- (black) and post-operative (grey). The visual representation (Box-and-whisker plot) and statistical analyses were aimed at directly quantifying plasma protein levels rather than assessing relative changes.

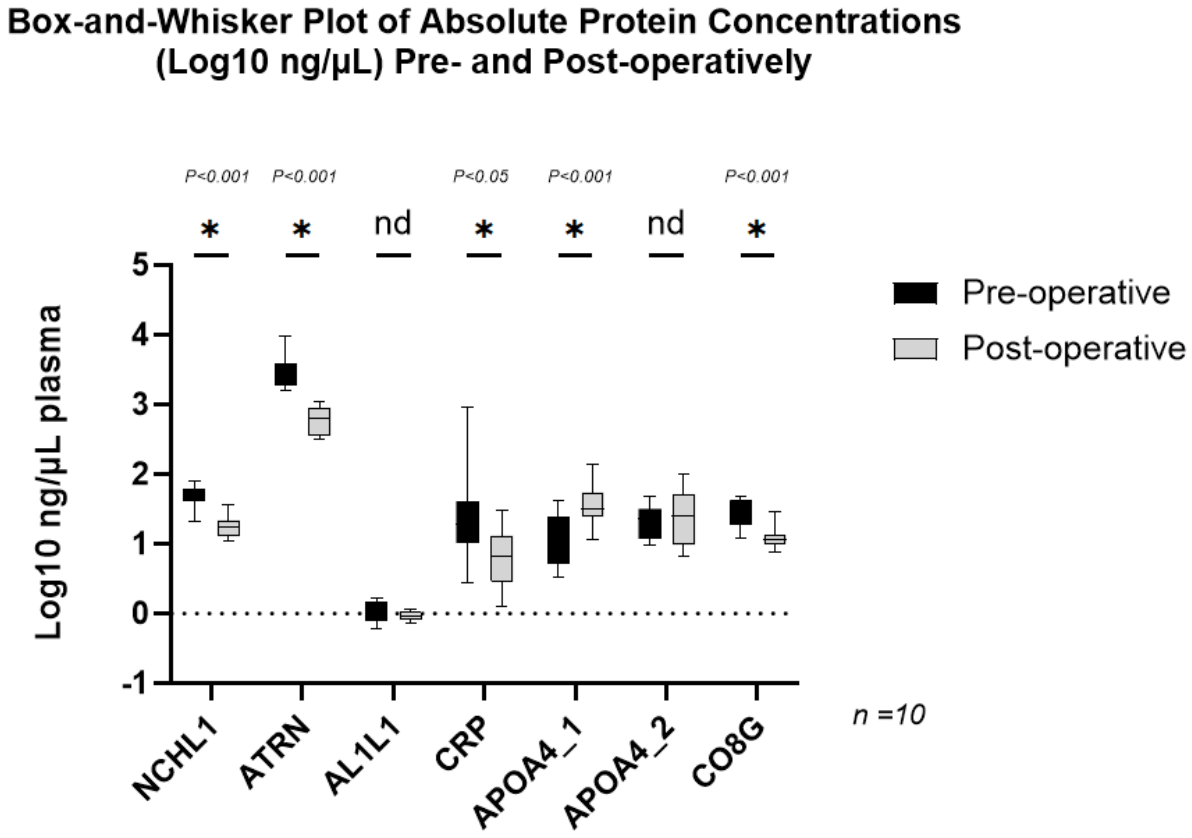

Figure 50. Box-and-whisker plot of absolute protein concentrations (Log10 ng/µL) before and after surgery. Box-and-whisker plots (min–max) with all individual data points shown illustrate absolute plasma concentrations ($\log_{10}$-transformed ng/µL) of seven targeted peptides representing six proteins (NCHL1, ATRN, AL1L1, CRP, APOA4_1, APOA4_2, and CO8G) in the OxAAA pilot cohort (n = 10). Each point represents an individual patient, thereby preserving the paired longitudinal structure of the dataset (pre-operative TP3 vs post-operative TP5/TPF). Statistical comparisons were performed using paired Student's t-tests with Benjamini–Hochberg false discovery rate (FDR) correction (Q = 0.02). Significance levels are indicated above each protein (*P < 0.05; **P < 0.001), while "nd" denotes non-significant change. $\log_{10}$ transformation was applied to improve visualisation across proteins spanning different concentration ranges and to stabilise variance without assuming normal distribution in graphical representation. This presentation explicitly accounts for within-individual changes and avoids the distributional assumptions inherent to summary bar plots with error bars.

Overview of statistical methodology used: multiple paired t-tests comparing pre- and post-operative states were used for each protein. Variance assumption: individual variance is assumed per group. Multiple comparisons correction: False Discovery Rate (FDR), using the two-stage step-up method (Benjamini, Krieger, and Yekutieli). Desired FDR (Q): 2.00%. Number of tests conducted: 7 (one per protein). Sample size: n = 10 paired plasma samples (Table 18).

Table 18. Summary of paired statistical comparisons between pre- and post-operative plasma protein levels. Paired t-tests were performed for each protein (n = 10 paired samples) to assess post-surgical changes. Individual group variance was assumed, and multiple comparisons were corrected using the two-stage step-up False Discovery Rate (FDR) method (Benjamini, Krieger, and Yekutieli) with a desired FDR (Q) of 2%. Significant differences were observed for NCHL1, ATRN, CRP, APOA4_1, and CO8G, confirming consistent trends detected in the fold-change analysis.

Protein	Discovery?	Pre-op Mean (log10 ng/µL)	Post-op Mean (log10 ng/µL)	P value	Q value	Difference (log10)	Significant?
NCHL1	Yes	1.676	1.238	0.000096	0.000146	0.4374 ↓	**Yes**
ATRN	Yes	3.464	2.774	0.006304	0.006430	0.6902 ↓	**Yes**
AL1L1	No	0.00287	-0.0316	0.520081	0.265241	ns	No
CRP	Yes	1.392	0.7946	0.015091	0.009236	0.5976 ↓	**Yes**
APOA4_1	Yes	1.092	1.544	0.008791	0.006725	-0.4514 ↑	**Yes**
APOA4_2	No	1.331	1.387	0.704312	0.307885	ns	No
CO8G	Yes	1.429	1.085	0.000035	0.000108	0.3439 ↓	**Yes**

Note: '↑' indicates increase post-operatively, '↓' indicates decrease post-operatively; 'ns' = not significant.

Significantly Decreased Proteins Post-surgery: NCHL1, ATRN, CRP, and CO8G showed notable decreases in plasma concentration after surgery. The reduction in CRP aligns with expected decreases in systemic inflammation following the procedure.

Significantly Increased Protein Post-surgery: APOA4_1 exhibited a notable rise in post-operative concentration, consistent with its previous behaviour in fold-change analyses, reinforcing its potential as a responsive biomarker.

Proteins with No Significant Change: AL1L1 and APOA4_2 did not exhibit significant pre- and post-operative differences, aligning with previous findings. As a complement to fold-change analysis, this absolute quantification confirms and expands upon prior results, providing precise measurements of actual plasma concentrations rather than relative shifts. The log10 scale allows visualisation of concentration changes over several orders of magnitude, highlighting biological relevance.

The absolute quantification analysis confirms the key findings observed in fold change and log2FC analyses. Importantly, this method provides clinically translatable values (ng/μL) that could be added to clinical prediction models. Significant post-operative reductions in NCHL1, ATRN, CRP, CO8G, and the increase in APOA4_1 remain consistent across all visualisations and statistical approaches, thereby strengthening their biological significance.

Discussion

This section interprets the results of the OxAAA pilot proteomic study by examining the interplay between technical and biological factors that influence protein quantification and expression. The discussion distinguishes artefacts arising from analytical processes, such as matrix effects, digestion variability, and ion suppression, from genuine biological variation related to surgical intervention and systemic physiological change. By disentangling these influences, the analysis provides a clearer understanding of the determinants shaping peptide detectability, quantitative reproducibility, and observed expression patterns in plasma. This distinction is essential for validating true biological signals and for ensuring that subsequent large-scale quantification within the OxAAA cohort reflects accurate, biologically meaningful differences rather than technical bias.

4.12 Interpretation of Technical and Biological Determinants of Protein Quantification and Expression

The data demonstrate that, of the seven peptides assayed, APOA4_1, CRP, ATRN, NCHL1, and CO8G showed high-confidence detection across all samples and statistically significant post-operative changes. Two peptides were considered marginal performers. APOA4_2 was quantifiable but variable (ns after FDR), and AL1L1 frequently fell below LOQ (detected in ~60% of samples), consistent with low signal-to-noise and inconsistent heavy-to-light ratios, suggesting ion suppression or suboptimal ionisation. Several technical limitations may have emerged, such as ion suppression, where the co-elution of abundant plasma peptides likely impeded the AL1L1 transitions, despite optimal selection criteria. Matrix effects, meaning variability in sample quality and lipemic interference, may have contributed to inter-patient signal fluctuations, particularly for low-abundance

targets. Peptide physicochemical properties, particularly highly hydrophobic or borderline-charged sequences (e.g., AL1L1), were associated with poor chromatographic peak shape and low fragmentation efficiency. Overall, protein-level quantification trends from both fold-change and absolute concentration analyses confirmed consistent post-operative decreases in NCHL1, ATRN, CRP, and CO8G, with APOA4_1 showing a moderate increase. AL1L1 and APOA4_2 remained essentially unchanged, reflecting stable baseline expression. These consolidated plots provided a clear and concise visual summary of protein behaviour across patients. From a biological standpoint, at TP5 (post-operation), decreases in CRP, NCHL1, ATRN, and CO8G and an increase in APOA4_1 were observed. The decline in CRP is compatible with the resolution of the acute postoperative response by TP5, whereas increased APOA4 may reflect lipid transport/remodelling during recovery. Inter-patient dispersion, most evident for APOA4_1, likely captures heterogeneity in convalescence and baseline metabolic status. This pilot application of the OxConCAT c-002 construct for absolute quantification in human plasma enabled the detection and quantification of most target peptides. However, a subset, especially the AL1L1 peptide, showed limited detectability and did not meet reliability thresholds (low median idotp; light S/N frequently < LOQ; < 3 transitions), likely due to ion suppression effects and physicochemical incompatibilities with LC–MS/MS conditions. These results highlight the need for iterative peptide selection and optimisation of chromatographic conditions for low-abundance targets. Further iterations may be used to develop and evaluate a next-generation OxConCAT construct that could incorporate newly selected peptides optimised for better detectability, ionisation efficiency, and quantification reliability. The next-generation OxConCAT construct could be planned to: (i) replace underperforming peptides (e.g., AL1L1) based on PRM screening (idotp, ppm, LOQ, CV); (ii) validate summed top 3 transitions for cohort-wide

quantitation; and (iii) confirm panel behaviour in a larger cohort with pre-specified QC exclusions and BKY/BH-controlled endpoints. This improved construct aims to overcome the limitations seen in the current analysis and enhance overall absolute quantification. Additionally, validation studies with larger patient cohorts are planned to confirm the clinical utility of these candidate biomarkers for disease monitoring and risk stratification.

Chapter 5 – OxConCAT Construct Redesign and Comparative Evaluation

Introduction

This chapter reports the iterative redesign of the OxConCAT construct to address analytical limitations identified in AAAQconCAT-C002. This redesign was directly informed by the peptide-level performance analyses described in Chapter 4. Although C-002 expressed efficiently and incorporated stable isotopes reliably, several peptides showed inconsistent detectability, incomplete digestion, and variable quantitative performance. Guided by these observations, we designed and evaluated two refined constructs (OxConCAT-V2.1 and OxConCAT-V2.2) with the goals of increasing proteolytic uniformity, improving peptide detectability, and standardising absolute quantification in plasma PRM workflows.

Rationale for Construct Redesign

5.1 Scientific motivations and analytical limitations of OxConCAT (AAAQconCAT-C002): Towards improving peptide quantification

The redesign of the OxConCAT construct was guided by data-informed refinement, using DIA-based peptide detection to improve compatibility with PRM workflows. Several peptides in the original construct showed limited detectability, likely due to ion suppression or unfavourable physicochemical properties. The updated construct, therefore, prioritised peptides with demonstrated detectability in discovery-oriented DIA datasets while recognising that DIA provides screening context rather than definitive

quantification. PRM with isotope-labelled standards remained the reference for peptide suitability. Accordingly, OxConCAT-V2 constructs retained a verified core set of proteins (six AAA-relevant proteins plus Attractin) and removed low-confidence targets. To improve reproducibility, the processing pipeline in Skyline was standardised to require at least three transitions per peptide, idotp ≥ 0.95, absolute mass error ≤ 5 ppm, consistent peak boundaries, and paired heavy/light co-elution.

Methods

Peptide Selection and Construct Refinement Workflow

5.2 Peptide Selection, Analytical Challenges, and Construct Refinement

The new OxConCAT followed a structured workflow (Table 19) integrating empirical validation and computational logic to optimise peptide detectability and analytical performance. Proteins relevant to AAA pathophysiology were selected for absolute quantification, and their peptides were retrieved from PeptideAtlas and ranked by observation frequency. Filtering criteria were applied as follows: only peptides between 8 and 15 amino acids were retained to avoid excessively long peptides that produce diffuse MS/MS spectra., and sequences containing cysteine (C), methionine (M), or internal arginine (R) or lysine (K) motifs known to generate unstable or ambiguous tryptic products (e.g., repeated KR motifs or established missed-cleavage hotspots) were excluded. Peptides mapping to multiple genomic locations or corresponding to inactive precursors were removed. The resulting set was codon-optimised for E. coli expression and validated by PRM using DIA guidance. Peptides showing poor or inconsistent detection were deprioritised in subsequent iterations. Validation through PRM revealed that some theoretically detectable peptides failed to ionise efficiently or were suppressed

in the plasma matrix, highlighting the limitations of purely *in silico* selection and emphasising the need for iterative empirical refinement.

Table 19. Workflow for peptide selection and construct refinement in the new OxConCAT design. This workflow outlines each step from protein selection to empirical validation, ensuring rigorous filtering based on detectability, suitability, and biological relevance.

Step	Description
Step 1	Select proteins relevant to AAA pathophysiology and biomarker discovery.
Step 2	Retrieve observed peptide sequences for selected proteins from PeptideAtlas.
Step 3	Rank peptides by number of supporting experiments and observation frequency.
Step 4	Apply filtering criteria: • Peptide length: 8–15 amino acids • Exclude C, M, internal R and K.
Step 5	Exclude peptides with multiple genomic mappings to avoid ambiguous protein inference.
Step 6	Remove signal peptides and pro-peptides representing inactive or cleaved forms.
Step 7	Assemble, construct, and optimise codons for efficient protein expression.
Step 8	Validate peptide detectability using PRM runs guided by DIA discovery data.
Step 9	Refine construct based on empirical detectability, retaining only robust targets.
Step 10	Apply quantitative QC thresholds in Skyline (≥3 transitions, idotp ≥ 0.95, |ppm| ≤ 5, S/N above LOQ) and document inclusion/exclusion with rationale.

5.3 Empirical validation using DIA overlap analysis with an automated script for peptide suitability

During the peptide refinement stage of the new OxConCAT construct, a detailed comparison was conducted between peptide candidates derived from three main sources: the original *in silico* script, DIA (TimsTOF) data, and Orbitrap Astral (Thermo Fisher)-derived outputs.[77] The objective was to identify peptides that were both analytically detectable and uniquely mapped to their target proteins, ensuring high-confidence and reproducible quantification across platforms. Several peptides initially included in the

script were found to be undetectable in both TimsTOF and Astral runs, indicating limited analytical value and leading to their systematic exclusion. Conversely, peptides demonstrating empirical overlap with either dataset were prioritised for retention, even if ranked lower in the initial selection hierarchy; overlap with two platforms (TIMS and Astral) reduces platform-specific detection artefacts. This overlap served as empirical confirmation of detectability and justified their inclusion in the refined construct. An illustrative case involved a peptide present in the original script but absent from both DIA and Astral data, which was replaced by a lower-ranked but empirically confirmed alternative. These examples demonstrated the necessity of combining automated ranking systems with manual expert curation to prevent overlooking analytically valuable peptides.[78] To maintain traceability, annotations were added to the construct documentation to flag uncertain entries (e.g., "unknown") and to justify manual interventions overriding automated filters. This iterative, evidence-based process enabled the construct to evolve from a theoretical model into a more empirically grounded and analytically robust standard. By integrating orthogonal data sources and manual curation, the resulting construct retained only those peptides that were both biologically relevant and experimentally validated, substantially improving the likelihood of successful quantification by PRM in plasma samples from AAA patients.

Peptides were filtered using strict biochemical criteria: optimal length (8–15 amino acids), absence of problematic residues (C, M, internal R or K), uniqueness to the target protein, and exclusion of pro-peptides or isoform-ambiguous sequences. Candidates were initially ranked by observation frequency in databases such as PeptideAtlas, though observation count alone was not considered sufficient for reliable detectability.[79]

Empirical overlap with DIA and Astral datasets became the primary retention criterion; candidate peptides were compared across three sources: (i) the in-silico script output, (ii)

TimsTOF DIA, and (iii) Astral DIA. Peptides detected in ≥1 empirical dataset and meeting biochemical criteria were retained for PRM validation; those absent across both empirical datasets were removed unless justified biologically (e.g., secreted/low-abundance targets with strong prior evidence). A colour-coded audit trail recorded status (TRUE/FALSE/UNKNOWN), empirical source(s), and curation notes. "UNKNOWN" entries were provisionally retained for a single PRM screen before final decision.

During iterative review, DIA- or Astral-only detections meeting all criteria were inserted into the construct, while low-ranked peptides with strong empirical signals were promoted. Non-redundancy and digestion efficiency were maintained throughout the refinement process. Once peptide selection was finalised, the gene construct was assembled using a modular design. An initiation sequence (methionine start codon followed by arginine) and a short N-terminal sacrificial tag were introduced to enhance expression efficiency. Short glycine-rich linkers (e.g., TGSG) were inserted between peptides to facilitate tryptic digestion without introducing undesired cleavage sites. At the C-terminus, a termination sequence and polyhistidine tag (His-tag) were added for affinity purification. CRP peptides were incorporated as internal retention-time and quality-control standards during LC–PRM/MS analysis. This empirically guided and manually curated design ensured that the final OxConCAT construct was analytically stable, biologically relevant, and reproducible across experimental runs. The process exemplified the power of iterative optimisation and empirical validation in the design of quantification constructs (Figure 51, Figure 52).

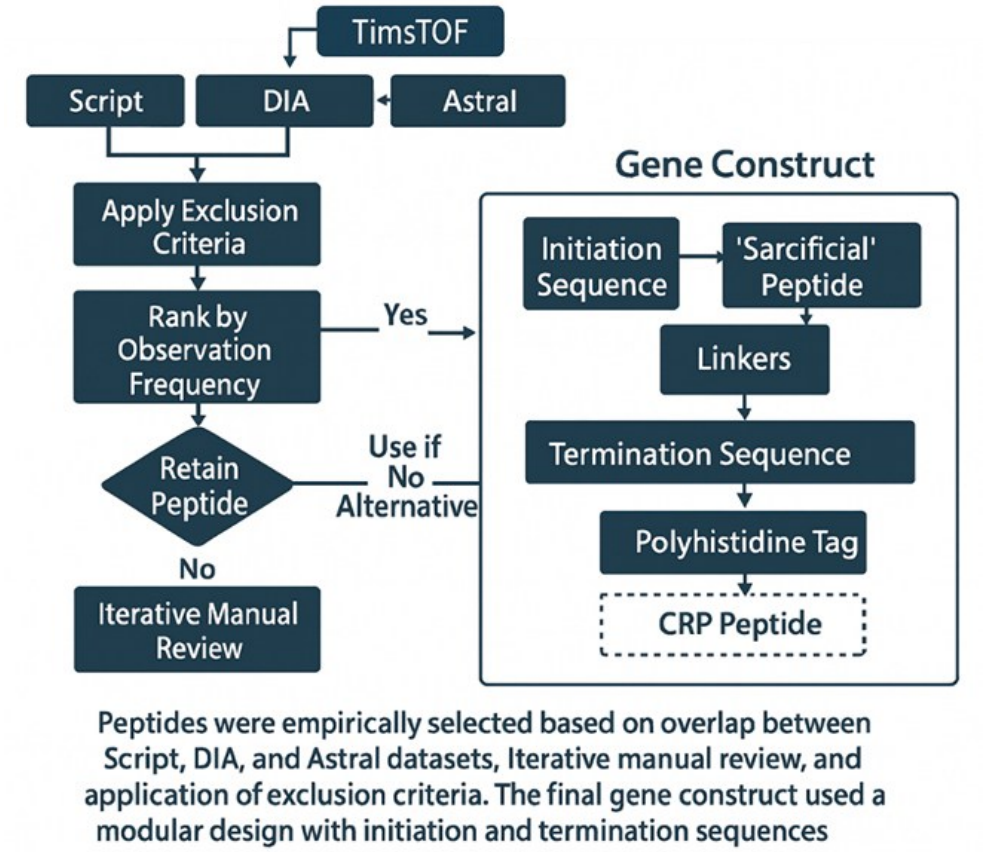

Figure 51. Workflow for Optimised Peptide Selection and Linker Integration in the OxConCAT Construct. This flowchart illustrates the methodological pipeline used to refine peptide selection and junction design for the OxConCAT construct. Starting from DIA-informed peptide identification, peptides are filtered based on physicochemical criteria, uniqueness, and empirical detectability. Glycine-rich linkers are inserted between peptides to preserve native-like tryptic cleavage sites and minimise structural hindrance. The workflow emphasises structural flexibility, native junction logic, and practical constraints related to downstream expression and digestion, resulting in a streamlined, quantifiable OxConCAT standard.

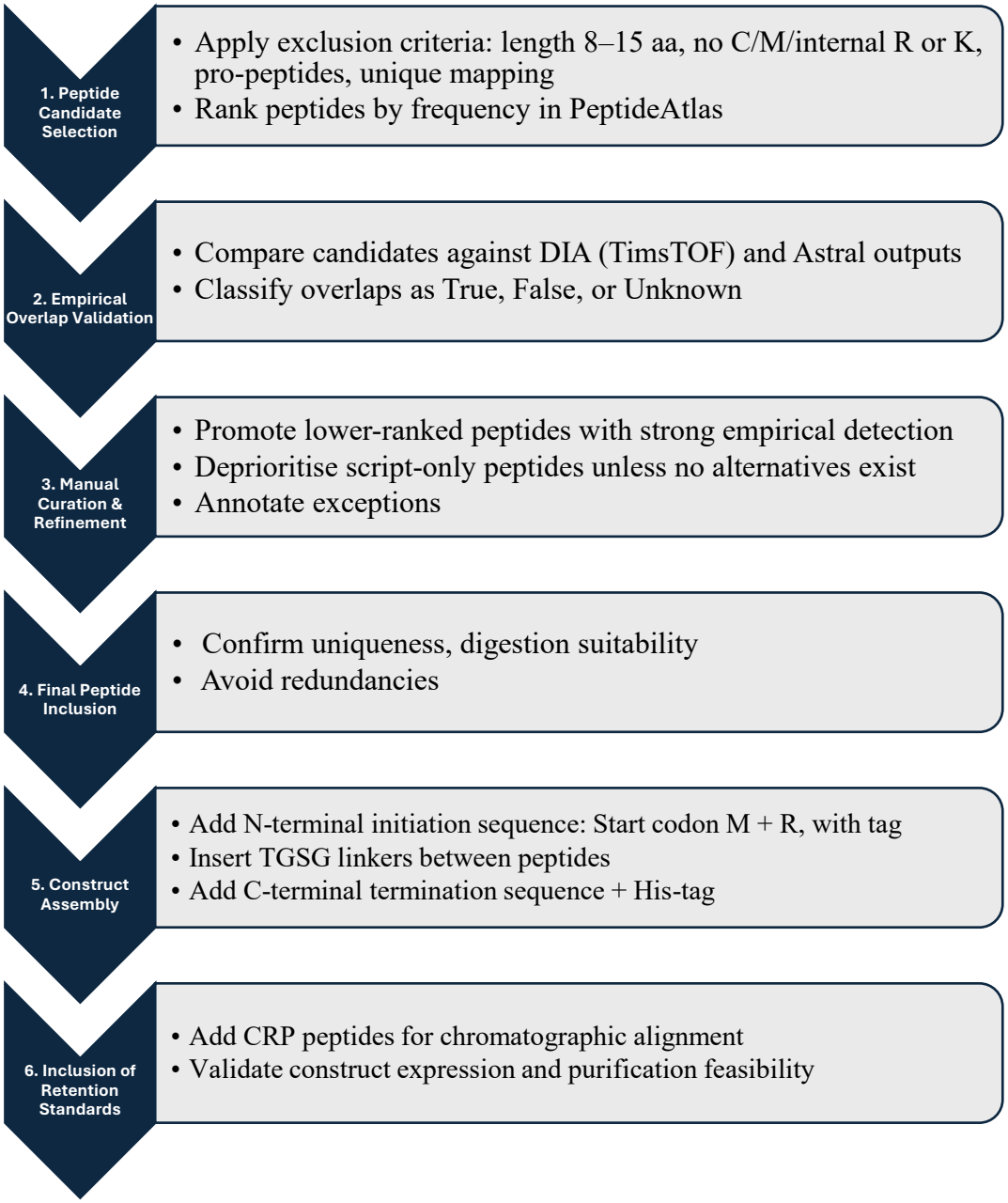

Figure 52. Stepwise Workflow for the Design and Empirical Refinement of the OxConCAT Construct. The flowchart summarises the iterative optimisation process, combining theoretical peptide prediction, empirical confirmation, and modular gene assembly to produce a robust OxConCAT standard for targeted plasma proteomics.

5.4 Peptide Junction Strategy and Linker Optimisation to Enhance Proteolytic Efficiency

A critical element of the OxConCAT redesign involved the strategic placement of peptide linkers to promote efficient tryptic digestion and preserve native-like cleavage patterns. Since trypsin cleaves after lysine (K) or arginine (R), the construct was assembled so that peptide junctions maintained a realistic enzymatic environment wherever possible.

To minimise digestion inefficiencies, a dual design strategy was implemented:

- Whenever feasible, peptides were joined so that at least one side of the junction retained a native-like context, typically ending with a K or R residue.
- Where this was not possible, junctions were engineered to ensure at least one accessible cleavage site, thereby reducing steric hindrance and enzymatic resistance.

To facilitate uniform cleavage, custom short linkers were introduced. These consisted mainly of glycine-rich sequences (TGSG), selected for their flexibility and minimal steric bulk, allowing spatial separation between adjacent peptides and preventing unwanted folding. TGSG was therefore selected over GS and GSG as it balances flexibility with minimal creation of internal semi-tryptic cleavage sites. Linkers frequently terminated in K or R to support proteolytic accessibility, and their precise composition was adapted according to the flanking peptide environment. This design reduced the formation of compact secondary structures that could obstruct trypsin access. The linker functioned as a molecular hinge, ensuring uniform digestion and reproducible peptide release for quantification. Conceptually, the resulting construct can be visualised as a flexible chain of structured peptide domains connected by soft, cleavable joints.

Each junction was evaluated in terms of its pre-peptide (upstream) and post-peptide (downstream) context. Because the downstream residue was predetermined by sequence design, linkers were primarily optimised to complement the pre-peptide end. Peptide order was also strategically arranged to favour junctions supporting efficient cleavage. Using this approach, a construct was generated that enhanced digestion efficiency, reduced steric interference, and ensured reproducible peptide release, key features for reliable quantification in PRM-based workflows (Figure 53).

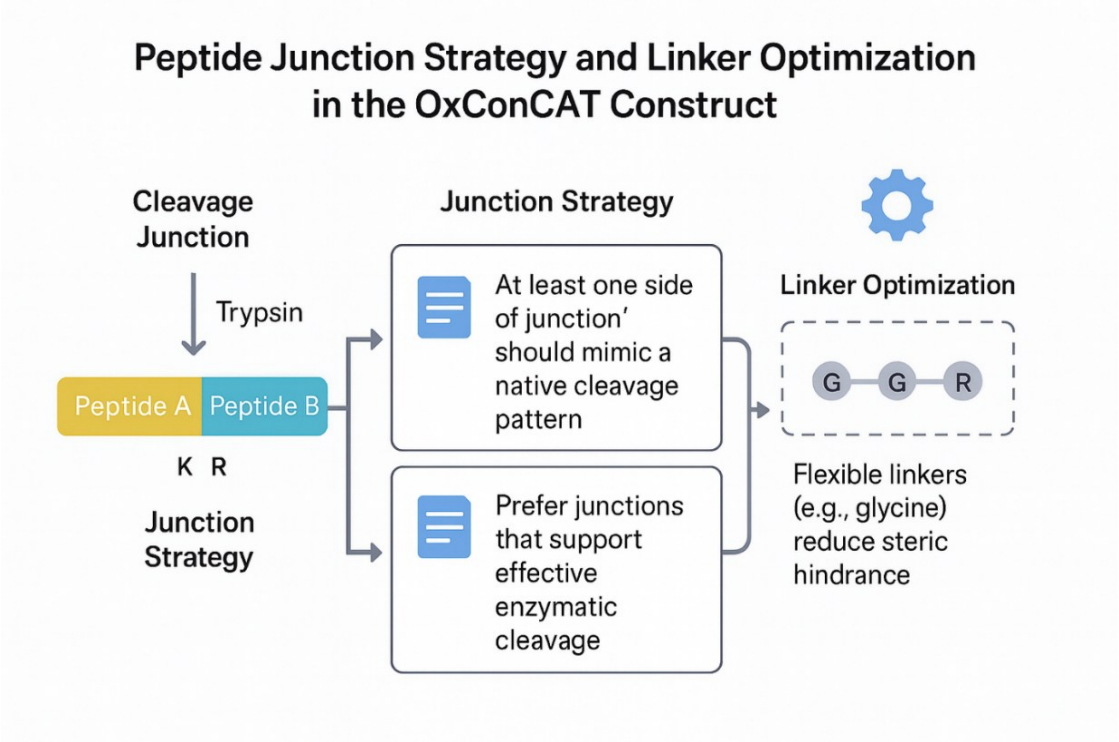

Figure 53. Peptide Junction and Linker Design in the OxConCAT Construct. This schematic illustrates how short glycine-rich linkers were inserted between peptides to maintain protease access and prevent steric hindrance. Cleavage sites were optimised to retain at least one native sequence context, ideally ending in K or R, ensuring consistent and efficient peptide release during trypsin digestion.

Results

The OxConCAT strategy underwent substantial refinement from the original C-002 construct to the revised constructs developed in this work (V2.1 and V2.2). This section critically compares these designs, analysing differences in structure, peptide content, and methodological underpinnings, while assessing how the modifications enhance theoretical validity, practical usability, and overall alignment with the project's analytical goals. Comparative evaluation revealed clear structural and compositional improvements in the redesigned constructs. The updated versions incorporated refined peptide panels, optimised linker architecture, and enhanced sequence balance to minimise aggregation and incomplete digestion. Theoretical modelling and sequence analysis further confirmed greater predicted proteotypic stability and more homogeneous peptide release. Collectively, these refinements improved the constructs' suitability for multiplexed absolute quantification, providing a more consistent and scalable framework for biomarker validation in plasma proteomics.

Comparative Analysis of Constructs

5.5 Structural and content differences between original OxConCAT (AAAQconCAT-C002) and revised versions

The redesigned OxConCAT constructs (V2.1 and V2.2) were compared to the original AAAQconCAT-C002 to assess improvements in design, peptide composition, and analytical performance. C-002, designed before linker optimisation was widely adopted in QconCAT workflows, placed peptides adjacently without inter-domain separation, increasing the likelihood of incomplete proteolysis. C-002 comprised 667 amino acids

(~73 kDa) cloned into pET21b(+), including three tryptic peptides per protein from ten AAA-related proteins. It lacked linkers, which could limit proteolytic uniformity. V2.1/V2.2 retained the same vector system, codon optimisation, CRP controls, retention standards, and His-tag but introduced empirical validation using dual DIA datasets. V2.1 used direct concatenation; V2.2 added TGSG linkers to improve trypsin accessibility and digestion consistency. A modular Attractin-only construct was also produced for targeted PRM analysis (Figure 54).

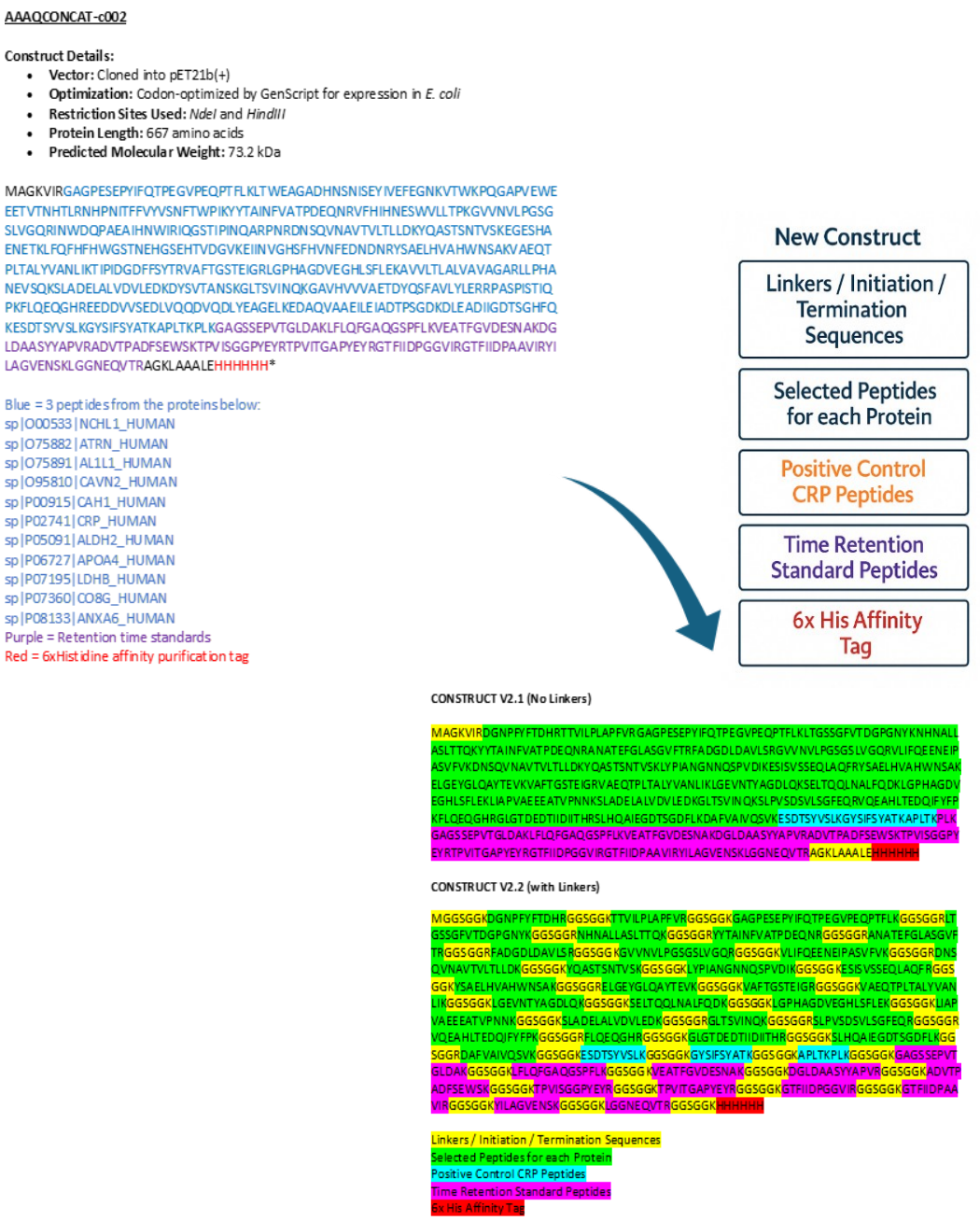

Figure 54. Comparative layout of the original OxConCAT construct (QconCAT-C-002) and revised constructs (V2.1 without linkers, V2.2 with TGSG linkers). Sequences are colour-coded: yellow = initiation/termination, green = target peptides, violet = retention-time standards, red = 6×His tag. The revised constructs remove undetectable peptides and introduce linkers to improve digestion efficiency and quantification reliability.

5.6 Theoretical soundness: proteotypic value, stability, and analytical predictability

The original C-002 construct offered broad protein coverage suitable for exploratory biomarker studies but did not account for digestion inefficiencies arising from juxtaposed peptides without linkers or consideration of native cleavage sites. This design often resulted in incomplete or inconsistent proteolysis, particularly in complex plasma matrices. The revised constructs adopted a targeted, empirically guided strategy. By integrating DIA-based peptide selection from two independent platforms, the inclusion of peptides that are both detectable and quantifiable in plasma was significantly improved. The incorporation of TGSG linkers in version V2.2 reduced steric hindrance, enhanced trypsin accessibility, and improved digestion uniformity. When possible, junctions were designed to preserve native-like tryptic environments, thereby lowering the risk of cleavage variability. The large size and complexity of C-002 also posed challenges for recombinant expression, purification, and digestion reproducibility; moreover, inclusion of low-detectability peptides unnecessarily consumed instrument time and data-processing resources. The revised, smaller multi-protein constructs, notably the Attractin-specific module, addressed these limitations by reducing molecular weight, simplifying purification workflows, and improving overall expression yield. By focusing on empirically validated peptides and modular construct design, the updated OxConCAT framework is predicted to achieve greater analytical reliability, digestion efficiency, and scalability. This flexibility allows for protein-specific validation studies without requiring synthesis of the entire multi-protein construct, enhancing both experimental efficiency and translational applicability.

Discussion

5.7 Discussion and Alignment with Research Goals

The original C-002 design was aligned with a broad, discovery-oriented strategy for absolute quantification of AAA biomarkers. While comprehensive, this approach was less suited to rapid clinical translation due to its inclusion of lower-confidence targets and the absence of digestion optimisation. The revised OxConCAT constructs better reflect the overarching aim of this thesis to develop robust, reproducible, and empirically validated standards for targeted quantification of AAA biomarkers. By prioritising depth over breadth and incorporating iterative refinement guided by empirical PRM and DIA evidence, the new designs are more closely aligned with the requirements of a clinically applicable assay pipeline (Figure 55).

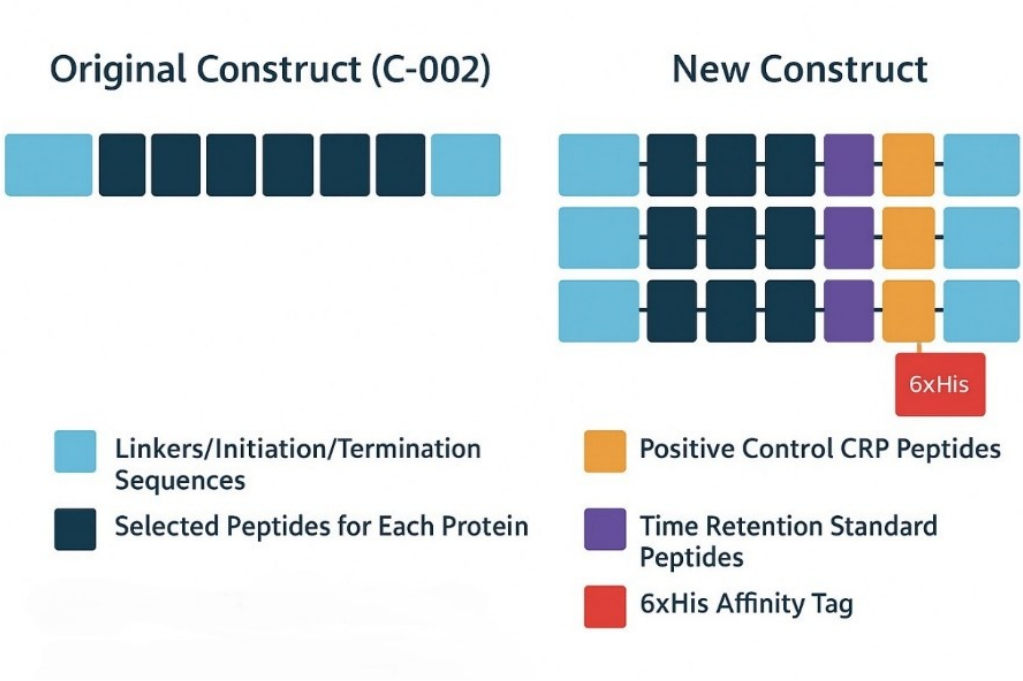

Figure 55. Comparison between the original OxConCAT construct (C-002) and the redesigned construct. The new design incorporates positive control CRP peptides, retention-time standards, and a 6×His affinity tag to enhance purification, retention alignment, and quantitative reliability compared with the original construct.

To summarise the key improvements, empirical validation was integrated at the selection stage using dual DIA datasets (TimsTOF DIA and Astral DIA). Linkers (in V2.2) were introduced to enhance protease accessibility and digestion reproducibility. Junction design incorporates native cleavage site mimicry to minimise digestion bias. Construct complexity was reduced to improve recombinant expression and simplify downstream workflows. Transparent documentation of peptide origin, validation status, and rationale for inclusion is provided. The design is modular, enabling the production of both multi-protein and single-protein constructs supporting protein-specific validation workflows (Table 20). The evolution from C-002 to the revised OxConCAT constructs represents a shift from a broadly inclusive, *in silico*-driven approach towards a focused, empirically validated, and digestion-optimised strategy.[80] These refinements strengthen the theoretical basis, practical utility, and translational potential of the construct, directly supporting the thesis objective of developing a reliable targeted proteomics workflow for AAA biomarker quantification. While MS/MS sequence coverage for the revised OxConCAT constructs (V2.1/V2.2) is still under active evaluation, the design changes summarised below were specifically implemented to improve empirical peptide detectability and overall MS/MS coverage relative to the original C-002 construct. A direct quantitative comparison of sequence coverage between constructs will be reported upon completion of ongoing validation experiments.

Table 20. Comparison between the original OxConCAT construct (C-002) and the revised constructs (V2.1/V2.2). Summary of major design, optimisation, and validation improvements implemented in the updated OxConCAT versions. The revised constructs incorporate empirical validation using DIA datasets, enhanced linker design for improved digestion, and modular architecture to enable targeted, clinically translatable proteomic quantification of AAA biomarkers.

Feature	Original C-002	Revised/New Construct (V2.1/V2.2)
Vector & Expression System	pET21b(+) codon optimised (*E. coli*)	Same vector and codon optimisation retained
Total length / MW	667 aa, ~73.2 kDa	Similar order of magnitude but adjusted length due to reorganisation and linker inclusion
Target Proteins	10 AAA-relevant proteins, each represented by 3 peptides	Reduced protein set, focusing on verified peptides from script, TimsTOF DIA, and Astral DIA; Attractin-specific construct was also generated
Peptide Sources	Selected from the literature and script without extensive empirical overlap filtering	Empirical overlap validation with DIA datasets (TimsTOF, Astral), prioritising empirically detectable peptides
Peptide Filtering	Avoided C, M, internal R/K, multi-genomic hits, pro-peptides	Same biochemical exclusion rules, but also ranked by experimental detection frequency and overlap with multiple MS datasets
Linkers	None in C-002	V2.2 incorporates short glycine-rich linkers (e.g., TGSG) between peptides to improve trypsin accessibility and digestion efficiency
Retention & Positive Controls	CRP positive control peptides (orange), retention time standards (purple)	Retained CRP and RT standards in the same colour-coding scheme
Affinity Tag	6x His tag at C-terminus	Same His-tag retained
Empirical Validation Stage	Limited PRM confirmation, DIA used post-design	PRM validation integrated into peptide selection, guided by DIA from two platforms
Special Design Notes	Sequential concatenation of peptides without consideration of native cleavage sites	Linker placement informed by native cleavage mimicry and steric accessibility considerations

Chapter 6 – GC×GC–MS Metabolomics for AAA Biomarker Discovery

Introduction

This chapter presents the metabolomic component of the OxAAA study, designed to complement the proteomic analyses described in previous chapters by providing an integrated view of systemic biochemical alterations associated with AAA and surgical intervention. Whereas proteomics characterises circulating protein abundance and pathway activity, metabolomics captures the downstream biochemical consequences of these molecular processes, thereby enhancing the interpretability of protein-level changes. Metabolomic profiling relies on analytical platforms such as LC–MS and gas chromatography-mass spectrometry (GC–MS) to detect small-molecule metabolites encompassing a wide range of polarity, volatility, and chemical structures. Because of this chemical diversity, no single analytical technique can comprehensively profile the entire metabolome. Highly polar metabolites, such as amino acids and organic acids, often require derivatisation to increase volatility and improve chromatographic separation, while low-polarity compounds such as lipids and esters are readily detectable without modification. Despite these challenges, GC–MS remains one of the most potent and reproducible platforms for analysing volatile and semi-volatile metabolites in complex biological matrices.[81] The introduction of comprehensive two-dimensional gas chromatography (GC×GC),[82] in combination with high-speed single quadrupole or high-resolution time-of-flight mass spectrometers (GC×GC–TOF–MS),[83–87] has substantially enhanced chromatographic resolving power. In GC×GC configurations, two columns with orthogonal stationary phases, typically non-polar and polar, are coupled in series, enabling the efficient separation of co-eluting compounds and markedly increasing

peak capacity and resolution. Within this framework, a pilot GC×GC–MS metabolomics study was conducted using plasma samples from the OxAAA cohort. The objective was to establish and optimise a robust metabolite extraction and derivatisation workflow tailored for AAA plasma, and to evaluate its suitability for high-resolution metabolite profiling and future large-cohort biomarker discovery. The GC×GC–MS platform provided enhanced separation and signal resolution compared with conventional one-dimensional GC–MS, facilitating confident metabolite identification and quantification. [88–93] The following sections describe the methodological framework for GC×GC–MS analysis (Sections 6.1–6.4), followed by results of metabolite identification and chromatographic performance (Sections 6.5–6.6), and statistical analyses including PCA, PLS–DA, volcano plots, fold-change analysis, and hierarchical clustering (Sections 6.7–6.11). Collectively, this metabolomic investigation complements the proteomic findings, providing a broader and more integrated understanding of the systemic biochemical responses associated with AAA and surgical intervention.

Methods

Method Development and Workflow Optimisation

Metabolite extraction from OxAAA plasma samples was carried out using a biphasic methanol/tert-butyl methyl ether (MTBE) protocol designed to maximise recovery across both polar and non-polar metabolite classes.[81] Each 200 µL plasma aliquot was mixed with methanol containing an internal standard (myristic acid-14,14,14-d_3) and vortexed to ensure complete homogenisation. MTBE was subsequently added, and the mixture was centrifuged at 4 °C to achieve clear phase separation. To enhance detection sensitivity and analytical coverage, the extract was divided into two processing streams (Figure 56). The

first fraction underwent chemical derivatisation to increase volatility and improve chromatographic performance for polar compounds. Derivatisation was achieved through methoximation with methoxyamine, followed by silylation with N-methyl-N-trimethylsilyl-trifluoroacetamide (MSTFA).[94] This two-step modification stabilised reactive carbonyl groups and introduced trimethylsilyl derivatives, improving separation, peak symmetry, and mass spectrometric response for amino acids, organic acids, and sugars. The second fraction was processed without derivatisation, allowing the profiling of native volatile and semi-volatile metabolites. Residual water was removed using anhydrous magnesium sulphate to prevent signal suppression and preserve chemical integrity.[95] This approach reduced sample handling variability and ensured higher recovery rates for metabolites incompatible with chemical modification. All samples were analysed using a comprehensive two-dimensional gas chromatography–mass spectrometry (GC×GC–MS) system (Shimadzu GC–MS QP2010 Ultra) equipped with a single quadrupole mass analyser. Although less sensitive than TOF instruments, high-speed quadrupole scanning offered sufficient spectral fidelity for metabolite identification. The first chromatographic dimension employed a non-polar column for volatility-based separation, while the second dimension used a medium-polarity column to provide orthogonal resolution. Data acquisition and processing were conducted using GC-MSolution, ChromSquare, and GC Image software packages. Metabolite identification was based on spectral matching against reference databases and external analytical standards.

The limit of detection (LOD) for each compound was estimated as:

$$LOD = \frac{3.3 \times \sigma}{S}$$

Where S is the slope of the external calibration and σ is the standard deviation of replicate responses at the lowest non-zero calibrant.[96]

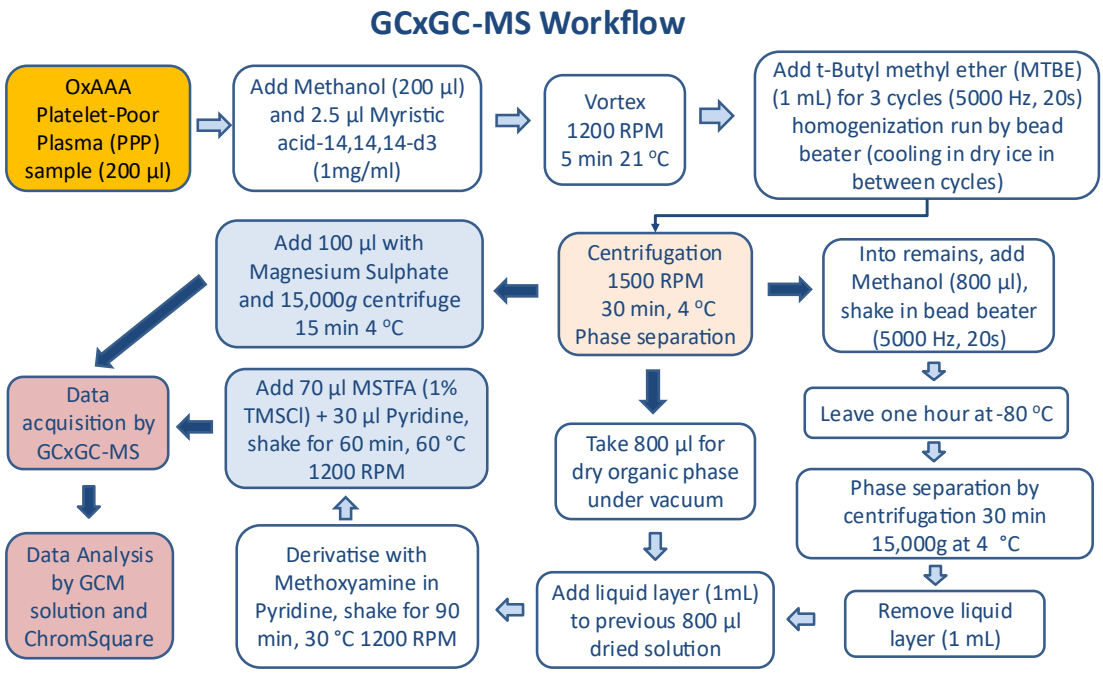

Figure 56. Metabolite extraction and derivatisation workflow for OxAAA plasma analysis. Plasma samples were separated into two analytical streams: one derivatised to enhance volatility and thermal stability (via methoximation and silylation) for improved GC separation of polar metabolites, and one non-derivatised fraction treated with anhydrous magnesium sulphate to preserve native composition and profile volatile non-polar compounds: this dual-stream strategy enhanced method robustness, metabolite recovery, and overall analytical sensitivity.

6.1 Identification of Plasma Metabolites via GC×GC–MS

Comprehensive two-dimensional gas chromatography–mass spectrometry (GC×GC–MS) was employed to profile plasma metabolites from the OxAAA cohort, following the extraction and derivatisation workflow described in Section 6.3. The biphasic methanol/tert-butyl methyl ether (MTBE) extraction yielded both organic and aqueous fractions, ensuring broad metabolite recovery across different chemical classes. The polar fraction was derivatised with methoxyamine hydrochloride and N-methyl-N-trimethylsilyl-trifluoroacetamide (MSTFA) to improve volatility and thermal stability, while the non-derivatised aliquot was treated with anhydrous magnesium sulphate to remove residual moisture and preserve native volatile compounds.

Analyses were performed on a Shimadzu QP2010 Ultra system configured for GC×GC–MS, comprising a non-polar first-dimension column coupled to an intermediate-polarity second-dimension column and interfaced with a single-quadrupole mass spectrometer. This orthogonal setup provided high peak capacity and minimised co-elution among metabolites with similar physicochemical properties. Data acquisition and processing were carried out using GC-MSolution, ChromSquare, and GC Image software packages, while compound annotation was achieved through comparison with analytical standards and electron-impact (EI) spectral libraries.

The analysis of OxAAA plasma extracts demonstrated the advantages of GC×GC separation over conventional one-dimensional GC-MS.[97] High-speed quadrupole scanning enabled the resolution of complex metabolite mixtures, identifying 104 distinct mass peaks (or "blobs") in derivatised fractions, many of which could not be discriminated using 1D GC-MS (Figure 57A), and 29 metabolites in the non-derivatised fraction. The GC×GC contour plot, resembling a topographic map, displayed first-dimension retention time along the x-axis (volatility), second-dimension retention time along the y-axis (polarity), and signal intensity along the z-axis (Figure 57B–C). This multidimensional visualisation provided a detailed representation of metabolite distribution and improved feature discrimination for subsequent annotation.

Among the metabolites detected in the non-derivatised fraction, squalene was of particular interest. Squalene, a triterpenoid hydrocarbon and key biochemical precursor in steroid biosynthesis, is challenging to identify due to its low density, hydrophobicity, and absence of distinct functional groups. Its detection within the OxAAA plasma samples demonstrated the capacity of the optimised workflow to recover neutral, low-abundance hydrophobic species. Squalene oxidation generates 2,3-squalene oxide, which undergoes enzyme-mediated cyclisation to form lanosterol, a precursor of cholesterol and

related sterols, underscoring its relevance to lipid metabolism and vascular biology. The corresponding chromatographic data are summarised in Table 21.

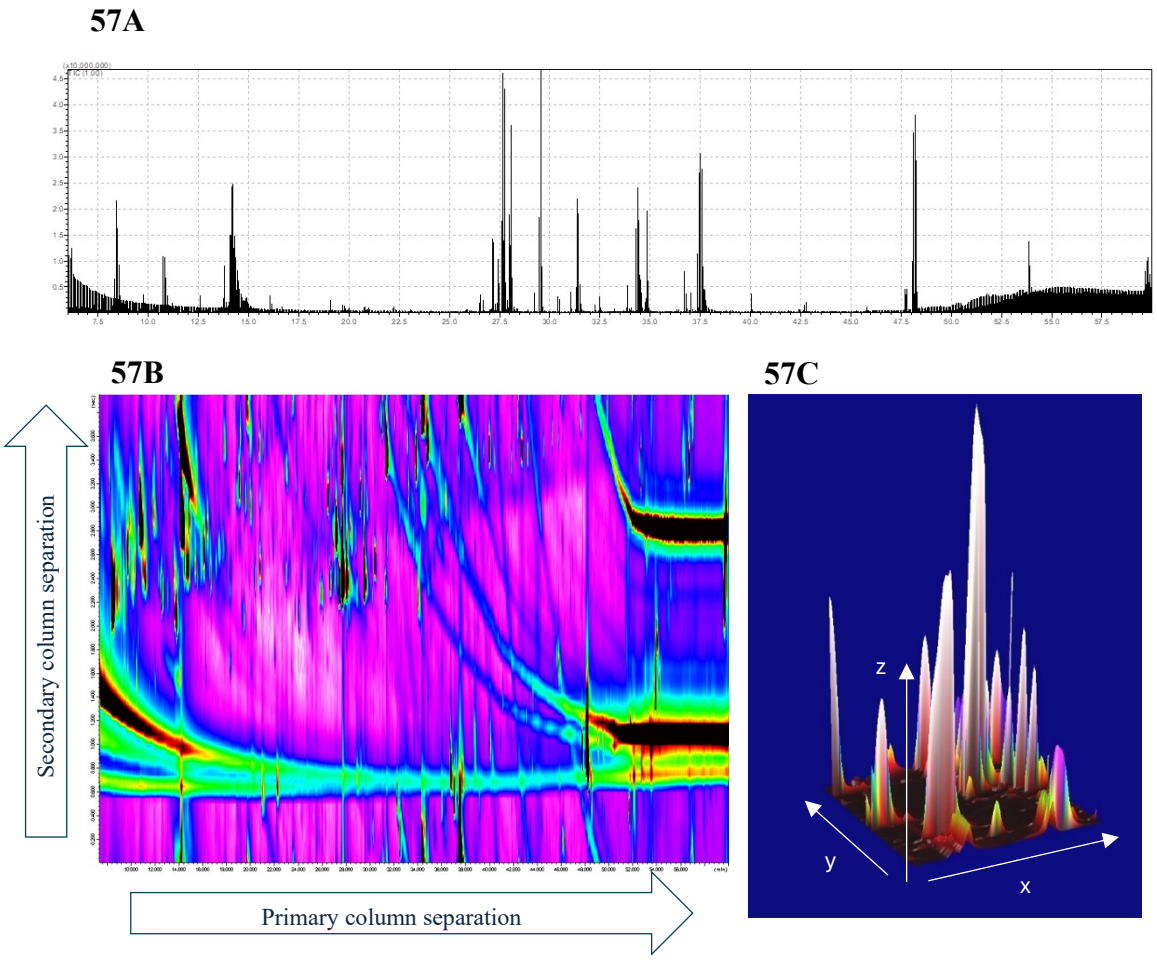

Figure 57. Chromatographic visualisation of plasma metabolite separation by GC×GC–MS. (A) Total Ion Chromatogram (TIC) of derivatised plasma analysed by one-dimensional GC-qMS, showing dense peak clustering and co-elution. (B) Two-dimensional GC×GC contour plot illustrating enhanced separation and identification of 104 molecular features, colour-coded according to spectral matching. (C) Three-dimensional ChromSquare representation displaying first- and second-dimension retention times on the x- and y-axes, respectively, with ion intensity mapped on the z-axis.

Table 21. Detection of squalene and associated neutral hydrophobic metabolites identified in OxAAA plasma samples. The identification of squalene confirmed the effectiveness of the optimised GC×GC–MS workflow for recovering non-polar metabolites, supporting the analytical breadth and reliability of the developed method.

ID	Metabolite Name	T^{1D}_R (min)	T^{2D}_R (sec)
1	Butane, 2-ethoxy-	11.114	0.85
2	Propane, 2-ethoxy-	11.648	0.8
3	1,3-Dioxan-5-ol	12.903	0.2
4	Nonane, 4,5-dimethyl-	15.517	0.95
5	Methoxyacetic acid, 2-tridecyl ester	15.65	0.95
6	1-Octanol, 2,2-dimethyl-	15.783	0.95
7	Dodecane, 2,6,11-trimethyl-	16.451	1
8	Nonadecane	16.785	1.05
9	1-Octanol, 2-butyl-	17.32	1.2
10	Phenol, 3,5-bis(1,1-dimethylethyl)-	17.994	1.65
11	Eicosane	18.722	1.3
12	Cyclopentanetridecanoic acid, methyl ester	19.861	1.65
13	Tetradecanoic acid, 12-methyl-, methyl ester	19.886	3.15
14	1-Docosene	20.612	2.7
15	Tetrapentacontane	21.524	1.45
16	Hexanedioic acid, dioctyl ester	21.73	1.8
17	2-methylhexacosane	22.395	1.7
18	Tricyclo[20.8.0.0(7,16)]triacontane, 1(22),7(16)-diepoxy-	22.759	3.55
19	1,2-15,16-Diepoxyhexadecane	23.014	2.85
20	Squalene	23.203	2.2
21	Cholest-5-en-3-ol (3.beta.)-, tetradecanoate	23.476	2.55
22	9-Octadecenal, (Z)-	23.621	3.25
23	9-Octadecenamide, (Z)-	23.68	2.8
24	7-Hexadecenal, (Z)-	24.142	2.5
25	Cholesta-3,5-diene	24.218	3.1
26	Cholesta-4,6-dien-3-ol, (3.beta.)-	24.552	3.1
27	3.alpha.-(Trimethylsiloxy)cholest-5-ene	25.022	3.3
28	Cholesterol	25.508	0.5
29	Pentatriacontane	26.753	3.2

6.2 Advantages Over Conventional 1D GC–MS

Compared with conventional one-dimensional gas chromatography–mass spectrometry (1D GC–MS), comprehensive two-dimensional GC×GC–MS provided substantial improvements in chromatographic resolution, analytical capacity, and quantitative reliability. The orthogonal configuration, combining a non-polar first-dimension column with a second column of intermediate polarity, significantly reduced co-elution artefacts and enhanced separation efficiency. This setup enabled the detection of 104 distinct molecular features in derivatised plasma fractions, representing a marked increase in peak capacity relative to 1D GC–MS. The additional separation dimension exploits two distinct physicochemical principles: volatility-driven retention in the first column and polarity- or functional group–based interactions in the second. As a result, GC×GC–MS can distinguish structurally similar metabolites that overlap in retention time under single-dimensional conditions, thereby improving both annotation reliability and spectral deconvolution.[98, 99]

Sharper, more symmetric peaks and reduced co-elution improved integration reliability and signal-to-noise. These improvements are particularly valuable for untargeted plasma metabolomics, where complex sample matrices often obscure low-abundance features. The enhanced detection of small polar compounds and semi-volatile lipids demonstrated the method analytical breadth, confirming GC×GC–MS as a powerful platform for comprehensive metabolic profiling in the OxAAA study.

Table 22. Advantages of GCxGC-MS Over One-Dimensional Gas Chromatography (1D GC-MS).

Feature	Advantages of GCxGC-MS over 1D GC-MS
Resolution and Separation	Provides superior separation due to the orthogonal two-dimensional layout, reducing co-elution of metabolites.
Sensitivity	Enhances signal-to-noise ratio by focusing compounds into sharper peaks, improving sensitivity.
Peak Capacity	Greatly increases peak capacity by using two columns with different selectivity.
Quantitative Accuracy	Improves quantitation of low-abundance analytes by better baseline separation.
Identification Confidence	Facilitates better compound identification using 2D retention time indices and mass spectral data.
Detection of Complex Mixtures	Enables detection of hundreds of analytes in complex biological samples with minimal overlap.
Data Visualization	Provides advanced visualisation in contour plots resembling topographic maps, aiding interpretation of dense datasets.
Volatility Range	Expands detection to a broader range of volatiles and semi-volatiles in a single run.

Metabolomic Profiling of OxAAA Plasma Pilot Cohort

6.3 Metabolite Extraction and Derivatisation Protocol Optimisation

Optimisation of the metabolite extraction and derivatisation workflow was performed using plasma samples from the OxAAA pilot cohort, comprising ten patients with matched pre-operative (TP3) and post-operative (TPF) samples. The aim was to establish a reproducible pipeline suitable for comprehensive metabolomic profiling and for detecting metabolic alterations associated with surgical intervention.

6.3.1 Sample Preparation

Metabolite extraction followed a biphasic methanol/water/tert-butyl methyl ether (MTBE) procedure to achieve broad recovery across polar and non-polar metabolite classes.[100] Plasma aliquots (200 µL) were thawed on ice and mixed with 225 µL of methanol containing an internal standard mixture, followed by vortexing for 10 seconds. Subsequently, 750 µL of MTBE was added, and the mixture was vortexed again before incubation on ice for 10 minutes to promote phase separation. To induce partitioning, 188 µL of LC–MS–grade water was added, and samples were briefly vortexed and centrifuged at 14,000 × rcf for 15 minutes at 4 °C. The resulting upper (organic) and lower (aqueous) phases were carefully collected into separate microtubes, dried under vacuum, and stored at −80 °C until derivatisation. Derivatisation of the dried extracts was conducted to improve the volatility and thermal stability of polar metabolites, facilitating efficient GC×GC separation. Each sample was reconstituted in 25 µL of methoxyamine hydrochloride in pyridine (20 mg/mL) and incubated at 30 °C for 60 minutes to stabilise carbonyl-containing compounds. A second step was then performed by adding 25 µL of N-methyl-N-trimethylsilyl-trifluoroacetamide (MSTFA) and incubating at 37 °C for 120 minutes. This two-step methoximation–silylation procedure converted hydroxyl and carboxyl groups to trimethylsilyl derivatives, enhancing volatility, improving chromatographic peak shape, and reducing adsorption on column surfaces.[101] A summary of the extraction and derivatisation workflow is provided in Table 23, outlining each procedural step and its analytical purpose.

Table 23. Summary of Metabolite Extraction and Analysis Workflow.

Step	Procedure	Purpose
1	Methanol/MTBE extraction	Phase separation for polar and non-polar metabolites
2	Centrifugation & separation	Isolate organic and aqueous layers
3	Vacuum drying	Remove solvents before derivatisation
4	Methoxyamine treatment	Stabilise carbonyl groups in metabolites
5	MSTFA treatment	Enhance the volatility of polar compounds
6	GCxGC-MS analysis	Two-dimensional separation and quantification
7	Data interpretation with ChromSquare	Feature detection and spectral matching

Derivatised extracts were analysed using GC×GC coupled to a quadrupole mass spectrometer (GC×GC–qMS, Shimadzu QP2010 Ultra). The analytical configuration included a non-polar first-dimension column for volatility-based separation and a second-dimension column of intermediate polarity to resolve structurally similar metabolites. Helium was employed as the carrier gas, with a programmed temperature gradient from 60 °C to 300 °C. The injection volume was 1 μL per sample, and data were acquired across a mass-to-charge (m/z) range of 50–600. This optimised sample preparation and derivatisation strategy provided improved reproducibility, peak definition, and metabolite recovery, forming the foundation for subsequent two-dimensional chromatographic analyses and statistical interpretation of the OxAAA plasma metabolome.[102, 103]

6.4 Data Acquisition and Comparative Chromatographic Performance

Data acquisition was performed using the Shimadzu GC×GC–qMS (QP2010 Ultra) system operated in high-speed scanning mode, enabling rapid data capture and improved resolution of closely eluting peaks.[104] This configuration provided the temporal precision necessary for comprehensive two-dimensional gas chromatography, effectively minimising co-elution and improving quantification of structurally similar metabolites within complex plasma matrices. Metabolite identification was conducted using ChromSquare for GC×GC visualisation and peak detection, complemented by NIST Mass Spectral Library and in-house spectral databases for compound matching. Each detected molecular feature, or "blob," was evaluated based on retention indices, spectral similarity, and intensity distribution. Three-dimensional chromatographic visualisations were generated, mapping first-dimension retention time (x-axis), second-dimension retention time (y-axis), and ion intensity (z-axis) to produce a topographic representation of the chromatographic landscape.[105] The analytical performance of the derivatised plasma workflow was initially benchmarked using conventional one-dimensional GC–qMS. The total ion chromatogram (TIC) from a representative pre-operative plasma sample (Patient 04; sample ID PLL4AS2-19TP3D) exhibited dense clustering and extensive overlap of peaks, particularly within the mid-to-late retention region, illustrating the inherent limitations of single-dimensional separation in complex biological matrices. Subsequent analysis of the same sample using GC×GC–MS revealed a substantial enhancement in chromatographic resolution, identifying 104 distinct molecular features. The orthogonal two-column configuration separated compounds according to volatility in the first dimension and polarity or functional group interactions in the second. This dual mechanism effectively reduced co-elution and improved annotation reliability. The resulting three-dimensional surface plot integrated both

retention dimensions with signal intensity, producing a topographic map of the plasma metabolome. Key metabolites, including lactic acid, urea, glucose, EDTA and cholesterol, were distinctly resolved, demonstrating the system ability to discriminate between chemically diverse species across a wide dynamic range. The pronounced separation of peaks and reduced spectral interference confirmed the superior resolving power of GC×GC–MS compared with 1D GC–MS, establishing it as the optimal platform for plasma metabolomic profiling in the OxAAA study.

Results

6.5 Overview of detected metabolites and annotation confidence levels

The optimised GC×GC–MS workflow yielded a comprehensive metabolic profile of OxAAA plasma samples, confirming its analytical precision and reproducibility. Across all derivatised fractions, 104 distinct molecular features were detected, of which 67 metabolites were confidently annotated following spectral validation. In parallel, 29 metabolites were identified in the non-derivatised fraction, consistent with previous pilot findings and validating the reproducibility of the dual-phase extraction strategy. Annotation was performed through spectral matching against reference libraries (NIST and in-house databases) and by comparison with retention indices. Confidence levels were assigned based on spectral similarity scores and chromatographic reproducibility across replicates. High-confidence annotations (Level 1) were confirmed using reference standards or spectra with similarity scores exceeding 900. In contrast, a smaller number of Level 2 annotations were classified as putative identifications with high spectral similarity but lacking direct standard confirmation. The identified metabolites encompassed diverse chemical classes, including organic acids (citric acid, lactic acid, 2-

ketoglutaric acid), amino acids (L-threonine, L-glutamic acid, L-valine), sugars and polyols (glucose, erythritol, ribitol), fatty acids (palmitic acid, oleic acid, dodecanoic acid), and sterols (cholesterol, cholest-5-en-3-ol, cholesterol isocaproate). This broad chemical distribution demonstrates the efficiency of the combined methanol/MTBE extraction and methoximation–silylation approach, enabling simultaneous detection of polar and non-polar metabolites within a single analytical framework. The high dimensionality of GC×GC–MS allowed effective discrimination of structurally similar or co-eluting compounds that are typically unresolved using 1D GC–MS. The topographic output visualised in Figure 58A–C displays the progressive increase in separation capacity, culminating in the identification of discrete, non-overlapping peaks distributed across both volatility and polarity axes. This level of chromatographic and spectral resolution provided the foundation for subsequent quantitative and multivariate analyses investigating metabolic changes associated with surgical intervention in AAA patients.

58A

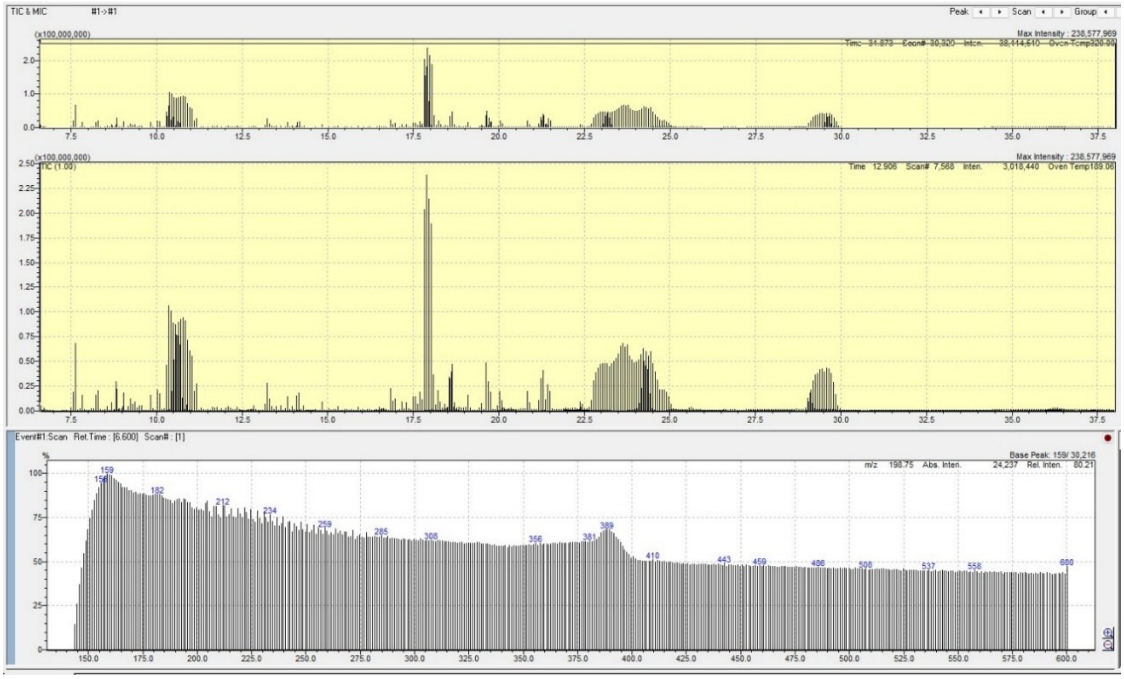

Figure 58A. One-dimensional GC–qMS Total Ion Chromatogram (TIC) of derivatised plasma from Patient 04 (pre-operative; PLL4AS2-19TP3D). The TIC demonstrates dense peak clustering and extensive overlap, particularly in the mid-to-late retention time range, highlighting the limited resolving capacity of single-dimensional separation. Such co-elution complicates confident metabolite identification and quantification. This 1D profile serves as a baseline reference illustrating the substantial resolution gains achieved with subsequent two-dimensional GC×GC separation.

58B

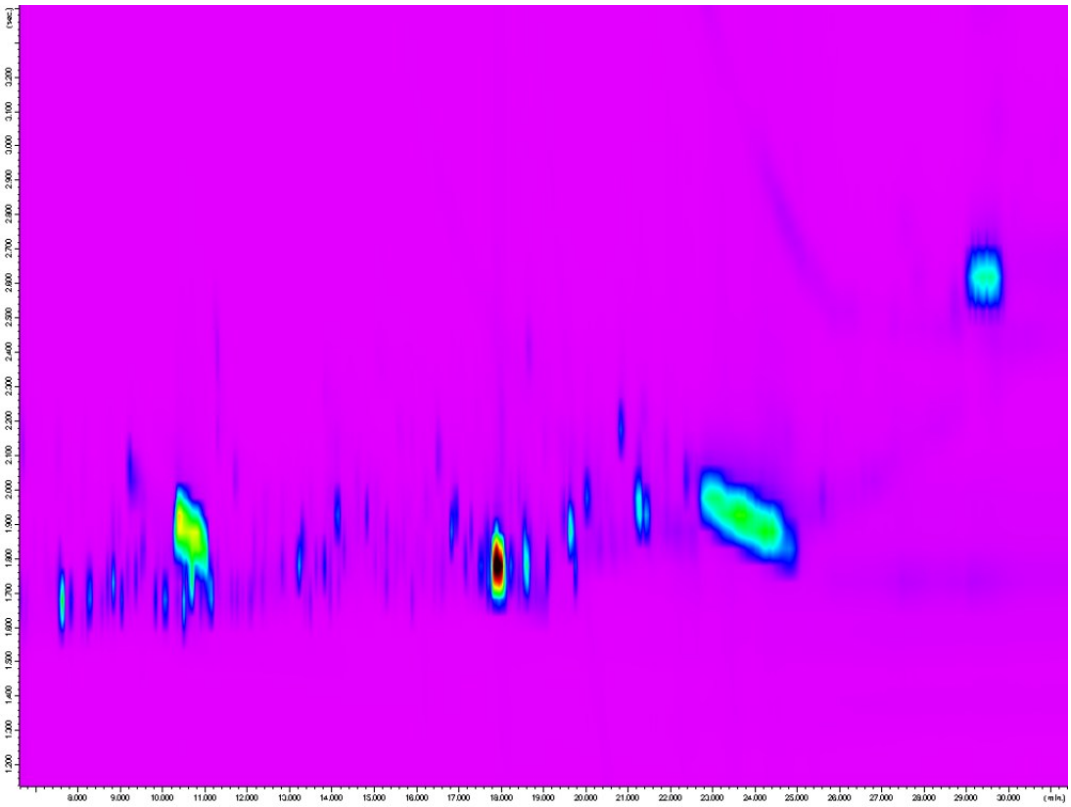

Figure 58B. Comprehensive two-dimensional GC×GC–MS contour plot of derivatised plasma from Patient 04 (pre-operative; PLL4AS2-19TP3D). The contour plot illustrates the markedly enhanced chromatographic resolution achieved with GC×GC–MS. The x-axis corresponds to the first-dimension retention time (volatility/hydrophobicity), and the y-axis represents the second-dimension retention time (polarity/functional interactions). Each discrete spot ("blob") represents a resolved molecular feature. Signal intensity is depicted by a colour gradient from blue (low abundance) to red (high abundance). A total of 104 distinct peaks were resolved, demonstrating the superior separation capacity of GC×GC–MS over conventional 1D GC.

58C

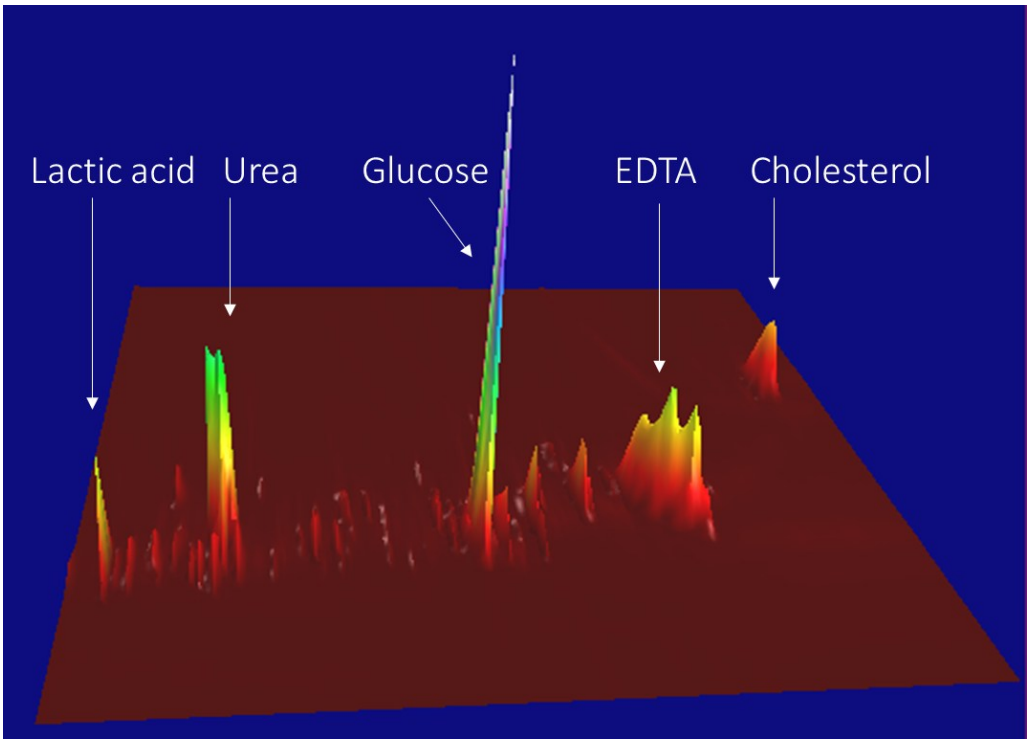

Figure 58C. Three-dimensional ChromSquare visualisation of GC×GC–MS output for derivatised plasma from Patient 04 (pre-operative; PLL4AS2-19TP3D). This 3D plot integrates first-dimension retention time (x-axis), second-dimension retention time (y-axis), and signal intensity (z-axis) to create a topographic representation of the GC×GC separation. Peak height reflects metabolite abundance, while the colour gradient (red → yellow → green) indicates increasing signal intensity. Key metabolites, including lactic acid, urea, glucose, EDTA (exogenous anticoagulant), and cholesterol, are annotated, demonstrating the platform's capability to resolve chemically diverse compounds within a complex plasma matrix.

6.6 Comparative coverage of derivatised fractions

The comparative evaluation of derivatised plasma fractions confirmed the broad analytical coverage achieved by the optimised GC×GC–MS workflow. The three-dimensional chromatographic output provided clear visual differentiation of metabolite elution profiles across both volatility and polarity dimensions, facilitating reliable annotation of key compounds spanning a wide dynamic range. Prominent features such as glucose, lactic acid, and cholesterol were detected with high signal intensity, reflecting both their natural plasma abundance and the efficiency of the derivatisation process in enhancing volatility and chromatographic separation. The detection of ethylenediaminetetraacetic acid (EDTA), originating from blood collection tubes and not biologically derived, with a distinct retention pattern and broad spectral footprint illustrated the platform sensitivity to both endogenous and exogenous compounds, underscoring the importance of recognising artefactual species introduced during sample handling. The topographical representation of peaks across the two chromatographic dimensions further demonstrated the capability of GC×GC–MS to resolve co-eluting and structurally related metabolites within complex plasma matrices, supporting confident compound identification and accurate quantification. In total, 67 metabolites were confidently identified from the derivatised fractions, encompassing multiple biochemical classes such as fatty acids, amino acids, sugars, and intermediates of energy metabolism. This coverage highlights the robustness of the two-step methoximation–silylation derivatisation and biphasic extraction protocol in achieving high analytical reproducibility and sensitivity for both polar and semi-polar species (Figure 59).

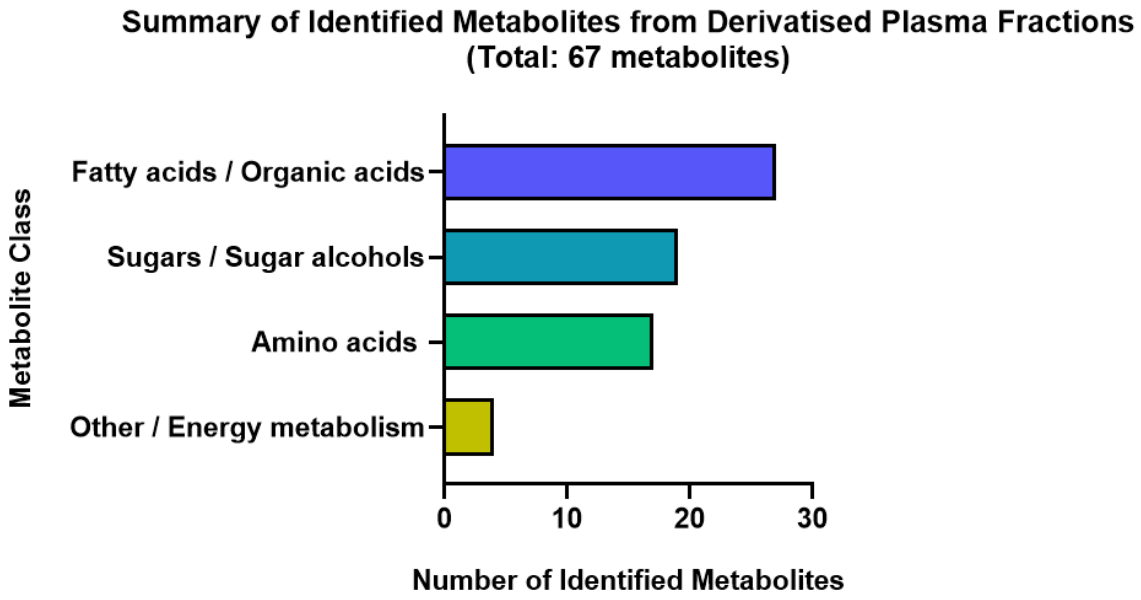

Figure 59. Summary of metabolites identified in derivatised plasma fractions. A total of 67 metabolites were identified and grouped into broad chemical classes. The optimised GC×GC–MS protocol achieved extensive coverage across the metabolic spectrum, including fatty acids and organic acids (n = 27), sugars and sugar alcohols (n = 19), amino acids (n = 17), and other metabolites involved in energy metabolism (n = 4). This distribution underscores the platform's ability to detect chemically diverse metabolites from complex plasma samples.

A comparison with earlier pilot workflows revealed a notable change in the detection profile of squalene, a highly hydrophobic triterpenoid precursor in cholesterol biosynthesis. Whereas squalene was consistently observed in prior analyses, it was only detected in trace amounts within the current optimised workflow. This reduction reflects the low volatility and limited derivatisation efficiency of squalene, but also indicates that the revised protocol favoured enhanced detection of polar and semi-polar metabolites, consistent with the objective of comprehensive plasma metabolome coverage. Its diminished signal in the derivatised stream highlights the inherent bias toward polar analytes, whereas its clear detection in the previous non-derivatised stream underscores the value of dual processing to retain coverage of neutral lipids. Collectively, these results demonstrate that the refined GC×GC–MS workflow achieved balanced sensitivity across

chemically diverse metabolite classes while maintaining reproducibility and reduced co-elution artefacts. This analytical foundation supported the subsequent application of multivariate analyses (Sections 6.7) to investigate metabolic shifts associated with surgical intervention in AAA patients.

Statistical Analyses of Pre- and Post-Surgical Metabolomic Profiles

6.7 Partial Least Squares Discriminant Analysis (PLS-DA)

Partial Least Squares Discriminant Analysis (PLS–DA) was applied to assess whether plasma metabolite profiles could differentiate pre-operative (TP3) from post-operative (TPF) samples in the OxAAA cohort. As a supervised multivariate approach, PLS–DA identifies the directions of greatest covariance between metabolite levels and predefined class labels, thereby maximising group separation while minimising intra-group variance. This makes it particularly suitable for analysing paired biological samples and detecting subtle systemic shifts. The PLS–DA model revealed a clear separation between TP3 and TPF groups (Figure 60). The first principal component (Component 1), accounting for 14.5% of total variance, captured the dominant metabolic signature distinguishing the two clinical states. In comparison, Component 2 (13.4% variance) reflected inter-individual variability, potentially linked to recovery rates, comorbidities, or treatment differences. The tighter clustering of post-operative samples suggested metabolic convergence after surgery, possibly indicating physiological stabilisation or partial restoration of homeostasis. This class separation confirmed that the surgical intervention induced systemic metabolic remodelling detectable at the plasma level. As PLS-DA is a supervised approach that may overfit class distinctions, its outcomes were interpreted

cautiously and cross-validated against unsupervised PCA and univariate statistical tests to ensure that observed separations reflected actual biological variation rather than model bias. The PLS–DA findings aligned with complementary analyses such as PCA, fold change, and volcano plots, collectively reinforcing the reliability and biological coherence of the observed shifts in metabolite composition. These data highlight the potential of GC×GC–MS plasma metabolomics to serve as a sensitive platform for monitoring post-surgical metabolic adaptation in AAA patients.

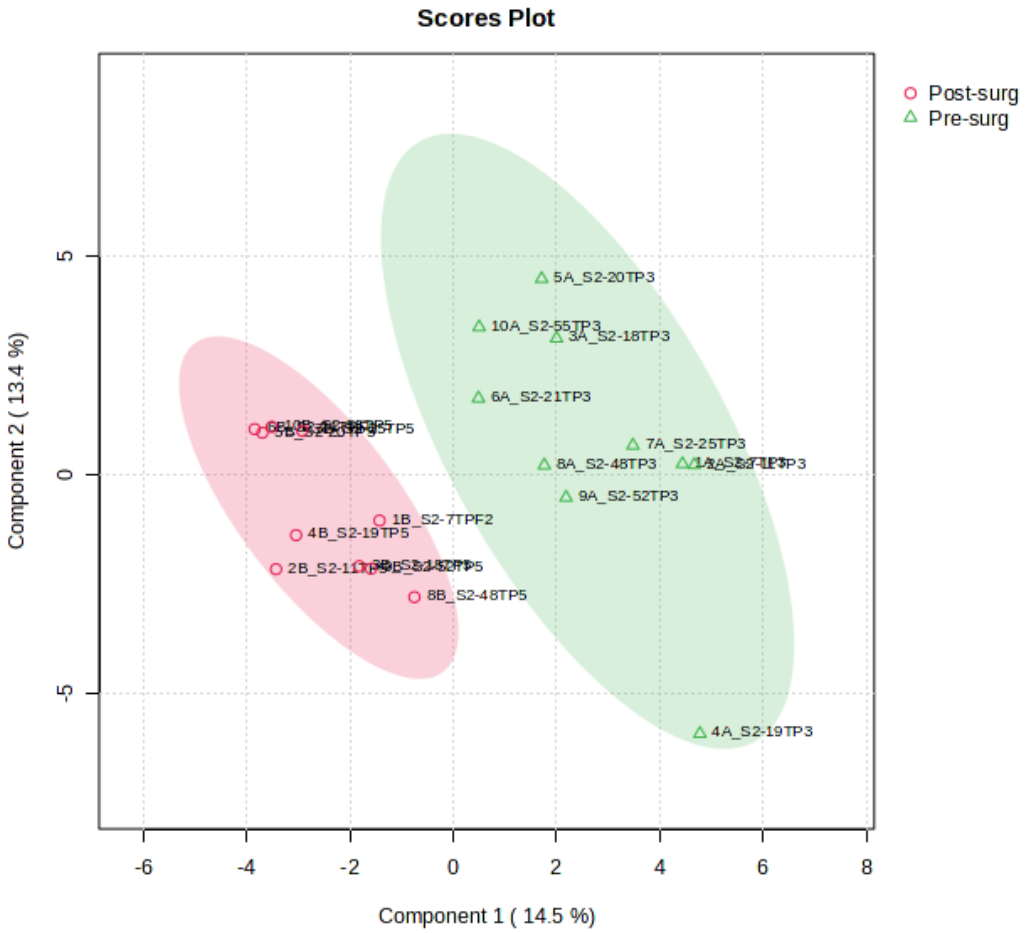

Figure 60. Partial Least Squares Discriminant Analysis (PLS-DA) – 2D Scores Plot of Plasma Metabolomic Profiles in the OxAAA Cohort. The plot shows a two-dimensional scores map derived from a PLS–DA model comparing pre-operative (TP3; green triangles) and post-operative (TPF; pink circles) plasma metabolomes. Component 1 (14.5%) captures the primary axis of metabolic discrimination, while Component 2 (13.4%) reflects secondary variation. Ellipses denote 95% confidence regions based on Hotelling's T^2 distribution. The group separation indicates consistent systemic metabolic changes following AAA repair.

6.8 Fold Change (FC) Analysis

The purpose of the fold change analysis is to provide an intuitive overview of metabolite alterations following surgery, highlighting both the direction and magnitude of change and complementing multivariate analyses with a metabolite-centric perspective. Fold change (FC) analysis was therefore performed on matched TP3 and TPF samples to quantify post-surgical metabolic modulation. The resulting $\log_2$-transformed FC values provided an overview of post-surgical metabolic modulation (Figure 61). A total of 22 metabolites were upregulated and 12 downregulated following surgery ($|\log_2 FC| > 1$), indicating a broad metabolic reorganisation. Upregulated metabolites included cholesterol isocaproate, erythritol, and L-threonine, patterns that are compatible with enhanced lipid mobilisation, oxidative stress adaptation, and increased protein synthesis during tissue recovery. Conversely, citric acid, glutamic acid, and dodecanoic acid showed significant decreases, suggesting transient suppression of the tricarboxylic acid (TCA) cycle, altered amino acid turnover, and modulation of lipid oxidation pathways. The spread of FC values across patients reflected inter-individual variability in metabolic response, potentially influenced by factors such as inflammation, medication, and post-operative recovery rate. These findings indicate a characteristic post-surgical metabolic fingerprint marked by shifts in lipid, amino acid, and energy metabolism. The directionality of changes aligns with the PLS–DA trends, reinforcing the evidence of systemic metabolic adaptation after AAA repair. Together, FC and multivariate analyses provide a consistent picture of metabolic reprogramming post-surgery. The combination of these approaches supports the identification of candidate metabolites for pathway-level interpretation and potential biomarker validation in larger patient cohorts.

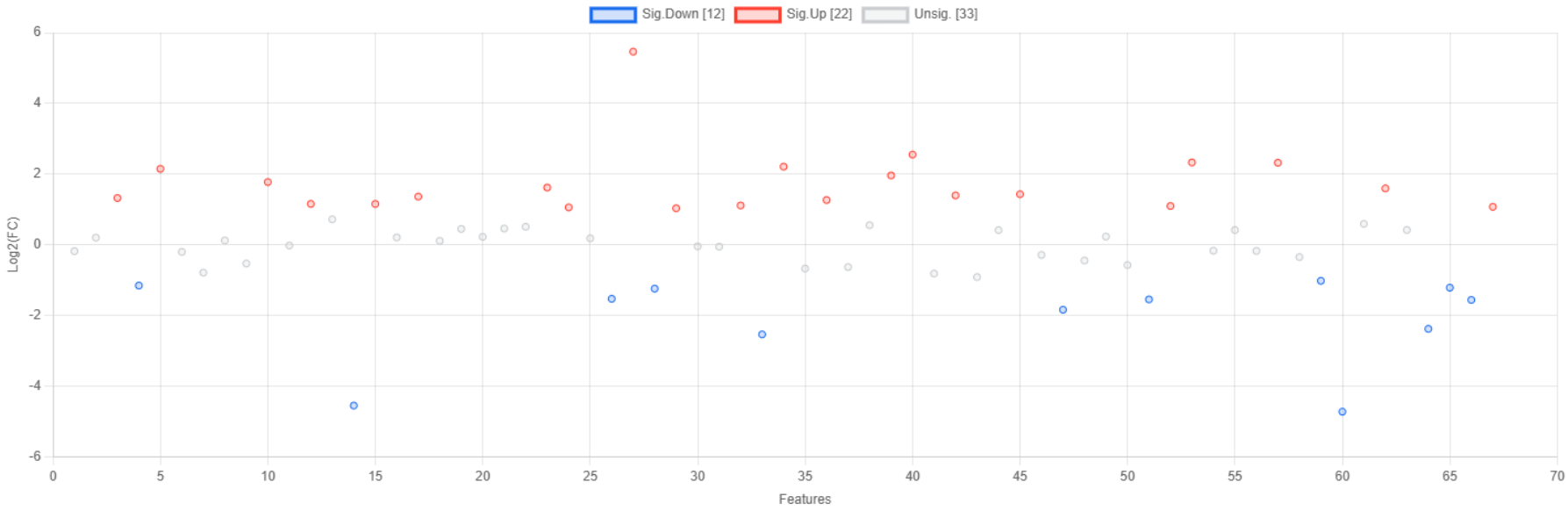

Figure 61. Fold change analysis highlighting directionality and magnitude of post-surgical metabolic alterations. Scatter plot showing $\log_2$-transformed fold change (FC) values comparing post-operative (TPF) to pre-operative (TP3) plasma samples for individual metabolites. Red points indicate significantly upregulated metabolites ($\log_2FC > 1$), blue points represent significantly downregulated metabolites ($\log_2FC < -1$), and grey points denote non-significant changes. The purpose of this figure is to visualise the overall balance and spread of metabolic responses following surgery, highlighting a predominance of upregulated metabolites and substantial inter-individual variability, consistent with global metabolic reprogramming after AAA repair.

6.9 Hierarchical Clustering Heatmap of Plasma Metabolites in the OxAAA Cohort

Hierarchical clustering analysis was performed to visualise global metabolic patterns and assess the degree of similarity among plasma samples collected before (TP3) and after (TPF) surgical repair of abdominal aortic aneurysm. The resulting heatmap revealed a distinct stratification between pre- and post-surgical samples, reflecting a clear metabolic reorganisation following surgery (Figure 62). The dendrogram structure identified two principal branches, corresponding to the pre-operative and post-operative groups, confirming that surgery induced a reproducible and coordinated shift in systemic metabolism. This unsupervised clustering outcome aligned closely with the PLS–DA results, providing independent validation of the observed class separation. Within the heatmap, several co-regulated metabolite clusters were apparent. One cluster exhibited uniform upregulation across post-operative samples, comprising metabolites such as erythritol, uric acid, and L-threonine, which are associated with oxidative stress regulation, purine metabolism, and protein turnover. In contrast, a second major cluster demonstrated downregulation of metabolites such as citric acid, glutamic acid, and octadecanoic acid, consistent with reduced activity of the tricarboxylic acid (TCA) cycle and modifications in fatty acid metabolism.

These complementary clusters point toward coordinated pathway-level responses, likely reflecting the metabolic adaptation and restoration of homeostasis following aneurysm repair. Although the group separation was well defined, some degree of inter-patient variability persisted, suggesting heterogeneous recovery trajectories influenced by factors such as medication, inflammation, or individual metabolic baseline. Nonetheless, the overall pattern confirmed that surgical intervention triggers a systemic biochemical reprogramming encompassing amino acid, lipid, and energy metabolism. Together with

fold change and multivariate analyses, the hierarchical clustering results provide a holistic view of the metabolic impact of surgery. The clear structural organisation of metabolite modules underscores the potential of plasma metabolomics to capture dynamic biochemical responses in AAA patients, offering insights into both recovery mechanisms and systemic physiological adaptation.

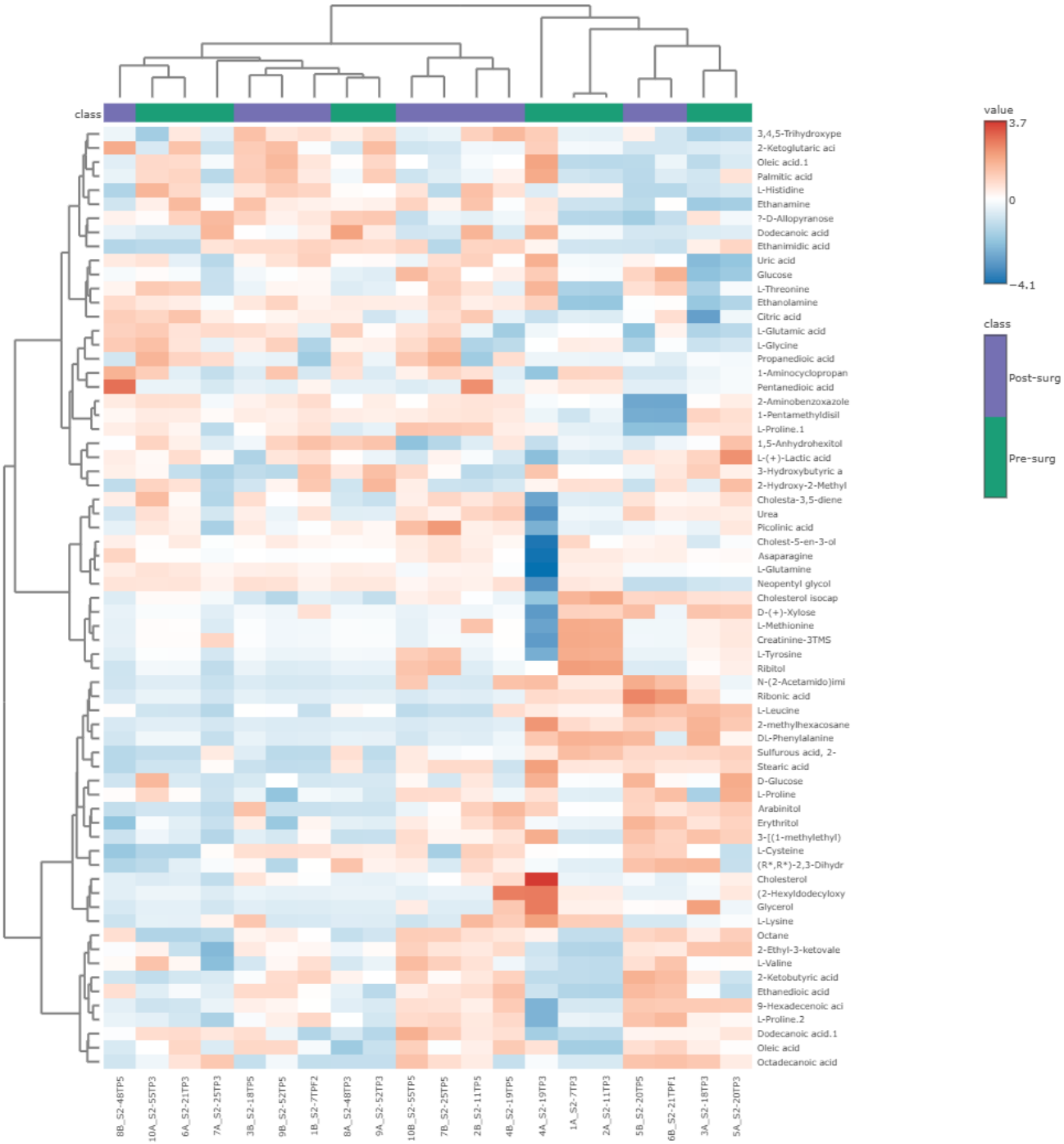

Figure 62. Hierarchical Clustering Heatmap of Plasma Metabolites in the OxAAA Cohort. Heatmap showing z-score normalised abundance of 67 identified plasma metabolites across 20 OxAAA samples. Each column corresponds to an individual sample grouped by surgical status (green = pre-surgery/TP3; purple = post-surgery/TPF). Rows represent individual metabolites identified via GC×GC–MS after derivatisation. Clustering was performed using Euclidean distance and complete linkage algorithms. The red-to-blue gradient denotes relative metabolite abundance, from high (red) to low (blue). Dendrograms display the hierarchical relationships among samples and metabolite expression profiles.

6.10 Principal Component Analysis (PCA) – Biplot

The PCA biplot provides an integrated visualisation of both sample clustering and the metabolites contributing most strongly to variance within the dataset. This combined view links metabolic profiles to their underlying biochemical drivers, allowing mechanistic interpretation of the patterns observed in the PCA scores plot. As shown in Figure 63, pre-surgical (TP3) and post-surgical (TPF) samples occupy distinct regions along the primary components, confirming the systemic metabolic realignment following abdominal aortic aneurysm repair. The orientation and magnitude of the metabolite loading vectors indicate their relative influence on these groupings. Metabolites such as erythritol, cholesterol, octadecanoic acid, and L-threonine align with the post-surgical cluster, suggesting increased abundance after intervention. These changes are consistent with enhanced lipid mobilisation, oxidative stress modulation, and anabolic recovery processes. Conversely, citric acid, glutamic acid, and dodecanoic acid project toward the pre-surgical group, reflecting reduced levels post-surgery and implying a transient downregulation of TCA cycle and amino acid metabolism pathways during recovery. The multidirectional spread of the loading vectors highlights that surgery-induced changes span several biochemical classes, fatty acids, amino acids, sugars, and sugar alcohols, underscoring the system-wide nature of the metabolic reprogramming. This integrative view complements the PCA scores and fold-change analyses, pinpointing metabolites that drive the observed class separation and providing a rational basis for prioritising targets in downstream validation and pathway mapping.

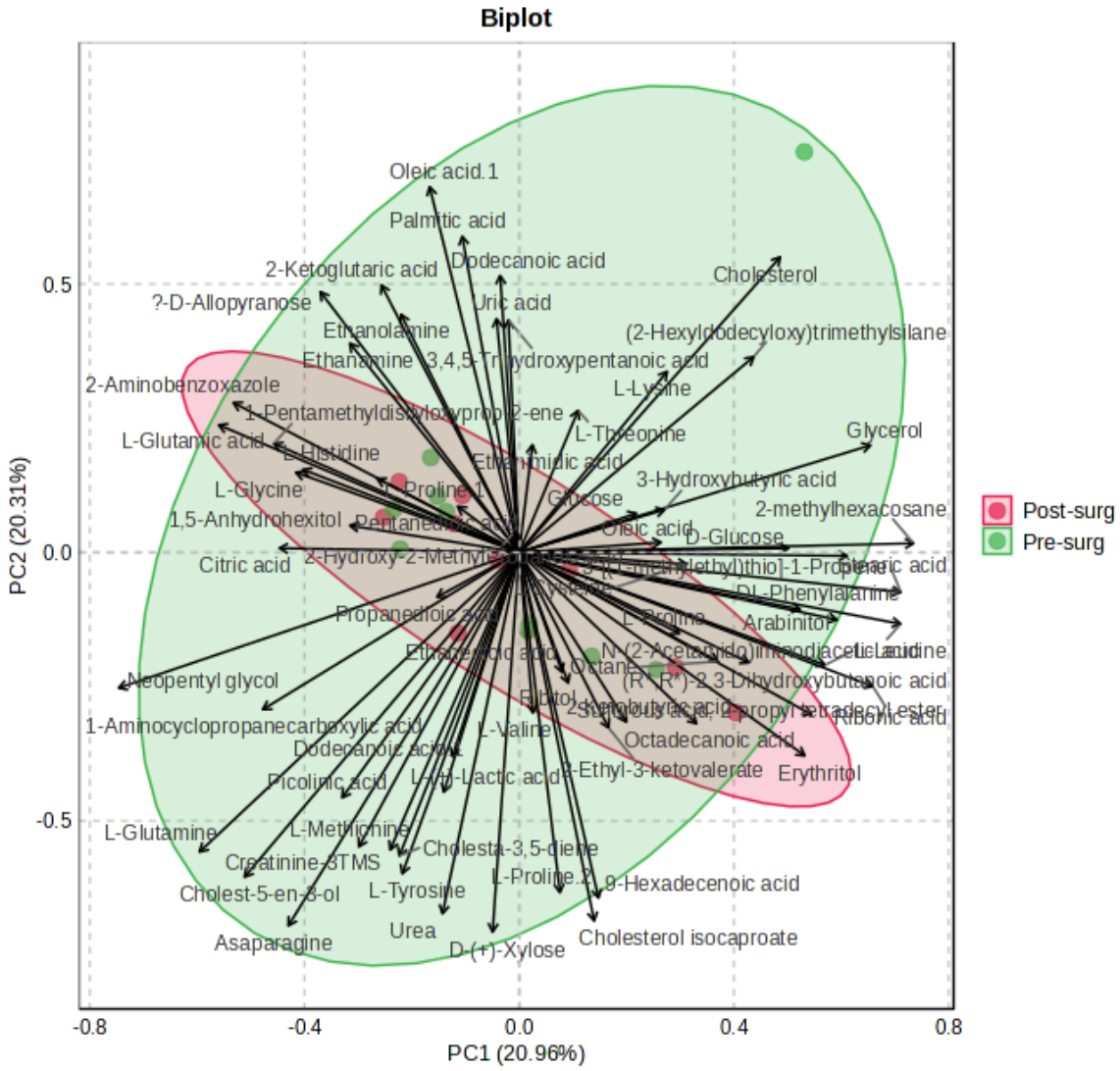

Figure 63. Principal Component Analysis (PCA) – Biplot. The PCA biplot combines sample scores and metabolite loadings to visualise variance structure. Each point represents an individual plasma sample (green triangles = TP3; pink circles = TPF). Arrows represent metabolites, with direction and length indicating their contribution to the principal components. Features located farther from the origin exert greater influence on group separation, revealing key metabolites associated with post-surgical metabolic reprogramming.

6.11 Volcano Plot of Differentially Abundant Plasma Metabolites (Post-surgical vs Pre-surgical Timepoints in OxAAA Patients

The volcano plot summarises the magnitude and statistical significance of plasma metabolite changes between pre-surgical (TP3) and post-surgical (TPF) timepoints in OxAAA patients (Figure 64). By integrating $\log_2$ fold change with $-\log_{10}$(p-value), this analysis highlights metabolites most responsive to surgical intervention while providing a global overview of post-operative metabolic modulation. Overall, the distribution of metabolites shows a predominance of positive fold changes, indicating that the majority of detected features increased in abundance following surgery. Using a significance threshold of $p < 0.05$ and a two-fold change cut-off ($|\log_2 FC| \geq 1$), eleven metabolites were identified as significantly upregulated post-operatively, while one metabolite was significantly downregulated. Among the most statistically significant changes, ethanedioic acid (oxalic acid) exhibited a marked increase ($\log_2 FC \approx 2.28$, $p \approx 1.8 \times 10^{-4}$), representing the strongest combined effect size and significance in the dataset. Several amino acids and related metabolites also showed consistent post-surgical increases, including L-proline ($\log_2 FC \approx 1.32$), L-valine ($\log_2 FC \approx 1.20$), L-cysteine ($\log_2 FC \approx 1.85$), and 2-ketobutyric acid ($\log_2 FC \approx 1.89$), suggesting enhanced amino-acid turnover and protein metabolism during recovery. Carbohydrate- and lipid-associated metabolites were similarly affected. Glucose ($\log_2 FC \approx 1.55$) and erythritol ($\log_2 FC \approx 1.70$) showed moderate but significant increases, consistent with altered energy handling and redox balance following surgical stress. Lipid-related features such as oleic acid ($\log_2 FC \approx 2.32$) and 9-hexadecenoic acid ($\log_2 FC \approx 1.08$) indicate changes in fatty-acid mobilisation and remodelling. Octane also displayed a significant post-operative increase ($\log_2 FC \approx 1.82$), potentially reflecting altered hydrocarbon or lipid-derived metabolic by-products.

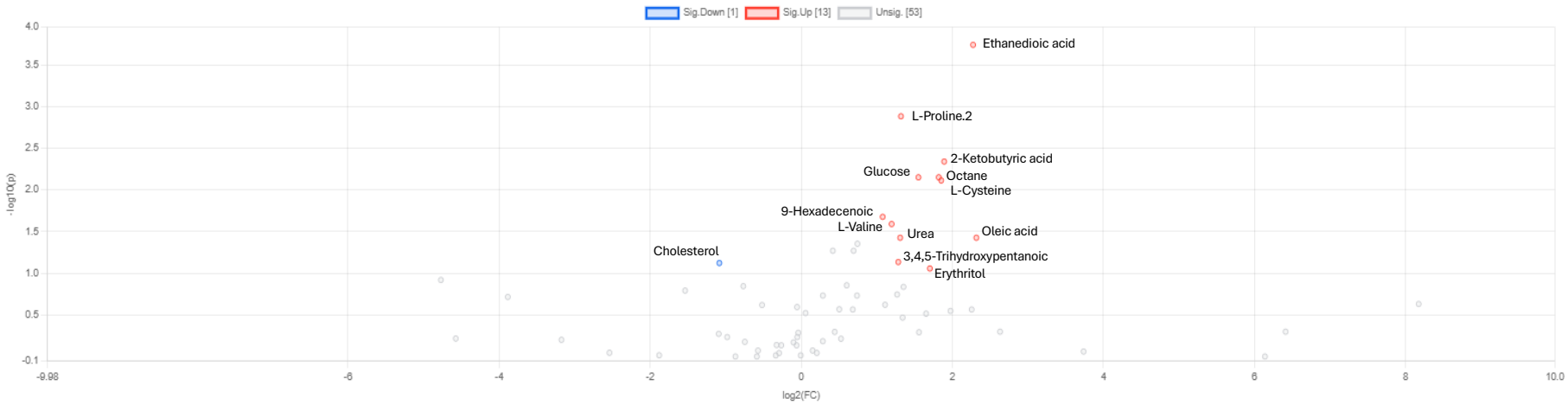

Figure 64. Differentially Abundant Plasma Metabolites (Post-Surgical vs Pre-Surgical Timepoints in OxAAA Patients). Volcano plot illustrating $\log_2$-transformed fold changes (post-surgical vs pre-surgical, TPF/TP3) plotted against $-\log_{10}$(p-values) for plasma metabolites measured in OxAAA patients (n = 10 matched pairs). Vertical dashed lines indicate a two-fold change threshold ($|\log_2 FC| = 1$), and the horizontal dashed line denotes the significance threshold (p = 0.05, raw paired test). Each point represents a metabolite; red points indicate significantly upregulated metabolites, blue points indicate significantly downregulated metabolites, and grey points represent non-significant features. Selected metabolites are annotated to facilitate biological interpretation of post-operative metabolic changes.

One metabolite, cholesterol, was significantly decreased after surgery ($log_2FC \approx -1.08$, $p < 0.05$), representing the only downregulated feature meeting the significance threshold. This reduction may reflect transient alterations in lipid transport or utilisation during the post-operative recovery phase. Although the total number of statistically significant metabolites is modest, the volcano plot reveals coherent, biologically interpretable trends that align with results from complementary multivariate analyses (PCA, PLS–DA, and fold-change profiling). Collectively, these findings support a coordinated post-surgical metabolic reorganisation involving amino-acid metabolism, lipid remodelling, and energy-related pathways. Even within a limited cohort size, reproducible metabolite-level changes were detected, underscoring the sensitivity of plasma metabolomics for capturing systemic responses to AAA repair and identifying candidates for targeted validation in larger patient cohorts. Each analytical method contributed complementary insights into data structure, group separation, and metabolite-level differences. The integrated analytical framework is summarised below (Table 24).

Table 24. Summary of statistical and multivariate analyses used for metabolomic data interpretation.

Figure	Analysis Type	Purpose	Rationale for Inclusion
Figure 60	Orthogonal Partial Least Squares Discriminant Analysis (PLS-DA) Scores Plot	Supervised classification of samples	Demonstrates separation between pre- and post-surgery metabolic profiles, highlighting intervention effects.
Figure 61	Fold Change (FC) Analysis Plot	Differential metabolite analysis	Identifies significantly up- and down-regulated metabolites. Visually quantifies the direction and magnitude of metabolic changes.
Figure 62	Hierarchical Clustering Heatmap	Unsupervised clustering of samples and metabolites	Reveals patterns of metabolic expression across individuals and timepoints. Clusters metabolites and samples into biologically meaningful groups.
Figure 63	PCA – Biplot	Metabolite contribution visualisation	Highlights which metabolites drive variation. Useful for biological interpretation of group separation seen in the PCA scores plot.
Figure 64	Volcano Plot	Combined magnitude and significance filtering	Highlights statistically significant and biologically relevant metabolites. Easily points to potential biomarkers.

Discussion

The comparison between one-dimensional (1D) and two-dimensional (2D) gas chromatography underscores the superior resolving power of GC×GC–MS for comprehensive plasma metabolomics, particularly in complex biological matrices. In this study, GC×GC–MS significantly improved peak resolution, separation efficiency, and metabolite coverage, enabling confident identification of 67 distinct metabolites from derivatised plasma samples within the OxAAA cohort. This represents a substantial advancement over conventional 1D GC–MS workflows, which were constrained by peak co-elution, limited sensitivity, and reduced chromatographic capacity.

The success of this analytical approach was driven by methodological optimisation across the extraction and derivatisation stages. The combined biphasic methanol/MTBE extraction and two-step derivatisation (methoximation followed by silylation) markedly enhanced the recovery and thermal stability of polar and semi-polar metabolites. These adjustments improved the detectability of compound classes typically underrepresented in standard GC–MS, including amino acids, organic acids, and sugars. The expanded metabolite spectrum achieved here addresses a major limitation of previous analyses in this cohort and supports the platform's suitability for downstream biomarker discovery.

Multivariate analyses confirmed the biological significance of these improvements. Partial Least Squares Discriminant Analysis (PLS–DA) demonstrated clear and reproducible separation between pre-operative (TP3) and post-operative (TPF) samples, indicating systemic metabolic remodelling in response to surgical intervention. The non-overlapping 95% confidence intervals and compact clustering of post-operative samples highlight the reproducibility and robustness of the metabolic distinctions. The PCA biplot further identified key metabolites contributing to this separation, most notably citric acid, glutamic acid, octadecanoic acid, cholesterol, erythritol, and L-threonine, which together

implicate coordinated shifts in lipid metabolism, amino acid turnover, carbohydrate utilisation, and oxidative stress responses. These pathways are consistent with the physiological stress and subsequent recovery following open AAA repair. Post-surgical upregulation of cholesterol, erythritol, and L-threonine, contrasted with reductions in citric acid and glutamic acid, is consistent with enhanced lipid mobilisation and altered TCA cycle flux. These signatures align with expected metabolic adaptations to surgical recovery and tissue remodelling.

Hierarchical clustering revealed structured patterns of metabolite co-regulation, suggesting pathway-level metabolic coordination rather than isolated compound shifts. Clusters of upregulated metabolites, such as cholesterol isocaproate, octadecanoic acid, and oleic acid, indicate concerted activation of lipid-related pathways, possibly reflecting energy substrate reallocation or compensatory lipolysis. Conversely, the downregulation of TCA intermediates and amino acids such as glutamate points toward a transient suppression of oxidative metabolism during recovery. These systemic adjustments may reflect the interplay between energy demand, inflammatory resolution, and anabolic repair following surgical intervention. Pairwise correlation analyses further revealed metabolite–metabolite associations that could indicate functional network dependencies and regulatory coupling between pathways. These relationships offer promising starting points for future validation and network-based biomarker studies within larger AAA populations.

An instructive methodological observation was the reduced detectability of squalene relative to earlier analyses. Its diminished signal likely reflects the limitations of derivatisation for highly hydrophobic compounds lacking reactive groups. This highlights an inherent analytical bias against neutral lipids and underscores the need for complementary lipidomic future strategies to achieve comprehensive metabolic coverage.

Despite this limitation, the optimised GC×GC–MS workflow markedly improved metabolite diversity and detection sensitivity, particularly for clinically relevant compounds including fatty acids, sugar alcohols, sterols, amino acids, and dicarboxylic acids, all key mediators of metabolic and inflammatory homeostasis.

The longitudinal, paired-sample design of the OxAAA study provided an additional advantage by minimising inter-individual variability and enhancing the ability to detect consistent, surgery-related metabolic shifts. This strengthens the biological interpretability of the results and increases confidence that the observed changes reflect genuine physiological responses rather than technical or demographic variability.

To mitigate platform bias against neutral lipids, future work will incorporate complementary shotgun/LC-MS lipidomics to extend coverage to steryl esters and long-chain triacylglycerols. Multivariate claims were supported by cross-validated PLS-DA and corroborated by unsupervised PCA and FDR-controlled univariate tests, reducing the risk of model over-interpretation in a modest sample.

Collectively, the integration of multivariate and correlation-based analyses offers a comprehensive depiction of metabolic adaptations following AAA repair. The findings highlight significant modulation of lipid and energy metabolism, redox balance, and amino acid pathways, providing biochemical insight into recovery processes. Moreover, the workflow established here forms an analytical foundation for future multi-omics integration with proteomic, transcriptomic, and clinical datasets within the OxAAA framework. Such integration could be pivotal for refining mechanistic understanding, improving risk stratification, and developing metabolite-based biomarkers to monitor post-surgical recovery and disease progression in AAA.

Chapter 7 – General Discussion and Conclusions

7.1 Overview

This thesis presents the development, optimisation, and application of complementary proteomic and metabolomic workflows for the quantitative characterisation of circulating plasma biomarkers in AAA. The work builds upon the OxAAA study framework, which integrates clinical, imaging, and molecular data to enhance disease prediction and management. Within this context, the overarching goal of the DPhil was to establish analytically robust and biologically interpretable mass spectrometry–based methods capable of accurately quantifying biomolecules in human plasma, with direct relevance to clinical translation and personalised patient monitoring. The ultimate objective underlying these developments is to improve the current OxAAA aneurysm growth prediction by incorporating precise proteomic quantification into the existing prediction model. Through the generation of reliable protein and metabolite data, this work seeks to refine biomarker-informed prediction tools that more effectively stratify patient risk, guide surveillance intervals, and inform surgical timing. Two complementary analytical streams were pursued:

1. A quantitative proteomic approach, centred on the design and implementation of the OxConCAT construct (C-002). This bespoke, isotopically labelled recombinant protein standard enables the absolute quantification of multiple plasma biomarkers using targeted parallel reaction monitoring (PRM).
2. A comprehensive metabolomic workflow based on two-dimensional gas chromatography coupled to mass spectrometry (GC×GC–MS), optimised to maximise metabolite coverage, reproducibility, and identification accuracy in plasma samples from AAA patients.

Together, these methods provide a dual-layered characterisation of the systemic biochemical changes associated with AAA surgery, integrating proteomic and metabolic perspectives. The work presented here, therefore, serves as a methodological and conceptual bridge between analytical innovation and clinical application, laying the foundation for the next phase of multi-omics validation and predictive modelling within the OxAAA study.

7.2 Methodological Development and Optimisation

7.2.1 Proteomics: The OxConCAT Quantification Framework

The OxConCAT construct was developed as a quantitative calibration tool to enable absolute measurement of circulating biomarkers identified in the OxAAA study and to refine the aneurysm-growth prediction algorithm. Designed to translate discovery findings into a clinically applicable framework, OxConCAT encodes stable isotope–labelled peptides from selected biomarkers within a single recombinant protein, allowing simultaneous, internally calibrated measurement of multiple plasma targets. This multiplexed approach enhances analytical consistency, minimises inter-assay variability, and enables reproducible comparison of protein abundances across cohorts. Peptide selection followed a rigorous multi-step process considering sequence uniqueness, absence of labile residues, efficient tryptic cleavage, and stable chromatographic behaviour. Empirical filtering of discovery datasets prioritised peptides with consistent plasma detectability and strong ionisation under both co-digestion and post-digest spike-in conditions, whereas peptides showing suppression or instability were excluded. Expression and purification of the OxConCAT protein were followed by systematic

optimisation of digestion and spike-in parameters. A spike-in level of 200 fmol per digest was identified as optimal, ensuring strong signals without detector saturation and maintaining linearity across a broad concentration range. The PRM approach was employed for its high specificity and precision, using PRM–PASEF acquisition on the timsTOF Pro to monitor multiple peptide transitions with high temporal and ion-mobility resolution. DIA was used in parallel as a complementary exploratory tool to characterise overall proteome variability and confirm that OxConCAT targets lay within physiologically relevant abundance ranges. This two-tiered strategy, DIA for contextual proteome mapping and PRM for quantitative precision, linked methodological optimisation with biological interpretation, providing both analytical depth and clinical relevance.

7.2.2 Metabolomics: Development of a GC×GC–MS Pipeline

The metabolomic component of this work focused on resolving the chemical complexity of plasma metabolites. GC×GC–MS offered superior separation and sensitivity over conventional one-dimensional GC–MS, enabling concurrent analysis of volatile, semi-volatile, and polar compounds. Method development optimised two critical steps: dual-phase extraction to separate polar and non-polar species, and sequential methoximation–silylation derivatisation to enhance volatility and stability. These refinements improved reproducibility and signal quality, leading to confident identification of 67 metabolites spanning amino acids, fatty acids, carbohydrates, organic acids, and sterols. Despite incomplete recovery of highly hydrophobic compounds such as squalene, the workflow achieved robust detection of central metabolic intermediates and demonstrated resilience

to batch effects, providing a solid foundation for future large-scale analyses and integrated omics studies.

7.3 Proteomic Interpretation: Biological and Analytical Dimensions

Application of the OxConCAT–PRM workflow to plasma from ten OxAAA patients, sampled pre- (TP3) and post-operatively (TPF), demonstrated the feasibility of absolute targeted quantification in complex plasma matrices. Most OxConCAT-encoded peptides were reproducibly detected, with five proteins showing consistent and statistically significant post-surgical changes: Attractin (ATRN), Neurochondrin-like 1 (NCHL1), C-reactive protein (CRP), Complement component C8 gamma chain (CO8G), and Apolipoprotein A-IV (APOA4).

Attractin and NCHL1

Both ATRN and NCHL1 showed marked reductions following surgery. ATRN, previously identified as elevated in patients with larger aneurysms, is associated with immune cell adhesion and thrombus organisation; its post-operative decrease is consistent with removal of aneurysm-associated thrombotic tissue and attenuation of chronic inflammatory activity. Similarly, NCHL1, implicated in extracellular matrix remodelling, appears downregulated as part of vascular repair and tissue healing processes initiated by surgical intervention.

Complement and inflammatory Proteins

CO8G and CRP both declined significantly after surgery, consistent with reduced systemic inflammation and complement activity once the aneurysmal thrombus and its

inflammatory burden were removed. These findings align with the expected post-operative resolution of acute-phase responses and systemic immune activation.

Lipid-Associated Proteins

APOA4 showed a modest but statistically significant post-operative increase, aligning with recovery-related adjustments in lipid transport. This pattern complements the GC×GC–MS metabolomic results, which revealed corresponding shifts in lipid and fatty acid metabolism, indicating coordinated proteomic–metabolomic adaptation to surgical repair.

Technical Considerations

Not all peptides met reliability thresholds. The AL1L1 peptide failed in roughly 40% of samples due to low ionisation efficiency and co-elution with abundant plasma components. These outcomes emphasise that physicochemical properties, particularly hydrophobicity and charge, remain critical determinants of peptide performance. Such insights will inform the next iteration of OxConCAT constructs, focusing on alternative peptide selection to enhance chromatographic behaviour, ionisation efficiency, and quantification reproducibility.

7.4 Metabolomic Interpretation and Physiological Context

GC×GC–MS provided an independent yet complementary view of systemic biochemical changes following AAA surgery. Compared with one-dimensional GC–MS, the two-dimensional approach substantially improved chromatographic resolution and metabolite coverage. The optimised workflow enabled identification of 67 metabolites across amino acids, organic acids, carbohydrates, fatty acids, and sterols, representing a significant

advance in metabolic profiling within the OxAAA cohort. Partial Least Squares Discriminant Analysis (PLS-DA) revealed separation between pre-operative (TP3) and post-operative (TPF) samples (Chapter 6, Section 6.7), supported by compact clustering of post-surgical profiles, evidence of reproducible metabolic remodelling, and cross-validation, and was further corroborated by PCA and FDR-controlled univariate testing. PCA loading plots identified citric acid, glutamic acid, octadecanoic acid, cholesterol, erythritol, and L-threonine as principal contributors, indicating coordinated shifts in lipid metabolism, amino-acid turnover, carbohydrate utilisation, and oxidative stress pathways.

These signatures reflect expected physiological adaptations during recovery from open AAA repair: increases in cholesterol, erythritol, and L-threonine alongside decreases in citric acid and glutamic acid suggest enhanced lipid mobilisation, redox adjustment, and transient modulation of oxidative metabolism. Hierarchical clustering and correlation analyses demonstrated pathway-level synchrony among lipid, amino-acid, and redox-related metabolites, underscoring network-driven responses rather than isolated compound shifts. The paired-sample design of the OxAAA study was critical for reducing inter-individual variability and isolating surgery-specific effects. Together, these findings reveal that AAA repair induces coordinated adjustments in lipid and energy metabolism, redox balance, and amino-acid utilisation, systemic adaptations characteristic of vascular recovery. The optimised GC×GC–MS workflow thus provides a platform for future integration with proteomic and clinical data to refine mechanistic understanding and predictive modelling of AAA growth and post-surgical recovery.

7.5 Technical and Biological Integration

Integrating proteomic and metabolomic results highlights the interplay between analytical precision and biological interpretation. The combination of OxConCAT-calibrated PRM and optimised GC×GC–MS increases confidence that observed molecular variations reflect genuine physiology rather than artefactual variability. Analytical validity was supported by isotope-labelled internal standards and retention-aligned PRM–PASEF in proteomics, and by internal standard–normalised, derivatisation-controlled GC×GC–MS in metabolomics. Biologically, the convergence of patterns across both datasets supports a consistent narrative: surgical repair triggers inflammatory resolution, metabolic adaptation, and vascular tissue remodelling. Together, these insights demonstrate how harmonised multi-omics approaches can translate molecular changes into clinically meaningful understanding.

7.6 Objectives Deferred Beyond the Thesis

While the thesis fulfilled its aims in method development, optimisation, and pilot application, particular broader objectives, such as international cohort validation and integrated omics analysis, were not completed within the DPhil timeframe. This reflected the prioritisation of achieving full analytical reproducibility and stability of the OxConCAT and GC×GC–MS workflows before large-scale deployment. The infrastructure for these subsequent phases is now in place. Over 400 plasma samples from cohorts in Oxford, Japan, Sweden, and the Netherlands have been collected and prepared. Cross-centre harmonisation will use a common OxConCAT lot, pooled-plasma QCs, and shared calibration/normalisation SOPs to ensure commutability and inter-laboratory comparability. This forthcoming phase aims to refine the OxAAA prediction algorithm

for aneurysm growth by integrating absolute proteomic quantification and detailed metabolic profiling with longitudinal clinical data. The expanded dataset will support improved prediction of aneurysm expansion at 12- and 24-month intervals, advancing biomarker-based risk stratification and personalised surveillance strategies.

7.7 Limitations

Several limitations should be acknowledged. First, the sample size of the pilot study limits the statistical power to detect smaller effect sizes, and biological variability between patients may have influenced some results. Second, despite careful optimisation, ion suppression and matrix effects remain inherent challenges in plasma proteomics and may have contributed to occasional inconsistencies in peptide detectability. Third, the GC×GC–MS metabolomics workflow, although improved in coverage, is biased toward volatile and semi-volatile compounds and does not capture the full lipidome or metabolite spectrum. Given the modest sample size (n=10 pairs), supervised models risk overfitting; we mitigated this by cross-validation, permutation testing, and triangulation with unsupervised PCA and FDR-controlled univariate analyses. Nevertheless, these limitations are partly mitigated by the methodological advances achieved: high reproducibility across technical replicates, consistency in fold-change directionality, and successful demonstration of absolute quantification across multiple proteins. The insights gained from these pilot data will guide the next stage of analytical refinement and biological validation.

7.8 Future Directions

Future work will expand upon the developments presented in this thesis through several complementary approaches:

1. **Refinement of subsequent OxConCAT Constructs**
    - Select alternative proteotypic peptides with improved chromatographic behaviour and ionisation.
    - Expand the panel with AAA-related proteins from discovery datasets.
    - Implement semi-automated expression/purification to increase yield and lot-to-lot consistency.
2. **International Cohort Validation and Prediction Algorithm Integration**
    - Apply OxConCAT–PRM to >400 plasma samples across four centres.
    - Quantify inter-centre variability using shared QCs and calibration curves.
    - Integrate absolute concentrations with longitudinal clinical data to evaluate aneurysm growth at 12 and 24 months and thereby improve the prediction algorithm.
3. **Combination of Proteomics with Metabolomics and Lipidomics**
    - Incorporate LC–MS–based lipidomics to complement the existing GC×GC–MS platform and enhance coverage of neutral and complex lipid species.
    - Use multivariate/multi-block models (e.g., DIABLO, MOFA) to map cross-pathway interactions linking proteins, metabolites, and lipids.
4. **Clinical Translation**
    - Down-select to a pragmatic PRM panel (e.g., 6–10 peptides) with predefined QC acceptance criteria.

- Establish clinical decision thresholds and intra-individual variability from repeated sampling.
- Coordinate with partner centres to embed assays into prospective clinical studies.

7.9 Concluding Remarks

This thesis reports the development and optimisation of quantitative proteomic and metabolomic workflows for translational application in AAA research, establishing an analytical foundation within the OxAAA framework. Through the creation of the OxConCAT construct, a bespoke isotopically labelled recombinant standard, absolute quantification of multiple plasma proteins was achieved with high precision and reproducibility. The complementary GC×GC–MS pipeline expanded the measurable metabolic landscape of plasma, improving both coverage and consistency. Together, these approaches revealed biologically coherent molecular changes following surgery, offering complementary insights into inflammation, energy metabolism, and vascular recovery. Although large-scale validation and integrated omics analyses were beyond the timeframe of this DPhil, the analytical groundwork established here now supports expansion to over 400 patient samples from international OxAAA cohorts in Oxford, Japan, Sweden, and the Netherlands. These studies will validate OxConCAT-based quantification across populations and refine the OxAAA aneurysm growth prediction algorithm by integrating molecular, clinical, and imaging data. In conclusion, the OxConCAT and GC×GC–MS pipelines represent important methodological advances towards a quantitative and integrative framework for studying AAA pathophysiology. Together, they provide the analytical precision, reproducibility, and scalability required

for future large-scale validation within the OxAAA and associated international cohorts. These workflows now form the technical foundation for the next phase of biomarker-informed predictive modelling, supporting the refinement of AAA growth algorithms and the broader goal of improving risk stratification and clinical decision-making in aneurysm management.

Supplementary Section S1.

Table S1. Comprehensive demographic and clinical data, aneurysm characteristics, and cardiovascular history of the OxAAA pilot cohort.

	Demographics Data and Examination at Baseline																							
Pilot Study Patient ID	Baseline sampling (TP3)	Follow-up sampling (TP5/TPF)	Age at Consent Date	Sex	Male?	Caucasian?	Height (m)	Weight (kg)	BMI	Distance from sternal notch to axilla (cm)	Distance from axilla to probe (cm)	Waist (cm)	Hips (cm)	Waist/Hip ratio	Systolic BP (mm Hg)	Diastolic BP (mm Hg)	Never Smoked	Ex-smoker	Current smoker	Type of tobacco consumed	Number of years of smoking	Pack Years	For ex-smoker: stopped duration
01	03/02/2014	01/08/2018	65	M	1	1	1.85	81.8	23.9	24	16	94	96	0.98	160	92	1	0	0				
02	17/03/2014	06/05/2014	81	M	1	1	1.78	91.0	28.7	21	18	113	110	1.03	100	72	0	0	1	Pipe	50	3	
03	21/05/2014	27/04/2014	80	M	1	1	1.67	60.0	21.5	19	14	85	83	1.02	140	70	0	0	1	Cigarettes/Cigars	50	46	
04	03/06/2014	01/10/2014	83	M	1	1	1.69	76.6	26.8			93	100	0.93			0	1	0	Cigars/Cigarettes	15	11.3	30
05	11/06/2014	30/07/2014	64	M	1	1	1.84	122.0	36.0			114	129	0.88	140	90	0	1	0	Cigarettes	40	40	4
06	16/06/2014	01/06/2016	72	F	0	1	1.54	54.4	22.9	18	12	82	95	0.86	170	96	0	1	0	Cigarettes	35	35	5
07	14/10/2014	01/11/2014	68	M	1	1	1.78	82.3	26.0	23	17	94	98	0.96	150	90	0	0	1	Cigarettes	40	40	
08	12/01/2016	14/04/2016	65	M	1	1	1.8	73.1	22.6	23	19	94	94	1.00			0	0	1	Cigarrettes/roll-ups	50	28	
09	04/02/2016	01/11/2016	74	M	1	1	1.62	82.5	31.4	24	18	92	97	0.95	158	98	0	1	0	Cigarettes	20	20	40
10	29/02/2016	01/04/2016	65	M	1	1	1.72	82.4	27.9	23	21	97	101	0.96	170	100	0	1	0	Cigars	20		25

	Cardiovascular History																												
Pilot Study Patient ID	**Diabetes**	Diagnosis - status unknown	Diabetes - lifestyle management	Diabetes - oral medication	Diabetes - insulin	**Hypertension**	**Hypercholesterolaemia**	**Peripheral vascular disease**	History of percutaneous arterial intervention	History of peripheral arterial bypass	History of venous disease treatment	**Coronary heart disease**	History of stable angina	History of myocardial infarction/acute coronary syndrome	History of percutaneous coronary intervention	History of coronary artery bypass graft	**Cerebral vascular disease**	History of TIA,	History of stroke	**Valvular heart disease**	**Cardiac arrhythmia**	**Family history of CHD**	**Family history of aneurysms**	**Alcohol consumption (units**	01 - Cardiovascular	02 - Respiratory	AAA size cm	Surgery	
01	**0**	0	0	0	0	**1**	**0**	**0**	0	0	0	**0**	0	0	0	0	**0**	0	0	**0**	**0**	**1**	**1**	**10**	0	0	3.9	OSR	
02	**0**	0	0	0	0	**0**	**0**	**0**	0	0	0	**0**	0	0	0	0	**0**	0	0	**0**	**1**	**0**	**0**	**2**	0	0	5.8	OSR	
03	**0**	0	0	0	0	**1**	**1**	**0**	0	0	0	**0**	0	0	0	0	**1**	1	0	**0**	**0**	**1**	**1**	**2**	0	0	6.7	OSR	
04	**0**	0	0	0	0	**1**	**1**	**1**	0	0	1	**1**	0	1	0	1	**0**	0	0	**0**	**0**	**0**	**0**	**10**	1	0	5.6	OSR	
05	**1**	0	0	1	0	**1**	**1**	**0**	0	0	0	**0**	0	0	0	0	**0**	0	0	**0**	**0**	**0**	**1**	**15**	0	0	8.5	OSR	
06	**0**	0	0	0	0	**1**	**1**	**1**	1	0	0	**0**	0	0	0	0	**0**	0	0	**0**	**0**	**0**	**0**	**0**	1	0	6	OSR	
07	**0**	0	0	0	0	**0**	**0**	**0**	0	0	0	**1**	1	0	1	0	**0**	0	0	**0**	**0**	**0**	**1**	**10**	1	0	5.6	OSR	
08	**1**	0	1	0	0	**1**	**1**	**0**	0	0	0	**0**	0	0	0	0	**0**	0	0	**0**	**0**	**1**	**0**	**5**	1	0	5.7	OSR	
09	**0**	0	0	0	0	**1**	**0**	**0**	0	0	0	**0**	0	0	0	0	**0**	0	0	**0**	**0**	**1**	**1**	**10**	0	1	5.3	OSR	
10	**1**	0	1	1	0	**1**	**1**	**0**	0	0	0	**0**	0	0	0	0	**0**	0	0	**0**	**0**	**1**	**0**	**0**	0	0	5.9	OSR	

Supplementary Section S2

Evaluation of Trypsin Cleavage Efficiency in the OxConCAT Standard Using FragPipe-Based DDA Analysis

Experimental Design and Sample Preparation

Trypsin digestion efficiency of the OxConCAT (Oxford Concatemer) construct was evaluated using purified OxConCAT protein in the absence of plasma matrix. A single production batch was analysed at four input amounts (50, 100, 200, and 500 fmol). All samples underwent identical tryptic digestion prior to LC–MS/MS analysis. This concentration range enabled assessment of potential concentration-dependent digestion effects while excluding matrix-related interference. Data were acquired using data-dependent acquisition (DDA) on high-resolution Orbitrap instrumentation.

Data Processing Workflow (FragPipe v23.0)

Raw DDA files were processed using FragPipe (v23.0), incorporating MSFragger (v4.3), Philosopher (v5.1.1), Percolator (v3.7.1), and IonQuant (v1.1.11) within a closed-search workflow.

Database Search

Database searching was performed under strict trypsin specificity, allowing cleavage C-terminal to lysine and arginine residues, with up to two missed cleavages permitted. Precursor mass tolerance was set to ±20 ppm and fragment mass tolerance to 20 ppm. Carbamidomethylation of cysteine was specified as a fixed modification, while

methionine oxidation and protein N-terminal acetylation were included as variable modifications. The FASTA database consisted exclusively of the OxConCAT sequence with appended decoy entries for false discovery rate estimation.

Validation and FDR Control

Peptide-spectrum matches were validated using Percolator. Protein-level false discovery rate (FDR) was controlled at 1% using a sequential picked FDR strategy. Protein inference was conducted using ProteinProphet to ensure confident protein-level assignment.

Quantification

Label-free quantification was performed using IonQuant with match-between-runs enabled. Intensity normalisation was applied across runs to ensure comparability between concentration points. All four datasets were processed jointly within a single workflow to maintain consistent identification and quantification criteria.

Global Peptide Identification and Missed Cleavage Distribution

Across the four input amounts (50–500 fmol), more than 40 OxConCAT-derived peptides were confidently identified at 1% protein-level FDR. The majority were fully cleaved. Six peptides exhibited evidence of a single missed cleavage event, and no peptides displayed more than one quantifiable missed cleavage. Missed cleavage frequency remained stable across the tested concentration range.

Quantification of Miscleavage Ratios

For peptides in which both correctly cleaved ("short") and miscleaved ("long") forms were detected, relative abundances were calculated using MS1 intensities derived from IonQuant. Miscleavage percentage was defined as:

$$\text{Miscleavage (\%)} = \frac{\text{Long peptide intensity}}{\text{Long + Short peptide intensity}} \times 100$$

Of the six peptides exhibiting missed cleavage, three produced sufficient signal for quantitative assessment.

ANXA6_HUMAN
Short: DLEADIIGDTSGHFQK
Long: DLEADIIGDTSGHFQKESDTSYVSLK
Long form abundance: 1.96%
Estimated cleavage efficiency: ~98%

CRP_HUMAN
Short: ESDTSYVSLK
Long: ESDTSYVSLKGYSIFSYATK
Long form abundance: 4.57%
Estimated cleavage efficiency: ~95.5%

LDHB_HUMAN
Short: SLADELALVDVLEDK
Long: SLADELALVDVLEDKDYSVTANSK
Long form abundance: 22.8%
Estimated cleavage efficiency: ~77–78%

No additional quantifiable miscleavage events were observed among the remaining peptides.

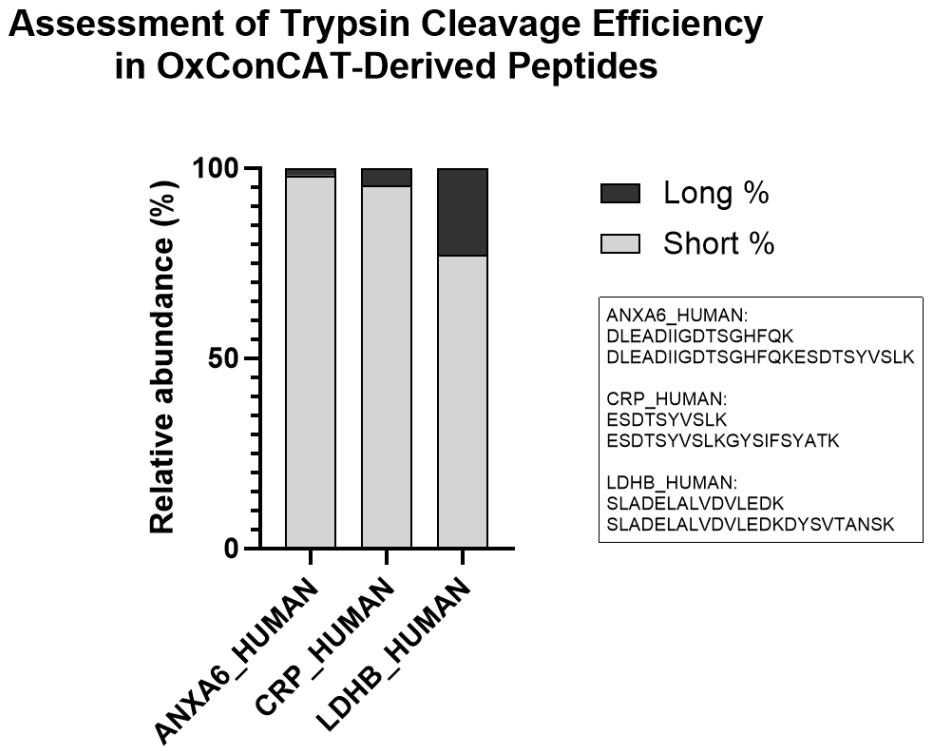

Figure S1. Evaluation of Trypsin Cleavage Efficiency in the OxConCAT Construct.
Trypsin digestion efficiency was assessed by re-searching DDA datasets using the full OxConCAT sequence while allowing up to two missed cleavages. For peptides in which both correctly cleaved (short) and miscleaved (extended) forms were detected, relative abundances were calculated from summed MS1 intensities across replicate injections. Bars represent the percentage contribution of correctly cleaved peptides ("Short %") and corresponding miscleaved forms ("Long %") for each OxConCAT-derived peptide. ANXA6 and CRP peptides demonstrated highly efficient cleavage (>95% correctly cleaved), whereas the LDHB peptide exhibited partial sequence-dependent resistance (~22% miscleavage). No additional quantifiable missed cleavages were detected among the remaining OxConCAT peptides. These findings confirm robust overall trypsin digestion of the OxConCAT construct, with only isolated peptide-specific deviations.

Concentration Independence of Cleavage Efficiency

The LDHB-derived peptide exhibited the highest miscleavage rate (~22%). Inspection of the local sequence revealed that the lysine cleavage site is flanked by acidic residues, a context that may reduce trypsin accessibility through local structural or electrostatic effects. In contrast, ANXA6- and CRP-derived peptides demonstrated efficient cleavage (<5% miscleavage), consistent with expected trypsin activity under denaturing conditions. Cleavage efficiency remained consistent across the 50–500 fmol range, indicating that the observed variability reflects sequence context rather than concentration-dependent digestion limitations. Overall, these results demonstrate efficient and reproducible tryptic digestion of the OxConCAT construct. Missed cleavage events were infrequent and confined to specific sequence contexts. The identification of a peptide with reduced cleavage efficiency underscores the importance of empirical validation and iterative optimisation during OxConCAT design to ensure optimal performance in absolute quantification workflows.

References

1. Abdul-Hussien, H., Hanemaaijer, R., Kleemann, R., Verhaaren, B.F.J., van Bockel, J.H., Lindeman, J.H.N.: The pathophysiology of abdominal aortic aneurysm growth: Corresponding and discordant inflammatory and proteolytic processes in abdominal aortic and popliteal artery aneurysms. J Vasc Surg. 51, 1479–1487 (2010). https://doi.org/10.1016/j.jvs.2010.01.057

2. Erbel, R., Eggebrecht, H.: Aortic dimensions and the risk of dissection. Heart. 92, 137–142 (2006). https://doi.org/10.1136/hrt.2004.055111

3. Kent, K.C.: Abdominal Aortic Aneurysms. New England Journal of Medicine. 371, 2101–2108 (2014). https://doi.org/10.1056/NEJMcp1401430

4. Abdominal aortic aneurysm screening for women is unlikely to be a fair use of NHS resources. (2018)

5. Vänni, V., Turtiainen, J., Hakala, T., Salenius, J., Suominen, V., Oksala, N., Hernesniemi, J.: Vascular comorbidities and demographics of patients with ruptured abdominal aortic aneurysms. Surgery. 159, 1191–1198 (2016). https://doi.org/10.1016/j.surg.2015.10.005

6. Golledge, J., Thanigaimani, S., Powell, J.T., Tsao, P.S.: Pathogenesis and management of abdominal aortic aneurysm. Eur Heart J. 44, 2682–2697 (2023). https://doi.org/10.1093/eurheartj/ehad386

7. Kessler, V., Klopf, J., Eilenberg, W., Neumayer, C., Brostjan, C.: AAA Revisited: A Comprehensive Review of Risk Factors, Management, and Hallmarks of Pathogenesis. Biomedicines. 10, (2022). https://doi.org/10.3390/biomedicines10010094

8. Gwon, J.G., Kwon, T.-W., Cho, Y.-P., Han, Y.J., Noh, M.S.: Analysis of in hospital mortality and long-term survival excluding in hospital mortality after open surgical repair of ruptured abdominal aortic aneurysm. Ann Surg Treat Res. 91, 303–308 (2016). https://doi.org/10.4174/astr.2016.91.6.303

9. Karkos, C.D.: Mortality After Endovascular Repair of Ruptured Abdominal Aortic Aneurysms. Archives of Surgery. 144, 770 (2009). https://doi.org/10.1001/archsurg.2009.132

10. Hołda, M.K., Iwaszczuk, P., Wszołek, K., Chmiel, J., Brzychczy, A., Trystuła, M., Misztal, M.: Coexistence and management of abdominal aortic aneurysm and coronary artery disease. Cardiol J. 27, 384–393 (2020). https://doi.org/10.5603/CJ.a2018.0101

11. Wanhainen, A., Van Herzeele, I., Bastos Goncalves, F., Bellmunt Montoya, S., Berard, X., Boyle, J.R., D'Oria, M., Prendes, C.F., Karkos, C.D., Kazimierczak, A., Koelemay, M.J.W., Kölbel, T., Mani, K., Melissano, G., Powell, J.T.,

Trimarchi, S., Tsilimparis, N., Antoniou, G.A., Björck, M., Coscas, R., Dias, N. V., Kolh, P., Lepidi, S., Mees, B.M.E., Resch, T.A., Ricco, J.B., Tulamo, R., Twine, C.P., Branzan, D., Cheng, S.W.K., Dalman, R.L., Dick, F., Golledge, J., Haulon, S., van Herwaarden, J.A., Ilic, N.S., Jawien, A., Mastracci, T.M., Oderich, G.S., Verzini, F., Yeung, K.K.: Editor's Choice -- European Society for Vascular Surgery (ESVS) 2024 Clinical Practice Guidelines on the Management of Abdominal Aorto-Iliac Artery Aneurysms. European Journal of Vascular and Endovascular Surgery. 67, 192–331 (2024). https://doi.org/10.1016/j.ejvs.2023.11.002

12. Chaikof, E.L., Dalman, R.L., Eskandari, M.K., Jackson, B.M., Lee, W.A., Mansour, M.A., Mastracci, T.M., Mell, M., Murad, M.H., Nguyen, L.L., Oderich, G.S., Patel, M.S., Schermerhorn, M.L., Starnes, B.W.: The Society for Vascular Surgery practice guidelines on the care of patients with an abdominal aortic aneurysm. J Vasc Surg. 67, 2-77.e2 (2018). https://doi.org/10.1016/j.jvs.2017.10.044

13. Beck, A.W., Sedrakyan, A., Mao, J., Venermo, M., Faizer, R., Debus, S., Behrendt, C.-A., Scali, S., Altreuther, M., Schermerhorn, M., Beiles, B., Szeberin, Z., Eldrup, N., Danielsson, G., Thomson, I., Wigger, P., Björck, M., Cronenwett, J.L., Mani, K.: Variations in Abdominal Aortic Aneurysm Care: A Report From the International Consortium of Vascular Registries. Circulation. 134, 1948–1958 (2016). https://doi.org/10.1161/CIRCULATIONAHA.116.024870

14. Thompson, S., Brown, L., Sweeting, M., Bown, M., Kim, L., Glover, M., Buxton, M., Powell, J.: Systematic review and meta-analysis of the growth and rupture rates of small abdominal aortic aneurysms: implications for surveillance intervals and their cost-effectiveness. Health Technol Assess (Rockv). 17, (2013). https://doi.org/10.3310/hta17410

15. Public Health England: Official Statistics Abdominal aortic aneurysm screening: 2018 to 2019 data, https://www.gov.uk/government/statistics/abdominal-aortic-aneurysm-screening-2018-to-2019-data

16. UK Health Security Agency: https://ukhsa.blog.gov.uk/2016/01/06/abdominal-aortic-aneurysm-aaa-screening-programme-an-important-milestone/, https://ukhsa.blog.gov.uk/2016/01/06/abdominal-aortic-aneurysm-aaa-screening-programme-an-important-milestone/

17. Smalley, D.M., Ley, K.: Plasma-derived microparticles for biomarker discovery. Clin Lab. 54, 67–79 (2008)

18. Anderson, N.L., Anderson, N.G.: The Human Plasma Proteome. Molecular & Cellular Proteomics. 1, 845–867 (2002). https://doi.org/10.1074/mcp.R200007-MCP200

19. Brzhozovskiy, A., Kononikhin, A., Bugrova, A.E., Kovalev, G.I., Schmit, P.-O., Kruppa, G., Nikolaev, E.N., Borchers, C.H.: The Parallel Reaction Monitoring-

Parallel Accumulation–Serial Fragmentation (prm-PASEF) Approach for Multiplexed Absolute Quantitation of Proteins in Human Plasma. Anal Chem. 94, 2016–2022 (2022). https://doi.org/10.1021/acs.analchem.1c03782

20. Li, J., Smith, L.S., Zhu, H.-J.: Data-independent acquisition (DIA): An emerging proteomics technology for analysis of drug-metabolizing enzymes and transporters. Drug Discov Today Technol. 39, 49–56 (2021). https://doi.org/10.1016/j.ddtec.2021.06.006

21. Clish, C.B.: Metabolomics: an emerging but powerful tool for precision medicine. Molecular Case Studies. 1, a000588 (2015). https://doi.org/10.1101/mcs.a000588

22. Gowda, G.A.N., Djukovic, D.: Overview of mass spectrometry-based metabolomics: opportunities and challenges. Methods Mol Biol. 1198, 3–12 (2014). https://doi.org/10.1007/978-1-4939-1258-2_1

23. Griffiths, W.J., Koal, T., Wang, Y., Kohl, M., Enot, D.P., Deigner, H.: Targeted Metabolomics for Biomarker Discovery. Angewandte Chemie International Edition. 49, 5426–5445 (2010). https://doi.org/10.1002/anie.200905579

24. Roberts, L.D., Souza, A.L., Gerszten, R.E., Clish, C.B.: Targeted Metabolomics. Curr Protoc Mol Biol. 98, (2012). https://doi.org/10.1002/0471142727.mb3002s98

25. Bellamkonda, K., Williams, M., Handa, A., Lee, R.: Flow Mediated Dilatation as a Biomarker in Vascular Surgery Research. J Atheroscler Thromb. 24, 779–787 (2017). https://doi.org/10.5551/jat.40964

26. Lee, R., Charles, P.D., Lapolla, P., Cassimjee, I., Huang, H., Kessler, B., Fischer, R., Handa, A.: Integrated Physiological and Biochemical Assessments for the Prediction of Growth of Abdominal Aortic Aneurysms in Humans. Ann Surg. 270, e1–e3 (2019). https://doi.org/10.1097/SLA.0000000000003154

27. Lee, R., Cassimjee, I., Huang, H., Lapolla, P., Ngetich, E., Chandrashekar, A., Charles, P., Kessler, B., Fischer, R., Handa, A.: Integrated Plasma and Tissue Proteomics Reveals Attractin Release by Intraluminal Thrombus of Abdominal Aortic Aneurysms and Improves Aneurysm Growth Prediction in Humans. Ann Surg. 275, 1206–1211 (2022). https://doi.org/10.1097/SLA.0000000000004439

28. Chen, Y., Wang, F., Xu, F., Yang, T.: Mass Spectrometry-Based Protein Quantification. Presented at the (2016)

29. Becker, C.H., Bern, M.: Recent developments in quantitative proteomics. Mutation Research/Genetic Toxicology and Environmental Mutagenesis. 722, 171–182 (2011). https://doi.org/10.1016/j.mrgentox.2010.06.016

30. Rozanova, S., Barkovits, K., Nikolov, M., Schmidt, C., Urlaub, H., Marcus, K.: Quantitative Mass Spectrometry-Based Proteomics: An Overview. Presented at the (2021)

31. Munro, V., Kelly, V., Messner, C.B., Kustatscher, G.: Cellular control of protein levels: A systems biology perspective. Proteomics. 24, (2024). https://doi.org/10.1002/pmic.202200220

32. Raffield, L.M., Dang, H., Pratte, K.A., Jacobson, S., Gillenwater, L.A., Ampleford, E., Barjaktarevic, I., Basta, P., Clish, C.B., Comellas, A.P., Cornell, E., Curtis, J.L., Doerschuk, C., Durda, P., Emson, C., Freeman, C.M., Guo, X., Hastie, A.T., Hawkins, G.A., Herrera, J., Johnson, W.C., Labaki, W.W., Liu, Y., Masters, B., Miller, M., Ortega, V.E., Papanicolaou, G., Peters, S., Taylor, K.D., Rich, S.S., Rotter, J.I., Auer, P., Reiner, A.P., Tracy, R.P., Ngo, D., Gerszten, R.E., O'Neal, W.K., Bowler, R.P.: Comparison of Proteomic Assessment Methods in Multiple Cohort Studies. Proteomics. 20, (2020). https://doi.org/10.1002/pmic.201900278

33. Joshi, A., Mayr, M.: In Aptamers They Trust. Circulation. 138, 2482–2485 (2018). https://doi.org/10.1161/CIRCULATIONAHA.118.036823

34. Parker, C.E., Borchers, C.H.: Mass spectrometry based biomarker discovery, verification, and validation--quality assurance and control of protein biomarker assays. Mol Oncol. 8, 840–58 (2014). https://doi.org/10.1016/j.molonc.2014.03.006

35. Coorssen, J.R., Padula, M.P.: Proteomics—The State of the Field: The Definition and Analysis of Proteomes Should Be Based in Reality, Not Convenience. Proteomes. 12, 14 (2024). https://doi.org/10.3390/proteomes12020014

36. Simpson, D.M., Beynon, R.J.: QconCATs: design and expression of concatenated protein standards for multiplexed protein quantification. Anal Bioanal Chem. 404, 977–989 (2012). https://doi.org/10.1007/s00216-012-6230-1

37. Lesur, A., Bernardin, F., Koncina, E., Letellier, E., Kruppa, G., Schmit, P.-O., Dittmar, G.: Quantification of 782 Plasma Peptides by Multiplexed Targeted Proteomics. J Proteome Res. 22, 1630–1638 (2023). https://doi.org/10.1021/acs.jproteome.2c00575

38. Pratt, J.M., Simpson, D.M., Doherty, M.K., Rivers, J., Gaskell, S.J., Beynon, R.J.: Multiplexed absolute quantification for proteomics using concatenated signature peptides encoded by QconCAT genes. Nat Protoc. 1, 1029–1043 (2006). https://doi.org/10.1038/nprot.2006.129

39. Kennedy, J.J., Whiteaker, J.R., Ivey, R.G., Burian, A., Chowdhury, S., Tsai, C.-F., Liu, T., Lin, C., Murillo, O.D., Lundeen, R.A., Jones, L.A., Gafken, P.R., Longton, G., Rodland, K.D., Skates, S.J., Landua, J., Wang, P., Lewis, M.T., Paulovich, A.G.: Internal Standard Triggered-Parallel Reaction Monitoring Mass Spectrometry Enables Multiplexed Quantification of Candidate Biomarkers in Plasma. Anal Chem. 94, 9540–9547 (2022). https://doi.org/10.1021/acs.analchem.1c04382

40. Ignjatovic, V., Geyer, P.E., Palaniappan, K.K., Chaaban, J.E., Omenn, G.S., Baker, M.S., Deutsch, E.W., Schwenk, J.M.: Mass Spectrometry-Based Plasma Proteomics: Considerations from Sample Collection to Achieving Translational Data. J Proteome Res. 18, 4085–4097 (2019). https://doi.org/10.1021/acs.jproteome.9b00503

41. Domon, B., Aebersold, R.: Mass Spectrometry and Protein Analysis. Science (1979). 312, 212–217 (2006). https://doi.org/10.1126/science.1124619

42. Halvey, P., Farutin, V., Koppes, L., Gunay, N.S., Pappas, D.A., Manning, A.M., Capila, I.: Variable blood processing procedures contribute to plasma proteomic variability. Clin Proteomics. 18, 5 (2021). https://doi.org/10.1186/s12014-021-09311-3

43. Hui, H.W.H., Kong, W., Goh, W.W. Bin: Thinking points for effective batch correction on biomedical data. Brief Bioinform. 25, (2024). https://doi.org/10.1093/bib/bbae515

44. Pietzner, M., Wheeler, E., Carrasco-Zanini, J., Kerrison, N.D., Oerton, E., Koprulu, M., Luan, J., Hingorani, A.D., Williams, S.A., Wareham, N.J., Langenberg, C.: Synergistic insights into human health from aptamer- and antibody-based proteomic profiling. Nat Commun. 12, 6822 (2021). https://doi.org/10.1038/s41467-021-27164-0

45. Rodríguez-Suárez, E., Whetton, A.D.: The application of quantification techniques in proteomics for biomedical research. Mass Spectrom Rev. 32, 1–26 (2013). https://doi.org/10.1002/mas.21347

46. Pappireddi, N., Martin, L., Wühr, M.: A Review on Quantitative Multiplexed Proteomics. Chembiochem. 20, 1210–1224 (2019). https://doi.org/10.1002/cbic.201800650

47. Annesley, T.M.: Ion Suppression in Mass Spectrometry. Clin Chem. 49, 1041–1044 (2003). https://doi.org/10.1373/49.7.1041

48. Kirsher, D.Y., Chand, S., Phong, A., Nguyen, B., Szoke, B.G., Ahadi, S.: Current landscape of plasma proteomics from technical innovations to biological insights and biomarker discovery. Commun Chem. 8, 279 (2025). https://doi.org/10.1038/s42004-025-01665-1

49. Solier, C., Langen, H.: Antibody-based proteomics and biomarker research—Current status and limitations. Proteomics. 14, 774–783 (2014). https://doi.org/10.1002/pmic.201300334

50. Zhang, Y., Fonslow, B.R., Shan, B., Baek, M.-C., Yates, J.R.: Protein Analysis by Shotgun/Bottom-up Proteomics. Chem Rev. 113, 2343–2394 (2013). https://doi.org/10.1021/cr3003533

51. Brownridge, P., Holman, S.W., Gaskell, S.J., Grant, C.M., Harman, V.M., Hubbard, S.J., Lanthaler, K., Lawless, C., O'cualain, R., Sims, P., Watkins, R., Beynon, R.J.: Global absolute quantification of a proteome: Challenges in the deployment of a QconCAT strategy. Proteomics. 11, 2957–2970 (2011). https://doi.org/10.1002/pmic.201100039

52. McGuire, J.N., Overgaard, J., Pociot, F.: Mass spectrometry is only one piece of the puzzle in clinical proteomics. Brief Funct Genomic Proteomic. 7, 74–83 (2008). https://doi.org/10.1093/bfgp/eln005

53. Pino, L.K., Searle, B.C., Yang, H.-Y., Hoofnagle, A.N., Noble, W.S., MacCoss, M.J.: Matrix-Matched Calibration Curves for Assessing Analytical Figures of Merit in Quantitative Proteomics. J Proteome Res. 19, 1147–1153 (2020). https://doi.org/10.1021/acs.jproteome.9b00666

54. NHS Health Research Authority: Oxford Abdominal Aortic Aneurysm Study - OxAAA, https://www.hra.nhs.uk/planning-and-improving-research/application-summaries/research-summaries/oxford-abdominal-aortic-aneurysm-study-oxaaa/

55. Lee, R., Antonopoulos, A.S., Alexopoulou, Z., Margaritis, M., Kharbanda, R.K., Choudhury, R.P., Antoniades, C., Channon, K.M.: Artifactual elevation of plasma sCD40L by residual platelets in patients with coronary artery disease. Int J Cardiol. 168, 1648–50 (2013). https://doi.org/10.1016/j.ijcard.2013.03.019

56. Scott, K.B., Turko, I. V., Phinney, K.W.: Quantitative Performance of Internal Standard Platforms for Absolute Protein Quantification Using Multiple Reaction Monitoring-Mass Spectrometry. Anal Chem. 87, 4429–4435 (2015). https://doi.org/10.1021/acs.analchem.5b00331

57. Lange, V., Picotti, P., Domon, B., Aebersold, R.: Selected reaction monitoring for quantitative proteomics: a tutorial. Mol Syst Biol. 4, (2008). https://doi.org/10.1038/msb.2008.61

58. Rauniyar, N.: Parallel Reaction Monitoring: A Targeted Experiment Performed Using High Resolution and High Mass Accuracy Mass Spectrometry. Int J Mol Sci. 16, 28566–28581 (2015). https://doi.org/10.3390/ijms161226120

59. Bruker Daltonik GmbH: Plasma proteomics goes high throughput – timsTOF Pro with PASEF and 4D feature alignment to quantify 500 plasma proteins in 11.5 min, https://www.evosep.com/wp-content/uploads/2021/05/1867805-lcms-151-plasmaproteomics-ebook.pdf?

60. Choi, S. Il, Jin, Y., Choi, Y., Seong, B.L.: Beyond Misfolding: A New Paradigm for the Relationship Between Protein Folding and Aggregation. Int J Mol Sci. 26, 53 (2024). https://doi.org/10.3390/ijms26010053

61. Anderson, N.L., Razavi, M., Pearson, T.W., Kruppa, G., Paape, R., Suckau, D.: Precision of Heavy–Light Peptide Ratios Measured by MALDI-TOF Mass

Spectrometry. J Proteome Res. 11, 1868–1878 (2012). https://doi.org/10.1021/pr201092v

62. Hoofnagle, A.N., Whiteaker, J.R., Carr, S.A., Kuhn, E., Liu, T., Massoni, S.A., Thomas, S.N., Townsend, R.R., Zimmerman, L.J., Boja, E., Chen, J., Crimmins, D.L., Davies, S.R., Gao, Y., Hiltke, T.R., Ketchum, K.A., Kinsinger, C.R., Mesri, M., Meyer, M.R., Qian, W.-J., Schoenherr, R.M., Scott, M.G., Shi, T., Whiteley, G.R., Wrobel, J.A., Wu, C., Ackermann, B.L., Aebersold, R., Barnidge, D.R., Bunk, D.M., Clarke, N., Fishman, J.B., Grant, R.P., Kusebauch, U., Kushnir, M.M., Lowenthal, M.S., Moritz, R.L., Neubert, H., Patterson, S.D., Rockwood, A.L., Rogers, J., Singh, R.J., Van Eyk, J.E., Wong, S.H., Zhang, S., Chan, D.W., Chen, X., Ellis, M.J., Liebler, D.C., Rodland, K.D., Rodriguez, H., Smith, R.D., Zhang, Z., Zhang, H., Paulovich, A.G.: Recommendations for the Generation, Quantification, Storage, and Handling of Peptides Used for Mass Spectrometry–Based Assays. Clin Chem. 62, 48–69 (2016). https://doi.org/10.1373/clinchem.2015.250563

63. Picotti, P., Aebersold, R.: Selected reaction monitoring–based proteomics: workflows, potential, pitfalls and future directions. Nat Methods. 9, 555–566 (2012). https://doi.org/10.1038/nmeth.2015

64. Shuford, C.M., Walters, J.J., Holland, P.M., Sreenivasan, U., Askari, N., Ray, K., Grant, R.P.: Absolute Protein Quantification by Mass Spectrometry: Not as Simple as Advertised. Anal Chem. 89, 7406–7415 (2017). https://doi.org/10.1021/acs.analchem.7b00858

65. Wenk, D., Zuo, C., Kislinger, T., Sepiashvili, L.: Recent developments in mass-spectrometry-based targeted proteomics of clinical cancer biomarkers. Clin Proteomics. 21, 6 (2024). https://doi.org/10.1186/s12014-024-09452-1

66. Taylor, P.J.: Matrix effects: the Achilles heel of quantitative high-performance liquid chromatography–electrospray–tandem mass spectrometry. Clin Biochem. 38, 328–334 (2005). https://doi.org/10.1016/j.clinbiochem.2004.11.007

67. Ding, W., Nakai, K., Gong, H.: Protein design via deep learning. Brief Bioinform. 23, (2022). https://doi.org/10.1093/bib/bbac102

68. Norn, C., Wicky, B.I.M., Juergens, D., Liu, S., Kim, D., Tischer, D., Koepnick, B., Anishchenko, I., Baker, D., Ovchinnikov, S., Coral, A., Bubar, A.J., Boykov, A., Valle Pérez, A.U., MacMillan, A., Lubow, A., Mussini, A., Cai, A., Ardill, A.J., Seal, A., Kalantarian, A., Failer, B., Lackersteen, B., Chagot, B., Haight, B.R., Taştan, B., Uitham, B., Roy, B.G., de Melo Cruz, B.R., Echols, B., Lorenz, B.E., Blair, B., Kestemont, B., Eastlake, C.D., Bragdon, C.J., Vardeman, C., Salerno, C., Comisky, C., Hayman, C.L., Landers, C.R., Zimov, C., Coleman, C.D., Painter, C.R., Ince, C., Lynagh, C., Malaniia, D., Wheeler, D.C., Robertson, D., Simon, V., Chisari, E., Kai, E.L.J., Rezae, F., Lengyel, F., Tabotta, F., Padelletti, F., Boström, F., Gross, G.O., McIlvaine, G., Beecher, G., Hansen, G.T., de Jong, G., Feldmann,

H., Borman, J.L., Quinn, J., Norrgard, J., Truong, J., Diderich, J.A., Canfield, J.M., Photakis, J., Slone, J.D., Madzio, J., Mitchell, J., Stomieroski, J.C., Mitch, J.H., Altenbeck, J.R., Schinkler, J., Weinberg, J.B., Burbach, J.D., Sequeira da Costa, J.C., Bada Juarez, J.F., Gunnarsson, J.P., Harper, K.D., Joo, K., Clayton, K.T., DeFord, K.E., Scully, K.F., Gildea, K.M., Abbey, K.J., Kohli, K.L., Stenner, K., Takács, K., Poussaint, L.L., Manalo, L.C., Withers, L.C., Carlson, L., Wei, L., Fisher, L.R., Carpenter, L., Ji-hwan, M., Ricci, M., Belcastro, M.A., Leniec, M., Hohmann, M., Thompson, M., Thayer, M.A., Gaebel, M., Cassidy, M.D., Fagiola, M., Lewis, M., Pfützenreuter, M., Simon, M., Elmassry, M.M., Benevides, N., Kerr, N.K., Verma, N., Shannon, O., Yin, O., Wolfteich, P., Gummersall, P., Tłuścik, P., Gajar, P., Triggiani, P.J., Guha, R., Mathew Innes, R.B., Buchanan, R., Gamble, R., Leduc, R., Spearing, R., dos Santos Gomes, R.L.C., Estep, R.D., DeWitt, R., Moore, R., Shnider, S.G., Zaccanelli, S.J., Kuznetsov, S., Burillo-Sanz, S., Mooney, S., Vasiliy, S., Butkovich, S.S., Hudson, S.B., Pote, S.L., Denne, S.P., Schwegmann, S.A., Ratna, S., Kleinfelter, S.C., Bausewein, T., George, T.J., de Almeida, T.S., Yeginer, U., Barmettler, W., Pulley, W.R., Wright, W.S., Willyanto, Lansford, W., Hochart, X., Gaiji, Y.A.S., Lagodich, Y., Christian, V.: Protein sequence design by conformational landscape optimization. Proceedings of the National Academy of Sciences. 118, (2021). https://doi.org/10.1073/pnas.2017228118

69. Abramson, J., Adler, J., Dunger, J., Evans, R., Green, T., Pritzel, A., Ronneberger, O., Willmore, L., Ballard, A.J., Bambrick, J., Bodenstein, S.W., Evans, D.A., Hung, C.-C., O'Neill, M., Reiman, D., Tunyasuvunakool, K., Wu, Z., Žemgulytė, A., Arvaniti, E., Beattie, C., Bertolli, O., Bridgland, A., Cherepanov, A., Congreve, M., Cowen-Rivers, A.I., Cowie, A., Figurnov, M., Fuchs, F.B., Gladman, H., Jain, R., Khan, Y.A., Low, C.M.R., Perlin, K., Potapenko, A., Savy, P., Singh, S., Stecula, A., Thillaisundaram, A., Tong, C., Yakneen, S., Zhong, E.D., Zielinski, M., Žídek, A., Bapst, V., Kohli, P., Jaderberg, M., Hassabis, D., Jumper, J.M.: Accurate structure prediction of biomolecular interactions with AlphaFold 3. Nature. 630, 493–500 (2024). https://doi.org/10.1038/s41586-024-07487-w

70. Goverde, C.A., Wolf, B., Khakzad, H., Rosset, S., Correia, B.E.: De novo protein design by inversion of the AlphaFold structure prediction network. Protein Sci. 32, e4653 (2023). https://doi.org/10.1002/pro.4653

71. Krokidis, M.G., Koumadorakis, D.E., Lazaros, K., Ivantsik, O., Exarchos, T.P., Vrahatis, A.G., Kotsiantis, S., Vlamos, P.: AlphaFold3: An Overview of Applications and Performance Insights. Int J Mol Sci. 26, (2025). https://doi.org/10.3390/ijms26083671

72. Hughes, C.S., Moggridge, S., Müller, T., Sorensen, P.H., Morin, G.B., Krijgsveld, J.: Single-pot, solid-phase-enhanced sample preparation for proteomics experiments. Nat Protoc. 14, 68–85 (2019). https://doi.org/10.1038/s41596-018-0082-x

73. Demichev, V., Messner, C.B., Vernardis, S.I., Lilley, K.S., Ralser, M.: DIA-NN: neural networks and interference correction enable deep proteome coverage in high throughput. Nat Methods. 17, 41–44 (2020). https://doi.org/10.1038/s41592-019-0638-x

74. Tyanova, S., Temu, T., Sinitcyn, P., Carlson, A., Hein, M.Y., Geiger, T., Mann, M., Cox, J.: The Perseus computational platform for comprehensive analysis of (prote)omics data. Nat Methods. 13, 731–740 (2016). https://doi.org/10.1038/nmeth.3901

75. Mellacheruvu, D., Wright, Z., Couzens, A.L., Lambert, J.-P., St-Denis, N.A., Li, T., Miteva, Y. V, Hauri, S., Sardiu, M.E., Low, T.Y., Halim, V.A., Bagshaw, R.D., Hubner, N.C., al-Hakim, A., Bouchard, A., Faubert, D., Fermin, D., Dunham, W.H., Goudreault, M., Lin, Z.-Y., Badillo, B.G., Pawson, T., Durocher, D., Coulombe, B., Aebersold, R., Superti-Furga, G., Colinge, J., Heck, A.J.R., Choi, H., Gstaiger, M., Mohammed, S., Cristea, I.M., Bennett, K.L., Washburn, M.P., Raught, B., Ewing, R.M., Gingras, A.-C., Nesvizhskii, A.I.: The CRAPome: a contaminant repository for affinity purification–mass spectrometry data. Nat Methods. 10, 730–736 (2013). https://doi.org/10.1038/nmeth.2557

76. Benjamini, Y., Krieger, A.M., Yekutieli, D.: Adaptive linear step-up procedures that control the false discovery rate. Biometrika. 93, 491–507 (2006). https://doi.org/10.1093/biomet/93.3.491

77. Goetze, S., van Drogen, A., Albinus, J.B., Fort, K.L., Gandhi, T., Robbiani, D., Laforte, V., Reiter, L., Levesque, M.P., Xuan, Y., Wollscheid, B.: Simultaneous targeted and discovery-driven clinical proteotyping using hybrid-PRM/DIA. Clin Proteomics. 21, 26 (2024). https://doi.org/10.1186/s12014-024-09478-5

78. Kitata, R.B., Yang, J., Chen, Y.: Advances in data-independent acquisition mass spectrometry towards comprehensive digital proteome landscape. Mass Spectrom Rev. 42, 2324–2348 (2023). https://doi.org/10.1002/mas.21781

79. Bollinger, J.G., Stergachis, A.B., Johnson, R.S., Egertson, J.D., MacCoss, M.J.: Selecting Optimal Peptides for Targeted Proteomic Experiments in Human Plasma Using In Vitro Synthesized Proteins as Analytical Standards. Methods Mol Biol. 1410, 207–21 (2016). https://doi.org/10.1007/978-1-4939-3524-6_12

80. Johnson, J., Harman, V.M., Franco, C., Emmott, E., Rockliffe, N., Sun, Y., Liu, L.-N., Takemori, A., Takemori, N., Beynon, R.J.: Construction of à la carte QconCAT protein standards for multiplexed quantification of user-specified target proteins. BMC Biol. 19, 195 (2021). https://doi.org/10.1186/s12915-021-01135-9

81. Yu, Z., Huang, H., Reim, A., Charles, P.D., Northage, A., Jackson, D., Parry, I., Kessler, B.M.: Optimizing 2D gas chromatography mass spectrometry for robust tissue, serum and urine metabolite profiling. Talanta. 165, 685–691 (2017). https://doi.org/10.1016/j.talanta.2017.01.003

82. Liu, Z., Phillips, J.B.: Comprehensive Two-Dimensional Gas Chromatography using an On-Column Thermal Modulator Interface. J Chromatogr Sci. 29, 227–231 (1991). https://doi.org/10.1093/chromsci/29.6.227

83. Mondello, L., Casilli, A., Tranchida, P.Q., Dugo, G., Dugo, P.: Comprehensive two-dimensional gas chromatography in combination with rapid scanning quadrupole mass spectrometry in perfume analysis. J Chromatogr A. 1067, 235–243 (2005). https://doi.org/10.1016/j.chroma.2004.09.040

84. Skoczyńska, E., Korytár, P., Boer, J. de: Maximizing Chromatographic Information from Environmental Extracts by GCxGC-ToF-MS. Environ Sci Technol. 42, 6611–6618 (2008). https://doi.org/10.1021/es703229t

85. Du, X., Zeisel, S.H.: SPECTRAL DECONVOLUTION FOR GAS CHROMATOGRAPHY MASS SPECTROMETRY-BASED METABOLOMICS: CURRENT STATUS AND FUTURE PERSPECTIVES. Comput Struct Biotechnol J. 4, e201301013 (2013). https://doi.org/10.5936/csbj.201301013

86. Egert, B., Weinert, C.H., Kulling, S.E.: A peaklet-based generic strategy for the untargeted analysis of comprehensive two-dimensional gas chromatography mass spectrometry data sets. J Chromatogr A. 1405, 168–177 (2015). https://doi.org/10.1016/j.chroma.2015.05.056

87. Weinert, C.H., Egert, B., Kulling, S.E.: On the applicability of comprehensive two-dimensional gas chromatography combined with a fast-scanning quadrupole mass spectrometer for untargeted large-scale metabolomics. J Chromatogr A. 1405, 156–167 (2015). https://doi.org/10.1016/j.chroma.2015.04.011

88. LECO Corporation; Saint Joseph, M.U.: https://gcms.cz/labrulez-bucket-strapi-h3hsga3/paper/PEG4D_CURRENCY_SPME_203-821-285.pdf, https://gcms.cz/labrulez-bucket-strapi-h3hsga3/paper/PEG4D_CURRENCY_SPME_203-821-285.pdf

89. Ralston-Hooper, K., Hopf, A., Oh, C., Zhang, X., Adamec, J., Sepúlveda, M.S.: Development of GCxGC/TOF-MS metabolomics for use in ecotoxicological studies with invertebrates. Aquatic Toxicology. 88, 48–52 (2008). https://doi.org/10.1016/j.aquatox.2008.03.002

90. Kempa, S., Hummel, J., Schwemmer, T., Pietzke, M., Strehmel, N., Wienkoop, S., Kopka, J., Weckwerth, W.: An automated GCxGC-TOF-MS protocol for batch-wise extraction and alignment of mass isotopomer matrixes from differential ^{13}C-labelling experiments: a case study for photoautotrophic-mixotrophic grown *Chlamydomonas reinhardtii* cells. J Basic Microbiol. 49, 82–91 (2009). https://doi.org/10.1002/jobm.200800337

91. Jeong, J., Zhang, X., Shi, X., Kim, S., Shen, C.: An efficient post-hoc integration method improving peak alignment of metabolomics data from GCxGC/TOF-MS. BMC Bioinformatics. 14, 123 (2013). https://doi.org/10.1186/1471-2105-14-123

92. Bean, H.D., Hill, J.E., Dimandja, J.-M.D.: Improving the quality of biomarker candidates in untargeted metabolomics via peak table-based alignment of comprehensive two-dimensional gas chromatography–mass spectrometry data. J Chromatogr A. 1394, 111–117 (2015). https://doi.org/10.1016/j.chroma.2015.03.001

93. Górecki, T., Harynuk, J., Panić, O.: The evolution of comprehensive two-dimensional gas chromatography (GC×GC). J Sep Sci. 27, 359–379 (2004). https://doi.org/10.1002/jssc.200301650

94. Misra, B., Olivier, M.: Metabolite Extraction and Derivatization of Plasma/ Serum Samples for High Resolution GC-MS- based Metabolomics v1, (2019)

95. Tarakhovskaya, E., Marcillo, A., Davis, C., Milkovska-Stamenova, S., Hutschenreuther, A., Birkemeyer, C.: Matrix Effects in GC–MS Profiling of Common Metabolites after Trimethylsilyl Derivatization. Molecules. 28, 2653 (2023). https://doi.org/10.3390/molecules28062653

96. Kromidas, S. ed: The HPLC-MS Handbook for Practitioners. Wiley (2017)

97. Raninen, K., Nenonen, R., Järvelä-Reijonen, E., Poutanen, K., Mykkänen, H., Raatikainen, O.: Comprehensive Two-Dimensional Gas Chromatography-Mass Spectrometry Analysis of Exhaled Breath Compounds after Whole Grain Diets. Molecules. 26, (2021). https://doi.org/10.3390/molecules26092667

98. Prodhan, M.A.I., McClain, C., Zhang, X.: Comprehensive Two-Dimensional Gas Chromatography Mass Spectrometry-Based Metabolomics. Presented at the (2021)

99. Zaid, A., Khan, M.S., Yan, D., Marriott, P.J., Wong, Y.F.: Comprehensive two-dimensional gas chromatography with mass spectrometry: an advanced bioanalytical technique for clinical metabolomics studies. Analyst. 147, 3974–3992 (2022). https://doi.org/10.1039/D2AN00584K

100. Fritsche-Guenther, R., Gloaguen, Y., Bauer, A., Opialla, T., Kempa, S., Fleming, C.A., Redmond, H.P., Kirwan, J.A.: Optimized Workflow for On-Line Derivatization for Targeted Metabolomics Approach by Gas Chromatography-Mass Spectrometry. Metabolites. 11, (2021). https://doi.org/10.3390/metabo11120888

101. Gutmann, F., Fritsche-Guenther, R., Dias, D.B., Kirwan, J.A.: Comparing the Extraction Performance in Mouse Plasma of Different Biphasic Methods for Polar and Nonpolar Compounds. J Proteome Res. 23, 2961–2969 (2024). https://doi.org/10.1021/acs.jproteome.3c00596

102. Mondello, L., Tranchida, P.Q., Dugo, P., Dugo, G.: Comprehensive two-dimensional gas chromatography-mass spectrometry: A review. Mass Spectrom Rev. 27, 101–124 (2008). https://doi.org/10.1002/mas.20158

103. Fiehn, O.: Metabolomics by Gas Chromatography-Mass Spectrometry: Combined Targeted and Untargeted Profiling. Curr Protoc Mol Biol. 114, 30.4.1-30.4.32 (2016). https://doi.org/10.1002/0471142727.mb3004s114

104. Shimadzu: Gas Chromatograph Mass Spectrometer GCMS-QP2010 Ultra, https://gcms.cz/labrulez-bucket-strapi-h3hsga3/jpo210001_0740e8553b/jpo210001.pdf?utm_

105. Shimadzu: ChromSquare GC×GC Software for Comprehensive Chromatography Data Analysis, https://www.shimadzu.co.uk/products/gas-chromatograph-mass-spectrometry/gc-ms-software/chromsquare/index.html

106. Ahmad, F.: Protein stability [determination] problems. Front Mol Biosci. 9, (2022). https://doi.org/10.3389/fmolb.2022.880358